

Diss ETH No. 18054

Metal-Ligand Cooperativity
in Rhodium and Platinum Amido Complexes:
C-H and Dihydrogen Activation
Chemistry

A dissertation submitted to the

ETH ZURICH

For the degree of

DOCTOR OF SCIENCES

Presented by

Federica Alessia Maria Ricatto

Dipl. Chem. Università degli Studi di Milano

Born on April 15, 1980

citizen of Milan, Italy

Accepted on the recommendation of

Prof. Dr. H. Grützmacher, examiner

Prof. Dr. A. Togni, co-examiner

Zürich 2008

A Marco

*Ho sceso, dandoti il braccio, almeno un milione di scale
e ora che non ci sei è il vuoto ad ogni gradino.
Anche così è stato breve il nostro lungo viaggio.
Il mio dura tuttora, né più mi occorrono
le coincidenze, le prenotazioni,
le trappole, gli scorni di chi crede
che la realtà sia quella che si vede.
Ho sceso milioni di scale dandoti il braccio
non già perché con quattr'occhi forse si vede di più.
Con te le ho scese perché sapevo che di noi due
le sole vere pupille, sebbene tanto offuscate,
erano le tue.*

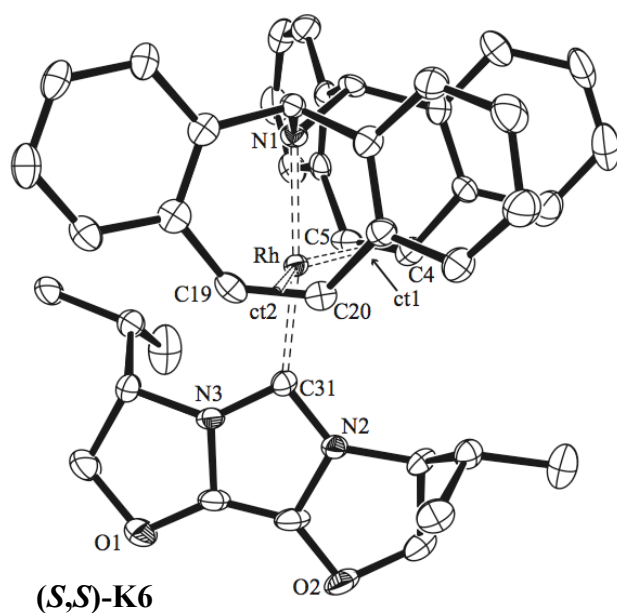
Eugenio Montale (Satura, Xenia II)

*I went down, giving you my arm, at least one million of stairs
and now, when you are no more here, it's the void on every step.
Also in such way our long journey has been short too.
Mine still goes on, and I need no more
coincidences, reservations,
traps, shames just those of people who thinks
that the reality is that what you see.
I went down millions of stairs giving you my arm
not just because four eyes are better viewing than two.
With you I went down 'cause I knew that between us
the only true pupils, notwithstanding such darkened,
were yours.*

Eugenio Montale (Satura, Xenia II)

Abstract

The *first chapter* of this thesis concerns the synthesis of new N-heterocyclic carbene rhodium(I) complexes bearing trop₂NH. Complexes [RhI(trop₂NH)(1,3-dimethylimidazolin-2-ylidene)] (**K3**), [RhCl(trop₂NH)(1,3-dicyclohexylimidazolin-2-ylidene)] (**K4**), [RhCl(trop₂NH)(1,3-bis-((S)-1-phenyl-ethyl)-2-ylidene)] ((**S,S**)-**K5**) and [RhCl(trop₂NH)((S)ValinolCarbene)] ((**S,S**)-**K6**) of general formula [RhX(trop₂NH)(NHC)] (X= Cl, I, OTf) have been obtained in good yield. The Introduction of chiral N-heterocyclic carbenes (derived from enantiomerically pure imidazolium salts) allows the formation of chiral complexes in the case of (**S,S**)-**K5** and (**S,S**)-**K6**.



Pentacoordinate Carbene rhodium(I) complexes have similar structures to those observed for the analogous phosphine complexes of trop₂NH in solution (NMR spectroscopy study) and in the solid state (X-ray spectroscopy study).

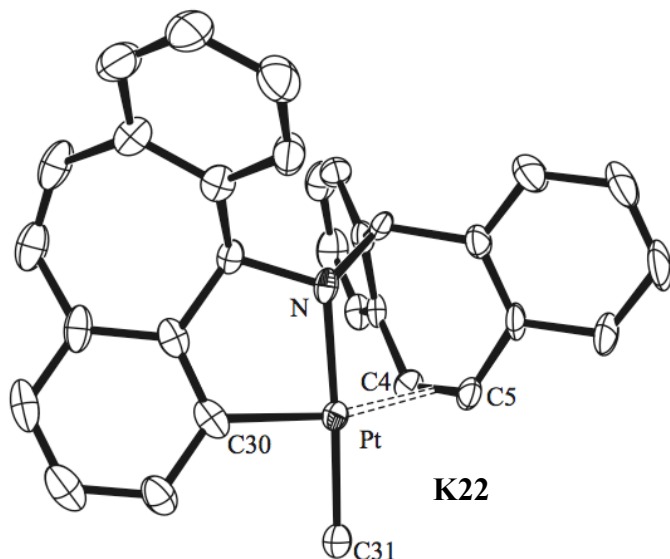
The tetracoordinate compound (**S,S**)-**K6** has been isolated and characterized by crystal structure analysis. Similarly to its phosphine analogue, (**S,S**)-**K6** has a saw-horse type structure.

Complexes **K3**, **K4**, (**S,S**)-**K5** and (**S,S**)-**K6** have been used as catalysts for transfer hydrogenation reactions. The compounds have lower activity than the phosphine-based system and no chiral induction has been observed when (**S,S**)-**K5** and (**S,S**)-**K6** have been employed.

The behavior in solution of the amides [RhX(trop₂N)(NHC)] **K7**, **K8**, (**S,S**)-**K9** and (**S,S**)-**K10** - derived from the deprotonation of amines **K3**, **K4**, (**S,S**)-**K5** and (**S,S**)-**K6** - has been studied. Complexes **K8**, (**S,S**)-**K9** and (**S,S**)-**K10** undergo *intra*-molecular C-H activation of the N-alkyl group of the carbene along the Rh-N bond of the amide and no products resulting from oxidative addition was detected. The cyclometalated rhodium(I) complexes have been fully characterized by NMR and X-ray spectroscopy.

The *second chapter* of this thesis describes the synthesis and reactivity of new alkyl platinum(II) complexes of trop₂NH of general formula [Pt(Me)₂(^Ytrop₂NH)] and [PtX(Me)(^Ytrop₂NH)] (X= OTf, OMs or BAr^F and Y= H, F or Ph).

These compounds have similar structures to the isoelectronic rhodium(I) complexes of trop₂NH.



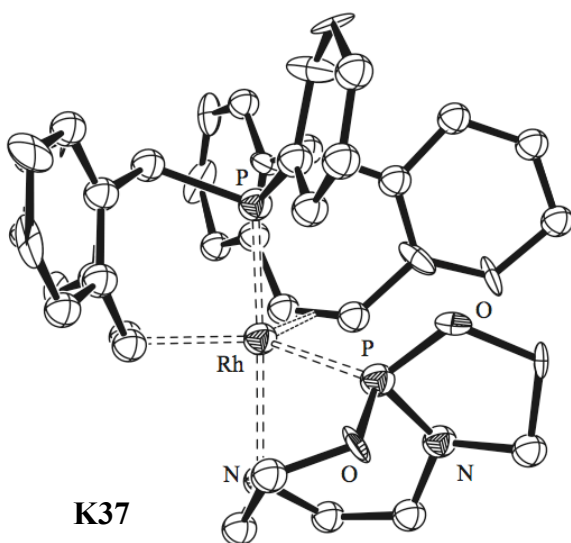
Thermal activation of complexes [Pt(Me)₂(^Ytrop₂NH)] **K20** (Y= H) and **K24** (Y= F) did not yield a reactive amide species by elimination of methane from the NH and methyl group but led to the stable square planar orthometallate compound **K22** and **K27**. [Pt(Me)₂(^{Ph}trop₂NH)] (**K25**) decomposes in solution at high temperature.

Formation of the amide has been achieved by deprotonation of complexes

[Pt(Me)(trop₂NH)] BAR^F with base (potassium *tert*-butoxide) but the amide most likely dimerizes in solution. To trap the formed amide before the formation of a dimeric species a suitable substrate (pentafluorobenzene, C₆HF₅) for the C-H activation was offered prior to the deprotonation reaction with the base. C₆HF₅ reacts with [Pt(Me)(trop₂NH)]BAR^F (**K29**) only upon addition of one equivalent of *t*BuOK. The product of the reaction is the pentafluorophenyl-platinum(II) compound **K35**.

DFT calculations support the activation of the substrate by 1,2-addition across the Rh-N bond. The process has a relatively low activation energy barrier (15 kcalmol⁻¹).

In the *third chapter* of this thesis preliminary studies regarding the reactivity of hydridophosphanes (HP) rhodium(I) complexes of trop₂PPh are described. Complex *Cis*-



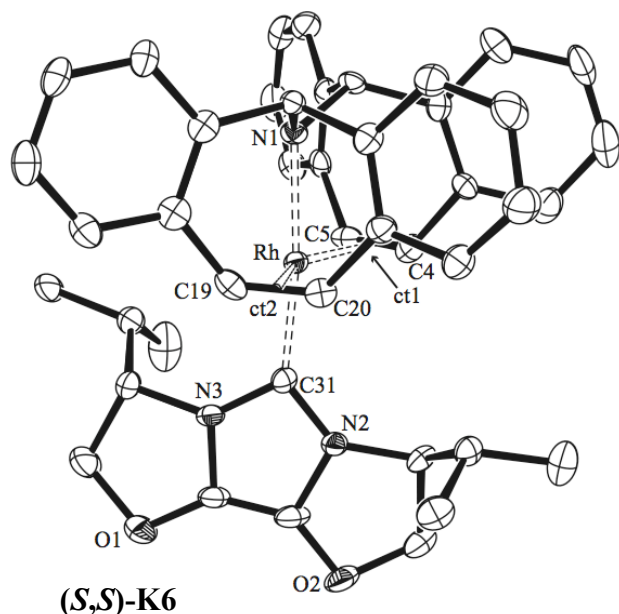
[Rh(trop₂PPh)(P(C₆H₁₃N₂O₂))] (**K37**) can be synthesized and converted to complex *trans*-[Rh(trop₂PPh)(P(C₆H₁₂N₂O₂))] (**K39**). **K39** has been found to react quantitatively in dihydrogen atmosphere to yield the hydride *trans*-[Rh(H)(trop₂PPh)(P(C₆H₁₃N₂O₂))] (**K40**).

DFT calculations show that compound **K39** has (calculated) distances for Rh-N and P-N of 2.445 Å and 1.975 Å. The dihydrogen molecule can easily displace the nitrogen of the hydridophosphanide moiety (weak interaction

Rh-N). The free pedant nitrogen of the HP ligand can act as internal base and assist the metal in the heterolytic activation of H₂.

Riassunto

Il *primo capitolo* di questa tesi riguarda la sintesi di nuovi complessi carbenici di rodio(I) di trop_2NH . I complessi $[\text{RhI}(\text{trop}_2\text{NH})(1,3\text{-dimethylimidazolin-2-ylidene})]$ (**K3**), $[\text{RhCl}(\text{trop}_2\text{NH})(1,3\text{-dicyclohexylimidazolin-2-ylidene})]$ (**K4**), $[\text{RhCl}(\text{trop}_2\text{NH})(1,3\text{-bis-}((S,S)\text{-1-phenyl-ethyl-2-ylidene}))]$ (**(S,S)-K5**) and $[\text{RhCl}(\text{trop}_2\text{NH})((S)\text{ValinolCarbene})]$ (**(S,S)-K6**) di formula generale $[\text{RhX}(\text{trop}_2\text{NH})(\text{NHC})]$ ($X = \text{Cl, I, OTf}$) sono stati sintetizzati in buone rese.



L'introduzione di carbeni N-eterociclici chirali (ottenuti da sali di imidazolio enantiomericamente puri) ha permesso di ottenere complessi chirali nel caso di **(S,S)-K5** e **(S,S)-K6**.

I complessi carbenici di rodio(I) pentacoordinati hanno strutture simili a quelle osservate per gli analoghi complessi fosfinici di trop_2NH in soluzione (studi di spettroscopia NMR) e allo stato solido (studi di spettroscopia a raggi X).

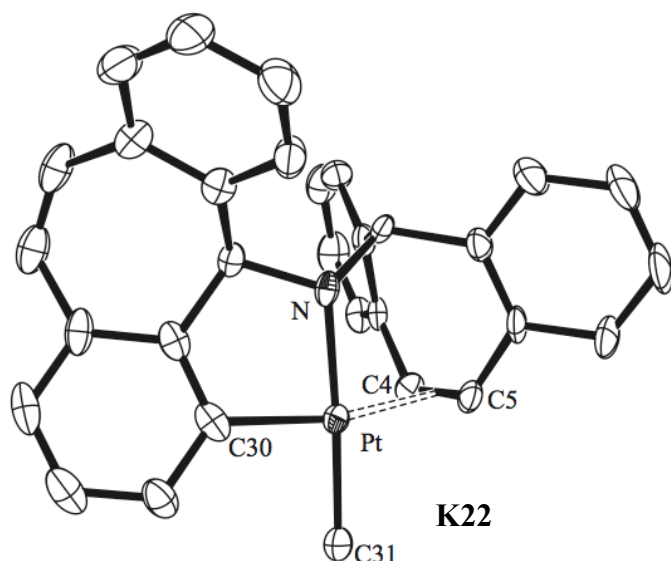
Anche il composto tetracoordinato **(S,S)-K6** è stato isolato e caratterizzato per analisi cristallografica. In maniera simile agli analoghi complessi fosfinici, **(S,S)-K6** ha una struttura a cavalletto.

I complessi **K3**, **K4**, **(S,S)-K5** e **(S,S)-K6** sono stati utilizzati come catalizzatori per reazioni di trasferimento di idrogeno. I complessi hanno minore attività catalitica rispetto ai sistemi fosfinici e nessun eccesso enantiomerico è stato osservato durante l'utilizzo di **(S,S)-K5** e **(S,S)-K6**.

E' stato inoltre studiato il comportamento in soluzione delle amidi $[\text{RhX}(\text{trop}_2\text{N})(\text{NHC})]$ **K7**, **K8**, **(S,S)-K9** e **(S,S)-K10**, ottenute per deprotonazione di **K3**, **K4**, **(S,S)-K5** e **(S,S)-K6**. I complessi **K8**, **(S,S)-K9** e **(S,S)-K10** subiscono l'attivazione intramolecolare del gruppo C-H (appartenente ai diversi sostituenti N-alchilici dei carbeni) attraverso il legame Rh-N dell'amide. Non si è mai osservata la formazione di prodotti derivanti da addizione ossidativa. I complessi metallaciclo di rodio(I) sono stati caratterizzati per spettroscopia NMR e raggi X.

Il *secondo capitolo* di questa tesi descrive la sintesi e la reattività di nuovi complessi alchilici di platino(II) di trop_2NH la cui formula generale è $[\text{Pt}(\text{Me})_2(\text{Ytrop}_2\text{NH})]$ e $[\text{PtX}(\text{Me})(\text{Ytrop}_2\text{NH})]$ ($X = \text{OTf, OMs}$ or BAr^{F} and $\text{Y} = \text{H, F}$ or Ph).

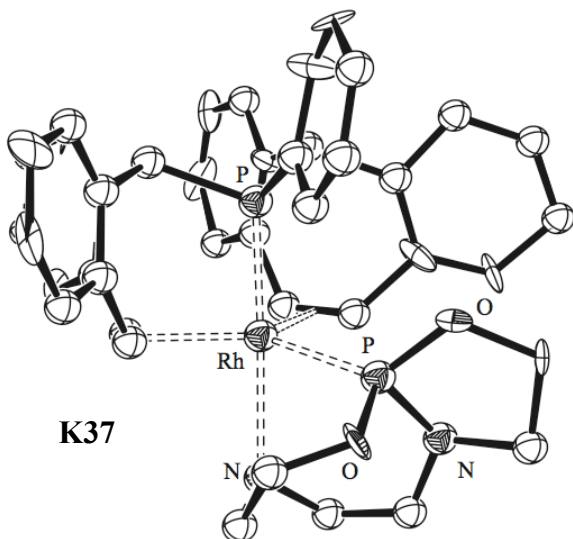
Questi composti hanno simili caratteristiche strutturali ai complessi isoelettronici di rodio(I) di trop₂NH.



L'attivazione termica di [Pt(Me)₂(^Ytrop₂NH)] **K20** (Y= H) e **K24** (Y= F) non produce, previa eliminazione di metano (formatosi da il gruppo NH e dal metile), specie amidiche reattive ma piuttosto porta alla formazione di specie planari quadrate **K22** and **K27** molto stabili. [Pt(Me)₂(^{Ph}trop₂NH)] (**K25**) si decompone in soluzione ad elevate temperature.

La formazione dell'amide è stata ottenuta per deprotonazione del complesso [Pt(Me)(trop₂NH)X] con una base (terbutossido di potassio) ma l'amide formatasi molto probabilmente dimerizza in soluzione. Per far reagire l'amide e prevenire la formazione di specie dimeriche è stato introdotto il substrato scelto per l'attivazione del C-H (in questo caso pentafluorobenzene C₆HF₅) prima della reazione di deprotonazione. C₆HF₅ reagisce con [Pt(Me)(trop₂NH)]BAR^F (**K29**) solo dopo l'aggiunta di *t*BuOK. Il prodotto della reazione è l'addotto

di pentafluorofenil-platino(II) **K35**.



Calcoli DFT sostengono l'ipotesi di attivazione del substrato per addizione 1,2 lungo il legame Rh-N dell'amide. Il processo ha una barriera energetica relativamente bassa (15 kcalmol⁻¹).

Nel *terzo capitolo* di questa tesi sono descritti gli studi preliminari condotti sulla reattività di complessi di idridofosforano (HP) rodio(I) di trop₂PPh.

Il complesso *Cis*-[Rh(trop₂PPh)(P(C₆H₁₃N₂O₂))] (**K37**) è facilmente sintetizzabile e può essere

convertito nella specie *trans*-[Rh(trop₂PPh)(P(C₆H₁₂N₂O₂))] (**K39**). **K39** reagisce quantitativamente in atmosfera di idrogeno formando l'idruro *trans*-[Rh(H)(trop₂PPh)(P(C₆H₁₃N₂O₂))] (**K40**).

Calcoli DFT dimostrano che il composto **K39** ha distanze (calcolate) Rh-N e P-N di 2.445 Å e 1.975 Å. La molecola di H₂ può facilmente sostituire l'atomo di azoto dell'idridofosforano (debole

interazione Rh-N). L'atomo di azoto dell'HP è libero di assistere come base interna l'attivazione eterolitica della molecola di H₂.

Table of Contents

Abstract	III
Riassunto	VII
Table of Contents.....	III
1 N-Heterocyclic Carbene Rhodium Complexes	7
1.1 Introduction.....	7
1.1.1 Electronic structure and Stability of Carbenes	7
1.1.1.1 Preparation of Free Diaminocarbenes.....	9
1.1.2 Carbene – Transition Metal Complexes	12
1.1.2.1 Synthesis	12
1.1.2.2 Electronic Properties	16
1.1.2.3 Catalytic Properties	17
1.1.3 Special Reactivity of NHC-Complexes	21
1.2 Aims	25
1.3 General Synthesis of [RhX(trop ₂ NH)(NHC)]	26
1.3.1 Characterization of [RhI(trop ₂ NH)(IMe)] and [RhCl(trop ₂ NH)(ICy)].....	28
1.3.2 Crystal structure of [RhCl(trop ₂ NH)(1,3-bis-((S)-1-phenyl-ethyl)imidazolin-2-ylidene)].....	29
1.3.3 Crystal structure of [Rh(trop ₂ NH)((S)-ValinolCarbene)]OTf.....	32
1.3.4 Additional NMR Data of [RhX(trop ₂ NH)(NHC)]	34
1.4 Deprotonation of [RhX(trop ₂ NH)(NHC)]	34
1.4.1 Determination of the Activation Energy (E _a) for the Ligand Inversion in (S,S)-K10.....	36
1.4.2 Transfer Hydrogenation.....	38
1.5 Reactivity of [RhX(trop ₂ NH)(NHC)].....	40
1.5.1 Reactivity of [Rh(trop ₂ NH)(ICy)].....	40
1.5.2 Reactivity of [Rh(trop ₂ NH)(S-ValinolCarbene)]	43
1.5.3 Reactivity of [RhCl(trop ₂ NH)(1,3-bis-((S)-1-phenyl-ethyl)imidazolin-2-ylidene)]	45
1.6 β-Functionalized Phenyl Isocyanide complexes.....	48
1.6.1 Crystal Structure of [RhCl(trop ₂ NH)(CNPh)].....	48
1.6.2 Synthesis of [RhCl(trop ₂ NH)(2-(trimethylsiloxy)phenylisocyanide)] and Crystal structure of [RhCl(trop ₂ NMe)(2-(trimethylsiloxy)phenylisocyanide)].....	50
1.6.4 PGSE experiments	53
1.7 Conclusions and Outlook	56
2 Platinum and Palladium Complexes	61
2.1 Introduction.....	61
2.1.2 C-H Activation by Late Transition Metals	64
2.1.2.1 Note on σ-complexes.....	65

2.1.2.2 Alkane Activation by Pt(II) Complexes – Mechanism for the C-H Activation Sequence	67
2.1.2.3 Note On The Rarity of Pt(IV)Pentacoordinate Complexes	72
2.1.3 Alkane Activation by Early Transition Metal Complexes	74
2.2 Aims	76
2.3 Synthesis of Pt(II) and Pd(II) Complexes	77
2.3.1 Thermal Activation in Benzene.....	80
2.4 Synthesis of [Pt(Me) ₂ (^Y trop ₂ NH)]	84
2.5 Synthesis of [Pt(Me)(X)(trop ₂ NH)]	89
2.6 Deprotonation Reaction.....	94
2.6.1 DFT Calculations	96
2.6.2 Activation of C ₆ F ₅ H	98
2.7 Conclusions and Outlook	100
3 Hydridophosphorane as Ligands for H₂ Activation	105
3.1 Introduction.....	105
3.1.1 Heterolytic Dihydrogen Activation in Complexes with Pendant Basic Group.....	105
3.1.2 Metallaphosphanides	109
3.2 Aims	111
3.3 Attempted synthesis of metallaphosphorane	112
3.4 Synthesis of [Rh(trop ₂ PPh)(HP)]	114
3.5 Reactivity of <i>trans</i> -[Rh(trop ₂ PPh)(HP)] with H ₂	119
3.6 DFT Calculations	122
3.7 Conclusions and Outlook	127
4 Experimental Section.....	131
4.1 General Comments.....	131
4.2 Preparation and Characterization.....	134
[RhCl(trop ₂ NH)(triphenylphosphine)] (K1)	134
[Rh(trop ₂ N)(triphenylphosphine)] (K2)	134
[RhI(trop ₂ NH)(1,3-dimethylimidazolin-2-ylidene)] (K3).....	135
[RhCl(trop ₂ NH)(1,3-dicyclohexylimidazolin-2-ylidene)] (K4)	136
[RhCl(trop ₂ NH)(1,3-bis-((S)1-phenyl-ethyl)imidazolin-2-ylidene)] ((S,S)-K5)	137
[Rh(trop ₂ NH)((S)-ValinolCarben)]OTf ((S,S)-K6)	138
[Rh(trop ₂ N)(1,3-dimethylimidazolin-2-ylidene)] (K7)	139
[Rh(trop ₂ N)(1,3-dicyclohexylimidazolin-2-ylidene)] (K8)	140
[Rh(trop ₂ N)(1,3-bis-(1-phenyl-ethyl)imidazolin-2-ylidene)] ((S,S)-K9).....	141
[Rh(trop ₂ N)((S)-ValinolCarbene)] ((S,S)-K10)	142
[Rh(trop ₂ NH)(1,3-dicyclohexylimidazolin-2-ylidene)] CHactivated (K11)	143

[Rh(trop ₂ NH)(ValinolCarben)] CHactivated (K12).....	145
[Rh(trop ₂ NH)(1-(1-phenyl-ethyl)imidazolin-2-ylidene)] ((S)-K13).....	147
[RhCl(trop ₂ NH)(CNC ₆ H ₅)] (K14).....	148
[RhCl(trop ₂ NH)(CNC ₆ H ₄ OSi(CH ₃) ₃)] (K15).....	149
[Rh(trop ₂ NH)(CN(Ph)OtBu)]K.....	150
[RhCl(trop ₂ NMe)(CNC ₆ H ₄ OSi(CH ₃) ₃)] (K16).....	151
[Rh(PF ₂ O ₂)(trop ₂ NH)(C ₇ H ₅ NO)] (K18).....	152
[Rh(trop ₂ NH)(μ-C ₇ H ₄ NO)] (K19).....	153
[Pt(Me) ₂ (trop ₂ NH)] (K20).....	154
[Pd(Me)(OTf)(trop ₂ NH)] (K21).....	155
[Pt(Me)(tropNHortho-trop)] (K22).....	156
Bis(3,7-Difluor-5H-dibenzo[a,d]cyclohepten-5-yl)amine (^F tropNH ₂) (133).....	157
3,7-Diphenyl-5H-dibenzo[a,d]cyclohepten-5-on (^{Ph} tropO) (136).....	158
3,7-Diphenyl-5H-dibenzo[a,d]cyclohepten-5-ol (^{Ph} tropOH) (137).....	159
5-Chlor-3,7-Diphenyl-5H-dibenzo[a,d]cyclohepten (^{Ph} tropCl) (138).....	160
Bis(3,7-Diphenyl-5H-dibenzo[a,d]cyclohepten-5-yl)amine (^{Ph} tropNH ₂) (139).....	161
[Pt(Me) ₂ (^F trop ₂ NH)] (K24).....	162
[Pt(^{Ph} trop ₂ NH)Me ₂] (K25).....	163
[Pt(^F tropNHortho- ^F trop)Me] (K26).....	164
[Pt(OTf)(Me)(trop ₂ NH)] (K27).....	165
[Pt(OMs)(Me)(trop ₂ NH)] (K28).....	166
[Pt(Me)(trop ₂ NH)]BAR ^F (K29).....	167
[Pt(Me)(^F trop ₂ NH)]BAR ^F (K30).....	168
[Pt(Me)(^{Ph} trop ₂ NH)]BAR ^F (K31).....	169
[Pt(Me)(trop ₂ NH)(PPh ₃)]OTf (K32).....	170
[Pt(Me)(trop ₂ N)] ₂ (K33).....	171
[Pt(X)(trop ₂ NH)Me(H)] ₂ (K34).....	172
[Pt(trop ₂ NH)Me(C ₆ F ₅)] (K35).....	173
[Pt(tropNH ₂)Me ₂].....	174
C ₆ H ₁₃ PN ₂ O ₂ (155).....	175
<i>cis</i> -[Rh(OTf)(trop ₂ PPh)(P(C ₆ H ₁₃ N ₂ O ₂))] (K37).....	176
<i>trans</i> -[Rh(OTf)(trop ₂ PPh)(P(C ₆ H ₁₂ N ₂ O ₂))] (K38).....	177
<i>trans</i> -[Rh(OTf)(trop ₂ PPh)(P(C ₆ H ₁₂ N ₂ O ₂))] (K39).....	178
<i>trans</i> -[Rh(H)(trop ₂ PPh)(P(C ₆ H ₁₃ N ₂ O ₂))] (K40).....	179
[RhCl(trop ₂ NMe)(P(OPh) ₃)].....	180
[Rh(trop ₂ NMe)(P(OPh) ₃)]OTf.....	181
4.3 Literature.....	182

5 Appendix 185

5.1 List of Abbreviations.....	185
--------------------------------	-----

5.2 Crystallographic Data.....	186
[RhCl(trop ₂ NH)(1,3-bis-((S)1-phenyl-ethyl)imidazolin-2-ylidene)] ((S,S)-K5)	186
[Rh(trop ₂ NH)((S)-ValinolCarben)]OTf ((S,S)-K6)	187
[Rh(trop ₂ NH)(1,3-dicyclohexylimidazolin-2-ylidene)] CHactivated (K11)	188
[RhCl(trop ₂ NH)(CNC ₆ H ₅)] (K14).....	189
[RhCl(trop ₂ NMe)(CNC ₆ H ₄ OSi(CH ₃) ₃)] (K16).....	190
[Rh(PF ₂ O ₂)(trop ₂ NH)(C ₇ H ₅ NO)] (K18).....	191
[Rh(trop ₂ NH)(μ-C ₇ H ₄ NO)] ₂ (K19).....	192
[Pt(Me) ₂ (trop ₂ NH)] (K20).....	193
[Pd(Me)(OTf)(trop ₂ NH)] (K21)	194
[Pt(Me)(tropNHortho-trop)] (K22)	195
[Rh(μ-Cl)(^F trop ₂ NH)] ₂ (K23).....	196
[Pt(Me) ₂ (^F trop ₂ NH)] (K24).....	197
[Pt(OMs)(Me)(trop ₂ NH)] (K28).....	198
[Pt(Me)(^{Ph} trop ₂ NH)]BAr ^F (K31)	199
[Pt(Me)(trop ₂ NH)(PPh ₃)]OTf (K32)	200
<i>cis</i> -[Rh(OTf)(trop ₂ PPh)(P(C ₆ H ₁₃ N ₂ O ₂))] (K37)	201
[RhCl(trop ₂ NMe)(P(OPh) ₃)].....	202
[Rh(trop ₂ NMe)(P(OPh) ₃)]OTf.....	203
Curriculum Vitae	185
Acknowledgment.....	207

1 N-Heterocyclic Carbene Rhodium Complexes

1.1 Introduction

The first chapter of this thesis is focused on the preparation of carbene complexes of rhodium (Chapter 1.3) and their application in transfer hydrogenation catalysis (Chapter 1.4.2). Especially, the reactivity of carbene amido complexes has been investigated and is discussed in Section 1.5. In the following introduction only general aspects of free carbenes and their complexes will be described. Topics concerning the stability of carbenes, their electronic properties and preparation will be presented in Chapter 1.1.1. Formation of carbenes metal adducts, their classification and application in catalysis, with a particular emphasis on asymmetric catalysis, will be reviewed in Chapter 1.1.2. A detailed section, Chapter 1.1.3, is dedicated to the special aspects of the reactivity of carbenes metal complexes, namely intramolecular C-H and C-C activation, which is of particular interest with respect to Section 1.5.

1.1.1 Electronic structure and Stability of Carbenes

In 2000 Bertrand defined carbenes as “neutral compounds featuring a divalent carbon atom with only six electrons in its valence shell”.¹ Two geometries are possible for this species: linear or bent. For the linear geometry the central carbon atom of the carbene can be described with an sp -hybridized valence electron configuration. The highest singly occupied orbitals are degenerate in energy (p_x and p_y) and the carbene is in a triplet ground state. In the bent geometry, the carbon atom adopts a sp^2 -type hybridization. One of the two p orbitals remains at the same energy level, while the other one is stabilized due to the acquired σ character (Figure 1.1). Most carbenes known today are bent.

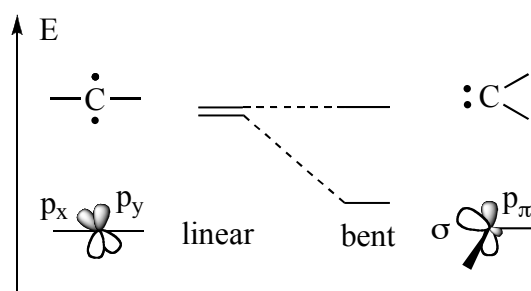


Figure 1.1: Relationship between the carbene bond angle and the nature of the frontier orbitals.

Figure 1.2 shows the four different scenarios possible for the electronic configuration of a bent carbene.

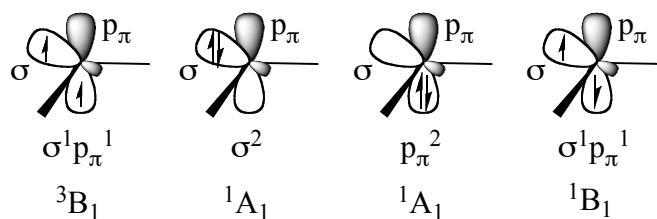


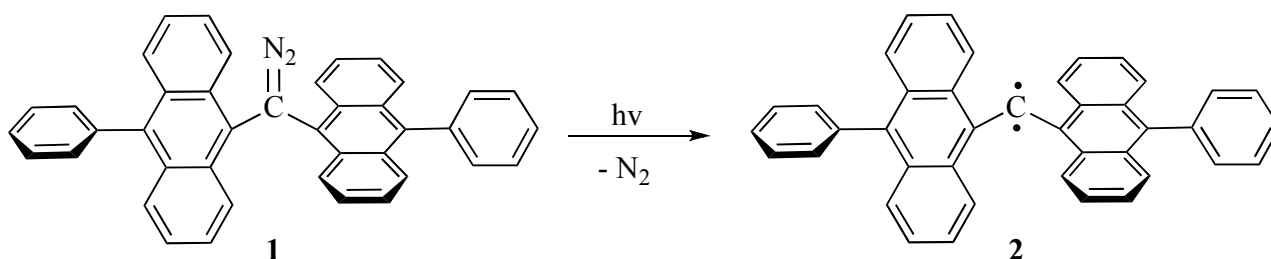
Figure 1.2: Possible electronic configurations of carbenes.

A first possibility is a triplet state, with two electrons with parallel spin in two different orbitals ($\sigma^1 p_\pi^1$ configuration, 3B_1 ground state). Two singlet states with paired electrons in the same orbital (σ^2 or p_π^2 configuration, 1A_1) can be also envisaged. Last, an excited singlet state is possible where the two paired electrons are in two different orbitals ($\sigma^1 p_\pi^1$ configuration, 1B_1).

The carbene configuration influences the energy of the σ and p_π orbitals. When the σ - p_π gap is small – smaller than the electron pairing energy – a triplet ground state is expected. This is the case for CH_2 which has triplet ground state more stable than the singlet ground state by 10 kcal mol^{-1} . The larger the energy gap σ - p_π becomes, the more stable the singlet state is stabilized. The σ - p_π energy difference is large when the substituents are σ -electron-withdrawing. Furthermore, the singlet state is stabilized by p -donors in α -position (stabilization via a bonding $(p-p)\pi$ interaction of the filled lone pairs at the donor and the unoccupied p -orbital at the central carbon). Harrison et al. studied the effect of the substituents on the ground state of the carbene.² The carbenes change from a triplet (ClI_2 , CH_2) to a significantly more stable singlet ground state when the substituents are changed from electropositive lithium to electronegative fluorine (CF_2).

Rather persistent triplet carbenes were obtained with sterically encumbering substituents, which stabilize these otherwise highly reactive carbenes through kinetic and thermodynamic effects (apart from rising the activation barrier for oligomerisation, the bulky substituents enforce a larger bonding angle at the central carbon which favors the triplet state).

This strategy has been adopted by Tamioka et al. to make triplet carbenes, which have a very long-life, as depicted in Scheme 1.1 showing the persistent triplet bis(9-anthryl)carbene (**2**).³



Scheme 1.1: Structure of triplet bis(9-anthryl)carbene (**2**).

Based on the current knowledge, it seems that singlet carbenes are easier to stabilize than triplet carbenes. Pauling made suggestions on how to stabilize such species.⁴ The key is to preserve their electroneutrality by the appropriate choice of substituents. This can be achieved in three different ways (Figure 1.3) and all of them have been studied experimentally.

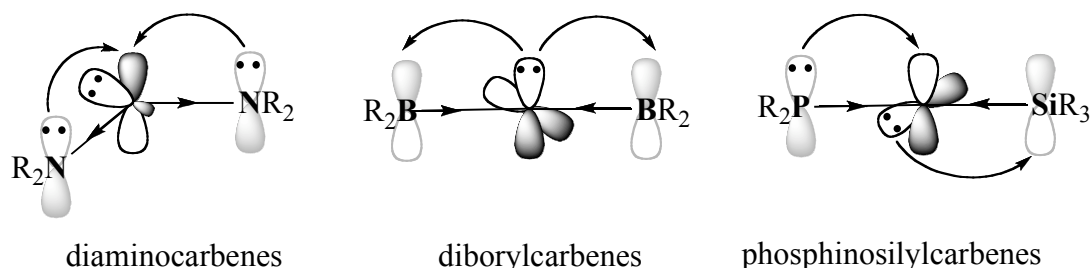
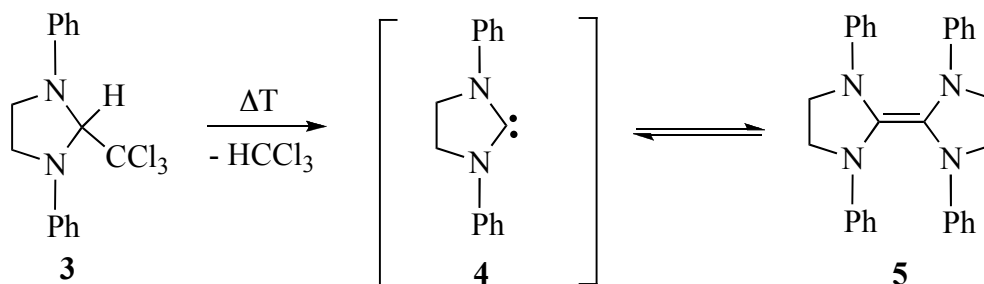


Figure 1.3: Electronic effects of the substituents.

Diaminocarbenes (Figure 1.3) with sufficiently bulky amino groups NR_2 could be isolated as crystalline substances. As in CF_2 (see above), the nitrogen centers in α -position serve as π -donor σ -acceptor substituents and stabilize electronically the singlet state. Remarkably, another possibility is to use two π -acceptor σ -donor substituents, as for example in diborylcarbenes, which likewise stabilize the singlet state despite the linear arrangement of the carbene. Finally, the combination of a π -donor (R_2P) and a π -acceptor (R_3Si), as for example phosphinosilylcarbenes, is suitable for the stabilization of a singlet carbene.

1.1.1.1 Preparation of Free Diaminocarbenes

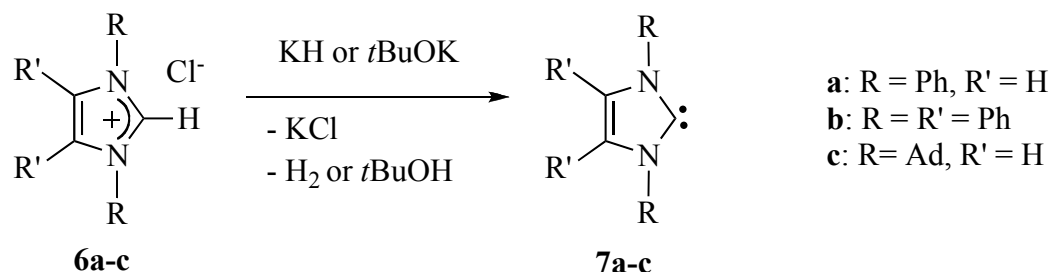
The first attempts to synthesize and isolate carbenes started in the early 1960s, when Wanzlick tried to prepare the 1,3-diphenylimidazolidin-2-ylidene (**4**) by thermal elimination of chloroform (Scheme 1.2),⁵ being aware of the stabilizing effect of amino substituents described above.



Scheme 1.2: The Wanzlick equilibrium.

The experiment was however not successful: Wanzlick isolated only the olefin **5**. Cross-coupling experiments did not support an equilibrium between **5** and the two carbene units **4**. In 1970,

Wanzlick and co-workers demonstrated that imidazol-2-ylidenes, which were trapped but not isolated, could be formed by deprotonation of the corresponding imidazolium salts with potassium *tert*-butoxide or potassium hydride, as depicted in Scheme 1.3.⁶



Scheme 1.3: Deprotonation of imidazolium salts by potassiumhydride.

Twenty years passed before the isolation of “*A stable Crystalline Carbene*”⁷ by Arduengo et al. was reported (Figure 1.4). Compound **7c** was obtained by deprotonation of the 1,3-di-1-adamantylimidazolium chloride (**6c**) (Scheme 1.3) with sodium or potassium hydride in presence of catalytic amounts *t*BuOK in almost quantitative yield. The colorless crystals of **7c** are thermally stable and melt at 240 – 241 °C.

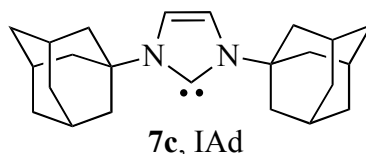


Figure 1.4: The first stable crystalline carbene isolated by Arduengo et al.

Herrmann and co-workers developed a more convenient preparative procedure, which employs liquid ammonia as solvent (homogeneous phase). Figure 1.5 shows differently substituted **8** – **10**, chiral **11** or bis- **12** carbenes prepared following this procedure.⁸

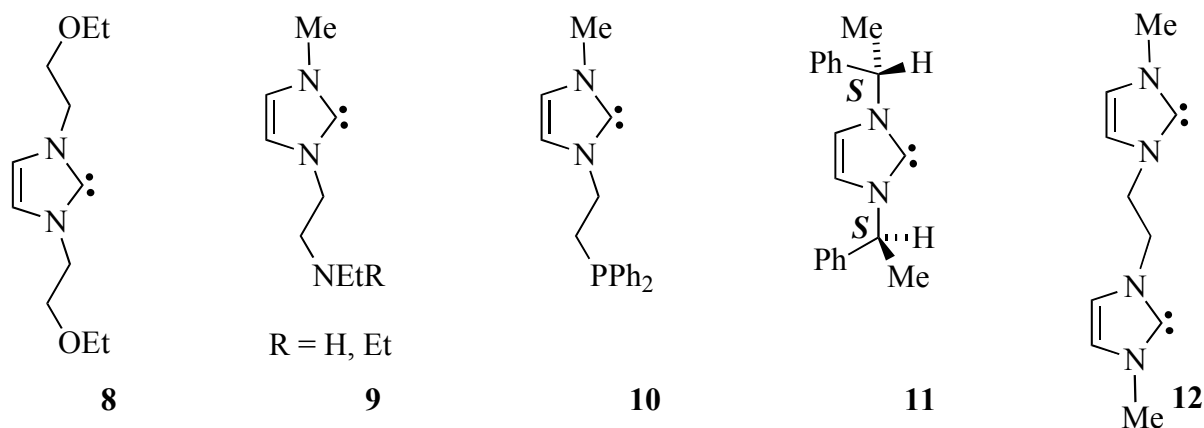
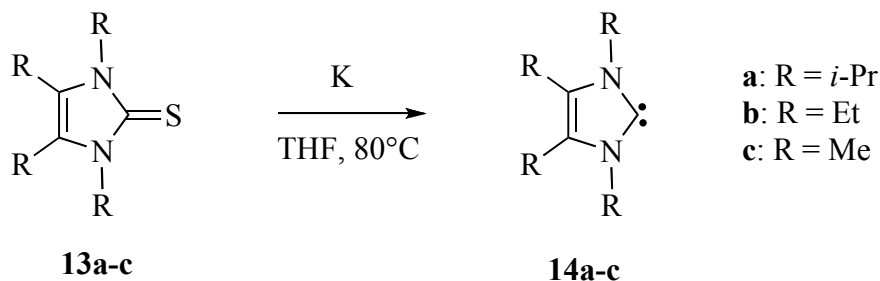


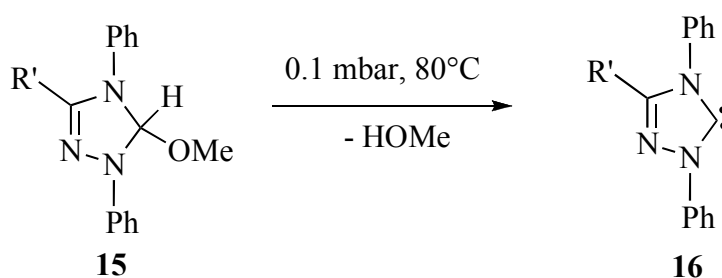
Figure 1.5: Examples of different carbenes isolated by Herrmann at al.

In 1993, Kuhn and co-workers synthesized alkyl-substituted N-heterocyclic carbenes **14a-c** by reduction of imidazol-2(3H)-thiones (**13a-c**) with potassium in refluxing THF.⁹ Scheme 1.4 shows an example of this procedure.



Scheme 1.4: Kuhn reaction.

Enders et al. reported in 1995 that the 1,2,4-triazol-5-ylidene (**16**) could be obtained in quantitative yield from the corresponding 5-methoxy-1,3,4-triphenyl-4,5-dihydro-1H-1,2,4-triazole (**15**) by thermal elimination (80°C) of methanol in vacuum (0.1 mbar), as depicted in Scheme 1.5. Compound **16** became the first commercially available carbene.¹⁰



Scheme 1.5: The synthesis of the first commercially available carbene.

Cyclic and acyclic aminocarbenes have been isolated using these methods: imidazolin-2-ylidenes (**17**), tetrahydropyrimid-2-ylidene (**18**), imidazol-2-ylidenes (**19**), 1,2,4-triazol-5-ylidenes (**20**), 1,3-thiazol-2-ylidenes (**21**) as well as acyclic diamino- (**22**), aminoxy- (**23**) and aminothiocarbenes (**24**).¹¹ These compounds are depicted in Figure 1.6.

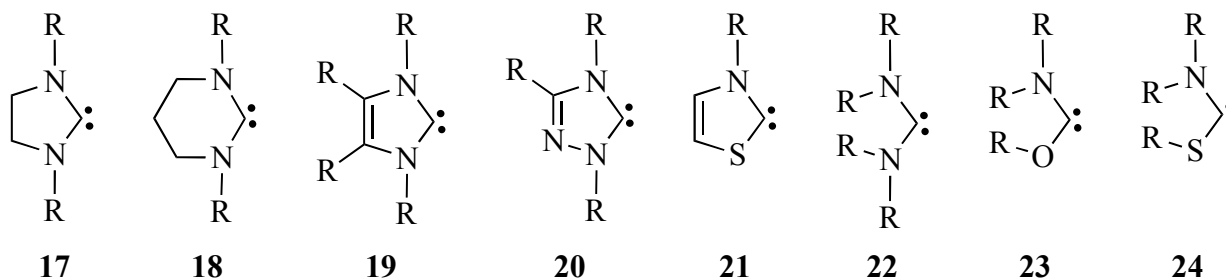


Figure 1.6: Aminocarbenes **17** – **24**.

Note that in all these carbenes the substituents are π -donors, one of which is always an amino group. This is mostly due to the higher stabilizing effect (due to superior π -donor ability) of amino versus alkoxy groups and also due to the higher steric shielding.

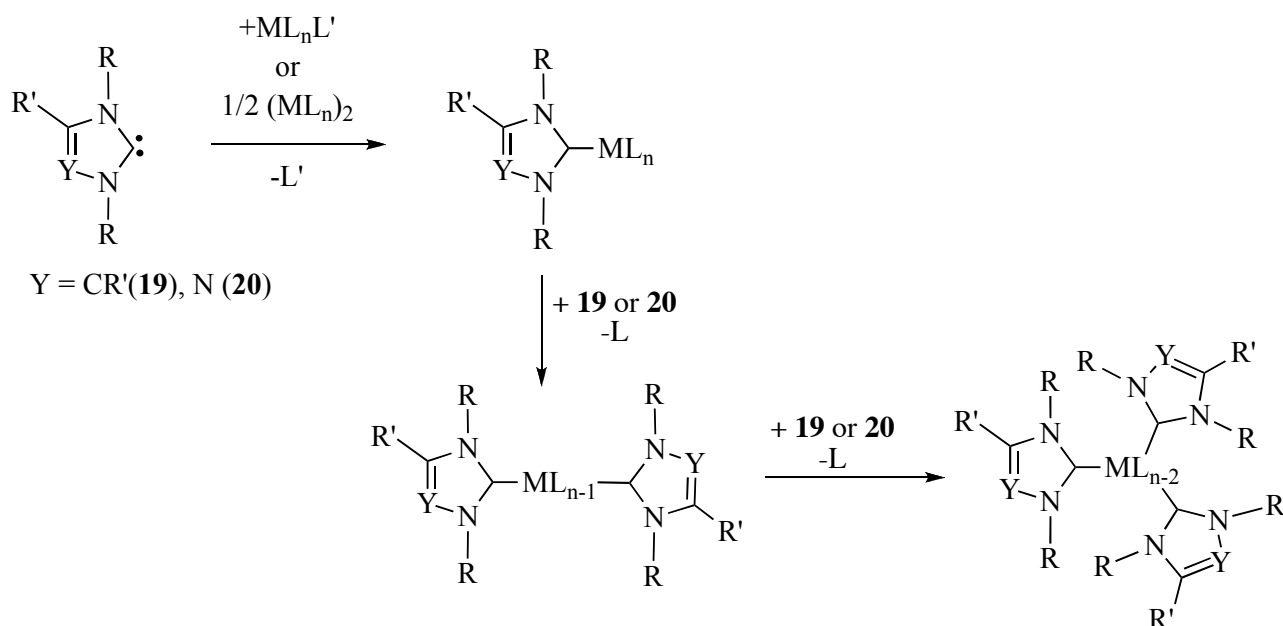
In ^{13}C NMR spectroscopy the carbene carbon of **17** – **18** appears at higher frequencies $\delta = 205 - 300$ ppm with respect to the corresponding salts at $\delta = 135 - 180$ ppm. The X-ray diffraction studies confirm the expected bent geometry (singlet carbenes), the observed bond angles are between $100 - 110^\circ$. The nitrogen atoms are in a planar environment and the N–C bond lengths are rather short ($1.32 - 1.37 \text{ \AA}$). This last feature indicates that the C–N bonds have partial double bond character due to the donation of the nitrogen lone pairs to the vacant orbital at the central carbene carbon center. This is confirmed by the sizable energy barriers for the rotation around the N–C bond for compounds of the type **22** and **23** measured by variable temperature NMR spectroscopy.

1.1.2 Carbene – Transition Metal Complexes

1.1.2.1 Synthesis

After the isolation of the first stable free carbenes by Arduengo and the development of new synthetic protocols for their preparation, the coordination chemistry of NHC-carbenes became a new research field to explore. Different strategies for the preparation of transition metal complexes of N-heterocyclic carbenes (NHCs) have been developed and they will be briefly discussed in this section (Schemes 1.6 – 1.11).

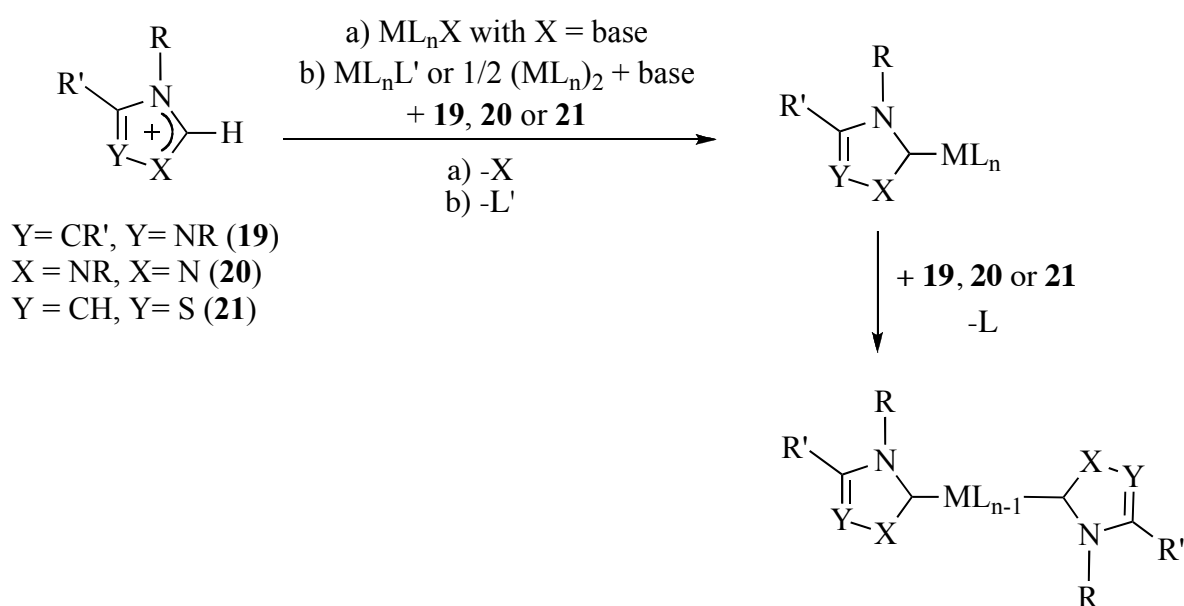
Organometallic precursors of type $\text{ML}_n\text{L}'$, bearing two-electron donor ligands, such as tetrahydrofuran, carbon monoxide, nitriles, phosphines, or pyridine, readily react with isolated free carbenes like imidazol-2-ylidenes (**19**) and triazol-2-ylidenes (**20**) as depicted in Figure I.6.¹² In the resulting complexes one of the ligands has been displaced by the carbene. In some cases, further ligand substitution can occur to give bis- and triscarbene complexes.¹³ In the case of carbonyl complexes $\text{M}(\text{CO})_n$ ($\text{M} = \text{Cr}, \text{Mo}, \text{W}, \text{Fe}, \text{Ni}$),¹² further substitution can require photolytic conditions.¹³ Dinuclear organometallic fragments of type $(\text{ML}_n)_2$ having bridging groups, like halogens or acetate groups, are split by N-heterocyclic carbenes to give the corresponding mononuclear complexes in excellent yields (Scheme 1.6).⁷



Scheme 1.6: Ligands substitution reactions.

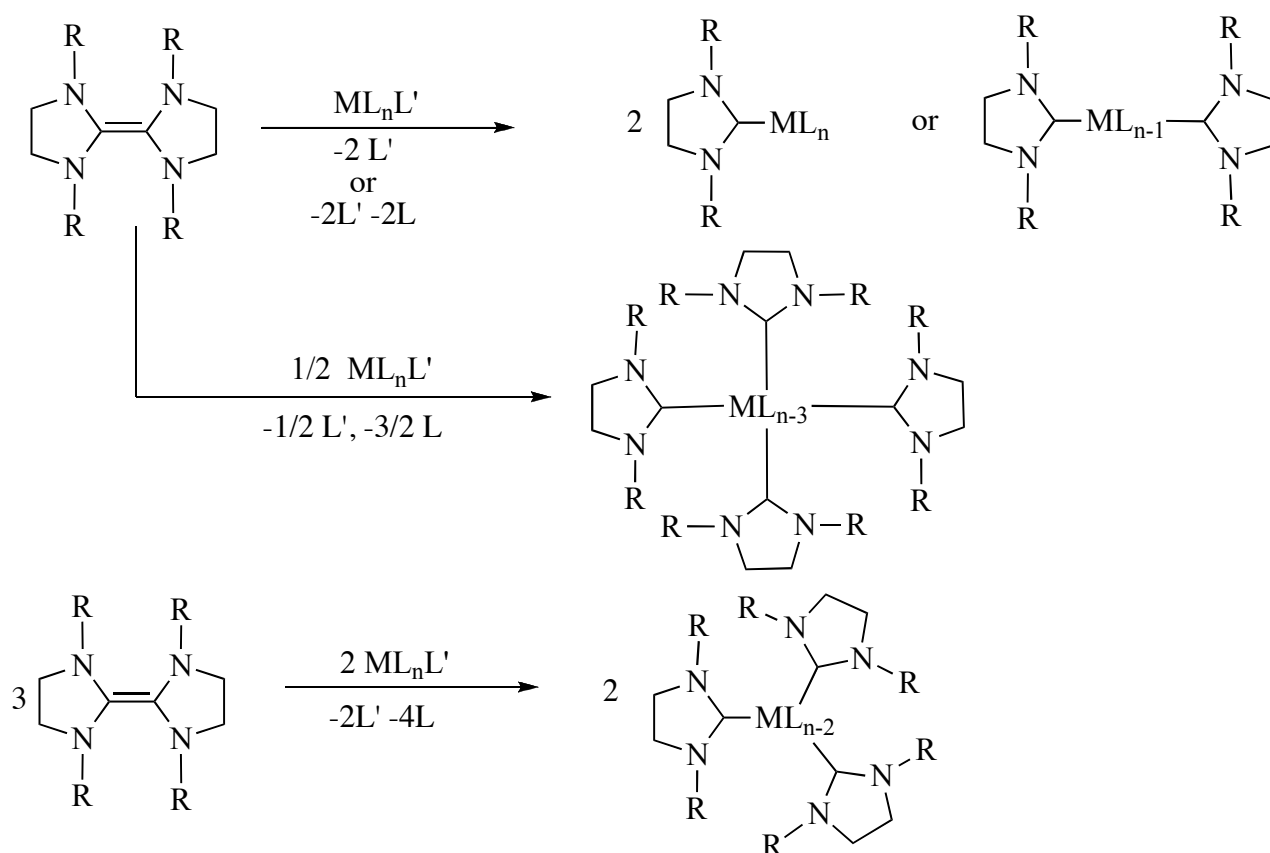
Scheme 1.7 shows a more general and widespread method, which was first discovered by Öfele in 1968.¹⁴ This is the direct deprotonation of an azolium salt in the presence of the appropriate organometallic fragment ML_nX or ML_nL' . When a complex of type ML_nX is employed, where X is a basic ligand such as hydride,¹⁴ alkoxide,¹⁵ or acetate,¹⁶ the use of an external base is not necessary. In fact, the ligand will affect the deprotonation of the imidazolium salt.

When compounds of type ML_nL' or $(ML_n)_2$ are employed the use of an organic base, such as triethylamine,¹⁷ is mandatory, as shown in Scheme 1.7.



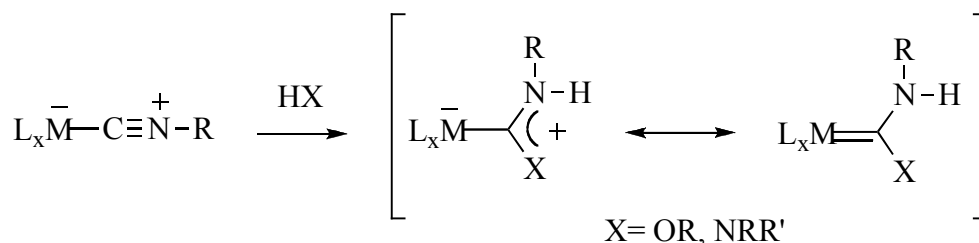
Scheme 1.7: Deprotonation of azolium salts prior to metallation.

Mono-, bis-, tris-, and even tetrakis-carbene complexes of various metals have been prepared by reaction of compounds of type ML_nL' or $(ML_n)_2$ with electron-rich olefins (Scheme 1.8).¹⁸



Scheme 1.8: Reaction of electron-rich olefin with organometallic fragments.

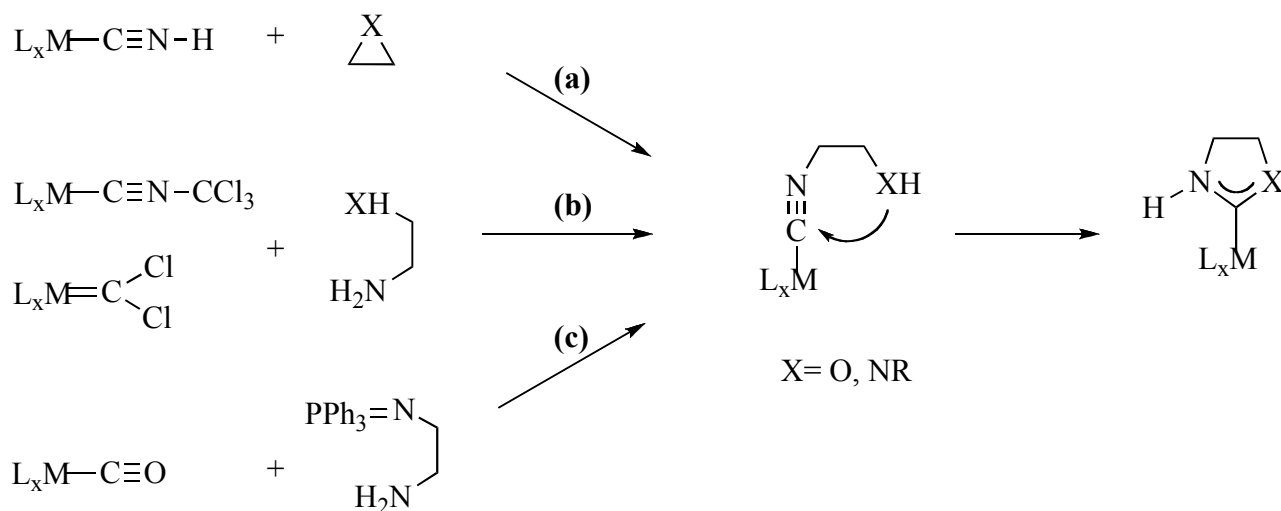
The inter- or intramolecular addition of N-nucleophiles to coordinated isocyanides is one of the most general synthetic approaches to diaminocarbene transition metal complexes (Scheme 1.9).¹⁹ In fact, isocyanides coordinated to metal centers can undergo nucleophilic attack at the terminal carbon atom by a variety of reagents.²⁰ In particular, with protic nucleophiles, such as alcohols and primary and secondary amines, the reaction yields metal-carbene complexes (Scheme 1.9).



Scheme 1.9: Nucleophilic addition of alcohols or imine to coordinated isocyanides.

The addition of nucleophiles HX to coordinated isocyanides usually leads to the formation of acyclic carbene complexes. On the other hand, the employment of functional isocyanides, which

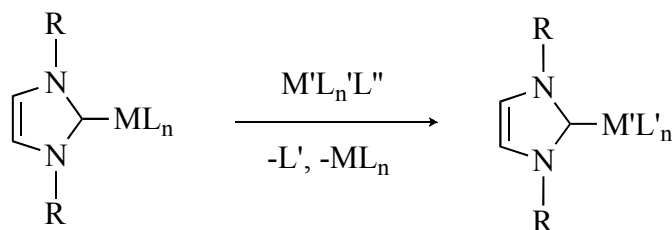
contain both the isocyanide group and the nucleophile in the same molecule, gives access to complexes with heterocyclic carbenes through an intramolecular 1,2 addition across the CN triple bond. Various synthetic methods have been developed to generate such functional aliphatic isocyanides at the metal center. Selected examples are: (a) the reaction of cyanometal acids with epoxides²¹ and aziridines,²² (b) the reaction of ethylenediamines or ethanolamine with trichloromethyl isocyanides²³ or dichlorocarbene complexes²⁴ and (c) the reaction of metal carbonyls with aminophosphinimines²⁵ (Scheme 1.10).



Scheme 1.10: Formation of carbene complexes from coordinated β -functional isocyanides.

Alternatively, Fehlhammer et al. have introduced readily available and stable 2-hydroxylalkyl isocyanides such as $\text{CNCH}_2\text{CH}_2\text{OH}$, in which the nucleophile and the isocyano group are already linked before coordination to the metal center. When suitably activated (by coordination to a transition metal) these ligands spontaneously cyclize to form oxazol-2-ylidenes complexes.²⁶

Carbene transfer reactions between transition metals are another option (Scheme 1.11).²⁷



Scheme 1.11: Transmetalation.

In particular the procedure developed by Lin et al. allows an easy access to N-heterocyclic carbenes complexes of silver. These compounds are subsequently employed for the synthesis of other metal-carbene systems. Transmetalation reactions using silver carbenes have been reported

for a variety of transition metals: Au(I), Cu(I), Cu(II), Ni(II), Pd(II), Pt(II), Rh(I), Rh(III), Ir(I), Ir(III), Ru(II), Ru(III) and Ru(IV). Recent reviews about silver N-heterocyclic carbenes have been published by Arnold,²⁸ Lin and Vasam.²⁹

1.1.2.2 Electronic Properties

While in the previous chapter the preparation of carbene metal complexes has been discussed, in the following one a brief description of the classification of metal-carbene bonds will be given.

Two extreme types of carbene complexes can be distinguished: the Fischer and the Schrock type, depending on the nature of the formal metal-carbon double bond (Figure 1.7a-b).

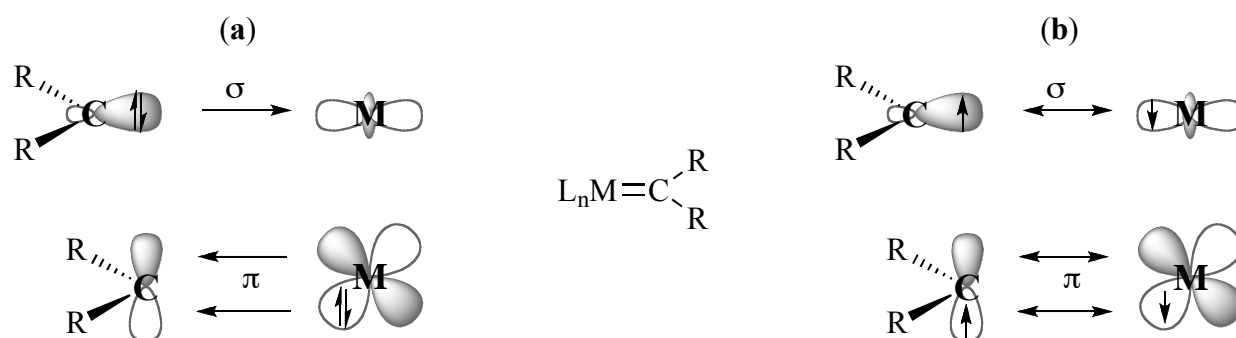


Figure 1.7: Representation of (a) Fischer carbene complexes and (b) Schrock carbene complexes.

In the Fischer carbene complexes, the carbene moiety serves as neutral 2-electron donor and coordinates to a metal center *via* the lone pair. The empty *p* orbital on the carbon is a weak acceptor for π -back donation from the metal (Figure 1.7a). In sum, a formally positive charge is build up on the carbon of the carbene (the back donation does not compensate the donation).

In contrast, the CR_2 group in the Schrock carbenes (Figure 1.7b) forms essentially two covalent bonds with the metal. Formally, the bond can be considered as the interaction of a triplet carbene with a metal fragment with at least two unpaired electrons (Chapter 1.1.1). Consequently, in a Schrock carbene complex the CR_2 group acts as an X_2 ligand.

Complexes containing a Fischer carbene are generally formed with low-oxidation state, late transition metals having π -acceptor ligands and the carbenes bearing at least a π -donor group, whereas complexes containing a Schrock carbene are usually formed with early transition metals in a high oxidation state having no π -acceptor ligands and carbene ligands bearing non- π -donor groups such as alkyl substituents.

N-heterocyclic carbene complexes do not really fit into this oversimplified picture. On the one hand, they could be classified as Fischer type carbene complexes, due to the presence of two

π -donor substituents. However, in practice N-heterocyclic carbenes (NHCs) serve as excellent σ -donors with little π -back bonding capacity³⁰ and as such bind extremely well to low-valent and high valent metal centers.³¹

1.1.2.3 Catalytic Properties

Due to their remarkable stability, NHC complexes became very popular as catalysts for various organic reactions. Their properties have been investigated and compared to those of commonly used phosphine complexes. Some examples of asymmetric catalyses will be discussed below as well.

Olefin metathesis

The ruthenium metathesis catalyst developed by Grubbs and co-workers, for which the Nobel Prize was awarded, is, without any doubts, the most important example of application of N-heterocyclic carbene complexes in catalysis. Significant improvements in terms of catalytic stability, activity and substrate range³² have been achieved by replacement of one of the two tricyclohexylphosphine ligands in the “first generation” of Grubbs catalyst **25** with bulky carbenes like IMes (1,3-dimesityl-4,5-imidazol-2-ylidene) (**27**) and SIMes (1,3-dimesityl-4,5-dihydroimidazol-2-ylidene, SIMes) (**28**), as shown in Figure 1.8.

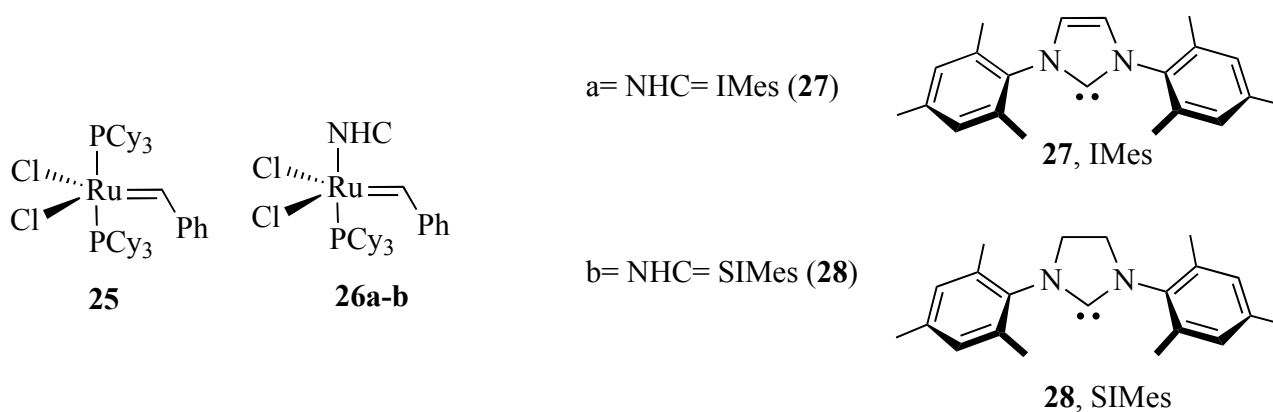


Figure 1.8: Grubbs metathesis catalysts.

Early mechanistic studies with compound **25** established that phosphine dissociation is a critical step. It has been demonstrated that catalysts containing sterically bulky electron-donating phosphine ligands display the highest catalytic activity.³³ This trend was explained on the basis of the increased *trans*-effect of larger and more basic phosphines, which was believed to accelerate dissociation of the second PR_3 ligand.

The “second generation” ruthenium olefin metathesis catalysts **26a-b** exhibit dramatically increased reactivity, due to the above mentioned electronic properties of the NHCs, which are

known to be superior donor ligands relative to trialkylphosphines. This characteristic is reflected in the increased labilization of the phosphine due to the greater *trans*-effect of the NHCs.

Coupling Reactions

NHC ligands have been used for the preparation of efficient palladium catalysts employed for C-C bond forming reactions. Among them the Heck reaction,³⁴ the Suzuki-Miyaura cross-coupling³⁵ and the Buchwald-Hartwig amination.³⁶

These palladium-mediated processes have been shown to proceed through a d^{10} -Pd(0) center. Hartwig, Cloke and Nolan suggested dissociation of one NHC to generate a PdL fragment, which then undergoes oxidative addition of RX (X= halide). A reaction pathway similar to that proposed in analogous phosphine systems.³⁷

Hydrogenation

RhCl(PPh₃)₃ (Wilkinson's catalysts) and [Ir(cod)(py)(PCy₃)]PF₆ (Crabtree's catalyst) (**29**) depicted in Figure 1.11 are the most widely used catalysts for homogeneous hydrogenation.

The Crabtree's catalyst shows remarkable catalytic activity but it has been shown to undergo decomposition reactions. To increase the catalytic activity, Nolan et al. synthesized complexes of type [(Ir(cod)(py)(NHC)]PF₆ **30**, **31** and **32** (Figure 1.9) by replacement of the phosphine ligand by a NHC carbene. The complexes show high activity (but still lower with respect to **29**) in the hydrogenation of C=C, C=O and N=O double bonds.³⁸

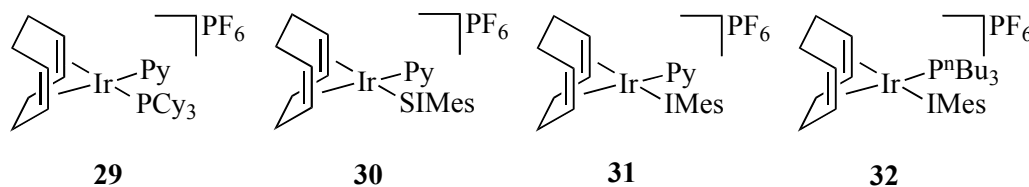


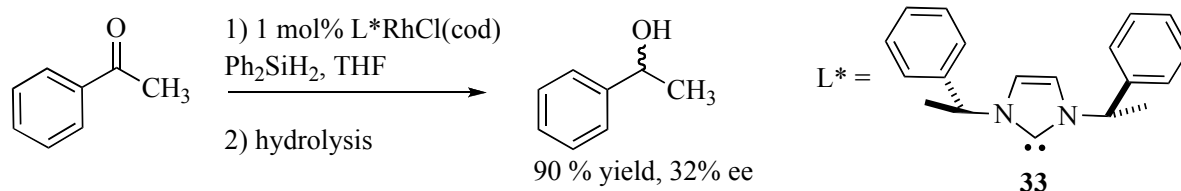
Figure 1.9: Hydrogenation catalysts.

Chiral N-Heterocyclic carbenes in asymmetric catalysis³⁹

The use of chiral NHC-metal complexes has been also explored in asymmetric catalysis. Enantiomerically pure complexes of N-heterocyclic carbenes can be obtained by (i) chiral substituents at the nitrogen atoms; (ii) a chiral ring framework; (iii) an element of axial chirality; (iv) an element of planar chirality; (v) a chiral backbone or alternatively; (vi) an oxazoline unit.

(i) The easiest and most direct way to produce chiral NHC ligands is indeed the design of systems in which the N-heterocyclic carbene bears chiral N-substituents (on the C-atoms adjacent to the nitrogen atoms in 1 and 3 positions within the ring). In 1996 Herrmann and Enders published the synthesis of the first chiral NHC. The synthetic strategy exploited the use of an enantiopure

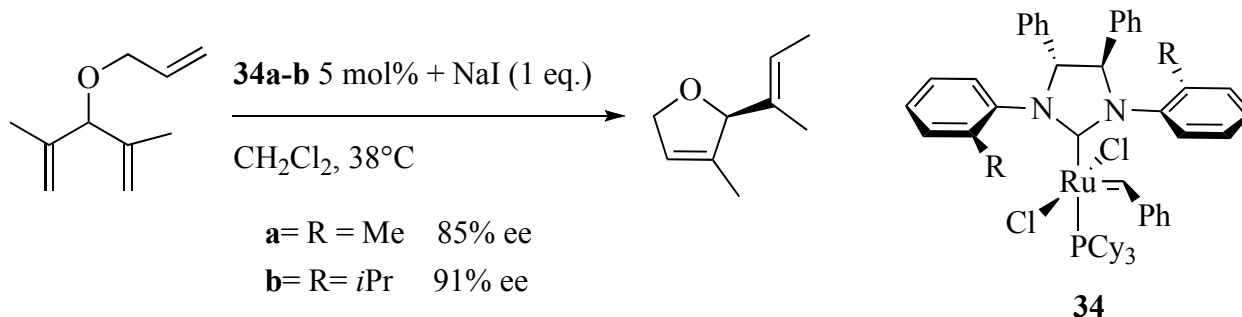
chiral amine.⁴⁰ This was converted to the imidazolium salt using the procedure already published by Arduengo.⁴¹ The chiral rhodium (I) complex obtained by reaction with ligand **33** was tested in the hydrosilylation of acetophenone (Scheme 1.12).



Scheme 1.12: Asymmetric hydrosilylation using the first chiral NHC.

The new catalyst displayed good activity but low stereoselectivity (32% ee), probably due to rapid internal rotation of the stereogenic substituents around the C-N axis and the flexibility of the substituents.

(ii) A second possibility to create stereogenic carbenes is to introduce a chiral backbone in the imidazolyl ring. The imidazolium salts are normally prepared from C₂-symmetric chiral vicinal diamines. The strategy has been used by Grubbs and co-workers and the resulting chiral ruthenium complexes **34a-b** have been tested in the stereoselective ring closing metathesis of olefins (Scheme 1.13).⁴²

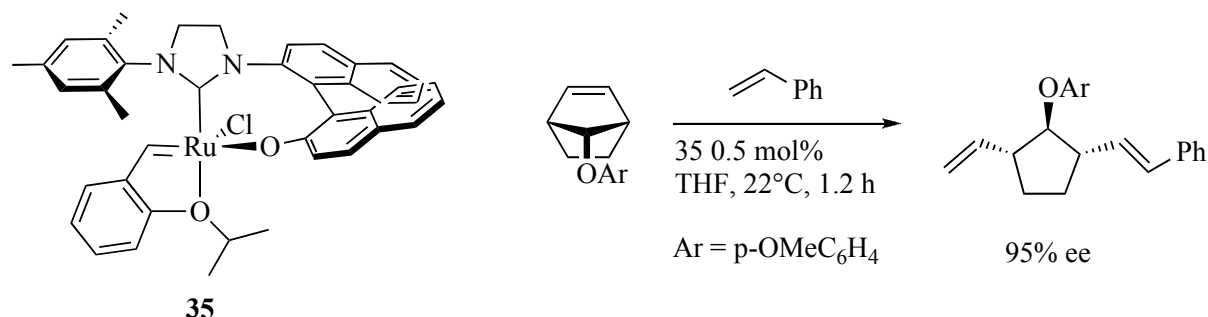


Scheme 1.13: Asymmetric ring closing metathesis.

Higher enantioselectivities were detected for ligands containing a 1,2-diphenylethylenediamine backbone than a 1,2-diaminocyclohexane skeleton. *Ortho*-monosubstituted N-aryl substituents in the carbene ligand lead to a greater selectivity than the more symmetrically mesityl-substituted derivative. This could be explained by the steric repulsion between the phenyl groups of the backbone and the *o*-aryl substituents on the N-substituent. The anti-conformation may transfer the chiral information to the active site of the catalyst more efficiently.

(iii) In 2002 Hoveyda et al. reported the synthesis of a novel chiral anionic bidentate carbene ligand combining an NHC unit with a phenolato donor and its application in asymmetric olefin

methathesis (Scheme 1.14).⁴³ Compound **35** gave interesting results in the asymmetric ring opening cross-metathesis.



Scheme 1.14: Ru-Catalyzed cross-metathesis catalysis.

(iv) The first example of chiral NHC having an element or planar chirality was reported by Bolm et al. at the beginning of 2002.⁴⁴ Later on, Togni et al. reported the synthesis of C2-chiral carbene ligand, using Ugi's chiral 1-ferrocenylethylamine as starting material, containing an element of planar chirality and a proper linker between the ferrocene and the imidazolyl unit.⁴⁵ Ugi's ferrocenylethylamine has been used for the synthesis of the chiral C2-symmetric tridentate PCP ligand **37** (related to the previous developed triphosphine Pigiphos **36**)⁴⁶ more recently published by the same group (Figure 1.10).⁴⁷ This phosphine-carbene ligand has been used in the nickel catalyzed hydroamination of acrylonitriles derivatives.⁴⁸

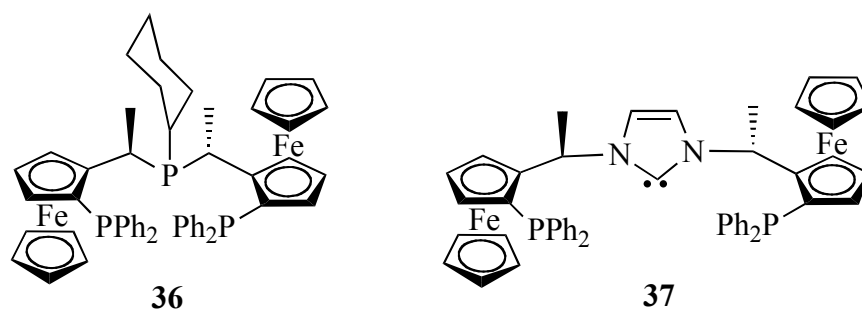
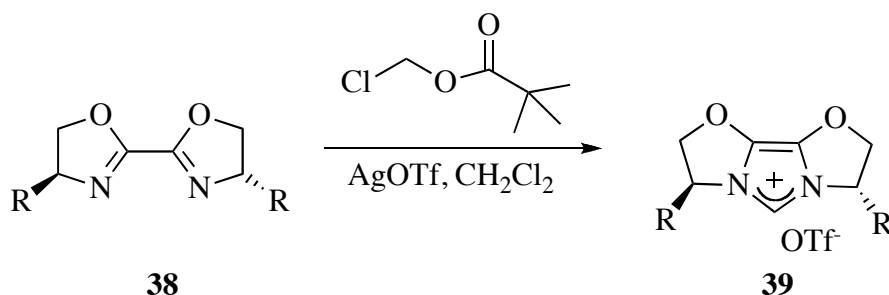


Figure 1.10: Togni's tridentate PCP ligand **37** and the Pigiphos **36**.

(v) The Burgess's group⁴⁹ and the Douthwaite's group⁵⁰ have focused their research on the synthesis of NHC carbenes linked by a chiral *trans*-cyclohexanediamine ligand. Unfortunately the performance in catalytic reactions is poor.

(vi) In 1998, Herrmann et al. reported the synthesis of the first carbene containing an oxazoline unit. More recently, in 2002, Glorius et al. reported the synthesis of the imidazolium salt **39** by

cyclizing the corresponding bisoxazoline **38** (Scheme 1.15).⁵¹ Various ligands (with different R groups) have been successfully used for palladium catalyzed Suzuki cross-coupling reactions.⁵²



Scheme 1.15: Synthesis of imidazolium salts from the corresponding bisoxazoline.

1.1.3 Special Reactivity of NHC-Complexes

The study of decomposition reactions of N-heterocyclic carbene metal complexes has always received great attention from the scientific community, first of all because of the extensive use of N-heterocyclic carbene ligands in catalysis as described above, secondly because degradation reactions are detrimental to the catalytic system. Several systems have been reported where the carbene ligands do not act as spectator ligands but undergo side reactions. Some of the most important examples from the recent literature will be discussed below, with a particular focus on reactions which are relevant for our studies.

Abnormal bindings motifs and rearrangement

The groups of Nolan⁵³ and Crabtree⁵⁴ reported iridium and palladium complexes bearing NHC ligands in abnormal binding motifs – namely C-4(5) binding (Figure 1.11a-b). The C-4(5) binding mode was previously considered as an unlike binding possibility because free carbene isolated by Arduengo et al. always adopted a C-2 binding mode, when complexed to a metal center. For compounds **40** and **41**, it is thought that C-4(5) binding is favored as a result of lower steric congestion around the metal center.

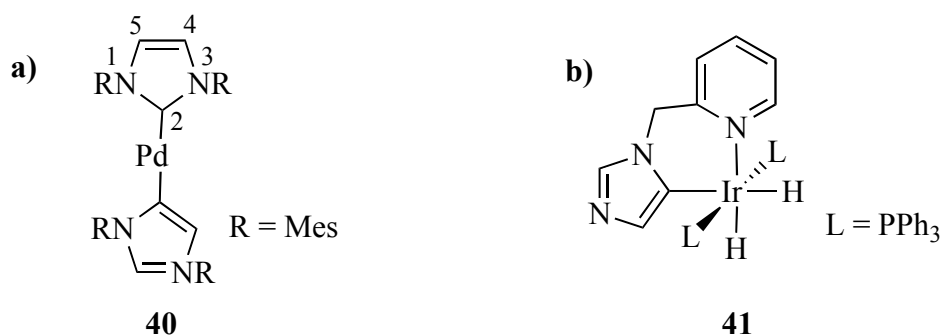
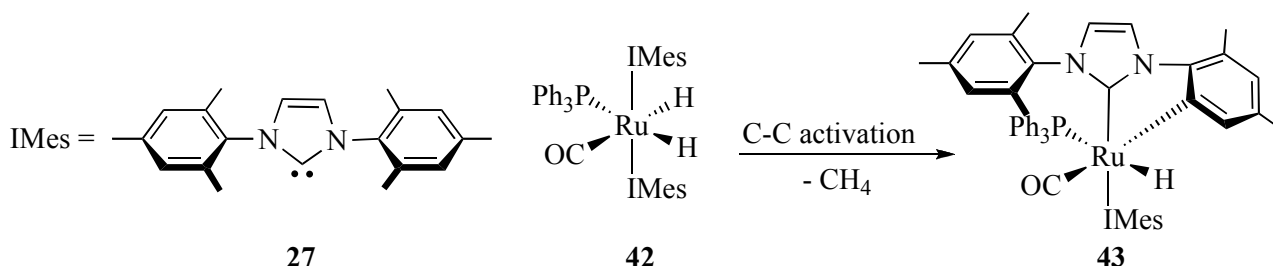


Figure 1.11: Abnormal binding modes for NHC ligands reported by Nolan (a) and Crabtree (b).

Rearrangement of N-heterocycle carbenes involving heterocycle cleavage has been documented by Waltman et al.⁵⁵ and the insertion of a carbene into a platinum-olefin bond has been reported recently by Fantasia et al.⁵⁶

C-C activation

In 2002, Whittlesey et al. reported an example of C-C activation.⁵⁷ Scheme 1.16 shows that thermolysis of a benzene solution of **42** afforded the C-C insertion product **43**, with release of one equivalent of methane after 16 days. The X-ray structure obtained for complex **43** shows that the ruthenium atom has inserted into one of the *ortho* Ar-CH₃ bonds of the IMes ligand (**27**) to give a new Ru-C bond as an integral part of a five-member metallacycle.

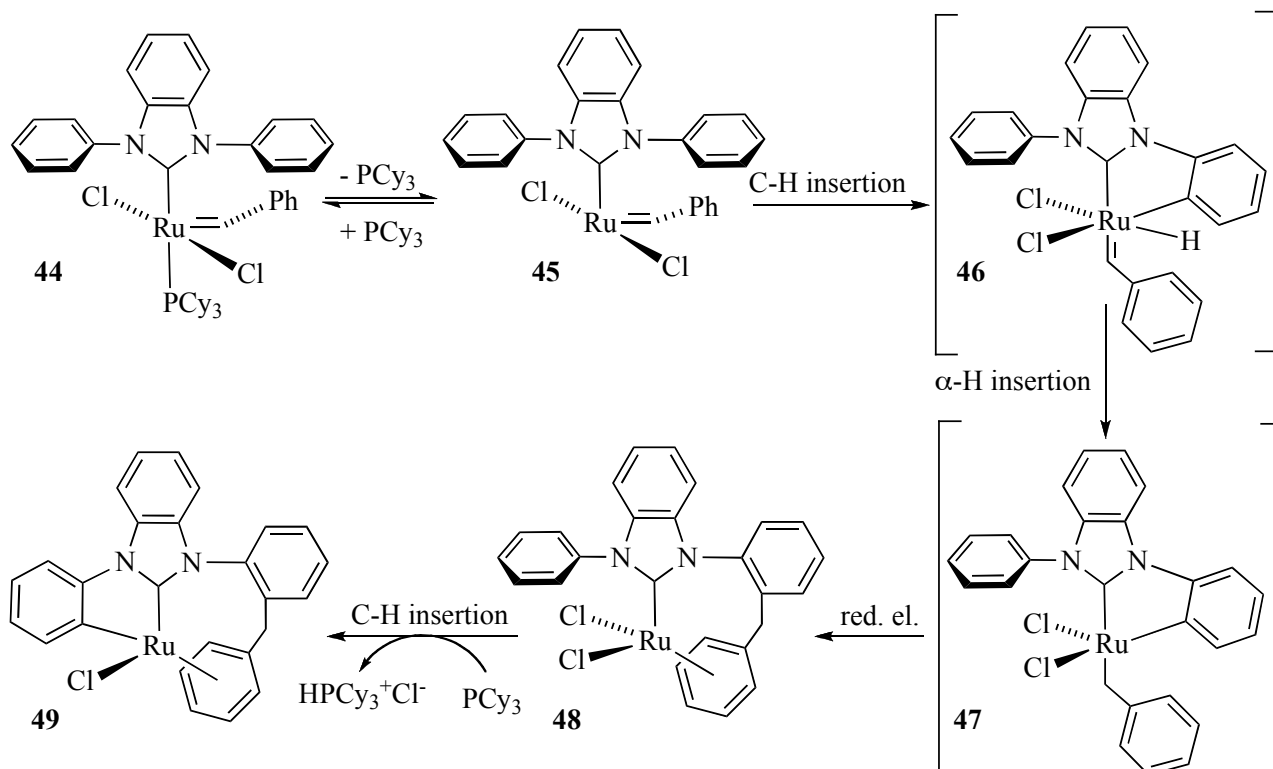


Scheme 1.16: Example of C-C activation by Whittlesey et al.

C-H activation

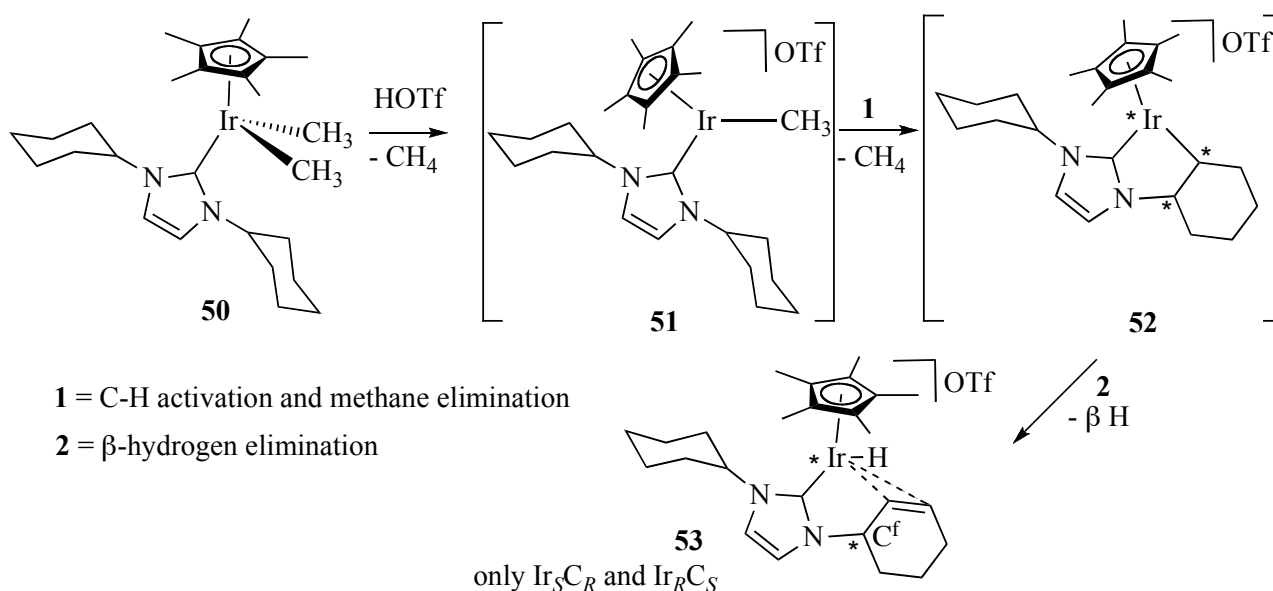
Very recently Grubbs et al. reported the double C-H activation⁵⁸ of an N-heterocyclic carbene ligand in the ruthenium olefin metathesis catalyst **44**.

One plausible mechanism for the decomposition of **44** has been hypothesized by Grubbs and it is presented in Scheme 1.17. Following phosphine dissociation, which is the initial step in ruthenium catalyzed olefin metathesis (see chapter 1.1.2.3), ruthenium hydride **46** may be formed by oxidative addition of an *ortho* C-H bond of an N-phenyl group to the ruthenium center. The resulting hydride then inserts at the α -carbon atom of the benzyldiene ligand to generate complex **47**. Formation of **48** could then occur by reductive elimination between the metallate phenyl carbon atom and the α -carbon atom of benzyldiene. Finally, C-H insertion together with the PCy₃-mediated elimination of HCl could generate complex **49**. Intermediate complexes **46** – **47** are only postulated and have not been observed by spectroscopic methods.



Scheme 1.17: Proposed mechanism for the double CH-activation for the metathesis catalyst **44**.

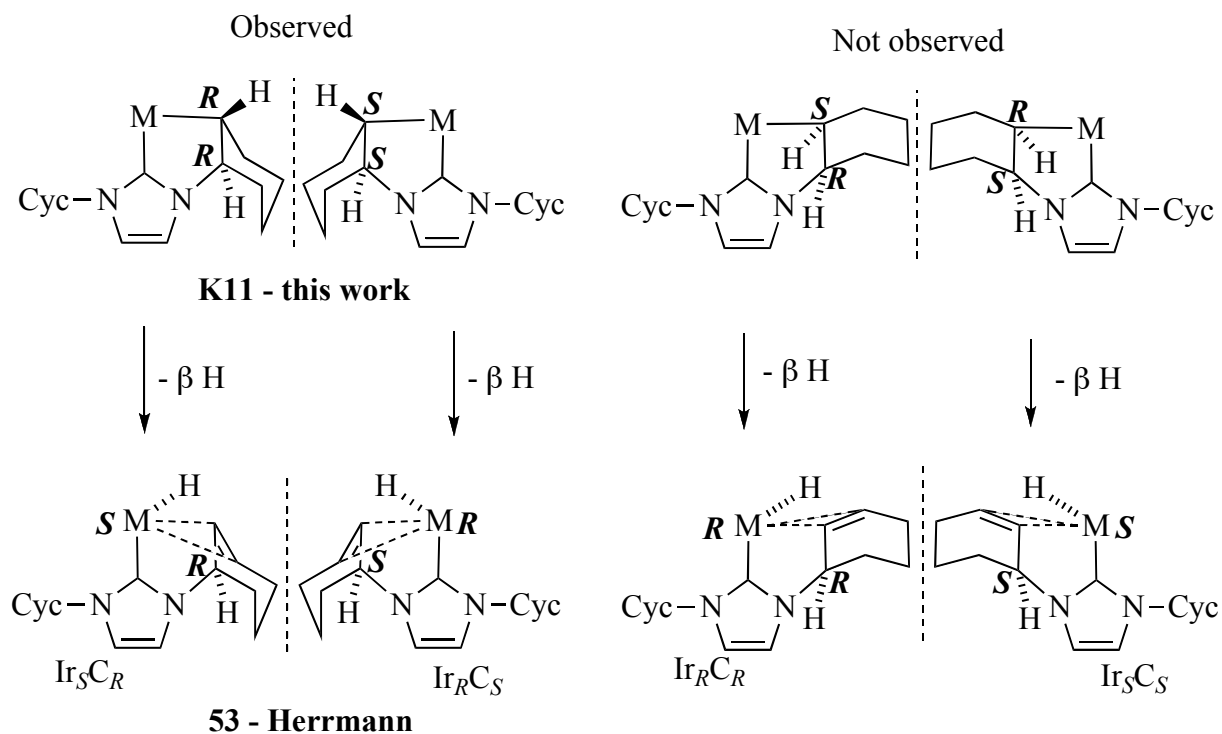
A C-H activation of the cyclohexyl moiety on a NHC ligand was already observed by W.A. Herrmann (Scheme 1.18).⁵⁹



Scheme 1.18: Formation of **53** by intramolecular C-H activation reported by Herrmann et al.

Herrmann et al. assumed that the cationic 16 electrons intermediate **51**, having a vacant coordination site at the metal centre, is required for the cyclometallation, a statement that is in

agreement with a previous suggestion of Bergman et al.⁶⁰ The cyclometallation/ β -hydrogen elimination results in the formation of stereogenic centers [(*) in Scheme 1.18] at the iridium and at the C^f carbon. Four isomers constituting two diastereomeric pairs of enantiomers could occur. Based on the ¹H NMR and the X-ray structural data for **53**, Herrmann et al. concluded that only the two enantiomers Ir_SC_R and Ir_RC_S are formed as depicted in Scheme 1.19.



Scheme 1.19: Stereochemistry of **53** (Herrmann) and **K11** (our work, see chapter 1.5.1).

The C-H activation of an *N*-*iso*-propyl group of a NHC ligand has been already observed by Yamaguchi et al. (Figure 1.12). A crystal structure of the product complex **54** is also available. The ¹H-NMR spectrum of **54** in C₆D₆ showed signals due to nonequivalent geminal protons on the carbon cyclometallate to iridium center at 3.95 and 2.26 ppm with coupling constant ²J_{HH} of 10 Hz, while the ¹³C resonance attributed to the cyclometallate methylene carbon is observed at 18.5 ppm.

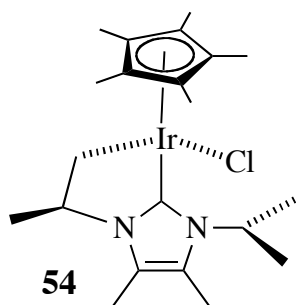


Figure 1.12: Example reported by Yamaguchi et al.

1.2 Aims

The purpose of this thesis was to continue and improve the research work started by T. Büttner. In his dissertation work Büttner describes the hydrogenation catalyst $[\text{RhCl}(\text{trop}_2\text{NH})\text{PPh}_3]$ (**K1**) (Scheme 1.20), where trop_2NH stands for bis(5-H-dibenzo[a,d]cyclohepten-5-yl)-amine, trivially called bistropamine.⁶¹ Deprotonation of **K1** leads to the neutral rhodium amide $[\text{Rh}(\text{trop}_2\text{N})\text{PPh}_3]$ (**K2**). This compound is able to heterolytically cleave dihydrogen to yield the rhodium-hydride amino complex $[\text{Rh}(\text{H})(\text{trop}_2\text{NH})]$. Both the isolated amide **K2** and the hydride complexes have been successfully used in catalytic hydrogenation reactions.⁶² It has been demonstrated that the active hydride species bears the hydrogen in equatorial position.

The main problems, already described in Büttner's thesis, of the above-mentioned system are the lability of the phosphine in axial position of **K2** and the isomerization of the reactive intermediate hydride $[\text{Rh}(\text{H})(\text{trop}_2\text{NH})\text{PPh}_3]$ to an air-stable and inactive complex in which the hydride adopts the apical position. The main aim of this thesis was to overcome these problems.

As already described in the introduction chapter, N-heterocyclic carbene ligands are capable of replacing phosphines. Carbenes have several advantages over the commonly utilized latter ligands, such as high thermal stability and resistance to dissociation from the metal center. In particular, results reported by Grubbs et al.^{32, 33} for the ruthenium metathesis catalysts and by Nolan et al.³⁸ for coupling and hydrogenation catalysts clearly show that a dramatic increase in reactivity can be achieved by replacement of the phosphine ligand by a carbene.

These features stimulated us to replace the phosphine ligand with a NHC ligand in the hydrogenation catalyst **K1**. Therefore, the first aim of the work presented in this chapter was the development of a protocol for the synthesis of novel chiral and achiral rhodium N-heterocyclic carbene complexes with bistropamine as co-ligand. We were interested in the study of the geometrical structures of the NHC complexes in comparison with the trialkylphosphine analogues, as well. The question to be addressed was whether or not complexes of general formula $[\text{RhX}(\text{trop}_2\text{NH})(\text{NHC})]$ (where X is a suitable coordinating counter anion) yield trigonal bipyramidal structures, similarly to the complexes reported by Büttner. In particular, we were intrigued by the possibility to synthesize a saw-horse type complex: $[\text{Rh}(\text{trop}_2\text{NH})(\text{NHC})]\text{X}$ (where X is a suitable non-coordinating counter anion). A further objective was to investigate the catalytic performance of NHC-rhodium bistropamine-based systems towards the catalytic transfer hydrogenation of simple ketones. In view of the increased catalytic activity of many NHC-complexes and specifically their stability, this seemed to be a promising approach to obtain high-performance $\text{Rh}(\text{trop}_2\text{NH})$ -complexes.

1.3 General Synthesis of [RhX(trop₂NH)(NHC)]

As already mentioned in Chapter 1.2, the first aim of this thesis was to develop a protocol for the synthesis of new chiral and achiral NHC-carbene rhodium complexes of Trop₂NH. Figure 1.13 shows the imidazolium salts used in the current study. The preparation of 1,3-dimethylimidazolium iodide⁶³ (IMe) (**55**) and 1,3-dicyclohexylimidazolium chloride⁶⁴ (ICy) (**56**) was performed using reported procedures. The enantiomerically pure imidazolium salts 1,3-bis-[(*S*)-1-phenyl-ethyl]imidazolium chloride⁸ (**57**) and the (*S*)-imidazolium triflate³⁶ (**58**) derived from the available (*S*)-valinol were prepared following Herrmann's and Glorius' protocols, respectively (the latter is shown in Scheme 1.15).

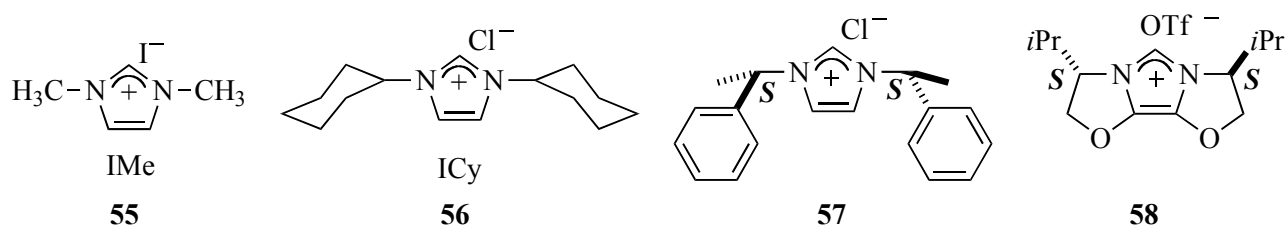
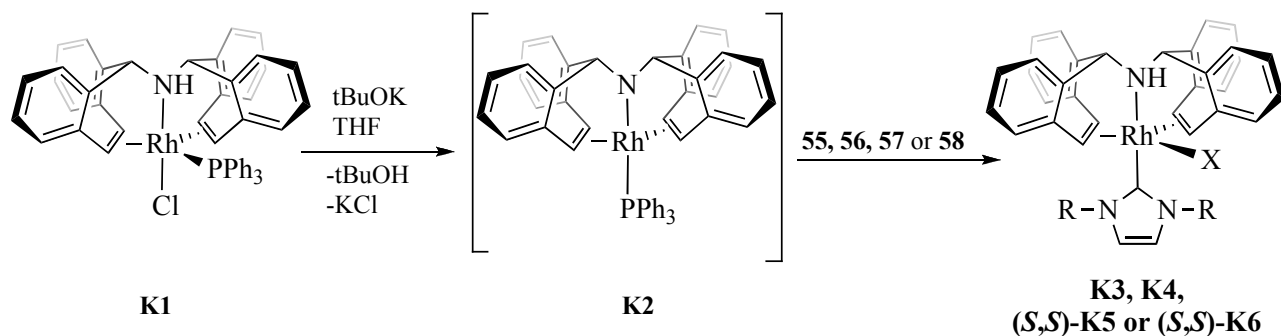


Figure 1.13: Imidazolium salts used in the present study.

For the synthesis of N-heterocyclic carbene rhodium(I) complexes of the general formula [RhX(trop₂NH)(NHC)] (where X is I, Cl or OTf, according to the imidazolium salt used) with bistropamine (trop₂NH) as co-ligand, two different methods have been tried (Chapter 1.1.2.1). The first method exploits a basic metal precursor such as [Rh(cod)(μ-OMe)]₂, as depicted in the general Scheme 1.7. The complexes [RhI(cod)(1,3-dimethylimidazol-2-ylidene)] and [RhCl(cod)(1,3-bis-(1-phenyl-ethyl)imidazol-2-ylidene)] were formed in good yields. However, the displacement of the cyclooctadiene ligand by the trop₂NH ligand did not occur. Even when the reaction was performed in the presence of dihydrogen, which in many cases leads to cyclooctane, cod could not be removed.

The successful synthetic route consists in the reaction of [Rh(trop₂N)(PPh₃)] (**K2**) – freshly prepared from [RhCl(trop₂NH)(PPh₃)] (**K1**) and stoichiometric amount potassium *tert*-butoxide in THF – with a slight excess of an imidazolium salt **55** – **58** (Figure 1.13). The rhodium-amide complex deprotonates the imidazolium salt, and the free carbene thus formed displaces the labile triphenylphosphine of complex **K2** to give the desired products in modest to good yields (up to 70%). These results demonstrate the superior binding properties of NHCs over phosphines as ligands.



Scheme 1.20: General procedure for the synthesis of [RhX(trop₂NH)(NHC)].

The reaction has many advantages over the other possible route, which utilizes the basic metal precursor [Rh(cod)(μ-OMe)]₂. The progress of the reaction between **K2** and the imidazolium salt can be easily followed by ³¹P NMR (from δ = 40.8 [d, ¹J_{RhP} = 124 Hz] to δ = -5.8 free PPh₃) and by the color change of the reaction mixture. The amide [Rh(trop₂N)(PPh₃)] is deep green and the NHC-rhodium complexes are red-orange. Figure 1.14 shows the isolated rhodium NHC-complexes **K3**, **K4**, **(S,S)-K5** and **(S,S)-K6**.

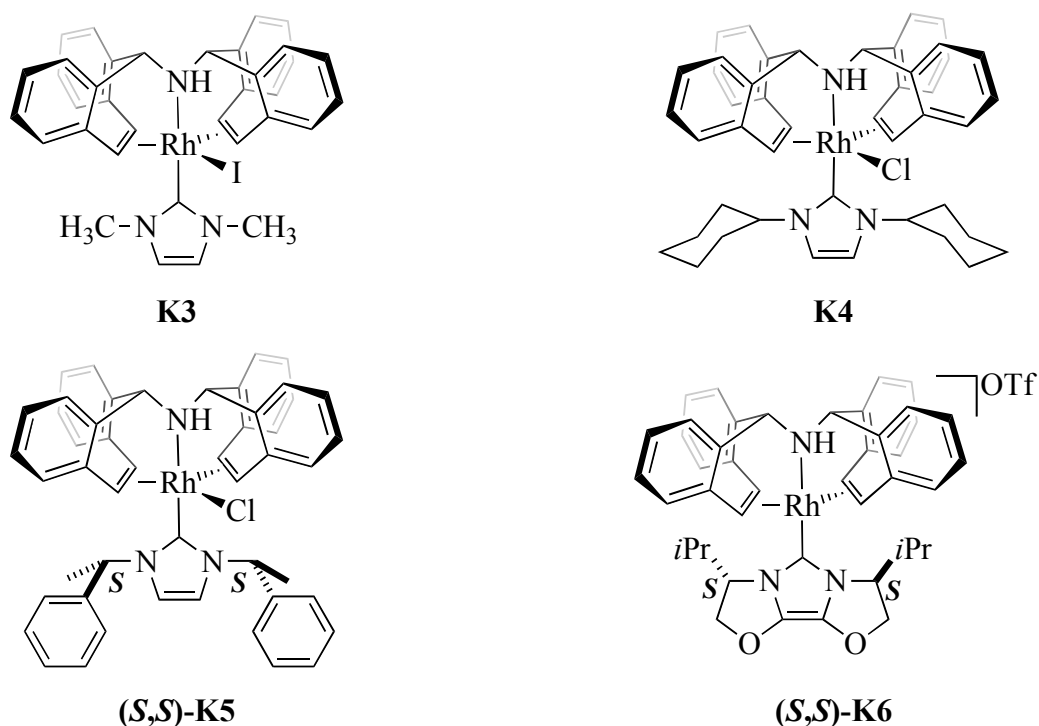


Figure 1.14: N-heterocyclic carbene rhodium(I) complexes synthesized in the present study.

1.3.1 Characterization of [RhI(trop₂NH)(IMe)] and [RhCl(trop₂NH)(ICy)]

Reaction of [RhCl(trop₂NH)(PPh₃)] (**K1**) with potassium *tert*-butoxide and one equivalent of 1,3-dimethylimidazolium iodine (**55**) allows the formation [RhI(trop₂NH)(1,3-dimethylimidazolin-2-ylidene)] (**K3**) in 40% yield. The product was further recrystallized from CH₂Cl₂ and *n*-hexane. No crystals of **K3** suitable for X-ray diffraction studies were obtained but the complex was characterized by NMR spectroscopy.

The ¹³C NMR spectrum of **K3** confirmed the coordination of the carbene moiety on the rhodium metal center. The carbon atom of the carbene displays a doublet at 168.1 ppm with a rhodium-carbon coupling constant of 50.0 Hz. Even though carbenes are strong σ-donor ligands, we never observed any displacement of the trop₂NH and the formation of bis-carbene rhodium complexes. The ¹³C NMR spectrum clearly indicates that the trop₂NH ligand is still bound to the metal center in a κ³-facial fashion. The bistropamine unit displays two doublets for the four olefinic carbons (with rhodium-carbon couplings of 14.3 Hz and 6.4 Hz) and one signal for the two benzylic ¹³C nuclei (Table 1.2). Furthermore, two different signals are displayed for the methyl substituents of the carbene at 40.4 and 45.8 ppm. This findings indicate that the carbene complexes have a trigonal bipyramidal - or saw-horse type structure - in which the ring plane of the carbene moiety is lying on the mirror plane running between the two trop units. One methyl is pointing towards the open side of the molecule, while the other one is pointing in the opposite direction approaching the benzannulated rings of the bistropamine ligand. This geometry was confirmed by X-ray analysis on crystals of compounds (**S,S**)-**K5** (Figure 1.15a-b) and (**S,S**)-**K6** (Figure 1.18a-b).

The ¹H NMR spectrum of **K3** shows two doublets for the four olefinic protons and one singlet for the two benzylic protons (Table 1.2). One of two olefin signals shows a resolved small coupling constant with the rhodium of about 2.7 Hz. The ¹H NMR chemical shifts of the methyl groups are not equivalent and at 4.28 and 4.33 ppm. The ¹³C and ¹H NMR spectra show sharp signals and give no indications for any dynamic phenomena detectable on the NMR time scale. The ¹⁰³Rh NMR chemical shift is at 1547 ppm.

Analogously to **K3**, [RhCl(trop₂NH)(1,3-dicyclohexylimidazolin-2-ylidene)] (**K4**) was synthesized. No crystals of **K4** suitable for X-ray diffraction studies were obtained and the complex was thoroughly investigated by NMR spectroscopy. Many similarities between **K3** and **K4** were observed. The ¹³C NMR spectrum shows as expected a doublet at 165.0 ppm (¹J_{RhC} = 49.3 Hz) for the N₂C=Rh unit. The two cyclohexyl groups are not equivalent to each other, but the CH₂ groups within each cyclohexyl substituent are related by mirror symmetry. Therefore,

only six different carbon signals are displayed for the CH₂ units and two signals for the two nonequivalent CH units (δ = 58.4 ppm and 58.8 ppm). The coordination of the bistropamine ligand is confirmed by ¹³C NMR and ¹H NMR spectroscopy. The ¹³C spectrum shows two doublets for the olefinic carbon atom and the ¹H NMR spectrum displays two doublets for the olefinic protons and one singlet for the benzylic ones (Table 1.2). Two multiplets are observed for the CH group of the cyclohexyl substituents of the imidazolyl moiety at δ = 4.42 ppm and 4.65 ppm. The ¹⁰³Rh NMR signal is at 1720 ppm in the range of the previous studied Rh-NHC complex **K3**.

1.3.2 Crystal structure of [RhCl(trop₂NH)(1,3-bis-((*S*)-1-phenyl-ethyl)imidazolin-2-ylidene)]

Crystals of the compound [RhCl(trop₂NH)(1,3-bis-((*S*)-1-phenyl-ethyl)imidazolin-2-ylidene)] (**(*S,S*)-K5**) suitable for X-ray analysis were grown by slow diffusion of *n*-hexane into a saturated dichloromethane solution of the compound. Figure 1.15a-b shows an ORTEP view of the molecular structure of **(*S,S*)-K5** (chiral point group: monoclinic P2). The molecule adopts the expected slightly distorted trigonal bipyramidal geometry around the rhodium center, with the carbene moiety in apical position, trans to the amine of the trop₂NH.

Pentacoordinate NHC-Rh(I) with distorted trigonal bipyramidal arrangement have been already reported in the literature by Gade and co-workers.⁶⁵ The Rh-C bond lengths to the olefinic carbons vary over a range from 2.165(6) to 2.213(8) Å in complex **(*S,S*)-K5**. The distance to the carbene carbon, Rh-C31, is somewhat shorter [2.051(7) Å] and lies within the typical range of values previously reported for NHC-Rh(I) complexes.⁴

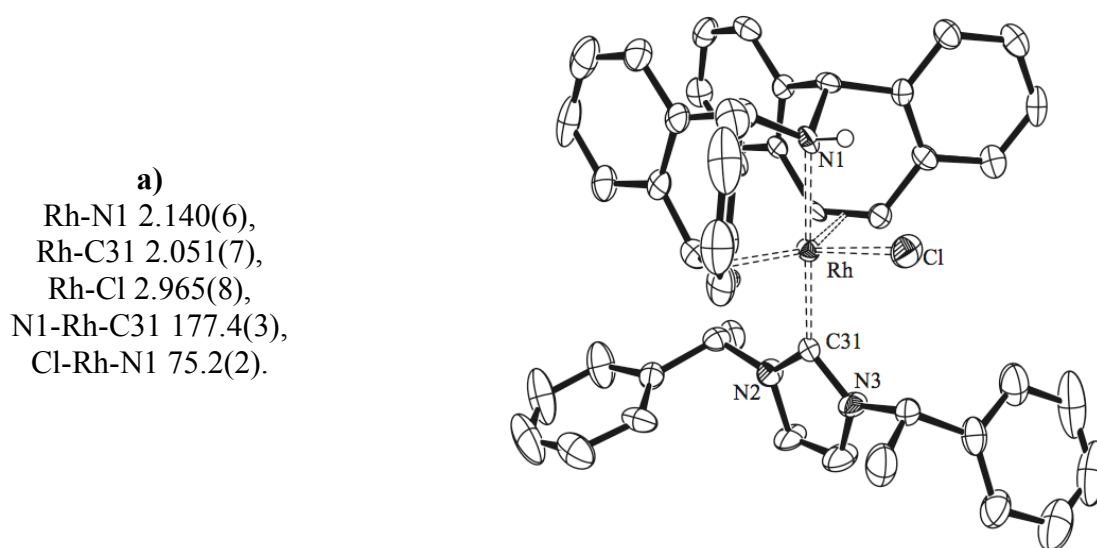


Figure 1.15a: ORTEP view of **(*S,S*)-K5** perpendicular to the Rh-carbene bond.

b)
 Rh-C5 2.165(6),
 Rh-C4 2.177(7),
 Rh-ct1 2.053(6),
 Rh-C19 2.199(6),
 Rh-C20 2.213(8),
 Rh-ct2 2.092 (7),
 C4-C5 1.412(8),
 C19-C20, 1.40(1),
 ct1-Rh-ct2 139.72(5),
 ct1-Rh-Cl 111.62(4),
 ct2-Rh-Cl 106.69(3).

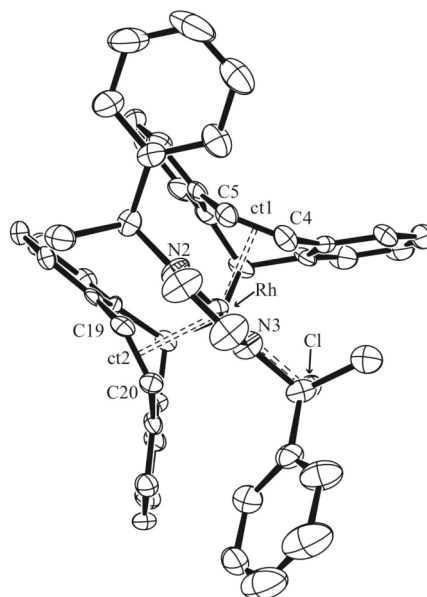
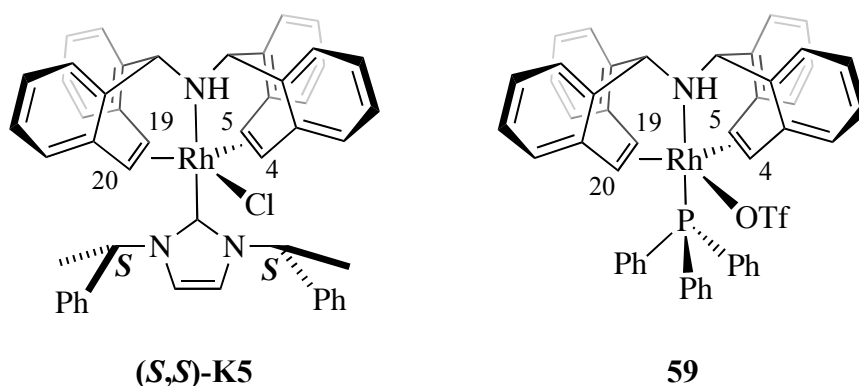


Figure 1.15b: ORTEP view of **(*S,S*)-K5** along the Rh-carbene bond. Thermal ellipsoids are drawn at 50% probability; all hydrogen atoms except at N1 are omitted for clarity. Selected bond lengths [Å] and angles [°]. ct = centroid of the olefin bond.

A comparison of structural parameters for **(*S,S*)-K5** and the known [Rh(OTf)(Trop₂NH)PPh₃] (**59**) reported by Büttner is given in Figure 1.16.⁶¹



Rh-C5, Rh-C4	2.165(6), 2.177(7)	2.172(2), 2.209(2)
Rh-C19, Rh-C20	2.199(6), 2.213(8)	2.168(2), 2.152(2)
Rh-NH	2.140(6)	2.150(2)
Rh-X	X= Cl 2.965(8)	X= OTf 2.381 (2)
N-Rh-X	X= Cl 75.2(2)°	X= OTf 90.70(8)°

Figure 1.16: Comparison of selected bond lengths and angles between **(*S,S*)-K5** and **59**.

Both complexes have a trigonal bipyramidal structure in which the C=C_{trop} units bind to the rhodium center with comparable bond distances. The replacement of the phosphine ligand by a N-heterocyclic carbene ligand does not cause any significant changes in the structure of the

rhodium bispromine complex **(S,S)-K5**. This is mainly due to the rigidity of the 5H-dibenzo[a,d]cyclohepten-5-yl (trop) skeleton which imposes a bite angle of approx. 90° for each nitrogen-olefin unit. The tetrahedral coordination sphere around the nitrogen center arranges the two trop substituents (and therefore the olefins) in a 120° angle to each other.

The Rh-Cl distance (2.965(8) Å) in **(S,S)-K5** is relatively long. Moreover, **(S,S)-K5** shows a distance between the chlorine atom and the NH proton of the bispromine moiety of approx. 2.37 Å. This latter interaction causes the narrowing of the Cl-Rh-N1 angle [$75.2(2)^\circ$] of about 15° from the trigonal plane and the elongation of the rhodium-chloride bond.

The structure of **59** shows a N-Rh-O angle of $90.70(8)^\circ$, with a deviation of only 0.70° from the trigonal plane of the bipyramidal structure.

As depicted in the ORTEP view along the Rh-carbene bond in Figure 1.15b and in the schematic representation of Figure 1.17a-b, **(S,S)-K5** lost the mirror plane present within the molecules **K3** and **K4** and shows only C_1 symmetry.

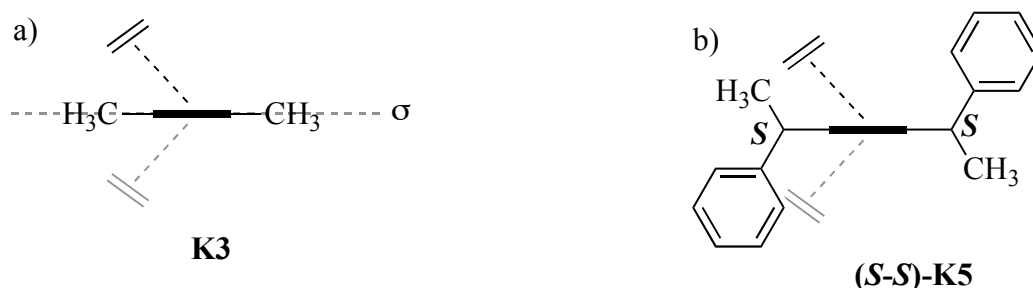


Figure 1.17a-b: Representation of **K3** (a) and **(S,S)-K5** (b) from below.

The molecular structure of **(S,S)-K5** is reflected by the NMR data. The ^1H NMR spectrum displays two doublets for the methyl groups at 1.93 ppm and at 2.25 ppm and two quartets for the $\text{NCH}(\text{Ph})(\text{CH}_3)$ units at 6.57 ppm and 8.3 ppm (all with $^3J_{\text{HH}} = 6.8$ Hz). Moreover, the trop_2NH displays more signals with respect to **K3** and **K4** due to the loss of symmetry. The ^1H NMR spectrum displays now two signals for the benzylic protons and four doublets for the olefinic ones (Table 1.2).

The ^{13}C NMR spectrum confirms the coordination of the NHC to the rhodium metal center. The carbene carbon shows a doublet at 168.6 ppm with $^1J_{\text{RhC}} = 49.6$ Hz. Two signals are displayed for the benzylic carbons and, due to line broadening; only two olefin resonances were detected (Table 1.2). As expected, the spectrum shows two singlets for the methyl groups ($\delta = 22.9$ ppm and 24.8 ppm) and two singlets for the $\text{NCH}(\text{Ph})(\text{CH}_3)$ units ($\delta = 57.8$ ppm and 58.4 ppm).

1.3.3 Crystal structure of [Rh(trop₂NH)((*S,S*)-ValinolCarbene)]OTf

Compound [Rh(trop₂NH)((*S,S*)-ValinolCarbene)]OTf (**(*S,S*)-K6**) was obtained in 65% yield as red microcrystals. Suitable crystals for X-ray analysis were grown by slow diffusion of *n*-hexane in a saturated dichloromethane solution of the compound. Figure 1.18a-b shows an ORTEP plot of the structure (chiral point group triclinic P1).

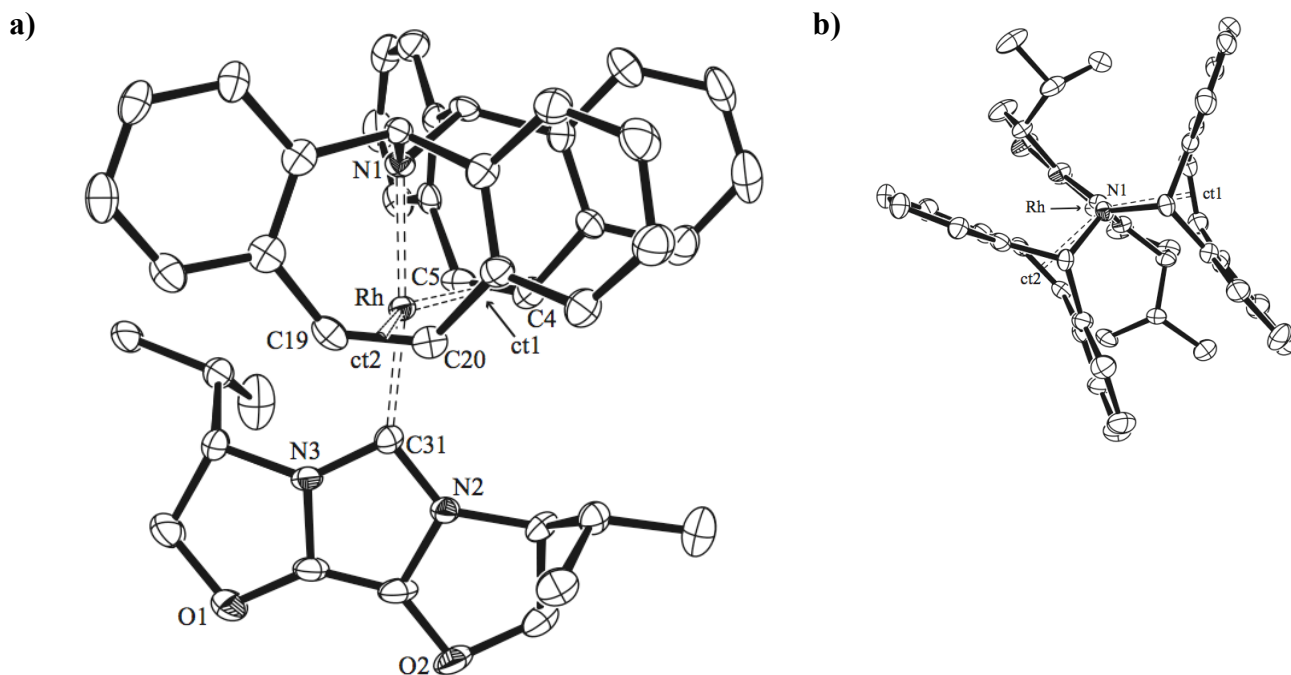


Figure 1.18a-b: ORTEP plot of (*S,S*)-**K6** a) view perpendicular to the Rh-carbene bond b) view along the Rh-carbene bond. Thermal ellipsoids are drawn at 50% probability; hydrogen atoms and the triflate counter anion are omitted for clarity. Selected bond lengths [Å] and angles [°]: Rh-N1 2.145(4), Rh-C31 1.992(5), Rh-C5 2.175(5), Rh-C4 2.172(4), Rh-ct1 2.056(5), Rh-C19 2.199(5), Rh-C20 2.204(5), Rh-ct2 2.088(5), C4-C5 1.408(7), C19-C20 1.393(7), N1-Rh-C31 173.51(19), ct1-Rh-ct2 147.03(6), C16-N1-C1 111.9(4), C16-N1-Rh 116.6(3), C1-N1-Rh 116.0(3). ct = centroid of the olefin bond.

All reported NHC-Rh(I) 16-electron complexes with a tertacoordinate Rh-center have a (sometimes slightly distorted) planar geometry.⁶⁶ In contrast, complex (**(*S,S*)-K6**) adopts a saw-horse type structure with a N1-Rh-C31 angle of about 173° and the ct1-Rh-ct2 angle of about 147°. There are no close contacts between the cation and the anion [Rh-OTf 4.751 Å]. Saw-horse type structures for stable 16-electron complexes have been rarely observed.⁶⁷ Some examples include the [Rh(trop₂NH)(PPh₃)]BAR^F (**60**) and [Rh(trop₂NH)(P(OPh)₃)]OTf (**61**) already reported by our research group.⁶⁸ (**(*S,S*)-K5**) is the first example of a rhodium-carbene complex with a saw-horse type structure. The Rh-C_{carbene} distance [1.992(5) Å] lies in the range of previously reported NHC-Rh(I) complexes.⁴ The Rh-C_{carbene} bond length is slightly shorter than the one observed for the

pentacoordinated compound [RhCl(trop₂NH)(1,3-bis-((*S*)-1-phenyl-ethyl)imidazolin-2-ylidene)] (**(*S,S*)-K5**) [2.051(7) Å]. The Rh-N1 distance of trop₂NH barely changes upon substitution of the *trans* ligand from PPh₃ or P(OPh₃) to NHC, both in trigonal bipyramidal structure such as (**(*S,S*)-K5**, **62** and **63**) and saw-horse structures such as (**(*S,S*)-K6**, **60** and **61**) (see Table 1.1).

Table 1.1: Comparison of the Rh-N bond lengths for trigonal bipyramidal and saw-horse structures.

Type of Structure/ Complex	Rh-N [Å]	Reference
<i>Trigonal Bipyramidal</i>		
(<i>S,S</i>)-K5	2.140(6)	this work
[Rh(trop ₂ NH)(PPh ₃)OTf] (62)	2.160(6)	Ref. 68
[Rh(trop ₂ NH)(P(OPh ₃)) ₂]OTf (63)	2.150(2)	Ref. 61
<i>Saw-horse</i>		
(<i>S,S</i>)-K6	2.145(4)	this work
[Rh(trop ₂ NH)(PPh ₃)] BArf ^F (60)	2.155(2)	Ref. 68
[Rh(trop ₂ NH)(P(OPh ₃))] OTf (61)	2.147(1)	Ref. 61

This type of behavior has been observed for other complexes as well. For example, in the second generation Grubbs catalysts, the Ru-P distance remains unaffected when the *trans* ligand changes from PCy₃ to IMes (IMes=1,3-bis(2,4,6-trimethyl)phenyl imidazol-2-ylidene).⁶⁹ Nolan and co-workers showed that the Pt-Cl distance is not affected in length when a *trans*-phosphine ligand is replaced by a NHC carbene ligand.⁷⁰

Compound (**(*S,S*)-K6**) has been studied by NMR spectroscopy. Both ¹³C NMR and ¹H NMR spectra confirmed the asymmetry of molecule (**(*S,S*)-K6**) which belongs, like (**(*S,S*)-K5**), to the point group C₁. In fact, many similarities between (**(*S,S*)-K5**) and (**(*S,S*)-K6**) have been observed.

In the ¹³C NMR spectrum, the trop-olefins carbons show four different doublets and the benzylic carbons display two singlets. As expected, the ¹H NMR shows four signals for the olefinic protons and two signals for the benzylic ones, as well. The chemical shifts are reported in Table 1.2.

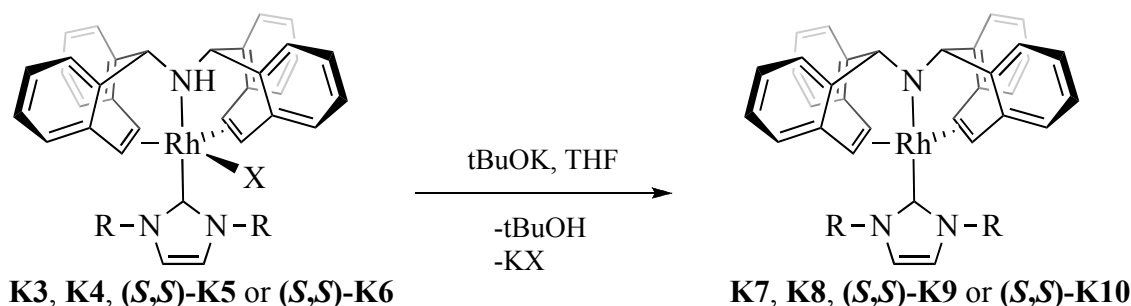
1.3.4 Additional NMR Data of [RhX(trop₂NH)(NHC)]

Table 1.2: Characteristic ¹H NMR ¹³C NMR data for **K3**, **K4**, (*S,S*)-**K5**, (*S,S*)-**K6**.

		$\delta^1\text{H}$ (ppm) [J_{HH} (Hz)]	$\delta^{13}\text{C}$ (ppm) [J_{RhC} (Hz)]
[RhI(trop ₂ NH)(IMe)] (K3)	benzyl	4.76	72.5
	olefin	4.92 [9.4], 5.11 [9.4]	69.9 [7.0], 70.4 [13.1]
[RhCl(trop ₂ NH)(ICy)] (K4)	benzyl	5.92	71.6
	olefin	4.86 [8.7], 6.36 [8.7]	71.0 [14.3], 71.9 [6.4]
[RhCl(trop ₂ NH)(57)] (<i>S,S</i>)- K5)	benzyl	4.73, 4.75	72.2, 72.3
	olefin	4.88 [9.1], 5.44 [9.1]	67.5, n.o.
[Rh(trop ₂ NH)(58)]OTf (<i>S,S</i>)- K6)	benzyl	4.98 [9.4], 5.51 [9.3]	69.5, n.o.
	olefin	4.73, 4.75	76.3, 77.6
[Rh(trop ₂ NH)(56)]OTf	benzyl	4.88 [9.1], 5.44 [9.1]	72.9 [8.2], 75 [7.2]
	olefin	4.98 [9.4], 5.51 [9.3]	77.1 [12.5], 77.3 [1.9]
[Rh(trop ₂ NH)(PPh ₃)OTf](56)	benzyl	4.91	72.7
	olefin	4.94 [9.3], 5.45 [9.3]	74.0 [6.9], 74.2 [13.3]

1.4 Deprotonation of [RhX(trop₂NH)(NHC)]

As mentioned in Chapter 1.2, the amide **K2** is the active species in catalysis, therefore the deprotonation of **K3**, **K4**, (*S,S*)-**K5** and (*S,S*)-**K6** to the corresponding amides was subsequently studied. The reaction is quantitative and occurs in THF at room temperature by addition of one equivalent of base e.g. potassium *tert*-butoxide, as shown in Scheme 1.21. The disappearance of the NH proton signals in the ¹H NMR spectra of **K7**, **K8**, (*S,S*)-**K9** and (*S,S*)-**K10** confirmed the deprotonation. Moreover, the colour of the solution changed from deep yellow (amine) to green (amide).



Scheme 1.21: Deprotonation of [RhX(trop₂NH)(NHC)] **K3**, **K4**, (*S,S*)-**K5** and (*S,S*)-**K6**.

The amides prepared in this way are shown in Figure 1.19. They could not be isolated but were characterized by NMR spectroscopy.

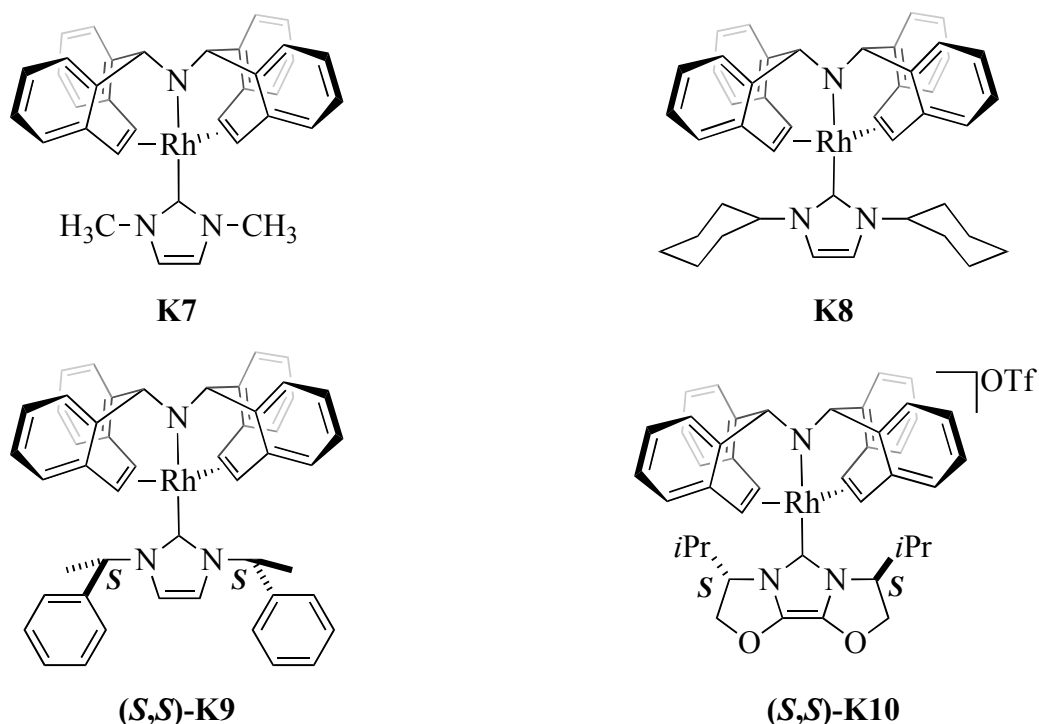


Figure 1.19: N-heterocyclic carbene rhodium(I) amido complexes.

K7, **K8**, **(S,S)-K9** and **(S,S)-K10** display simplified ^1H NMR and ^{13}C NMR spectra when measured at room temperature. Moreover, the spectra show broad signals, which reflect the dynamic behavior of the amides in solutions. These observations suggest either rapid rotation of the carbene ligand (not likely) or fast inversion at the nitrogen and rhodium centers, probably *via* a planar transition state.⁷¹ This second hypothesis is more probable and this type of inversion has been already proposed for the analogue phosphine system. This process leads to an exchange of the positions of the olefinic protons H_A and H_B as shown schematically in Figure 1.20.

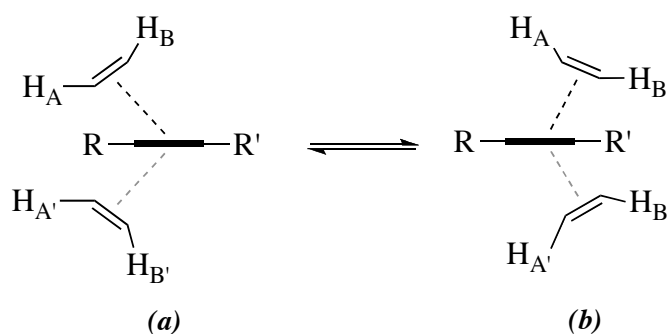


Figure 1.20: Inversion of the amide.

1.4.1 Determination of the Activation Energy (E_a) for the Ligand Inversion in (*S,S*)-K10

The ^1H NMR spectrum recorded at room temperature of the rhodium amide (*S,S*)-K10 derived from the deprotonation of (*S,S*)-K6 shows broad signals (Figure 1.21h). When the spectrum is recorded at low temperature the signals become sharper. Figure 1.21a shows that at 220 K an enhanced resolution of the resonances can be detected. We assume that at low temperature the amide has a saw-horse structure. The assumption is supported by the following observations. The ^1H NMR spectrum at 220 K displays four different doublets for the olefinic signals and one signal for both benzylic protons as we previously observed for **K3** and **K4**, which have trigonal bipyramidal structures. Four doublets for the methyl groups and two broad singlets for the *CH* group of the isopropyl groups (at 2.14 ppm and 2.93 ppm) are observed at low temperature. At room temperature only one broad peak for the *CH* group can be detected. Furthermore, the ^{13}C NMR spectrum confirms the proposed coordination mode of the trop ligand. The olefinic carbon signals are displayed as four doublets at 72.9 ppm ($^1J_{\text{RhC}} = 6.2$ Hz), 74.4 ppm ($^1J_{\text{RhC}} = 6.8$ Hz), 78.6 ($^1J_{\text{RhC}} = 15.9$ Hz) and 79.1 ($^1J_{\text{RhC}} = 16.6$ Hz). In addition, two singlets for the benzylic carbons ($\delta = 80.8$ ppm and 80.9 ppm) are present. The doublet at 160.6 ppm with $J_{\text{RhC}} = 44$ Hz is attributed to the Rh=C carbene carbon. In order to obtain quantitative data for the exchange process indicated in Figure 1.20, the ^1H NMR spectrum of (*S,S*)-K10 was recorded at eight different temperatures between 220 and 300 K (Figure 1.21a-h).

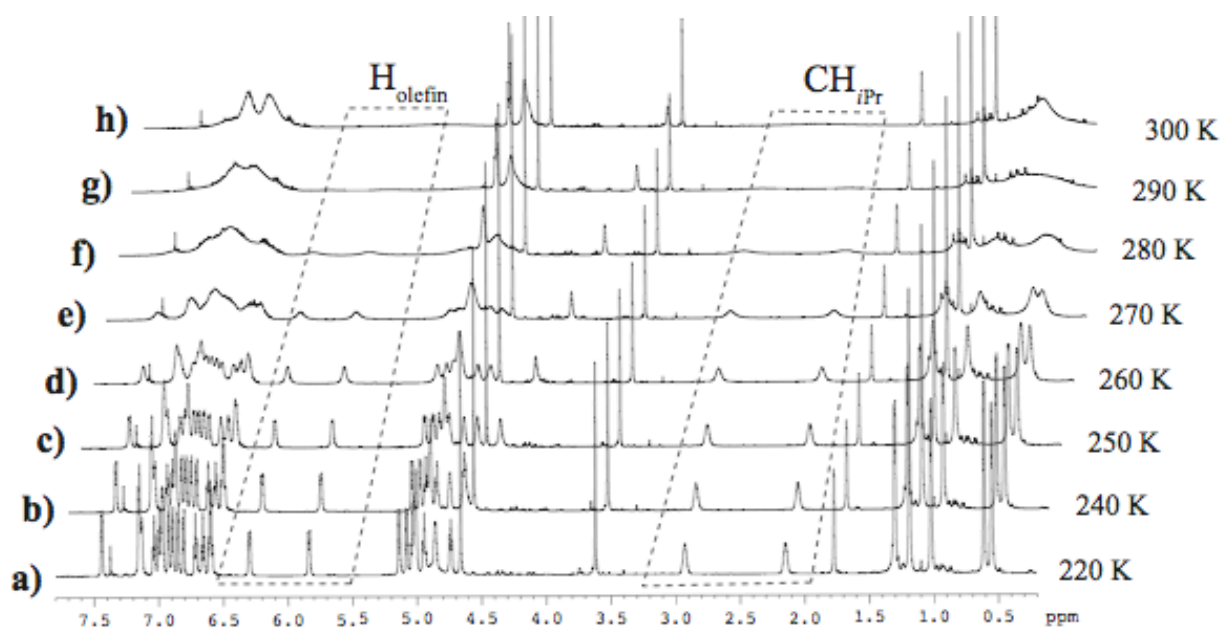


Figure 1.21a-h: Temperature dependent NMR spectra ($[\text{D}_8]$ THF, 700 MHz) at 220 K (a), 240 K (b), 250 K (c), 260 K (d), 270 K (e), 280 K (f), 290 K (g) and 300 K (h) of the amide (*S,S*)-K10.

The shapes of the resonances corresponding to the methyl groups have been simulated using the MEXICO program package.⁷² The coupling constants, the chemical shifts and the rate of the exchange for each temperature have been arranged in a matrix and used as input for the program. The kinetic data - the rate constants at different temperatures - were used to obtain the activation parameters for the exchange process occurring in **(S,S)-K10** using the Eyring equation (1).

$$\text{Eyring Equation: } k = \frac{k_B T}{h} e^{-\frac{\Delta H^\ddagger}{RT}} e^{\frac{\Delta S^\ddagger}{R}} \quad (1)$$

Where: $k_B = 1.381 \times 10^{-23}$ [J K⁻¹] Boltzmann constant, $h = 6.626 \times 10^{-34}$ [J s] Plank constant, $R = 8.3145$ [J mol⁻¹ K⁻¹] Universal Gas Constant, $T =$ absolute temperature in K, $\Delta S^\ddagger =$ activation entropy [J mol⁻¹ K⁻¹], $\Delta H^\ddagger =$ activation enthalpy [kJ mol⁻¹].

Reformulated as follows: (2) and (3).

$$\ln \frac{k}{T} - \ln \frac{k_B}{h} = -\frac{\Delta H^\ddagger}{RT} + \frac{\Delta S^\ddagger}{T} \quad (2)$$

$$R \ln \frac{kh}{Tk_B} = -\Delta H^\ddagger \frac{1}{T} + \Delta S^\ddagger \quad (3)$$

The activation parameters can be derived from the intersection and the slope of the regression line by plotting $R \ln(kh/TK_B)$ vs. the reciprocal absolute temperature (Figure 1.22).

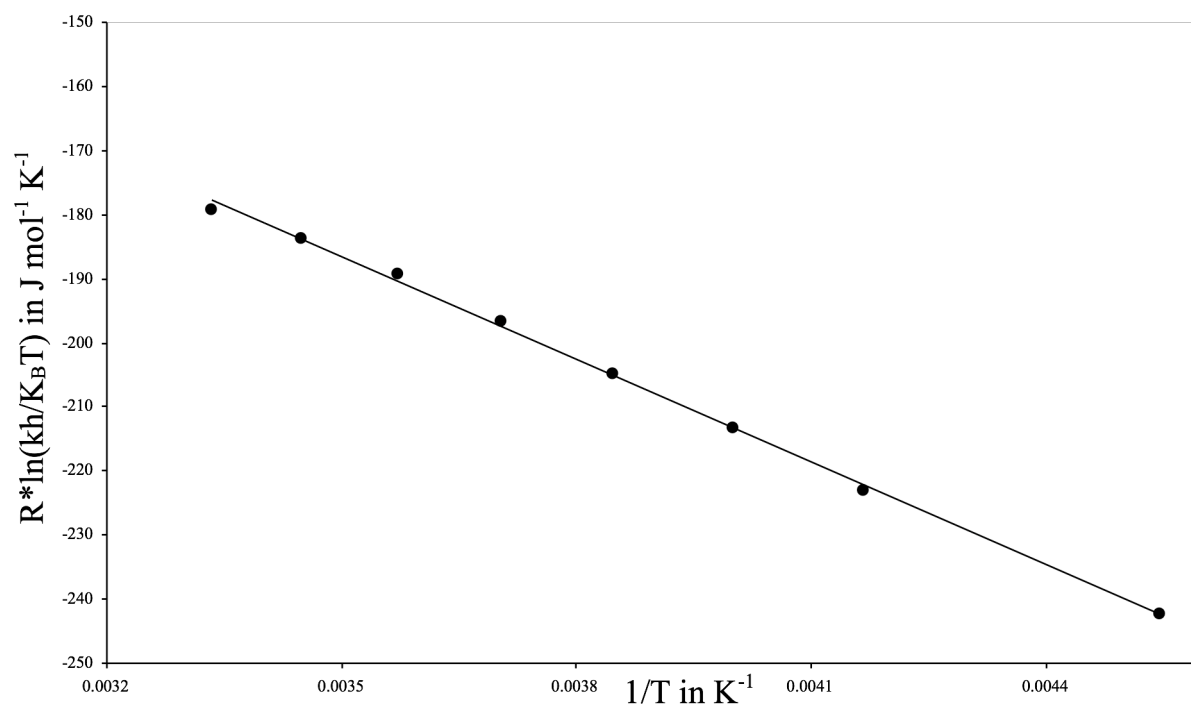


Figure 1.22: Eyring plot using the rate constant determined from the NMR simulation vs. T^{-1} with least square linear fit.

From the Eyring plot (Figure 1.23) a value of 53 kJ mol^{-1} was determined for the enthalpy of activation (ΔH^\ddagger), 13 kJ mol^{-1} higher compared to $[\text{Rh}(\text{trop}_2\text{N})(\text{PPh}_3)]$ (**K2**). The entropy of activation (ΔS^\ddagger) is slightly negative: $-0.12 \text{ J mol}^{-1} \text{ K}^{-1}$ indicating a more ordered or more rigid structure for the activated complex in comparison to the ground state structure. Similar data were obtained for complex **K2** ($\Delta S^\ddagger = 24 \text{ J mol}^{-1} \text{ K}^{-1}$ and $\Delta H^\ddagger = 40 \text{ kJ mol}^{-1}$).⁶¹ These results are in agreement with the planar transition state which we assume for the inversion process of the trop_2N ligand.

1.4.2 Transfer Hydrogenation

The results obtained so far were promising enough to test the carbene complexes as catalysts for transfer hydrogenations. The preparation of **K3**, **K4**, (**S,S**)-**K5** and (**S,S**)-**K6** from **K1** clearly showed the superiority of the NHCs over the phosphine as σ -donor ligands and we expected to obtain catalysts with an enhanced stability. The formation of the amides **K7**, **K8**, (**S,S**)-**K9** and (**S,S**)-**K10** showed a similar behavior of the NHCs complexes with respect to **K1**. Therefore, **K3**, **K4**, (**S,S**)-**K5** and (**S,S**)-**K6** were tested in the catalytic transfer hydrogenation of acetophenone to 1-phenylethanol using ethanol as hydrogen source and potassium *tert*-butoxide as base.[†] Among the tested catalysts, complex (**S,S**)-**K6** showed the highest activity (Figure 1.23), achieving turnover frequencies of about 1000 h^{-1} (calculated at 23% conversion). The reaction stops at 50% conversion, for yet unknown reasons. Complexes **K3**, **K4** and (**S,S**)-**K5** display an initial turnover frequency lower than that of (**S,S**)-**K6**.

These results show that the carbene complexes are less effective in transfer hydrogenation reactions compared to the comparable triphenylphosphine complex $\text{Rh}(\text{trop}_2\text{N})(\text{PPh}_3)$ ^{62, 68}, most probably due to the steric congestion of the complexes by the N-substituents on the NHC carbenes. These prevent the approach of the substrate towards the catalyst. Nolan and co-workers reached the same conclusions.³⁸ In fact, the cationic iridium carbene complexes published in 2001, although effective in the hydrogenation of simple olefins, are less active than the Crabtree's catalyst **29**, (see Figure 1.9.)

The HPLC analysis[‡] of 1-phenylethanol obtained by transfer hydrogenation with catalysts (**S,S**)-**K6** and (**S,S**)-**K5** shows no enantiomeric excess of the product. The lack of stereoselectivity is

[†]Molar ratios catalyst:acetophenone=1:1000, Ethanol= 8.5, tBuOK= 0.01. The progression of the catalysis was followed by GC analysis on a Hewlett Packard HP 6890 Series GC, column: Machery Nagel Permabond CW20M-DF-0.25 (25 m x 0.32 mm x 0.21 μm), Separation of 1-phenyl-ethanol from acetophenone: temperature: $120 \text{ }^\circ\text{C}$ isotherm; H_2 pressure: 0.34 bar; retention times: acetophenone: 1.95 min.; 1-phenylethanol: 2.63 min.

[‡]HPLC Agilent Series 1100 with Uv detector (DAD 210nm), column Chiracel OD-H (4.6 x 250mm, particle 5 μl), hexane/isopropanol 90/10, 0.5 ml/min, 25°C . Retention times: 12.1 m(R), 13.2 m(S).

unknown but could be simply due to the fact that the stereogenic centers are too remote from the active site. Note that no satisfying results (32% ee) were obtained either in the catalytic hydrosilylation of acetophenone with [RhCl(cod)(1,3-bis-((*S*)-1-phenyl-ethyl)imidazolin-2-ylidene)] (see Scheme 1.12).

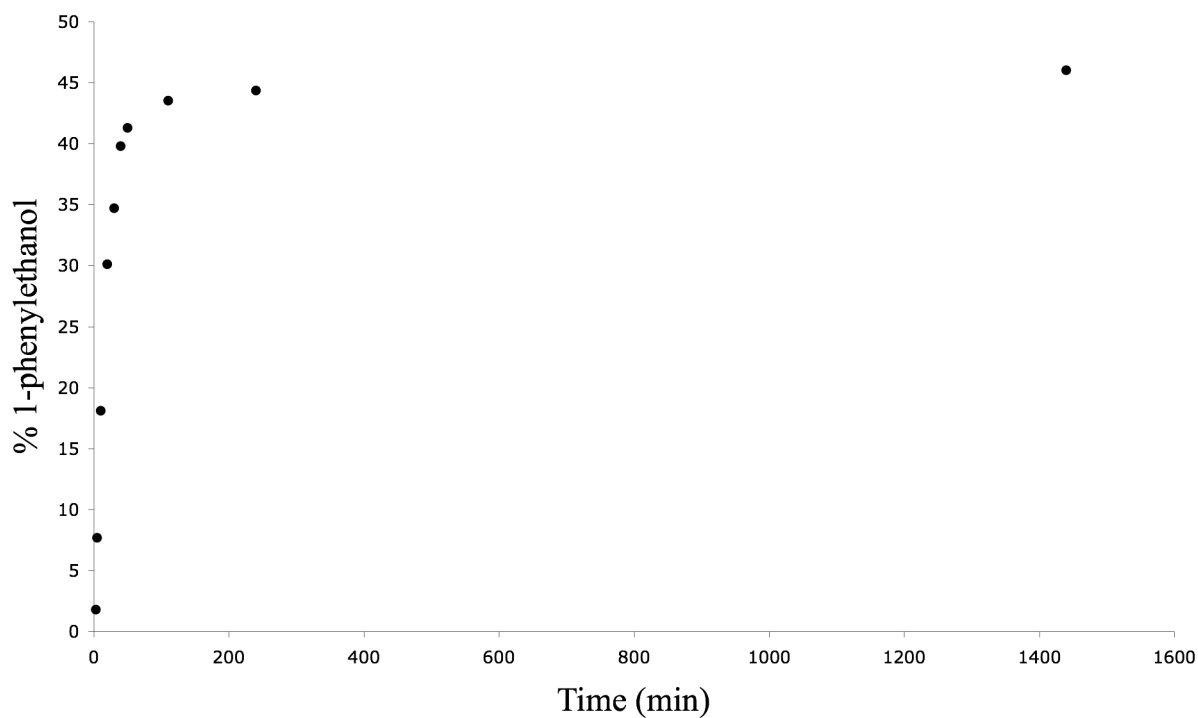


Figure 1.23: Time dependence of the catalytic transfer hydrogenation of acetophenone with complex (*S,S*)-**K6**. Molar ratios catalyst : acetophenone = 1 : 1000, Ethanol= 8.5, *t*BuOK= 0.01.

1.5 Reactivity of [RhX(trop₂NH)(NHC)]

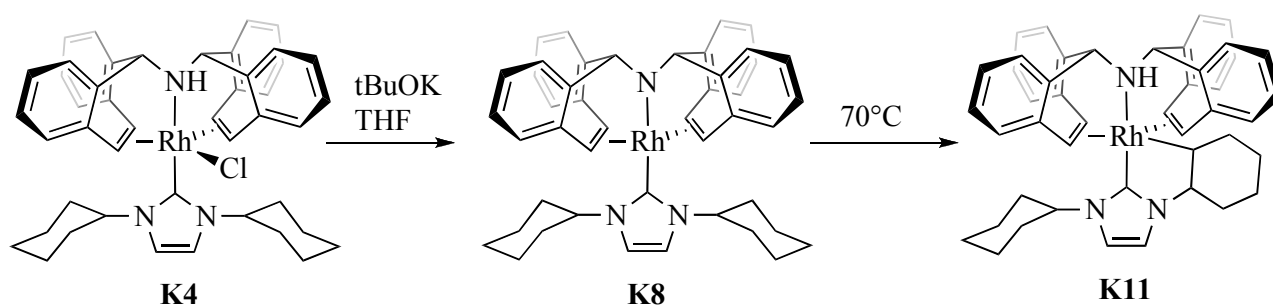
Despite several reports (see Chapter 1.1.2.3), which described enhanced performance of N-heterocyclic carbene complexes over comparable phosphine complexes, especially with respect to catalyst stability and activity, in our catalytic system such a replacement did not produce the desired effect. Indeed, the catalytic results obtained for the NHC complexes of rhodium(I) show that, although **K3**, **K4**, (*S,S*)-**K5** and (*S,S*)-**K6** catalyze to some extent the transfer hydrogenation of benzophenone, they are still much less active than **K1**.^{62, 68} Moreover, the use of chiral complexes, such as (*S,S*)-**K5** and (*S,S*)-**K6**, did not produce any stereoselectivity in the product.

In order to better understand the catalytic system and address future synthetic strategies for the preparation of new ligands toward a more fruitful direction, we further investigated the reactivity of compounds **K3**, **K4**, (*S,S*)-**K5** and (*S,S*)-**K6** in basic conditions. As will be shown below, these investigations added a new aspect in the “degradation” chemistry of NHCs complexes mentioned in (Chapter 1.1.3).

1.5.1 Reactivity of [Rh(trop₂NH)(ICy)]

Both the amino [RhI(trop₂NH)(IME)] (**K3**) and the amido complex [Rh(trop₂N)(IME)] (**K7**) are stable in solution for several weeks at room temperature and at relatively high temperatures (70 °C). No decomposition products were detected by ¹H NMR spectroscopy.

On the contrary, the amide [Rh(trop₂N)(1,3-dicyclohexylimidazol-2-ylidene)] (**K8**) reacts at 70°C slowly to give the five-member metallacycle **K11** (Scheme 1.22). As discussed below, we assume an intramolecular C-H activation reaction of the CH group in the cyclohexyl substituent across the Rh-N bond to be responsible for this transformation.



Scheme 1.22: Formation of the orthometallate rhodium complex **K11**.

Suitable crystals for X-ray analysis were grown by slow diffusion of *n*-hexane in a saturated THF solution of **K11**. Figure 1.24a-b display ORTEP plots of the structure of **K11** determined by a X-ray diffraction analysis. The carbene moiety is still C2-bound to the metal center – that is no

“abnormal” coordination mode is observed (Chapter 1.1.3) – in axial position *trans* to the amine group of the trop₂NH ligand. The angle N3-Rh-C13 is about 170°, slightly distorted from the ideal angle of 180° for an ideal trigonal bipyramidal structure. The Rh-C_{olefin} bond lengths are slightly shorter compared to the structure of [RhCl(trop₂NH)(1,3-bis-((*S,S*)-1-phenyl-ethyl)imidazolin-2-ylidene)] ((*S,S*)-**K5**), due to the *trans* influence of the activated cyclohexyl unit.

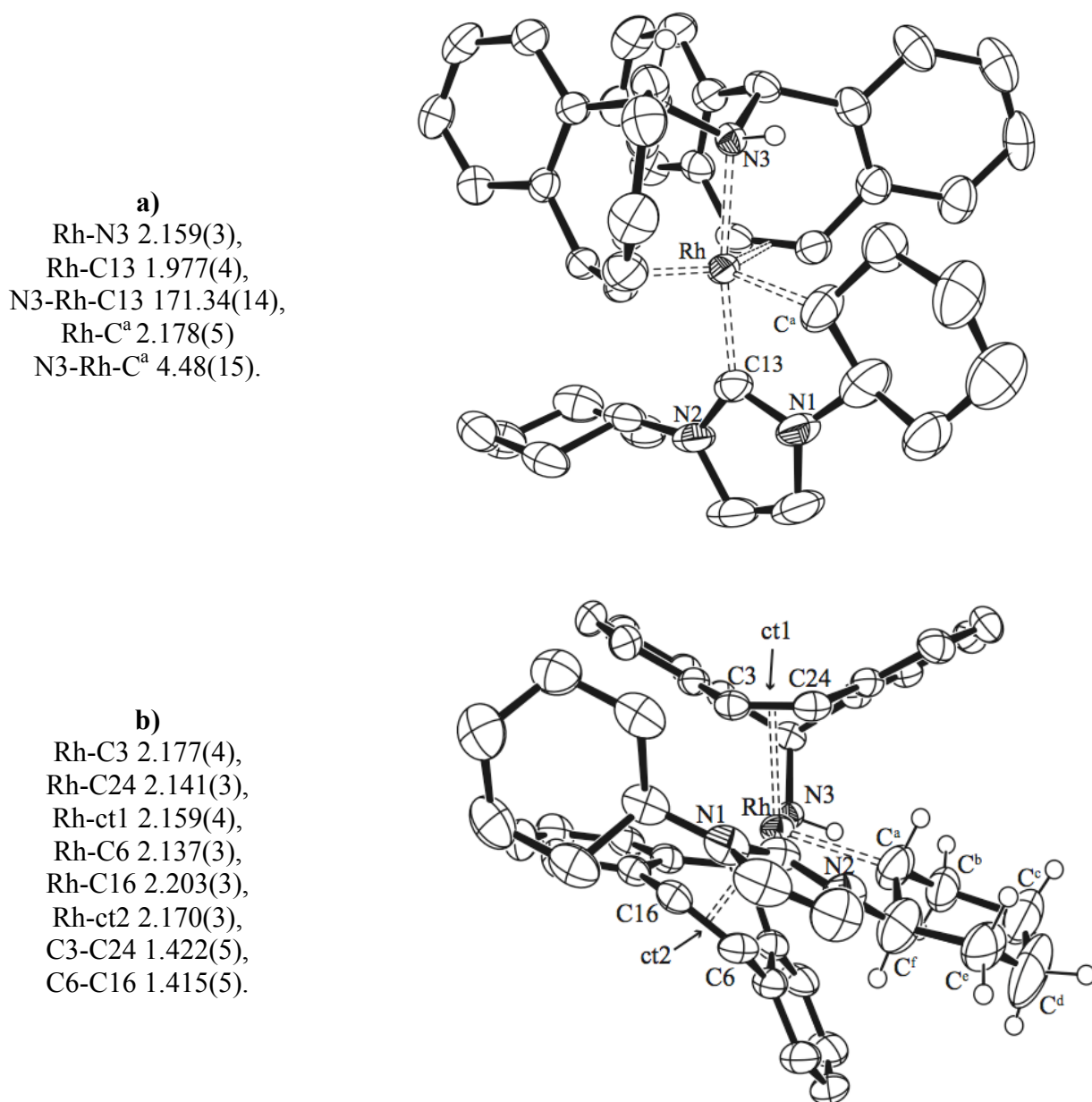


Figure 1.24a-b: ORTEP view of **K11**. Thermal ellipsoids are drawn at 50% probability; hydrogen atoms are omitted for clarity except for the NH and the activated cyclohexyl substituent. Selected bond lengths [Å] and angles [°] are reported. ct = centroid of the olefin bond.

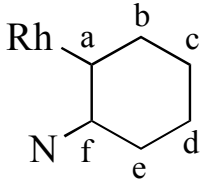
Selected NMR data of diagnostic value for compound **K11** are listed in Table 1.6. The ¹H NMR spectrum shows four different signals for the olefinic protons and two different singlets for the

benzylic ones. This observation is in accord with the lower symmetry of **K11** when compared to $[\text{RhCl}(\text{trop}_2\text{NH})(\text{ICy})]$ (**K4**) (only two signals for the olefinic protons and one signal for benzylic ones, see Table 1.2). Moreover, the chemical shifts of the characteristic protons of the trop_2NH are shifted to lower frequencies compared to $[\text{RhCl}(\text{trop}_2\text{NH})(\text{ICy})]$ (**K4**) indicating higher ($d \rightarrow \pi^*$)-back donation from the metal center to the olefins as a consequence of the higher *trans* effect of the alkyl unit present in **K11** compared to the chloride in **K4**.

The stereochemistry of compound **K11** was determined by ^1H NMR spectroscopy and by evaluation of the magnitude of the coupling constants between different nuclei (Table 1.3). These results are in perfect agreement with the X-ray diffraction study.

In particular, protons in C^a and C^f position show characteristic resonances: a broad triplet at 2.24 ppm and a well-resolved doublet of triplets at 3.94 ppm, respectively. The value found for the coupling constant between these two nuclei is of 11 Hz, a typical value for vicinal coupling constants between hydrogen nuclei with a dihedral angle of about 180° . Therefore, the two protons in C^a and C^f position must be *anti* to each other. This assignment was further confirmed by $^1\text{H}^1\text{H}$ -COSY experiment: the two protons show only close contacts to the axial and equatorial protons in position C^b and C^e , respectively.

Table 1.3: ^1H NMR and ^{13}C NMR data for complex **K11**.

	^1H δ (ppm)	^{13}C δ (ppm)	J_{RhC} (Hz)
	2.24 (a)	35.0	20
	0.24 (a §), 0.11 (e §)	30.26	
	0.83 (a §), 1.29 (e §)	29.19	
	1.29 (a §), 1.77 (e §)	25.63	
	1.39 (a §), 2.44 (e §)	33.37	
	3.94 (a §)	68.25	

\S : a= axial; e= equatorial.

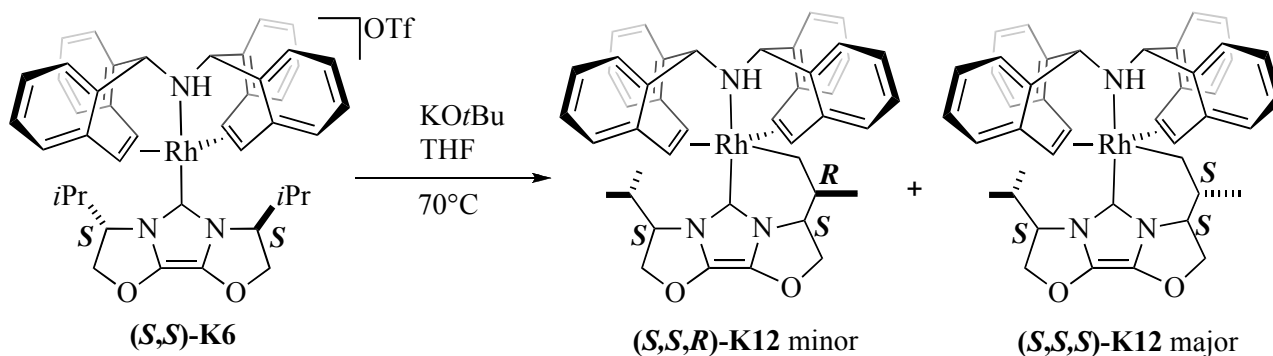
The most representative signals found in the ^{13}C NMR spectrum is at 176.0 ppm with $^1J_{\text{RhC}} = 51.87$ Hz and it is attributed to the $\text{Rh}=\text{CN}_2$ moiety. Moreover, the presence of a doublet at 35.1 ppm with $^1J_{\text{RhC}}$ of 20 Hz (attributed to the carbon C^a) further confirmed the formation of the cyclometallate species.

In contrast to the complex reported by Herrmann et al. (see Scheme 1.18), **K11** is stable and does not undergo β -hydrogen elimination therefore allowing its isolation. Note that four isomers (*R,R*),

(*S,S*), (*R,S*) and (*S,R*) of compound **K11** are possible, but only the pair of enantiomers (*R,R*) and (*S,S*) depicted in Scheme 1.19 has been isolated. We assume that the stereoselectivity in the addition of the NH bond along the R-N bond is governed by the minimization of 1,3-diaxial interactions and gauche interactions within the cyclohexyl unit which favours the formation of the enantiomers (*R,R*) and (*S,S*).

1.5.2 Reactivity of [Rh(trop₂NH)(*S*-ValinolCarbene)]

In presence of a base, complex (*S,S*)-**K6** decomposes quantitatively after three days at 70°C to the *ortho*-metallate Rh(I) complexes (*S,S,R*)-**K12** and (*S,S,S*)-**K12**, depicted in Scheme 1.23.



Scheme 1.23: Intramolecular C-H activation of the isopropyl group in complex (*S,S*)-**K6**.

No crystals suitable for X-ray diffraction study were obtained and the complexes (*S,S,R*)-**K12** and (*S,S,S*)-**K12** were analyzed and characterized by NMR spectroscopic techniques.

The ¹⁰³Rh NMR spectrum shows two signals at 520 ppm and at 543 ppm. Two diastereoisomers are formed in a ratio of 2:1 (determined by ¹H NMR through integration of the protons signals of the CH group of the isopropyl groups which show doublets of septets at 3.1 ppm and 3.17 ppm, respectively).

The ¹H NMR spectrum shows the presence of the ligand trop₂NH bound to the metal in a κ³-facial fashion. Due to the low symmetry of the molecule, all benzylic and olefinic protons are non-equivalent (Table 1.6). Moreover, the spectrum shows the presence of only three methyl groups in the minor (doublets at 0.51 ppm, 0.95 ppm and 1.25 ppm) as well as in the major product (doublets at 0.87 ppm, 0.98 ppm and 1.23 ppm). This observation indicates the C–H activation of one of the four methyl groups of the isopropyl substituents (compare with the results observed by Yamaguchi et al.; Figure 1.12). The two proton signals at 0.23 ppm and 1.08 ppm for the minor compound and 0.52 ppm and 0.63 ppm for the major compound have been attributed to the geminal protons of the CH₂ group bonded to the rhodium metal center. No signals were observed in the hydride region.

In the ^{13}C NMR spectrum, two signals for the benzylic carbons and four signals for the olefinic ones were recorded (Table 1.6). The resonance of the metal-bonded methylene nucleus is observed as doublet at 22.9 ppm (minor isomer) with $^1J_{\text{RhC}} = 28.7$ Hz and at 24.9 ppm (major isomer) with $^1J_{\text{RhC}} = 28.4$ Hz (Table 1.4 and 1.5). The stereochemistry of the two diastereoisomers has been assigned by NMR experiments and by evaluation of the magnitude of various spin-spin coupling constants. The assignment of the chemical shifts is given in Table 1.4 and 1.5.

Table 1.4: ^1H NMR and ^{13}C NMR data for complex **(S,S,R)-K12** minor.

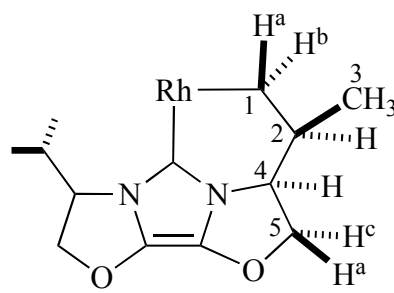
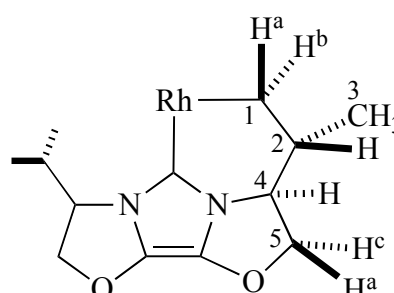
<i>Minor</i>	^1H δ (ppm)	^{13}C δ (ppm)	
	C ¹	0.23 (H ^a) 1.08 (H ^b)	22.9
	C ²	0.51	12.6
C ³	2.14	34.8	
C ⁴	4.54	62.4	
C ⁵	5.04 (H ^c) 4.68 (H ^a)	78.7	

Table 1.5: ^1H NMR and ^{13}C NMR data for complex **(S,S,S)-K12** major.

<i>Major</i>	^1H δ (ppm)	^{13}C δ (ppm)	
	C ¹	0.52 (H ^a) 0.63 (H ^b)	24.9
	C ²	1.50	40.9
C ³	0.87	20.8	
C ⁴	4.09	63.8	
C ⁵	4.44 (H ^c) 5.05 (H ^a)	82.1	

The formation of two diastereoisomers in ratio 2:1 can be explained with the help of the double-barreled Newman projections of **(S,S,R)-K12** and **(S,S,S)-K12**, which are shown in Figure 1.25a-b. In the minor conformation the methyl in axial position and the C-Rh bond on the adjacent carbon atom are *gauche* with respect to each other. Moreover, 1,3-diaxial interactions between the methyl group and the trop₂NH ligand on one side and the proton on the adjacent carbon atom on the

other side disfavour the formation of (*S,S,R*)-**K12**. In summary, the axial conformation of the minor conformer is energetically less favourable than the equatorial conformation, because of 1,3-diaxial interactions and *gauche* interactions (see the Newman projections of Figure 1.25a-b).

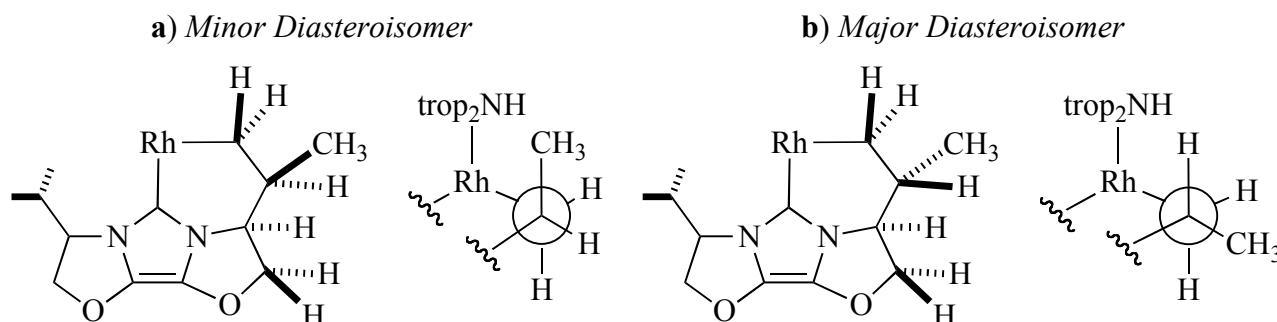
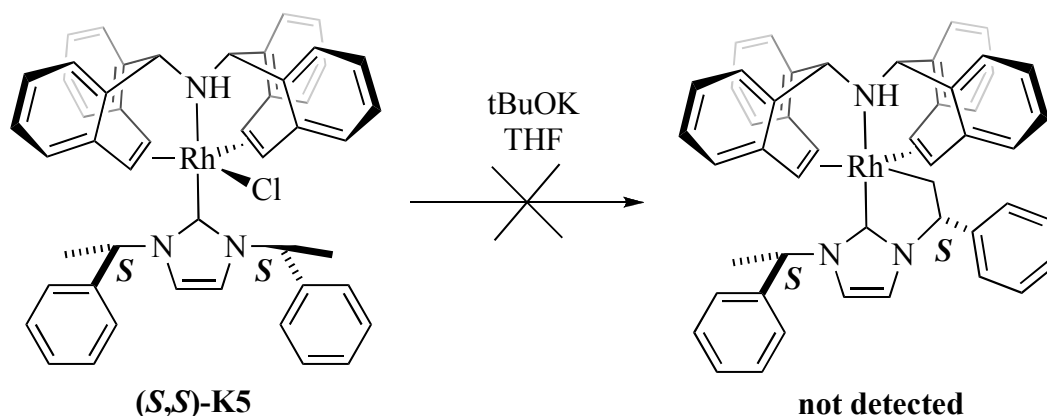


Figure 1.25a-b: Newman projections of (*S,S,R*)-**K12** minor (a) and (*S,S,S*)-**K12** major (b).

1.5.3 Reactivity of [RhCl(trop₂NH)(1,3-bis-((*S*)-1-phenyl-ethyl)imidazolin-2-ylidene)]

The behavior of complex [RhCl(trop₂NH)(1,3-bis-((*S*)-1-phenyl-ethyl)imidazolin-2-ylidene)] (*(S,S)*-**K5**), has been investigated at room temperature under basic conditions. (*(S,S)*-**K5**) has been deprotonated by one equivalent of base (potassium *tert*-butoxide) to the amide (*(S,S)*-**K9**). After two days at room temperature, the ¹H NMR signals of the amide (*(S,S)*-**K9**) disappeared and new compounds were detected (Scheme 1.24).



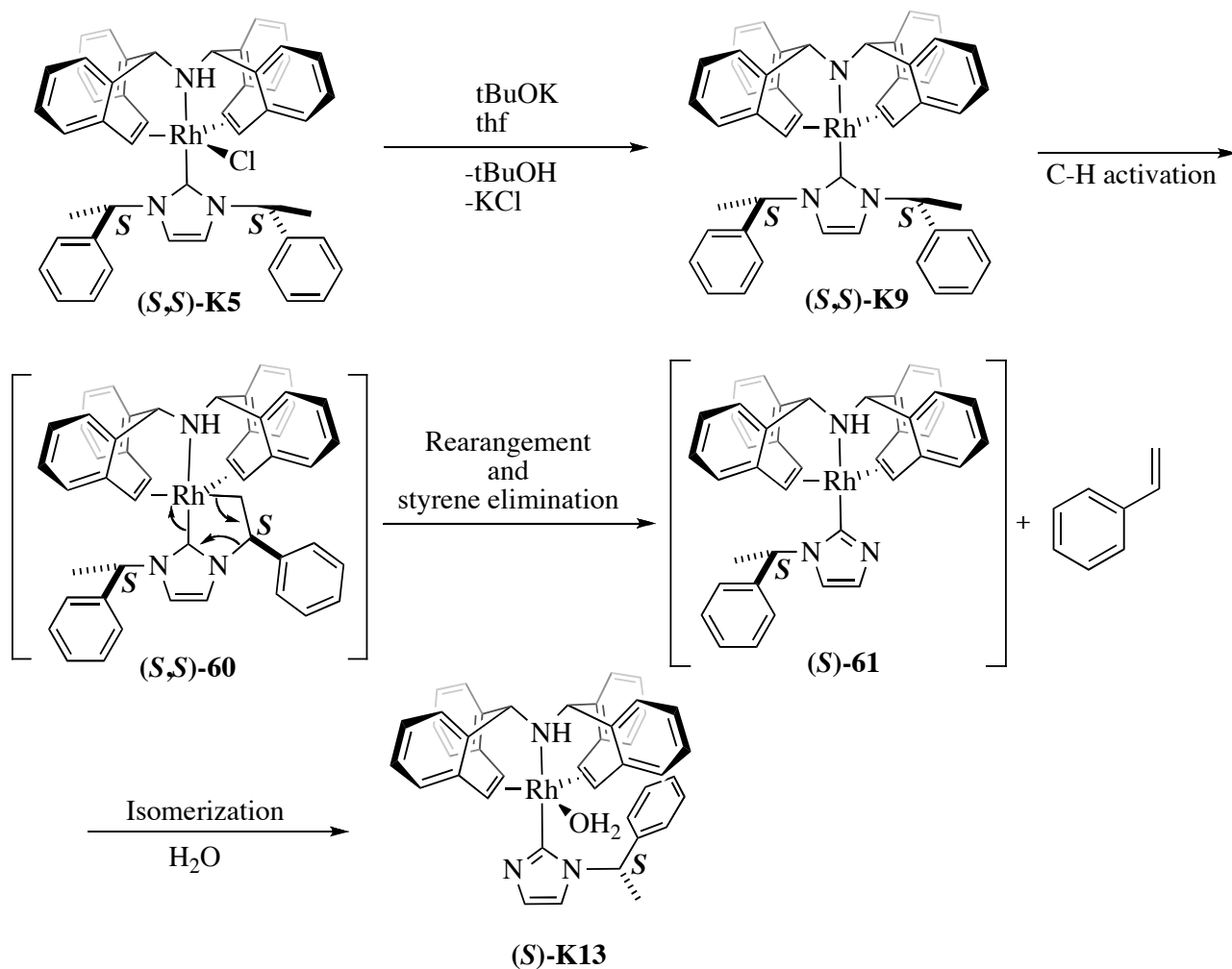
Scheme 1.24: Further reaction of (*(S,S)*-**K5**).

The ¹H NMR spectrum of the product derived from (*(S,S)*-**K5**, showed four different doublets for the olefinic protons and two for the benzylic ones (Table 1.6). Moreover, only one doublet for the methyl group and one quartet for the proton relative to the NCH(Ph)(CH₃) unit were found, which indicated that one of the N-bonded CH(Ph)(CH₃) groups was transformed. The reaction solution

showed an AMX spin system and a ^1H ^{103}Rh HMQC NMR experiment showed no contacts between the rhodium containing molecule and the species giving rise to this set of resonances. By comparison with literature data, this AMX spin system was identified as the one of styrene. Clearly, the decomposition reaction of with the amide (**(S,S)-K9**) took a different course.

Because no crystals of the product suitable for X-ray structure analysis could be grown, the structure of (**S**)-**K13** was elucidated by various NMR experiments. These showed that the complex contains one coordinated water molecule (δ ^1H = 3.17 ppm). The position of the phenyl group was determined from the measured ^1H ^1H NOESY interactions. Through space contacts between the NH group of the bistropamine, the water molecule and the protons of the aryl group in *ortho*, *para* and *meta* positions were detected. These observations suggest that probably the phenyl ring is pointing toward the open side of the molecule. Moreover, the NH chemical shift in (**S**)-**K13** is at 0.65 ppm, shifted more than 4 ppm compared to the starting material [RhCl(trop₂NH)(1,3-bis-(*S*-1-phenyl-ethyl)imidazolin-2-ylidene)] (**(S,S)-K5**). This difference can be explained by the strong shielding induced by the ring current of the benzene ring, pointing toward the NH moiety. Hence, we propose the structure shown in Scheme 1.25 for (**S**)-**K13**.

A plausible mechanism for the formation of (**S**)-**K13** is also shown in Scheme 1.25. In the first step, the metallacycle (**(S,S)-58**) is formed by C-H activation of one of the methyl groups of the 1-phenyl-ethyl substituents on the imidazolium ring across the Rh-N bond of the amide, in analogy with the C-H activation processes leading to **K11** and **K12**. Subsequently, the metallacycle (**(S,S)-60**) rearranges under elimination of one molecule of styrene (driving force of the reaction) to yield (**S**)-**61**. Finally, coordination of one molecule of water present in the system could lead to the product (**S**)-**K13** which we experimentally observed at the end of the reaction cascade. A mechanism involving β -elimination (or α -elimination) from species (**S**)-**61** seems very unlikely. The cyclometallate species (**S**)-**61** is electronically saturated (18 electrons complex) and therefore cannot undergo a classical β -hydrogen elimination. Moreover, the ^1H NMR did not display any hydride signals.



Scheme 1.25: A plausible mechanism for the formation of (S)-K13.

Table 1.6: Characteristic chemical shifts of ^{13}C and ^1H for the benzylic and olefinic protons of complexes K11, (S,S,R)-K12 (minor = m), (S,S,S)-K12 (Major = M) and (S)-K13.

		^1H δ (ppm)	^{13}C δ (ppm)	J_{RhC} (Hz)
K11	benzyl	4.31, 4.39	72.3, 72.4	
	olefin	3.20, 3.56, 3.79, 4.29	51.7, 54.7, 56.4, 61.9	8.7, 8.4, 10, 8
K12	benzyl	4.27, 4.31 <i>m</i>	72.03, 72.09 <i>m</i>	
		4.29 (overlapping) <i>M</i>	72.02, 72.09 <i>M</i>	
	olefin	3.89, 3.75, 4.26, 4.37 <i>m</i>	51.56, 55.14, 51.73, 59.73 <i>m</i>	8.5, 8.6, 8.3, 8.3 <i>m</i>
		3.84, 3.78, 4.09, 4.31 <i>M</i>	51.39, 51.56, 54.91, 59.43 <i>M</i>	7.9, 8.6, 8.6, 9.2 <i>M</i>
(S)-K13	benzyl	4.07, 4.69	70.5, 71.2	
	olefin	4.04, 4.52, 5.93, 6.89	67.2, 70.4, 73.6, 79.8	n.d., n.d., 15.9, 14.1

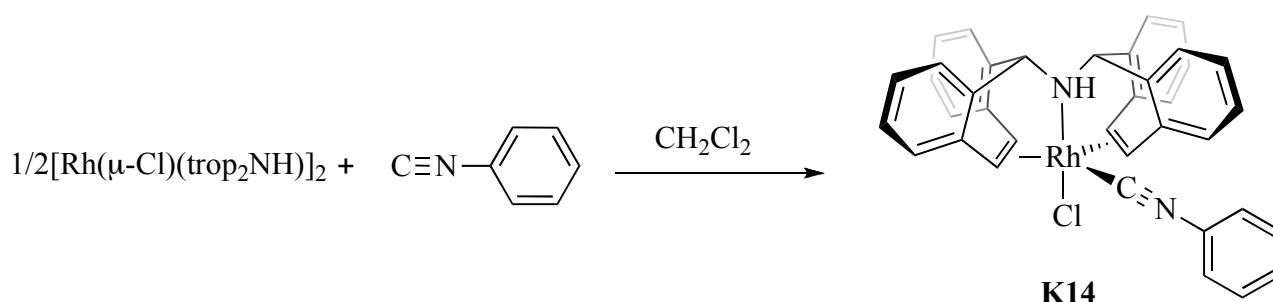
1.6 β -Functionalized Phenyl Isocyanide complexes

As previously discussed in Chapter 1.4.2, **K3**, **K4**, (*S,S*)-**K5** and (*S,S*)-**K6** showed lower catalytic performance with respect to the phosphine system, previously reported by our research group.^{62, 68} The reason of such decreased reactivity is yet unclear but likely the steric hindrance of the N-alkyl substituents of the carbene ligand is responsible for this drop of reactivity. A new type of decomposition reaction has been discovered for compounds of general formula $[\text{RhX}(\text{trop}_2\text{NH})(\text{NHC})]$ whereby the N-alkyl groups at the NHC carbene ligand become intramolecularly activated under the formation to stable metallacycles (see Chapters 1.5). This type of reaction takes place when the reactive Rh-N bond and CH bonds of the N-alkyl groups are in proximity as in **K8**, (*S,S*)-**K9**, and (*S,S*)-**K10** whereas the methyl substituted carbene in **K7** did not undergo a further reaction. Although it is not clear, why the activity of the NHC complexes as transfer hydrogenation catalysts is generally lower, the observed intramolecular C-H activation reaction is clearly one way of catalyst deactivation.

Therefore, we tried to synthesize carbene complexes, which do not carry a N-bonded substituent. This can be simply achieved by replacing the NR unit in the heterocyclic carbene ligand by an oxygen center. This goal can be accomplished, for example, by reacting suitable β -functionalized phenyl isocyanide complexes (see Chapter 1.1.2.1).

1.6.1 Crystal Structure of $[\text{RhCl}(\text{trop}_2\text{NH})(\text{CNPh})]$

The coordination chemistry of phenylisocyanide⁷³ as ligand in rhodium- trop_2NH complexes has been investigated. The reaction with the rhodium precursor $[\text{Rh}(\mu\text{-Cl})(\text{trop}_2\text{NH})_2]$ gave almost quantitatively the new compound $[\text{RhCl}(\text{trop}_2\text{NH})(\text{CNPh})]$ (**K14**) (Scheme 1.26).



Scheme 1.26: Preparation of **K14**.

Complex **K14** was characterized by NMR spectroscopy. The signals for the olefinic and benzylic protons of the trop ligand give rise to two doublets at 5.5 ppm and one singlet at 4.41 ppm, respectively, in the ^1H NMR spectrum.

The quaternary carbon of the isocyano group was not detected in the ^{13}C NMR spectrum. The coordination of the phenylisocyanide is proven by a strong absorption band at 2131 cm^{-1} in the IR spectrum (stretching frequency of the CN group). Furthermore, the complex has been characterized by X-ray diffraction studies. Suitable crystals were obtained by slow diffusion of *n*-hexane in a THF solution of **K14**. Figure 1.26 shows an ORTEP plot of the structure of $[\text{RhCl}(\text{trop}_2\text{NH})\text{CNPh}]$ (**K14**). The pentacoordinate complex has a trigonal bipyramidal structure, bearing the phenylisocyanide ligand in equatorial position.

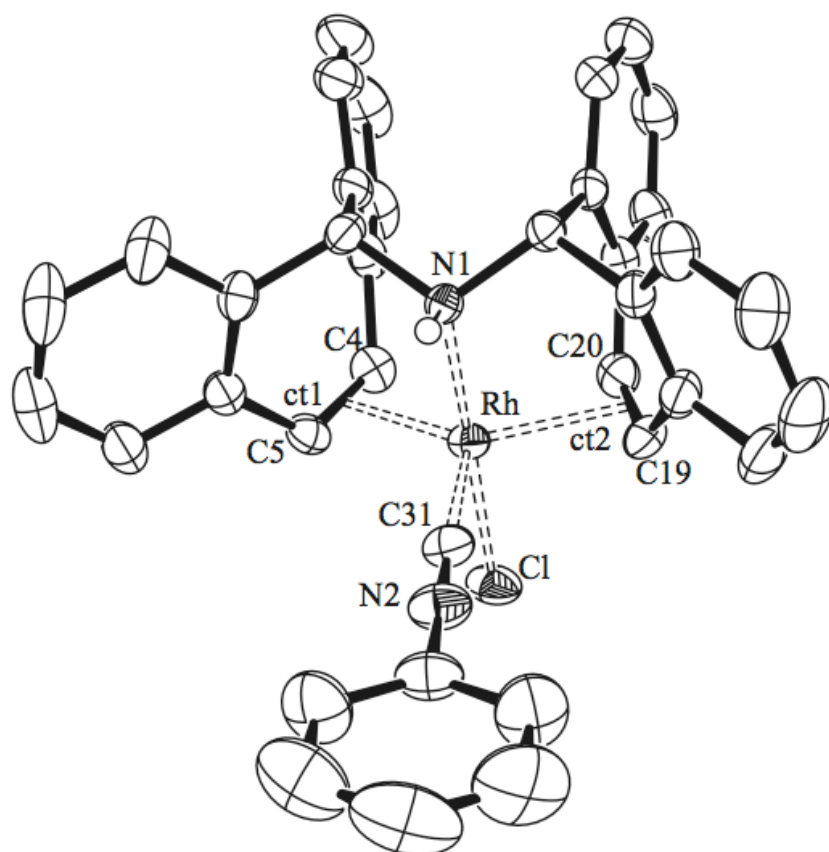
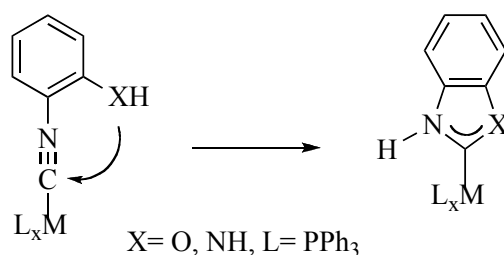


Figure 1.26: ORTEP view of **K14**. Thermal ellipsoids are drawn at 50% probability; hydrogen atoms are omitted for clarity except for the NH. Selected bond lengths [\AA] and angles [$^\circ$]: Rh-Cl 2.3710(4), Rh-N 2.094(1), Rh-C31 2.028(2), Rh-C4 2.161(2), Rh-C5 2.129(2), Rh-ct1 2.022(2), Rh-C19 2.198(2), Rh-C20 2.197(2), Rh-ct2 2.080(2), N1-Rh-Cl 178.43(4), N1-Rh-ct1 90.45(3), N1-Rh-ct2 91.34(4), N1-Rh-C31 90.50(6). ct = centroid of the olefin bond.

The phenyl ring of the isocyanide is lying in the plane of the trigonal bipyramid. The Rh-C bond length is of 2.03 \AA , the chlorine counter anion is in apical position, coordinated to the metal with a distance of 2.37 \AA . The olefinic bond lengths are in the range of previously reported bistropamine rhodium complexes.

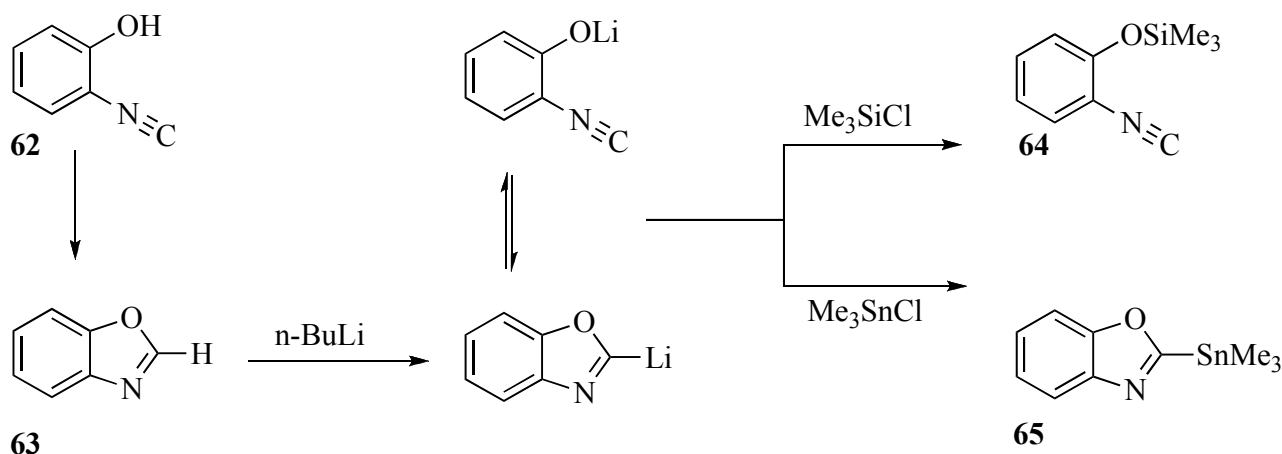
1.6.2 Synthesis of $[\text{RhCl}(\text{trop}_2\text{NH})(2\text{-(trimethylsiloxy)phenylisocyanide})]$ and Crystal structure of $[\text{RhCl}(\text{trop}_2\text{NMe})(2\text{-(trimethylsiloxy)phenylisocyanide})]$

The synthesis of a β -functionalized aryl isocyanide complex of rhodium was subsequently studied. In β -functionalized aryl isocyanides the electrophilic isocyanide and the nucleophilic substituent are suitably oriented to allow an intramolecular nucleophilic attack as depicted in Scheme 1.27. The geometry and the aromaticity of the resulting ligand serve as a driving force for this reaction (Chapter 1.1.2.1).



Scheme 1.27: Formation of carbene complexes from coordinated β -functional phenyl isocyanides.

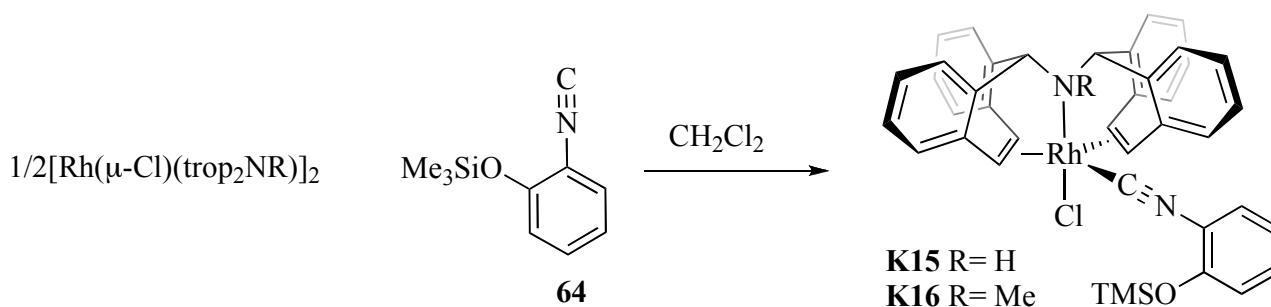
The synthesis of 2-hydroxyphenyl isocyanide (**62**) was attempted first. Differently from aliphatic isocyanides, the free 2-hydroxyethyl isocyanide (**63**) is not stable and cyclizes to benzoxazole **64**.⁷⁴ Lithiation of **64** leads to an equilibrium between lithiated **63** and **62**. Reaction of the mixture with Me_3SiCl yields regiospecifically 2-(trimethylsiloxy)phenyl isocyanide (**64**), while reaction with Me_3SnCl gives the C-metallate 2-trimethylstannylbenzoxazole (**65**) (Scheme 1.28).⁷⁵



Scheme 1.28: Preparation of 2-(trimethylsiloxy)phenyl isocyanide **64**.

The isocyanide **64** was readily coordinated to the rhodium metal fragment, in a similar way to **K14**, as shown in Scheme 1.29. The reaction of an excess of **64** with a dichloromethane suspension

of $[\text{Rh}(\mu\text{-Cl})(\text{trop}_2\text{NH})]_2$ yields complex $[\text{RhCl}(\text{trop}_2\text{NH})(2\text{-}(\text{trimethylsiloxy})\text{phenylisocyanide})]$ (**K15**) as yellow powder.



Scheme 1.29: Synthesis of **K15** and **K16**.

The ^1H NMR and ^{13}C NMR spectra show the expected features for pentacoordinate trop_2NH rhodium complexes, with doublets at 5.35 ppm and 5.58 ppm for the olefinic protons and a singlet at 4.40 ppm for the benzylic proton in the range expected for similar trop_2NH complexes. The ^{13}C NMR spectrum displays a doublet at 161.75 ppm with a rhodium-carbon coupling of 37.75 Hz.

No suitable crystals of **K15** were obtained for X-ray diffraction studies but the related complex $[\text{RhCl}(\text{trop}_2\text{NMe})(2\text{-}(\text{trimethylsiloxy})\text{phenylisocyanide})]$ (**K16**) has been synthesized and crystallized from a concentrated dichloromethane solution. Figure 1.27 shows the structure of **K16** determined through a single crystal X-ray diffraction study.

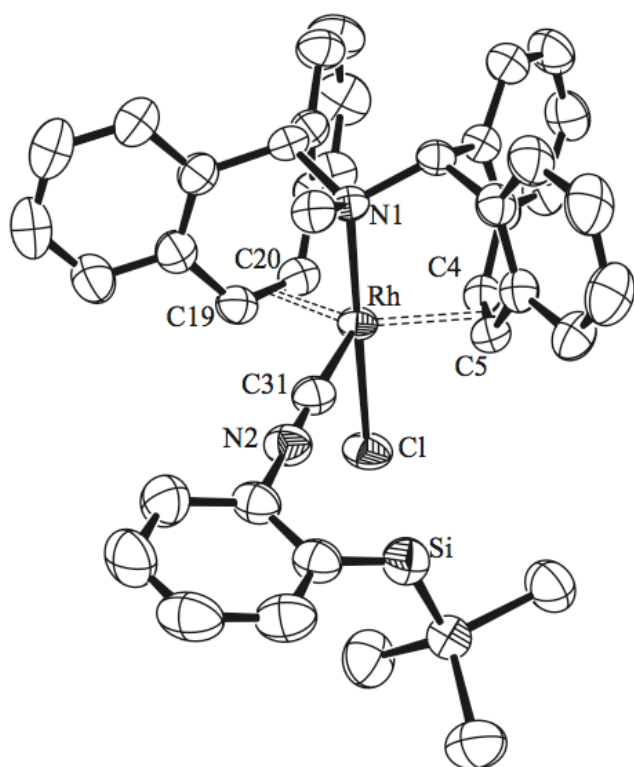
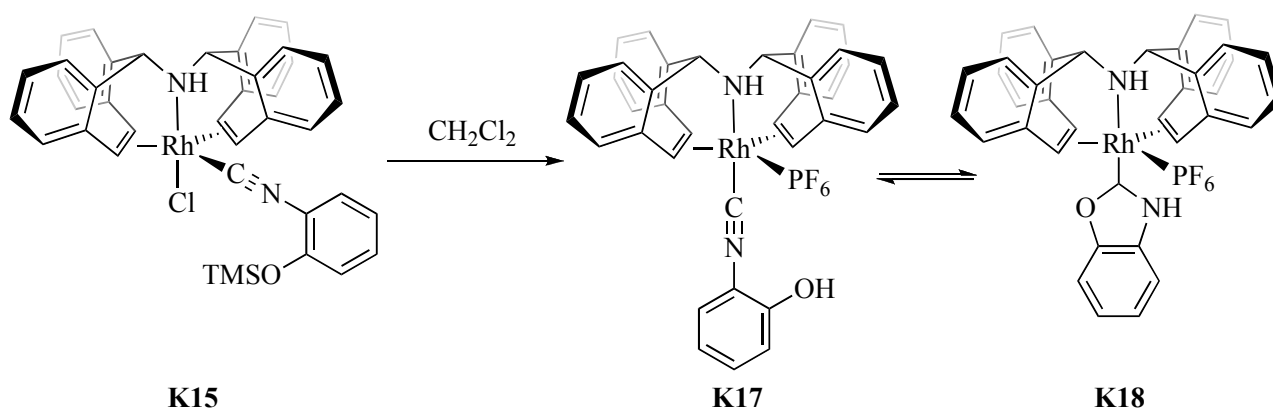


Figure 1.27: ORTEP view of **K16**. Thermal ellipsoids are drawn at 50% probability; hydrogen atoms are omitted for clarity. Selected bond lengths [Å] and angles [°]:
 Rh-Cl 2.3393(7),
 Rh-N1 2.122(2),
 Rh-C31 2.038(3),
 Rh-C4 2.189(3),
 Rh-C5 2.183(3),
 Rh-ct1 2.07(3),
 Rh-C19 2.178(3),
 Rh-C20 2.175(3),
 Rh-ct2 2.07(3),
 N1-Rh-Cl 178.36(6),
 N1-Rh-C31 96.23(9).
 ct = centroid of the olefin bond.

1.6.3 Synthesis of [RhOTf(trop₂NH)(2,3-dihydrobenzoaxol-2-ylidene)]

It has been shown that the electrophilicity of coordinated isocyanide is directly correlated with the positive charge on the carbon atom.⁷⁶ Therefore, the chloride abstraction was planned, prior to the cleavage of the protecting group of the alcohol. The reaction has been performed in the presence of a halide scavenger, e.g. Et₃OPF₆, as depicted in Scheme 1.30.



Scheme 1.30: Synthesis of [RhOTf(trop₂NH)(2,3-dihydrobenzoaxol-2-ylidene)] **K18**.

The reaction progress was followed by NMR spectroscopy. After a few days, the formation of the alcohol **K17** and of the cyclized carbene [RhOTf(trop₂NH)(2,3-dihydrobenzoaxol-2-ylidene)] (**K18**) could be detected. The ¹H NMR spectrum displays characteristic peaks at 9.8 ppm for the OH resonance and at 13.7 ppm for the NH resonance. All the attempts to obtain larger quantities of pure **K18** through crystallization from the reaction mixture failed and resulted in the decomposition into unidentified material. By chance, single crystals of a comparable complex, **K18'**, of sufficient quality were obtained in one experiment by slow diffusion of *n*-hexane into the reaction mixture in THF (with Et₃OPF₆ as chloride scavenger), which allowed the structure determination of **K18'** (Figure 1.28).

The pentacoordinate complex has a trigonal bipyramidal structure. The counter anion PF₂O₂⁻, resulting from the hydrolysis of the PF₆⁻ counter anion, is coordinated to the metal center and the bond length between the rhodium center and the oxygen of the PF₂O₂⁻ group is of 2.35 Å. The carbene moiety is apical position, like the previously synthesized NHC complexes **K3**, **K4**, (**S,S**)-**K5** and (**S,S**)-**K6**. The bond length Rh-C31 is of about 1.97 Å, only slightly shorter than the one for **K5** (2.05 Å). The olefin bond lengths are in the range of other similar compounds.

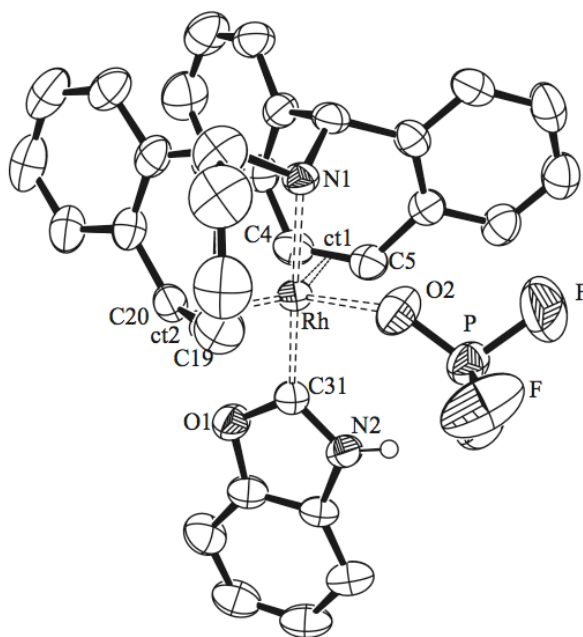
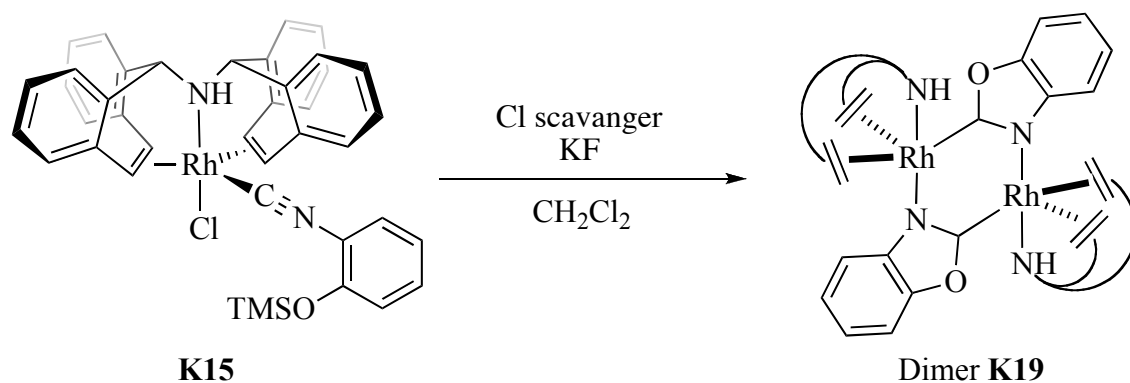


Figure 1.28: ORTEP view of **K18'**. Thermal ellipsoids are drawn at 50% probability; hydrogen atoms are omitted for clarity. Selected bond lengths [\AA] and angles [$^\circ$]: Rh-N1 2.153(9), Rh-C31 1.97(1), Rh-C4 2.17(1), Rh-C5 2.16(1), Rh-ct1 2.0(1), Rh-C19 2.19(1), Rh-C20 2.17(1), Rh-ct2 2.0(1), Rh-O2 2.347(9), NH₂-O(PO₂F₂) 3.754(5), N1-Rh-C31 178.6(4), N1-Rh-O2 79.1(3), N1-Rh-ct1 90.2(3), N1-Rh-ct2 90.5(3). ct = centroid of the olefin bond.

1.6.4 PGSE experiments

The mixture of compounds **K17/K18** has been tested for transfer hydrogenation catalysis under comparable conditions to those used in experiments with **K3**, **K4**, (**S,S**)-**K5** and (**S,S**)-**K6** (Chapter 1.4.2). A ratio catalyst to substrate (benzophenone) 1:10'000 has been used. As reducing agent *i*PrOH was employed (0.5 M). Potassium *tert*-butoxide was used as base (70 eq) and the catalytic test was performed at 60°C.

Under such conditions compound **K18** displayed a TOF of 1040 h⁻¹ measured after one hour and of 188 h⁻¹ after 48 hours, and a TON calculated after 48 hours of 9000 h⁻¹. Even though the catalyst cannot undergo intramolecular C-H activation, it does not show higher activity compared to the triphenylphosphine complex. Again, the reason for this low activity is not unambiguously clear but a deactivation pathway of **K17/K18** as catalyst could be due to dimerization under formation of a six membered dimetallaheterocycle under the employed basic conditions. Indeed, the formation of such a dimeric species **K19** was observed when the synthesis of **K18** from **K15** was attempted in the presence of KF (Scheme 1.31).



Scheme 1.31: Formation of the dimer **K19**.

Based on the chemical shift at 14 ppm⁷⁶, the NH of the carbene in compound **K18** is highly acidic. It is therefore reasonable to assume, that this NH function is more easily deprotonated than the NH function of the trop₂NH ligand. Suitable X-ray structure of the dimeric compound **K19**, were obtained by slow diffusion of *n*-hexane in a THF solution of **K19** and Figure 1.29 shows the ORTEP plot of the structure as a result of a single crystal diffraction study.

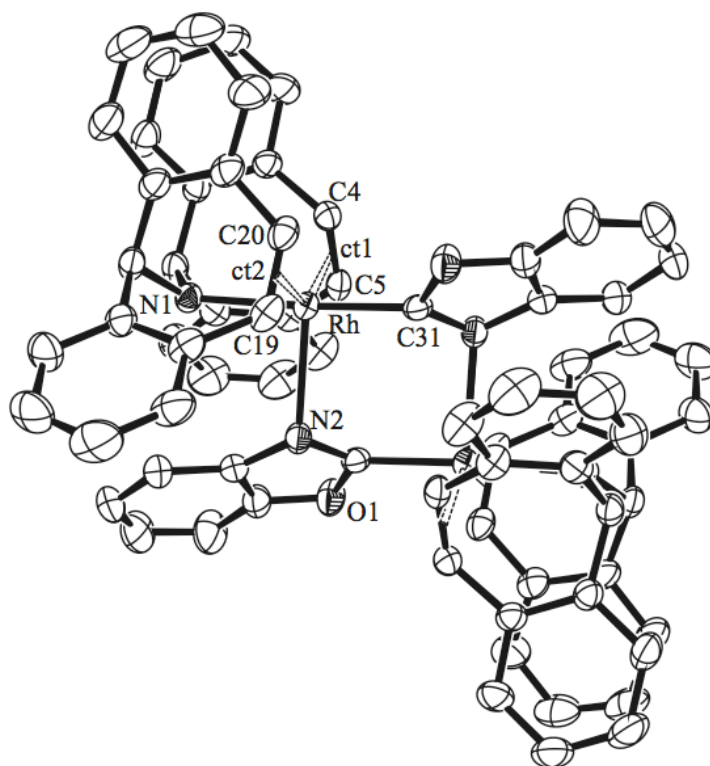


Figure 1.29: ORTEP view of **K19**. Thermal ellipsoids are drawn at 50% probability; hydrogen atoms are omitted for clarity. Selected bond lengths [Å] and angles [°]: Rh-N1 2.172(2), Rh-C4 2.156(3), Rh-C5 2.185(3), Rh-ct1 2.05(3), Rh-C19 2.164(3), Rh-C20 2.168(3), Rh-ct2 2.05(3), Rh-C31 2.000(2), Rh-N2 2.374(2), ct1-Rh-ct2 133.77(7), N1-Rh-N2 88.26(8), N1-Rh-C31 176.04(9). ct = centroid of the olefin bond

The complex **K19** consists of a dirhodaheterocycle in which each Rh center has a trigonal bipyramidal coordination sphere. The carbene units are placed in axial position with a bond length Rh-C31 of about 2.00 Å (compare the monomer **K18'** which shows a bond length rhodium-carbene of 1.97 Å). The deprotonated NH of the carbene is coordinated to the metal center in the equatorial position with a distance of about 2.4 Å, significantly longer than the Rh-N bond length to the bistropamine ligand (2.17 Å). The olefinic bonds are marginally shorter than normally found in similar pentacoordinate rhodium complexes. To further confirm the dimerization of compound **K18** in solution and not only in the solid state, we determined the diffusion coefficient (D) of **K19** by PGSE[§] measurements in CD₂Cl₂. A PGSE NMR diffusion measurement⁷⁷ consists of a spin echo sequence in combination with the application of pulsed field gradients. The diffusion constant (D) can be calculated from equation (1):

$$\ln\left(\frac{I}{I_0}\right) = -(\gamma\delta)^2 G^2 \left(\Delta - \frac{\delta}{3}\right) D \quad (1)$$

G = gradient strength, Δ = delay between the midpoints of the gradient, δ = diffusion coefficient, D = gradient length.

The slope of the regression line by plotting $\ln(I/I_0)$ (I/I_0 = observed spin echo intensity/intensity without gradient) vs. G^2 allows determining D (Figure 1.30).

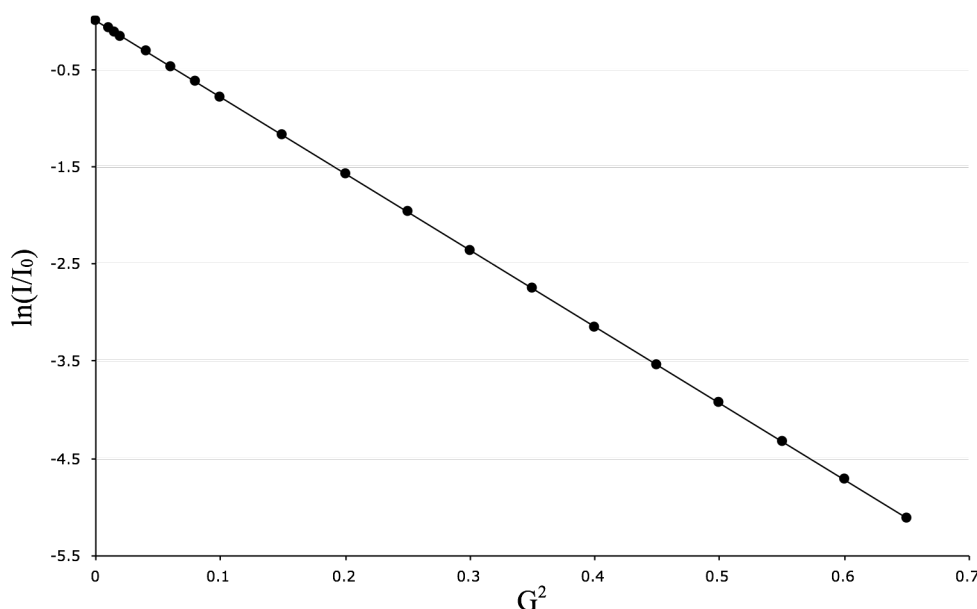


Figure 1.30: Plot of $\ln(I/I_0)$ vs. G^2 .

[§] Pulsed Field Gradient Spin-Echo (PGSE)

Compounds with small hydrodynamic radii move faster, and reveal larger diffusion coefficients D . The D -value can be related to the hydrodynamic radii of the molecule *via* the Stocks-Einstein equation (2) (this allows for a viscosity correction).

$$D = \frac{kT}{6\pi\eta r_H} \quad (2)$$

$k = 1.381 \times 10^{-23}$ [JK⁻¹] Boltzmann constant, T = absolute temperature, η = viscosity, r_H = hydrodynamic radii

Table 1.7 shows the Diffusion coefficient (D), hydrodynamic radii (r), and spherical volume (V) of **K19** determined by the PGSE measurement. The volume of the molecule (V_{calc}) in a dichloromethane solution is 1264 Å³. This is in agreement with the volume of the molecule calculated from the crystal structure (V_{Crystal}). Therefore we conclude that molecule **K19** is predominantly a dimer in solution as well.

Table 1.7: Diffusion coefficient (D), hydrodynamic radii (r), and spherical volume (V) of **K19** in CD₂Cl₂ (400 MHz, 298 K)[†].

Solvent	NMR nucleus	D [10^{-10} m ² s ⁻¹]	r_H [Å]	V_{calc} [Å ³]	V_{Crystal} [Å ³]
CD ₂ Cl ₂	¹ H	7.87	6.7	1264	1476

[†] Calibration with HDO/D₂O: $m = 2.005 \times 10^{-3}$, $\Delta = 167.75$ ms, $\delta = 1.75$ ms, $D = 1.902$. Measured: $m = -7.863 \times 10^{-4}$, $\Delta = 300$ ms, $\delta = 2$ ms, $\eta = 0.4173 \times 10^{-3}$ Kgs⁻¹m⁻¹.

1.7 Conclusions and Outlook

A suitable and convenient method for the preparation of new N-heterocyclic carbene rhodium(I) complexes bearing the trop₂NH ligand could be developed. It consists in the reaction of a phosphine rhodium amido complex with an imidazolium salt which proceeds under displacement of the phosphine ligand by the N-heterocyclic carbene (NHC) ligand which is formed in situ. This method allows a variety of complexes to be synthesized and chiral complexes are readily available from enantiomerically pure imidazolium salts such as **57** and **58**.

The successful formation of **K3**, **K4**, (**S,S**)-**K5** and (**S,S**)-**K6** from **K2** by displacement of the triphenylphosphine ligand clearly shows the better binding properties of NHCs as a strong σ -donor ligands and importantly clearly demonstrate the lability of the PPh₃ ligand in **K2**.

By extensive X-ray diffraction and NMR spectroscopic studies, the close similarity of NHC and phosphine complexes of the type [Rh(trop₂NH)(L)]⁺ (L = PR₃, NHC) was clearly established. Importantly, the structure determination for (**S,S**)-**K6** clearly shows that these cations have likewise saw-horse type structures (trigonal bipyramids with one missing equatorial corner).

The quantitative deprotonation of the NHC complexes was accomplished with stoichiometric amounts of base (potassium *tert*-butoxide). The resulting amido complexes are highly dynamic on the NMR-time scale and show inversion at the nitrogen and rhodium centers probably *via* a planar transition state. In the particular case of **(S,S)-K10** the activation energy for the inversion was determined and the values calculated are in agreement with those measured for **K2**.

Despite the described analogous features of [Rh(trop₂N)(NHC)] and [Rh(trop₂N)(PPh₃)] and the lower lability of NHCs, the catalytic activity of the N-heterocyclic carbene amides in transfer hydrogenations was disappointingly lower with respect to **K2**. This result is attributed to higher steric congestion caused by the N-substituents, which block the approach of the substrate to the Rh-N bond as reactive site. Furthermore, when the chiral compounds **(S,S)-K5** and **(S,S)-K6** were employed, no enantiomeric excess could be detected. The reason for this lack of stereoselectivity and the low activity is not fully understood at this stage of the investigations.

Possible deactivation routes were discovered. The N-alkyl groups of the NHC ligands can easily undergo *intra*-molecular C-H activation across the Rh-amide bond under relatively mild conditions to form cyclometallate complexes. These processes clearly occur with N-bonded isopropyl- (see **(S,S)-K6**), 1-ethyl-phenyl- (see **(S,S)-K5**) and cyclohexyl groups (see **K5**). In one special case, a further rearrangement reaction under extrusion of styrene has been observed. These intramolecular C-H activation reactions are the first of their kind and demonstrate that C-H bonds can successfully be added across late transition metal amide bonds. This observation does not only add a new facet to the decomposition of fashionable NHC ligands but may be of conceptual importance for the development of systems capable of C-H activations in general (*vide infra*).

In order to circumvent the intramolecular C-H activation of the NHC ligands, **K18** was synthesized, where an oxygen atom replaces one R-N group. Disappointingly, **K18** showed low catalytic activity in transfer hydrogenation reactions due to the formation of dimeric species in solution **K19**.

In summary we conclude that the incorporation NHC ligands into Rh(trop₂NH) complexes does not improve the catalytic performance as initially hoped. While in the phosphane complexes the P-bonded substituents point away from the reactive Rh-N site, the N-bonded substituents in NHC complexes do block this site and kinetically slow down the catalytic performance. Furthermore, unexpected deactivation reactions were observed. The best candidate for an active carbene complex will probably be a dioxycarbene, where both nitrogen atoms are replaced by oxygens, but such species have not been isolated yet, probably due to their great instability (Chapter 1.1.1).

Thus, the best co-ligands in Rh(trop₂N)-based catalysts remain phosphines despite their lability. A way to overcome this obstacle may be to increase the thermodynamic stability of the complexes by an additional chelating effect. The conceivable tetrachelate ligand, shown in Figure 1.31, may fulfill such characteristic.

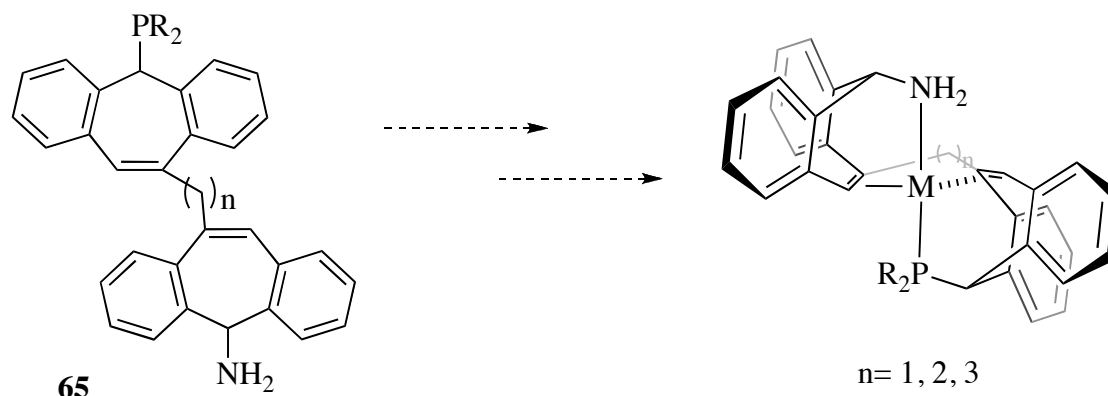


Figure 1.31: Conceivable tetrachelate ligand.

- ¹ D. Bourissou, O. Guerret, F.P. Gabbai, G. Bertrand, *Chem. Rev.*, **2000**, 100, 39.
- ² J.F. Harrison, *J. Am. Chem. Soc.*, **1971**, 93, 4112; J.F. Harrison, C.R. Liedtke, J.F. Liebman, *J. Am. Chem. Soc.*, **1979**, 101, 7162.
- ³ H. Tomioka, E. Iwamoto, H. Itakura, K. Hirai, *Nature*, **2001**, 412, 626.
- ⁴ L.J. Pauling, *J. Chem. Soc. Chem. Commun.*, **1980**, 688.
- ⁵ H.W. Wanzlick, H.J. Kleiner, *Angew. Chem. Int. Ed. Engl.*, **1962**, 1, 2375.
- ⁶ H.W. Wanzlick, H.J. Schönherr, *Liebigs. Ann. Chem.*, **1970**, 731, 176; H.W. Wanzlick, H.J. Schönherr, *Chem. Ber.*, **1970**, 103, 1037.
- ⁷ A.J. Arduengo III, R. L. Harlow, M. Kline, *J. Am. Chem. Soc.*, **1991**, 113, 361.
- ⁸ W.A. Herrmann, M. Elison, J. Fischer, C. Köcher, G.R.J. Arthus, *Chem. Eur. J.*, **1996**, 2, 772; W.A. Herrmann, C. Köcher, L.J. Goossen, G.R.J. Arthus, *Chem. Eur. J.*, **1996**, 2, 1627.
- ⁹ N. Kuhn, T. Kratz, *Synthesis*, **1993**, 561.
- ¹⁰ D. Enders, K. Breuer, G. Raabe, J. Runsink, J.H. Teles, J. P. Melder, K. Ebel, S. Brode, *Angew. Chem. Int. Ed. Engl.*, **1995**, 34, 1021.
- ¹¹ D. Bourissou, O. Guerret, F.P. Gabbai, G. Bertrand, *Chem. Rev.*, **2000**, 100, 39-91 and references therein.
- ¹² K. Öfele, W.A. Herrmann, D. Mihalios, M. Elison, E. Herdtweck, W. Scherer, J. Mink, *J. Organomet. Chem.*, **1993**, 459, 177.
- ¹³ K. Öfele, M. Herberhold, *Z. Naturforsch.*, **1973**, 28b, 306.
- ¹⁴ K. Öfele, *J. Organomet. Chem.*, **1968**, 12, P42.
- ¹⁵ C. Köcher, W.A. Herrmann, *J. Organomet. Chem.*, **1997**, 532, 261.
- ¹⁶ W.A. Herrmann, C.P. Reisinger, M. Spiegler, *J. Organomet. Chem.*, **1998**, 557, 93.
- ¹⁷ D. Enders, H. Gielen, G. Raabe, J. Runsink, J. Teles, *H. Chem. Ber.*, **1997**, 130, 1253.
- ¹⁸ For a review see: M.F. Lappert, *J. Organomet. Chem.*, **1988**, 358, 185.
- ¹⁹ C.Y. Liu, D.Y. Chen, G.H. Lee, S.M. Peng, S.T. Liu, *Organometallics*, **1996**, 15, 1055 and references therein.

- ²⁰ Reviews on coordination chemistry of isocyanides: (a) E. Singleton, H.E. Oosthuizen, *Adv. Organomet. Chem.*, **1983**, 22, 209. (b) P.M. Treichel, *Adv. Organomet. Chem.*, **1993**, 11, 21.
- ²¹ W. Beck, W. Weigand, U. Nagel, M. Schaal, *Angew. Chem. Int. Ed. Engl.*, **1984**, 23, 377; E. Bär, A. Völkl, F. Beck, W.P. Fehlhammer, *J. Chem. Soc. Dalton Trans.*, **1986**, 863.
- ²² W.P. Fehlhammer, E. Bär, B. Boyadjiev, *Z. Naturforsch.*, **1986**, 41b, 1023.
- ²³ G. Beck, W.P. Fehlhammer, *Angew. Chem. Int. Ed. Engl.*, **1988**, 27, 1344.
- ²⁴ P.J. Brothers, W.R. Roper, *Chem. Rev.*, **1988**, 88, 1293.
- ²⁵ R.Z. Ku, D.Y. Chen, G.H. Lee, S.M. Peng, S.T. Liu, *Angew. Chem. Int. Ed. Engl.*, **1997**, 36, 2631.
- ²⁶ U. Kernbach, W.P. Fehlhammer, *Inorg. Chim. Acta*, **1995**, 235, 299.
- ²⁷ S.T. Liu, T.Y. Hsieh, G.H. Lee, S.M. Peng, *Organometallics*, **1998**, 17, 993.
- ²⁸ P.L. Arnold, *Heterot. Chem.*, **2002**, 13, 534.
- ²⁹ I.J.B. Lin, C.S. Vasam, *Comments. Inorg. Chem.*, **2004**, 25, 75.
- ³⁰ L. Cavallo, A. Correa, C. Constabile, H. Jacobsen, *J. Organomet. Chem.*, **2005**, 690, 5407.
- ³¹ W.A. Herrmann et al., *J. Organomet. Chem.*, **1998**, 557, 93.
- ³² M. Scholl, S. Ding, C.W. Lee, R.H. Grubbs, *Org. Lett.*, **1999**, 1, 953.
- ³³ E.L. Dias, S.T. Nguyen, R.H. Grubbs, *J. Am. Chem. Soc.*, **1997**, 119, 3887.
- ³⁴ C. Yang, S.P. Nolan, *Synlett*, **2001**, 1539
- ³⁵ G.A. Grasa, M.S. Viciu, J. Huang, C. Zhang, M.L. Trudell S.P. Nolan, *Organometallics*, **2002**, 21, 2866
- ³⁶ G.A. Grasa, M.S. Viciu, J. Huang, S.P. Nolan, *J. Org. Chem.*, **2001**, 66, 7729.
- ³⁷ J.F. Hartwig, *Angew. Chem. Int. Ed.*, **1998**, 37, 2046.
- ³⁸ A.C. Hillier, H.M. Lee, E.D. Stevens, S.P. Nolan, *Organometallics*, **2001**, 20, 4246; H.M. Lee, T. Jiang, E.D. Stevens, S.P. Nolan, *Organometallics*, **2001**, 20, 1255; L.D. Vasquez-Serrano, B.T. Owens, J.M. Buriak, *Chem. Commun.*, **2002**, 2518.
- ³⁹ A detailed review on the topic: V. César, S. Bellemin-Laponnaz, L.H. Gade, *Chem. Soc. Rev.*, **2004**, 33, 619.
- ⁴⁰ W.A. Herrmann, L.J. Goossen, C. Köcher, G.R.J. Artus, *Angew. Chem. Int. Ed.*, **1996**, 35, 2805.
- ⁴¹ A. J. Arduengo, III, U.S. Patent N°5.182.405, 1993.
- ⁴² T.J. Seiders, D.W. Ward, R.H. Grubbs, *Org. Lett.*, **2001**, 3, 3225.
- ⁴³ J.J. Van Veldhuizen, S.B. Garber, J.S. Kinsbury, A.H. Hoveyda, *J. Am. Chem. Soc.*, **2002**, 124, 4954.
- ⁴⁴ C. Bolm, M. Kesselgruber, G. Raabe, *Organometallics*, **2002**, 21, 707.
- ⁴⁵ D. Broggini, A. Togni, *Helv. Chim. Acta*, **2002**, 85, 2518.
- ⁴⁶ P. Barbaro, C. Bianchini, A. Togni, *Organometallics*, **1997**, 16, 3004.
- ⁴⁷ S. Gischig, A. Togni, *Organometallics*, **2003**, 22, 618.
- ⁴⁸ L. Fadini, A. Togni, *Chem. Commun.*, **2003**, 30.
- ⁴⁹ M.C. Perry, X. Cui, K. Burgess, *Tetrahedron: Asymmetry*, **2002**, 13, 1969.
- ⁵⁰ L.G. Bonnet, R.E. Douthwaite, B.M. Kariuki, *Organometallics*, **2003**, 22, 4187.
- ⁵¹ F. Glorius, G. Altenhoff, R. Goddard, C. Lehmann, *Chem. Commun.*, **2002**, 2704.
- ⁵² G. Altenhoff, R. Goddard, C. Lehmann, F. Glorius, *J. Am. Chem. Soc.*, **2004**, 126, 15195.
- ⁵³ H. Lebel, M.K. Janes, A.B. Charette, S.P. Nolan, *J. Am. Chem. Soc.*, **2004**, 126, 5046.
- ⁵⁴ S. Gründemann, A. Kovacevic, M. Albrecht, J.W. Faller, R.H. Crabtree, *J. Am. Chem. Soc.*, **2002**, 124, 10473.
- ⁵⁵ A.W. Waltman, T. Ritter, R.H. Grubbs, *Organometallics*, **2006**, 25, 4238.
- ⁵⁶ S. Fantasia, H. Jacobsen, L. Cavallo, S.P. Nolan, *Organometallics*, **2007**, 26, 3286.
- ⁵⁷ R.F.R. Jazzar, S.A. Macgregor, M.F. Mahon, S.P. Richards, M.K. Whittlesey, *J. Am. Chem. Soc.*, **2002**, 124, 4944

- ⁵⁸ S.H. Hong, A. Chlenov, M.W. Day, R.H. Grubbs, *Angew. Chem. Int. Ed.*, **2007**, 46, 5148.
- ⁵⁹ M. Prinz, M. Grosche, E. Herdtweck, W.A. Herrmann, *Organometallics*, **2000**, 19, 1692.
- ⁶⁰ Y. Ma, R.G. Bergman, *Organometallics*, **1994**, 13, 2548.
- ⁶¹ T. Büttner, Diss. ETH No. 15503, Zürich, **2004**, "Synthesis and Reactivity of Penta Coordinated Rhodium Amine-Diolefin Complexes".
- ⁶² P. Maire, T. Büttner, F. Breher, P. Le Floch, H. Grützmacher, *Angew. Chem. Int. Ed.*, **2005**, 44, 6318.
- ⁶³ A.J. Arduengo III, US Patent, 5.077.414.
- ⁶⁴ E.A. Mistyukov, *Mendeleev Commun.*, **2006**, 258.
- ⁶⁵ V. César, S. Bellemin-Laponnaz, L.H. Gade, *Eur. J. Inorg. Chem.*, **2004**, 3436.
- ⁶⁶ W.A. Herrmann, G.D. Frey, E. Herdtweck, M. Steinbeck, *Adv. Synt. Catal.*, **2007**, 349, 1677; M. Moser, B. Wucher, D. Kunz, F. Rominger, *Organometallics*, **2007**, 26, 1024; K. Denk, P. Sirsch, W.A. Herrmann, *J. Organomet. Chem.*, **2002**, 649, 219; X. Yu, B.O. Patrick, B.R. James, *Organometallics*, **2006**, 25, 2359; J.M. Praetorius, M.W. Kotyk, J.D. Webb, R. Wang, C.M. Crudden, *Organometallics*, **2007**, 26, 1057.
- ⁶⁷ M. Ogasawara, D. Huang, W.E. Streib, J.C. Huffmann, N. Gallego-Planas, F. Maseras, O. Eisenstein, K.G. Caulton, *J. Am. Chem. Soc.*, **1997**, 119, 8642.
- ⁶⁸ T. Zweifel, J.-V. Naubron, T. Ott, H. Grützmacher, *Angew. Chem. Int. Ed.*, **2008**, 47, 3245.
- ⁶⁹ M.S. Sanford, J. A. Love, R.H. Grubbs, *J. Am. Chem. Soc.*, **2001**, 123, 6543.
- ⁷⁰ S. Fantasia, J.L. Petersen, H. Jacobsen, L. Cavallo, S.P. Nolan, *Organometallics*, **2007**, 26, 5880.
- ⁷¹ P. Maire, T. Büttner, F. Breher, P. Le Floch, H. Grützmacher, *Angew. Chem. Int. Ed.*, **2005**, 44, 6318.
- ⁷² A.D. Bain, G.J. Duns, *Can. J. Chem.*, **1996**, 74, 819.
- ⁷³ W.P. Weber, G.W. Gokel, I.K. Ugi, *Angew. Chem. Int. Ed.*, **1972**, 6, 530.
- ⁷⁴ J.P. Ferris, F.R. Antonucci, R.W. Trimmer, *J. Am. Chem. Soc.*, **1973**, 95, 919.
- ⁷⁵ P. Jutzi, U. Gilge, *J. Organomet. Chem.*, **1983**, 246, 159.
- ⁷⁶ M. Tamm, F.E. Hahn, *Coord. Chem. Rev.*, **1999**, 182, 175.
- ⁷⁷ P.S. Pregosin, E. Martinez-Viviente, P.G.A. Kumar, *Dalton Trans.*, **2003**, 4007.

2 Platinum and Palladium Complexes

The *intra*-molecular C-H activation of alkyl groups has been described in Chapter 1. As it will be later discussed, the activation of alkanes along a M-X bond is often observed for early transition metal complexes, whereas for complexes with late transition metals, C-H activation *via* an oxidative addition mechanism is common. In the literature, there are no examples of alkane activation along a M-X bond with M being a late transition metal. The complexes reported in the first chapter of this thesis represent therefore rare and interesting examples albeit the C-H activation process occurred only in an *intra*-molecular fashion. There is a high interest in achieving *inter*-molecular C-H activations and this prompted us to synthesize isoelectronic platinum complexes of trop_2NH and explore their reactivity. It is known that platinum complexes are capable of activating alkanes as it will be discussed in the following introduction. Since we were interested only in the C-H activation process, the discussion will focus on this step and on the different systems present in the literature. In particular, a detailed section has been dedicated to platinum chemistry (Chapter 2.1.2) and to 1,2-additions (Chapter 2.1.3).

2.1 Introduction

Despite the progresses made in synthetic chemistry and the capability of organic chemists in converting nearly every class of organic compounds into different chemicals, converting alkanes into functionalized chemicals still represent a challenge. The inertness of this class of saturated compounds towards selective synthetic reagents is mostly due to the stable C-C and C-H bonds.[§] Alkanes lack empty orbitals of low energy or occupied orbitals of high energy that could readily participate in chemical reactions (differently from olefins and alkynes).

Radical reactions started by chlorine atoms have been long known [equation (1)] and the alkyl radical produced can be converted to other kinds of organic molecules [equation (2)]. However, this process is not very selective.



Alkanes do also react at elevated temperatures in oxygen atmosphere (combustion) but normally the products formed undergo faster reaction in comparison with alkanes and proceed to the

[§]For alkanes the C-H bond energies values are in the range of 90 to 98 kcalmol⁻¹ for primary and secondary C-H bonds; in methane this energy is 104 kcalmol⁻¹. (S.W. Benson, *Thermochemical Kinetics*, Wiley, New York, ed 2, 1976, p.309).

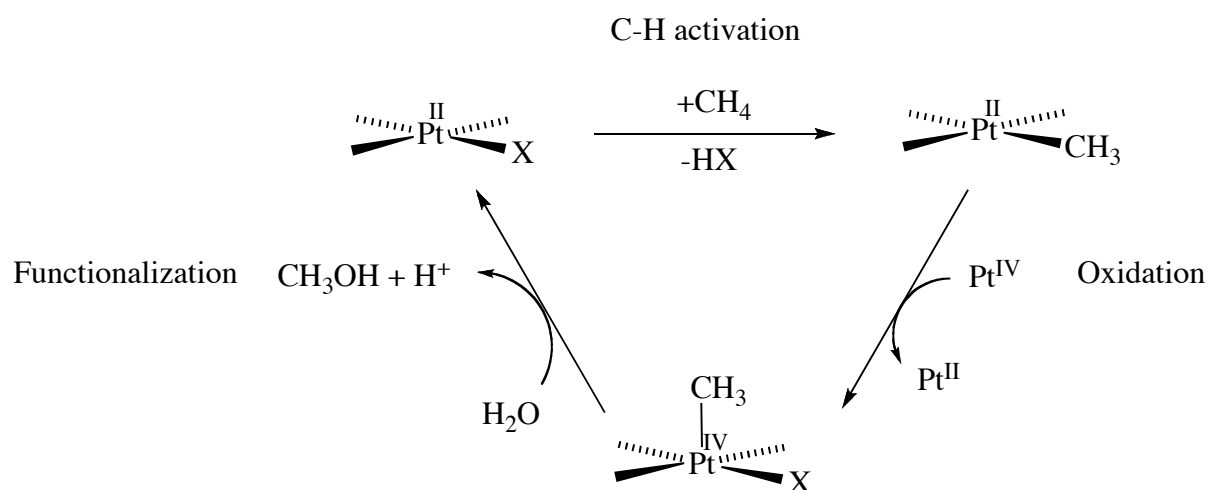
thermodynamically stable and economically unattractive carbon dioxide and water. For this reason the current use of alkanes in combustion processes is focused on the production of energy.

Cracking and thermal dehydrogenation (at high energy and temperatures) converts alkanes into more reactive and valuable olefins.

However, due to their inertness, alkanes are little exploited as starting material for the creation of more valuable chemicals, despite their abundance in nature as natural gas and major component of petroleum.

Chemists have been interested in the activation of alkanes and during the last decades it has been demonstrated that organometallic complexes are capable of activating C-H bonds. These efforts are discussed in a series of reviews.^{1a-k}

During the late 50s and early 60s, platinum salts in heavy water were used as catalyst for the incorporation of deuterium into hydrocarbons. The first example reported in the literature of a catalytic system able to convert methane into methanol in acidic media was the Pt-based system, normally referred as to the “Shilov system”, depicted in Scheme 2.1. The Shilov catalytic cycle consists of three major steps, each of which has been studied separately. Every single step may consist of several different elementary reactions and this makes the overall mechanism very complex and highly dependent on the particular system under consideration and on the specific reaction conditions.



Scheme 2.1: The Shilov System.

Despite the fact that equimolar quantities of Pt(IV) as oxidant are needed – which is a great disadvantage – the Shilov system inspired new research in this area.

2.1.1 Classification of C-H Activation Reactions

Today significant insight has been acquired concerning the mechanistic nature of metal-mediated C-H activation. According to the overall stoichiometry, the C-H activation reactions are conveniently divided in five different classes.

Oxidative addition:

Oxidative addition reactions are common for electron-rich, low valent complexes of the late transition metals such as Re, Fe, Ru, Os, Rh, Ir, Pt. In the reaction depicted in equation (3), the reactive species $[L_nM^x]$ has a free coordination site and it is electronically unsaturated in order to accommodate the two electrons supplied by R and H. Normally, the species is generated *in situ* by thermal activation or photolysis and is almost always unstable. In order for the reaction to occur the presence of an accessible $(n + 2)$ oxidation state for the metal is also necessary.



Sigma-bond metathesis:

The σ -bond metathesis consists of an exchange of σ -bonds. Often, the hydrogen transfers from a ligand to another in a concerted way, through a four-centers, four-electron transition state, which avoids the change in oxidation state of the metal from n to $(n + 2)$, typical for oxidative additions. This mechanism is often found with complexes containing electron-deficient d^0 metal centers that cannot undergo oxidation at the metal (complexes of early transition metals in high oxidation states).



Generally R and R' in equation (4) are both alkyl groups and the overall reaction can be described as an alkyl exchange, rather than a net C-H activation. The possible formation of C-C bonds has never been encountered yet.

The σ -bond metathesis has been studied for late transition metals as well, an example being the cationic Ir(III) species studied by Jensen and co-workers.² Unfortunately, for this system the mechanism is not clear yet. The oxidative addition will lead to an unusual, but not unprecedented, Ir(V) species therefore the σ -bond metathesis seems more probable since it avoids the Ir(V) oxidation state.

Metalloradical activation:

For this class of reaction mechanism, the only example was published by Wayland and co-workers.³ They have found that rhodium(II) porphyrine complexes exist in a monomer-dimer equilibrium and can reversibly activate C-H bonds of alkanes forming two porphyrine fragments as depicted in equation (5), where Porph= porphyrine.



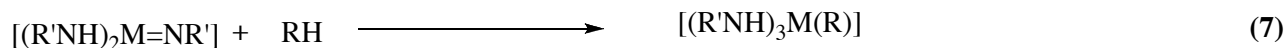
The transition state of the reaction is believed to be constituted by two molecules of rhodium. The two metal fragments are arranged in a linear fashion. One rhodium attacks the carbon atom of the alkane and the other one abstracts the hydrogen atom. This is the only example of such a type of reaction present in the literature.

Electrophilic activation:

Frequently late or post transition metals like Pd^{2+} , Pt^{2+} , Pt^{4+} , Hg^{2+} activate alkanes in strong acid media. The organometallic unit (which is presumed to exist in solution) $[\text{L}_n\text{M}^{x+2}(\text{X}_2)]$ formally substitutes the proton of the alkane [as depicted in equation (6)] – hence the term “electrophilic” substitution.

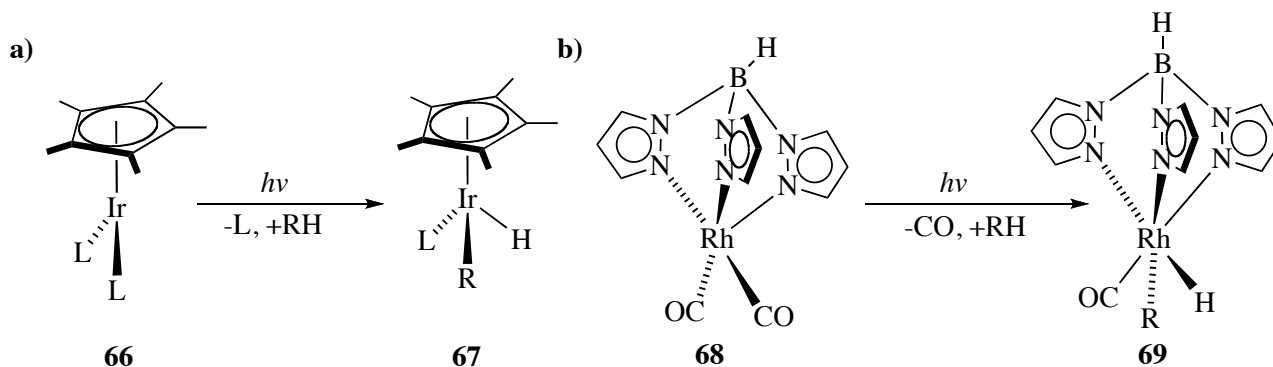
*1,2-addition:*

This important class of C-H activation reaction is depicted in equation (7) and is typically observed for early transition metal complexes and involves the activation of a C-H bond along a M-X bond. The reaction leads to a new compound where the alkyl fragment only is directly attached to the metal center.

**2.1.2 C-H Activation by Late Transition Metals**

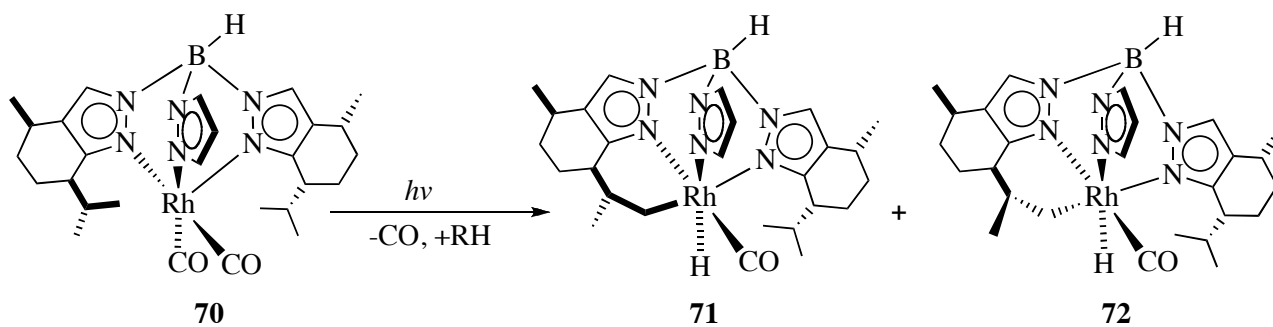
Even though platinum, a late transition metal, was known to activate C-H bonds already in the late 50's, from the great instability of metal hydride complex such as $[\text{Pt}(\text{CH}_3)(\text{H})(\text{PPh}_3)_2]$, it was long believed that the oxidative addition of an alkane might not be a feasible reaction. Only in 1982, Crabtree published a stable alkyl-iridium complex, derived by oxidative addition of cyclopentane to $[\text{Ir}(\text{H})_2(\text{PPh}_3)_2]$.⁴ In the same year Bergman⁵ and Graham⁶ published independent studies on the reactivity toward alkanes of $[\text{Ir}(\text{Cp}^*)\text{L}_2]$ (66) (where $\text{L} = \text{PMe}_3$ or CO and $\text{Cp}^* = \eta^5\text{-C}_5\text{Me}_5$) and $[\text{Rh}(\text{Tp}')(\text{CO})_2]$ (68) (where $\text{Tp}' = \text{tris-(3,5-dimethylpyrazolyl)borate}$), as shown in Scheme 2.2a-b.

The active unsaturated 16 electrons species, which could undergo thermal activation of alkanes, was formed by induced elimination of a labile ligand (such as carbon monoxide) from **66** or **68**. The species formed were particularly reactive and unstable; therefore the reactions were performed in the substrate as solvent. The *inter*-molecular oxidative addition lead to species such as **67** and **69**.



Scheme 2.2a-b: Reactivity of [Ir(Cp*)L] fragments (a) and of [Rh(Tp')(CO)] fragments (b).

Since then, several examples of C-H activation reactions appeared in the literature; especially *intra*-molecular processes. Among them, the activation of the isopropyl group within the menthol modified tris(pyrazolyl)borate rhodium complex **70** has been recently reported by Tolman et al. In this particular case a mixture of the two *intra*-molecular activation products **71** and **72** in a 85:15 ratio were formed from the oxidative addition of a methyl group (Scheme 2.3).⁷



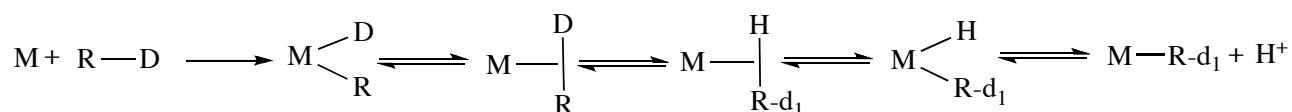
Scheme 2.3: Intramolecular C-H activation of a menthol substituted rhodium fragment.

2.1.2.1 Note on σ -complexes

The activation of C-H bonds by oxidative addition has been long believed to occur via a three-centered transition state formed by the metal center and the C-H bond of the substrate. Only after the discovery of η^2 -H₂ complexes by Kubas, it was proposed that similar adducts could be formed by the interaction of the C-H unit and the metal center.

This new hypothesis explained the observation of isotopomer distributions by Pt(II) salts in acidic deuterated solutions, known since the late 50's. Such process requires multiple C-H bond

activations and functionalizations once the substrate entered the coordination sphere of the metal center, as depicted in Scheme 2.4.

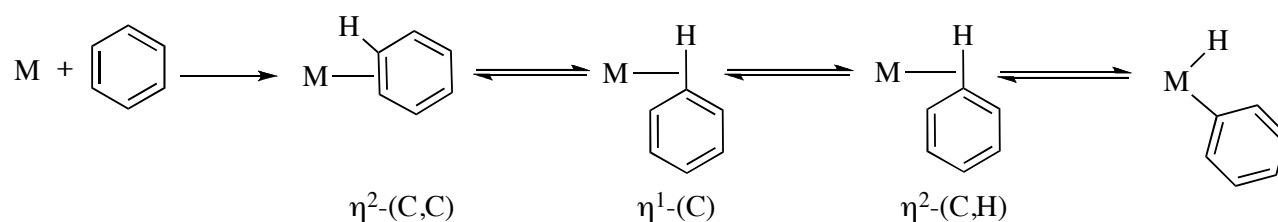


Scheme 2.4: Isotopomer distributions promoted by Pt(II) salts in acidic deuterated solutions.

Hydrocarbons σ -complexes are now believed to be the intermediates of almost all C-H activation reactions. Even though they could not be yet directly observed, many observations support their existence.

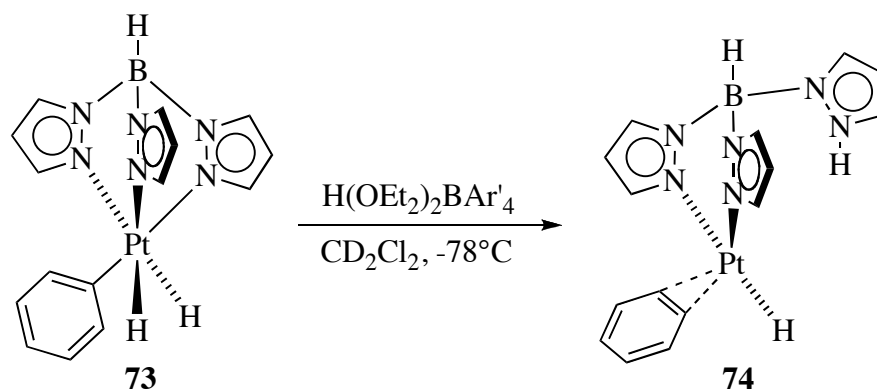
The only complex sufficiently stable to be detected on the NMR-time scale is the [Re(Cp)(CO)(cycloheptane)] adduct formed by flash photolysis in a frozen matrix or in solution.⁸ The quintet resonance signal detected at $\delta = -2.32$ ppm has been attributed by the authors to the alkane complex [Re(Cp)(CO)(cycloheptane)]. Another related example is the Fe(porphyrine) heptane complex, which has been characterized by X-ray diffraction by Reed et al. The crystallographic data show a large void above the porphyrine plane occupied by an *n*-octane solvent molecule.⁹ The iron-carbon bond distance of 2.5 Å and 2.8 Å are in the range of commonly observed agostic C-H interactions.¹⁰

Similarly, isotope exchange has been observed for aromatic substrates as well. These hydrocarbons are generally more easily activated because of their filled π -orbitals that can interact with the unoccupied orbitals of the metal center. The slippage of the phenyl unit that occurs during the C-H activation process is shown in Scheme 2.5.



Scheme 2.5: Ring slippage of benzene.

An example for the $\eta^2\text{-(C,C)}$ coordination mode has been published by Brookhart et al.¹¹ The complex was formed from the (Tp')Pt system **73**, shown in Scheme 2.6. The $\eta^2\text{(C}_6\text{H}_6\text{)}$ -compound **74** has been characterized by X-ray diffraction studies and by NMR spectroscopy.



Scheme 2.6: η^2 -(C,C) coordination mode of benzene.

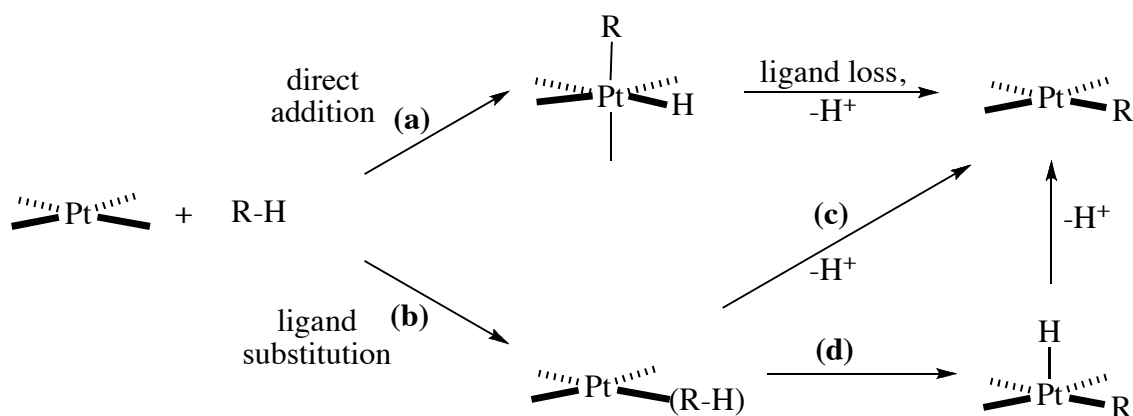
The ^{13}C NMR and ^1H NMR spectra of **74** show one resonance for the aromatic CH carbons and protons. The ^1H NMR signal attributed to the benzene is shifted to low frequencies ($\delta = -30.1$ ppm).

2.1.2.2 Alkane Activation by Pt(II) Complexes – Mechanism for the C-H Activation Sequence

After the discovery of C-H activation reactions performed by platinum complexes, different scenarios for this step were envisaged and these are depicted in Scheme 2.7.

The direct oxidative additions depicted in path (a) from Pt(II) complexes to octahedral Pt(IV) complexes appear to be extremely rare due to the high instability of the six-coordinate Pt(IV) intermediate with respect to the reactants.

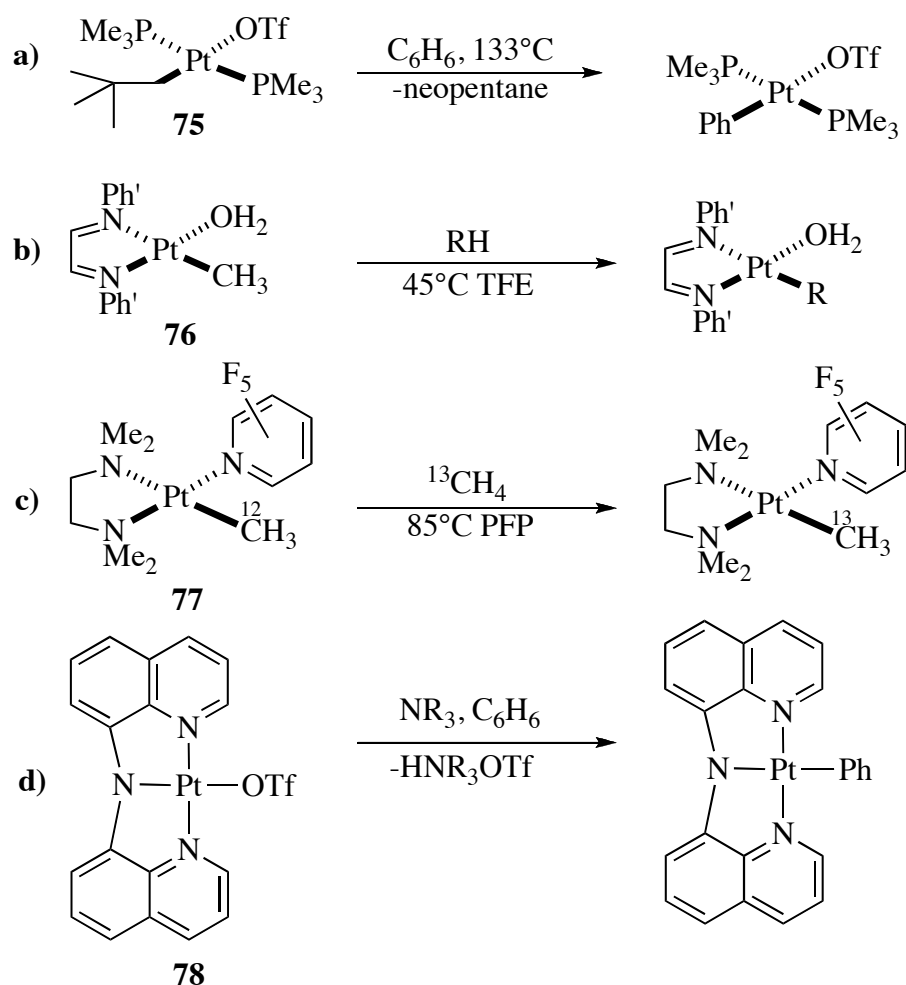
Most likely, the majority of the systems studied so far go through a Pt(II) σ -alkane complex intermediate such in path (b). In mechanism (c) (which is called “electrophilic mechanism”) the σ -alkane adduct is directly deprotonated, while in mechanism (d) the σ -alkane undergoes oxidative addition and forms a Pt(IV) pentacoordinate intermediate, which is subsequently deprotonated to form the Pt(II) alkyl product.



Scheme 2.7: C-H activation sequence: different possibilities.

The approach of the alkane to the platinum complex to form a σ -alkane adduct, following path (b), needs the presence of a free coordination site on the metal. This feature has been elucidated by early studies on tetracoordinate Pt(II) complexes, which showed that complexes bearing labile groups undergo much easier and faster C-H activation reactions.

One of the earliest examples reported in the literature supporting this hypothesis is the intermolecular activation of deuterated benzene at 133°C by the phosphine alkyl Pt(II) complex **75** (Scheme 2.8a), where the presence of the labile trifluoromethanesulfate (triflate, OTf) provides the free coordination site necessary for the approach of the substrate.¹² Scheme 2.8b-c shows similar examples published by the groups of Labinger and Bercaw: in the case of the (tmeda)-complex¹³ **77** (where tmeda= N,N,N',N'-tetramethylethylenediamine) the labile ligand is pentafluoropyridine, whereas in the diimine Pt(II) complexes **76** developed and studied in collaboration with the Norwegian group of Tilstet,¹⁴ this role is played by a water or TFE (trifluoroethanol) molecule. This system has been further investigated by Chen and co-workers, as well.^{154-c}

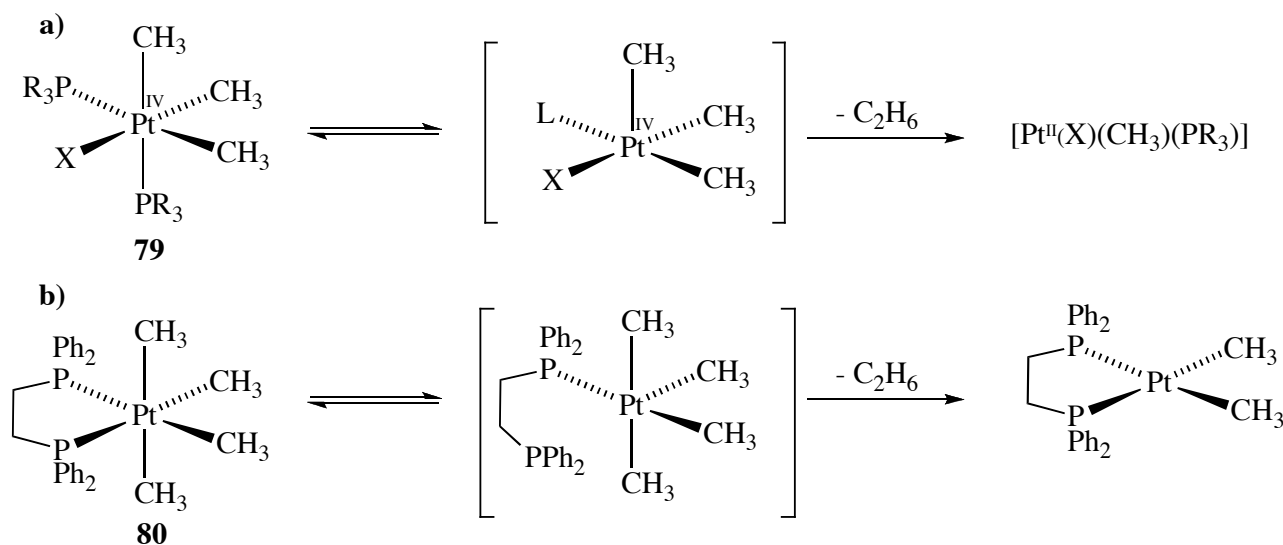


Scheme 2.8a-d: Pt(II) tetracoordinate complexes bearing labile ligands.

In complex **78** of Figure 2.8d the alkane coordinates upon decooordination of the labile triflate. The alkane is subsequently deprotonated by an external base.¹⁶ The related chlorine-based system is not active under the same reaction conditions, proving the need of a labile ligand in the platinum complex, to allow the coordination of the substrate. For the latter base-promoted reaction the formation of a σ -complex prior to C-H activation could explain the increased acidity of the substrate and subsequent easier deprotonation. On the contrary, the formation of a σ -complex for the previously discussed examples could be explained in terms of lower activation energy for such species to undergo oxidative addition.

Information about the mechanisms involved in the breaking of a carbon-hydrogen bond could be obtained by studying reactions of C-C reductive elimination from Pt(IV) complexes, even if for a long time Pt(IV) alkyl hydride complexes were not synthetically accessible.

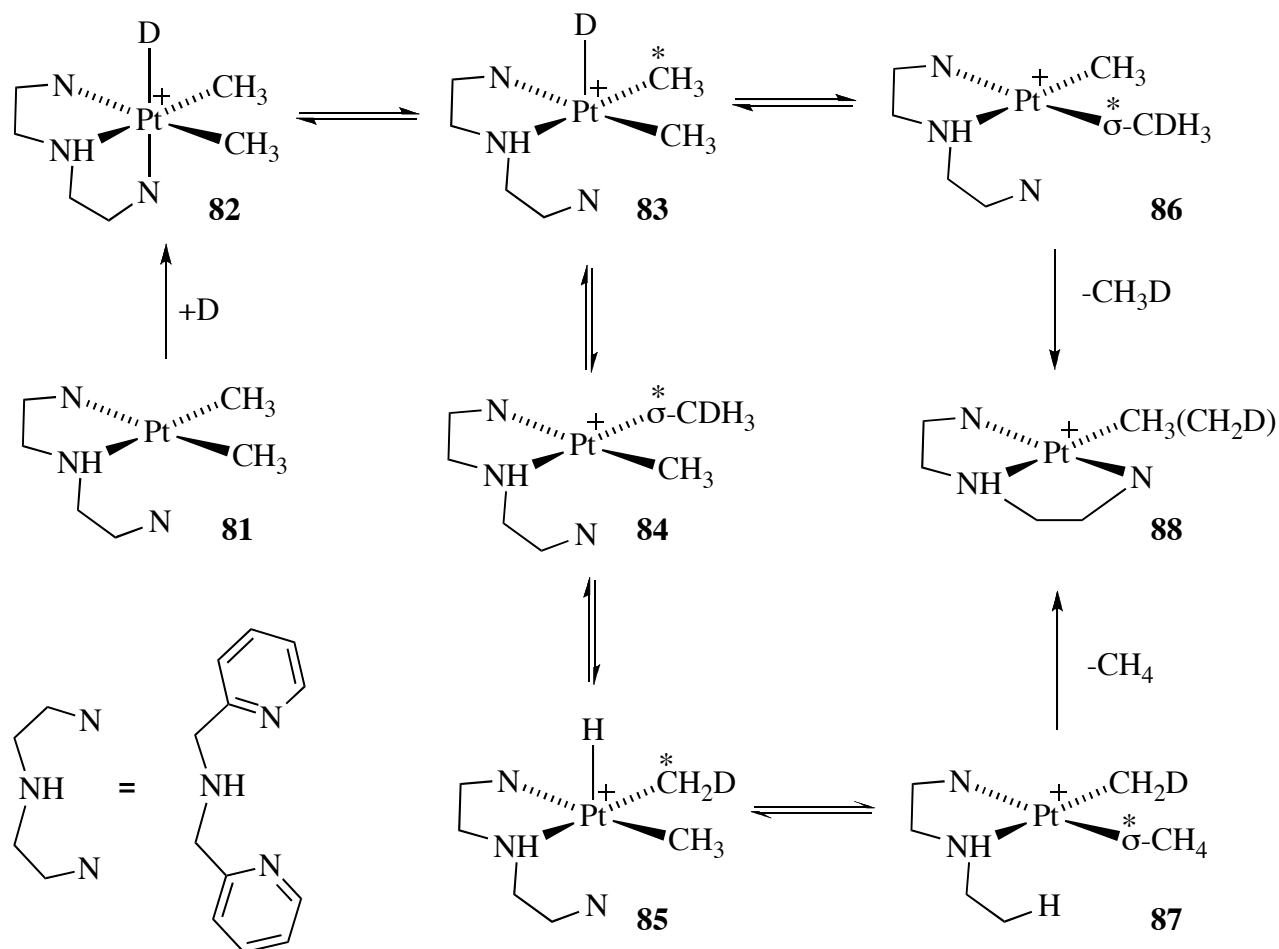
In the example reported in Scheme 2.9a the rate of the reductive elimination of ethane from a pentacoordinate Pt(IV) complex $[\text{PtX}(\text{Me})_3(\text{PR})_2]$ (**79**) is strongly inhibited by addition of phosphine proving that the system undergoes first dissociation of a ligand to form a pentacoordinate species prior to the C-C coupling reaction.¹⁷



Scheme 2.9a-b: Reductive elimination from Pt(IV) alkyl complexes.
Where $\text{PR}_3 = \text{PMe}_2\text{Ph}$, PMePh_2 or PMe_3 and $\text{X} = \text{halide}$.

More recently, the mechanism has been confirmed during a study on the $[\text{Pt}(\text{Me})_4(\text{dppe})]$ (**80**) [$\text{dppe} = \text{bis}(\text{diphenylphosphino})\text{ethane}$] as illustrated in Scheme 2.9b. In this case the partial dissociation of the chelating phosphine ligand dppe provides access to the reactive unsaturated species.¹⁸

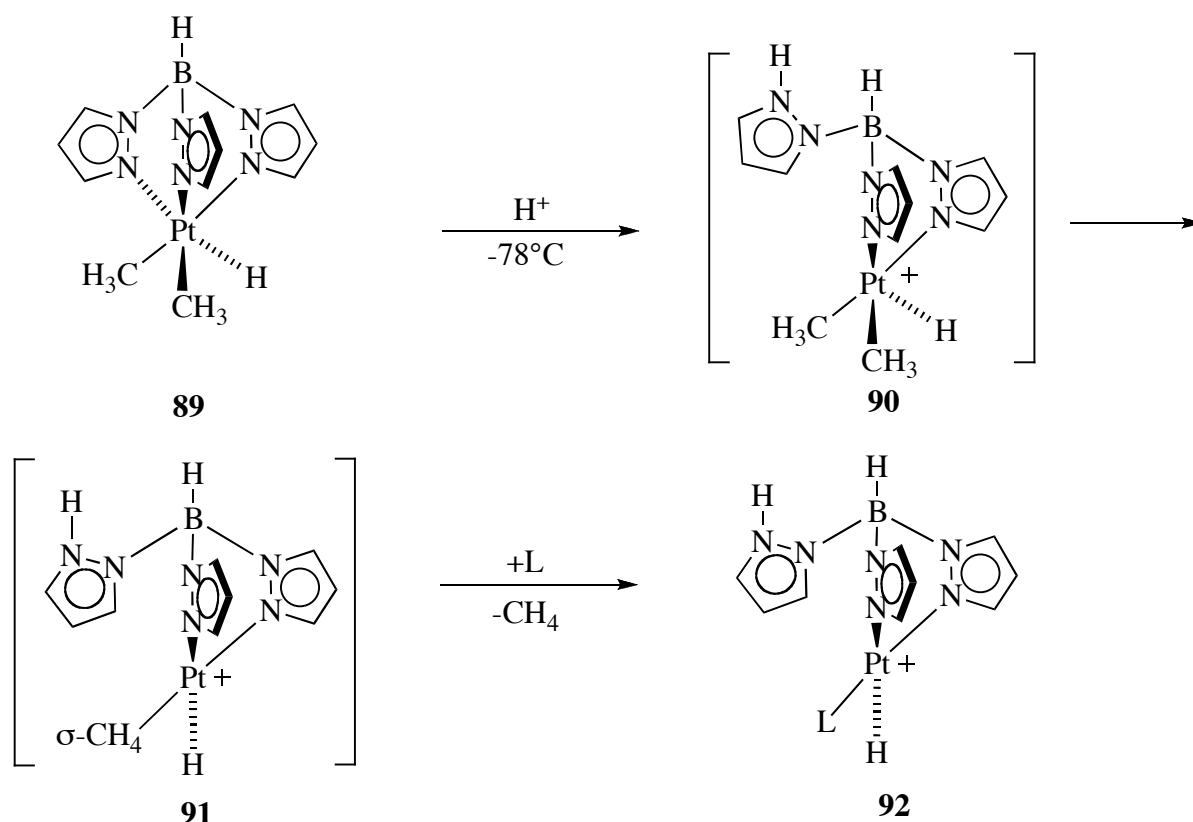
These results are supported by studies on the C-H reductive elimination conducted with alkyl hydrides of Pt(IV). Different research groups have been able to synthesize and isolate complexes of this type.¹⁹ An example is shown in Scheme 2.10.



Scheme 2.10: C-H reductive elimination studies from a Pt(IV) alkyl hydride complex.

The deuteride complex $[\text{Pt}^{\text{IV}}(\text{Me})_2(\text{D})(\kappa^3\text{-bpma})]^+$ (**82**) (bpma = bis(pyridylmethyl)amine) depicted in Scheme 2.10 was obtained by protonation with deuterated acids of $[\text{Pt}^{\text{II}}(\text{Me})_2(\kappa^2\text{-bpma})]$ (**81**).²⁰ The scrambling of deuterium was observed only in the methyl group *trans* to the amine (*) in **83**, **84** and **85**, whereas the elimination of methane was detected exclusively from the position *cis* to the amine (*) in **86** and **87**.²¹ These observations can be explained by the fact that, with respect to the methyl group, the hydride (or deuteride) has higher *trans* influence on the pyridyl moiety, which become therefore more labile than the amine. Moreover, the easier elimination of CH_4 from the position *cis* to the amine is due to the geometry of the bpma ligand. The pyridyl can only replace the methyl *cis* to the amine to yield the square planar platinum(II) methyl complex **88**.

An other ligand recently used to stabilize a Pt(IV) alkyl hydride is the already mentioned Tp' ligand (Scheme 2.2b). The three nitrogen atoms of the ligand can stabilize a hexacoordinate Pt(IV) complex by capping one face of the octahedron. The trimethylplatinum(IV) complexes of Tp' are very stable even at elevated temperatures and the reductive elimination of ethane to yield platinum(II) complexes has never been observed.²² On the other hand, mixed methyl-hydrido complexes such as [Pt(Me)₂(H)(Tp')] (**89**), are reactive. The reaction depicted in Scheme 2.11 is promoted by acids.

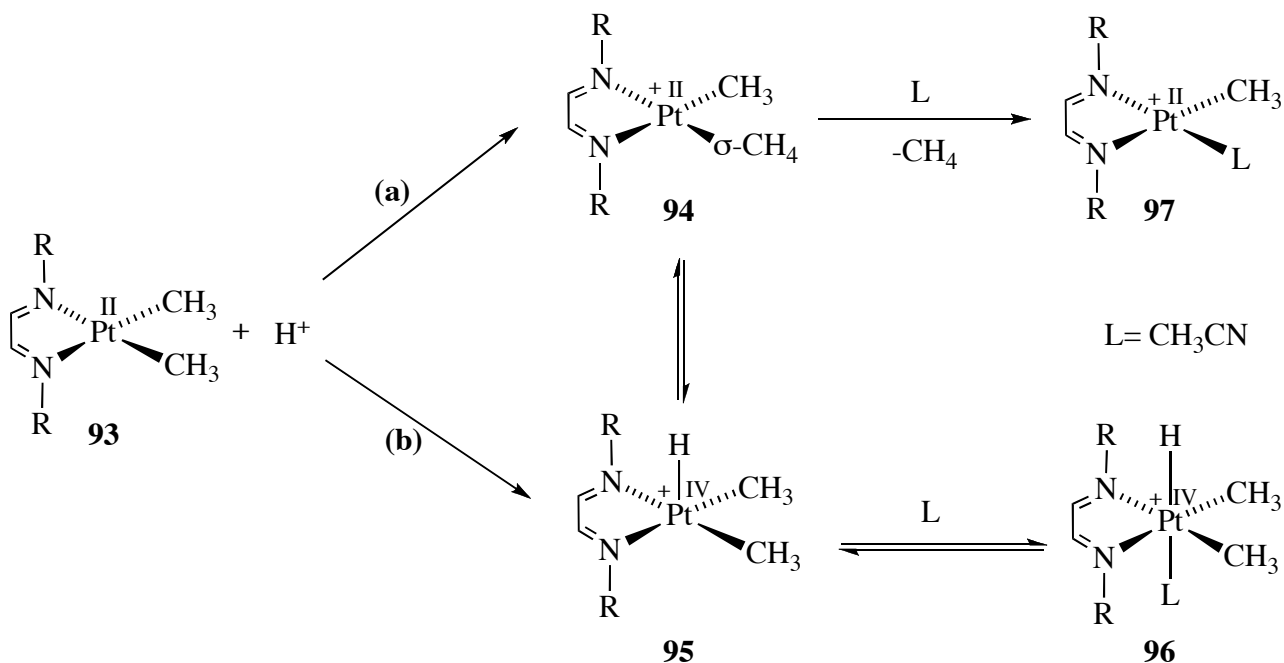


Scheme 2.11: Formation of Pt(II) complexes with κ^2 -Tp' ligand.

The proposed Pt(IV) pentacoordinate species **90** is unstable and thus undergoes loss of methane through **91**. While the Pt(II) methane complex has never been observed, the use of trapping agents ($\text{L} = \text{CNCH}_3$) allows the isolation of square planar Pt(II) complexes bearing the κ^2 -Tp' ligand having one protonated pyrazole group (**92**).²³

Finally, extensive studies on direct protonation of Pt(II) methyl diimine complexes, such as the ones in Scheme 2.12 (**93**), shed light on the mechanism of C-H activation. These results are summarized in two review articles.^{1f,k} Two different scenarios are envisaged: (a) the direct protonation at the methyl group to form the methane σ -complex **94** or (b) the protonation at the metal center to form the methyl(hydrido)platinum(IV) complex **95**. Experimental evidence was

obtained for the metal being the kinetic site of protonation. In the diimine platinum(II) complexes under investigation the use of acetonitrile as trapping agent prevents the formation of the methane σ -complex **94** from the reactive pentacoordinate species **95** and the subsequent reductive elimination to yield **97**. Moreover, an increase in concentration of acetonitrile yields the methyl(hydrido)platinum(IV) complex **96**.²⁴



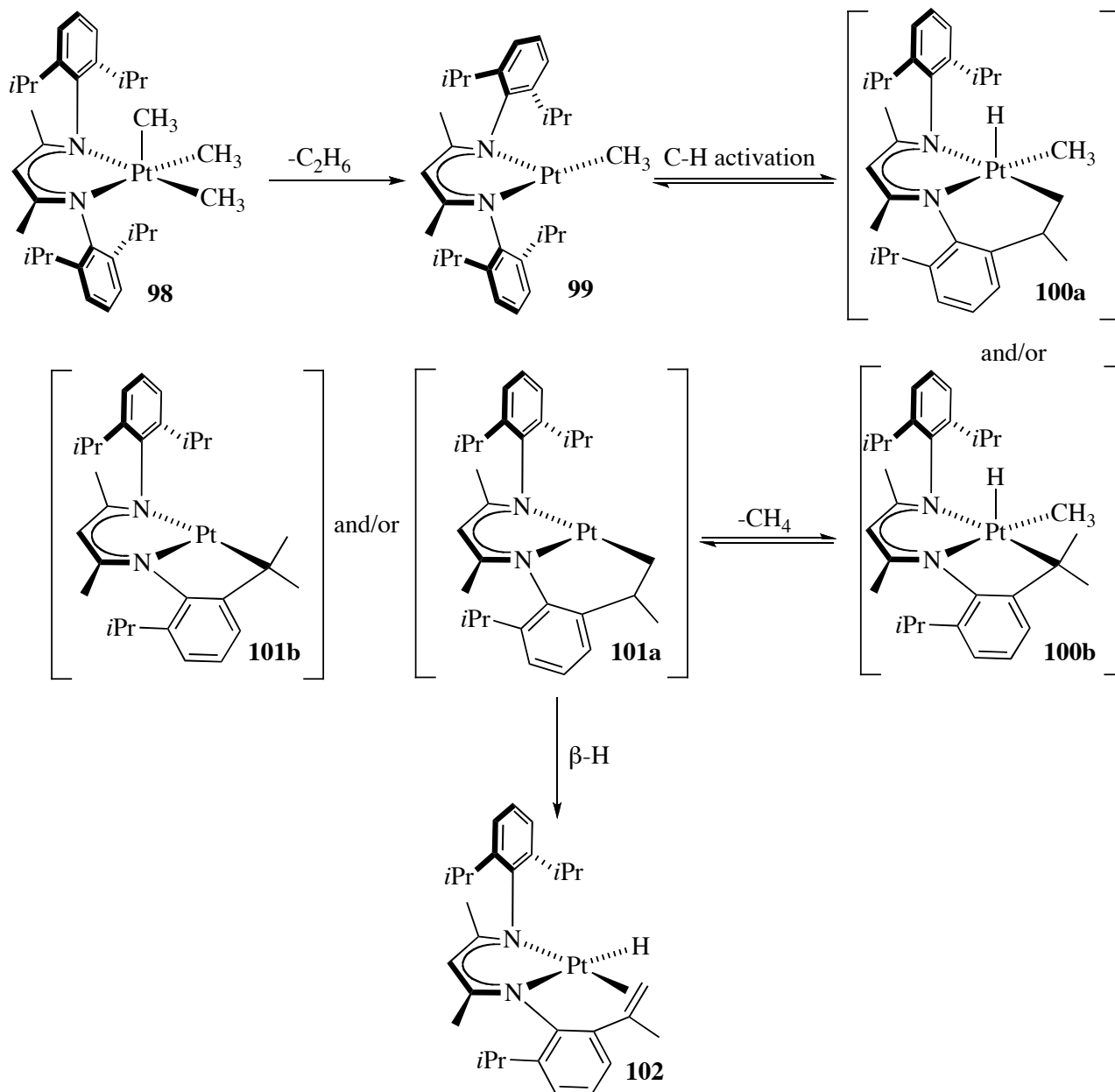
Scheme 2.12a-b: Mechanism for the protonation of Pt(II) complexes: (a) direct protonation at the methyl group or (b) protonation at the metal center. R is a substituted phenyl group.

In conclusion, in these diimine systems the protonation occurs preferentially at the platinum center and by the principle of microscopic reversibility this indicates that the C-H activation proceeds by oxidative addition: path (b) and (d) in Scheme 2.7.

2.1.2.3 Note On The Rarity of Pt(IV)Pentacoordinate Complexes

The pentacoordinated platinum (IV) complexes, shown until now as intermediates, are particularly reactive and have been directly observed only recently. One of such rare examples is the one reported by Goldberg and co-workers and is depicted in Scheme 2.13.²⁵ Thermolysis of [Pt(Me)₃(nacnac)] (**98**) (nacnac = {[(*o*-^{*i*}Pr₂C₆H₃)NC(CH₃)₂CH]⁻) leads to elimination of ethane and formation of **102**. The mechanism of the reaction is believed to be the one shown in the scheme: **98** eliminates ethane to form **99**, subsequently intramolecular C-H activation of the isopropyl group leads to a metallacycloplatinum(IV) complex (**100a** or/and **100b**). The latter adduct eliminates methane to form **102a-b**, which then undergoes β -elimination to yield the product (**102**).²⁶

It has been postulated that the great stability of the nacnac pentacoordinate platinum complexes is due to the anionic ligand: indeed the formation of a pentacoordinate neutral complex prevents the coordination of the counter anion.



Scheme 2.13: Mechanism for the formation of Pt hydrido alkane complex.

Related complexes recently isolated are shown in Figure 2.1a-b. In compound **103** the coordination of the anion is avoided by the use of a non-coordinating tetraarylborate as counterion.²⁷ Interestingly, neither dichloromethane or diethylether used as solvent in the reaction mixture seem to coordinate to the free coordination site of the molecule.

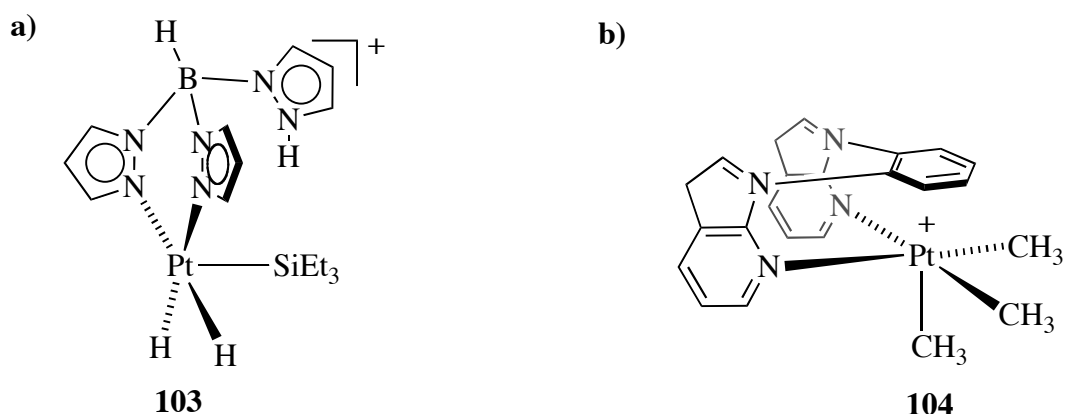
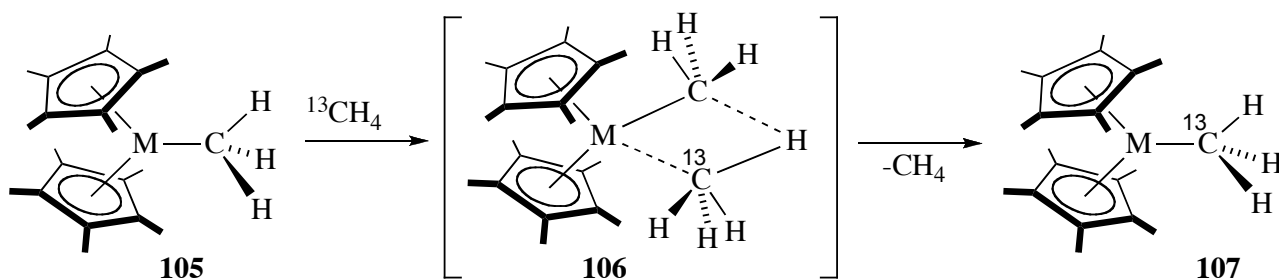


Figure 2.1a-b: Other examples of Pt(IV) pentacoordinate alkyl complexes.

In the example **104**, recently published by Wang et al., the pentacoordinate arrangement around the metal center is accomplished by the use of a bulky N-N chelating ligand. Complex **104** has been characterized by X-ray diffraction studies.²⁸ The sixth coordination site of the Pt(IV) is completely capped by the phenyl linker between the two azaindolyl units of the ligand.

2.1.3 Alkane Activation by Early Transition Metal Complexes

While the platinum complexes described in Section 2.1.2 react *via* oxidative addition and reductive elimination, several metal complexes – namely those with early transition metal centers – are believed to react *via* a concerted pathway. In such cases the oxidative addition is energetically prohibited because no electrons are available in the metal d-orbitals. One of the earliest reports on this reaction type is the one of Watson, depicted in Scheme 2.14.²⁹ The yttrium complex [Y(Me)(Cp*)₂] (**105**) exchanges with ¹³CH₄ to yield the isotope labeled complex **107**.

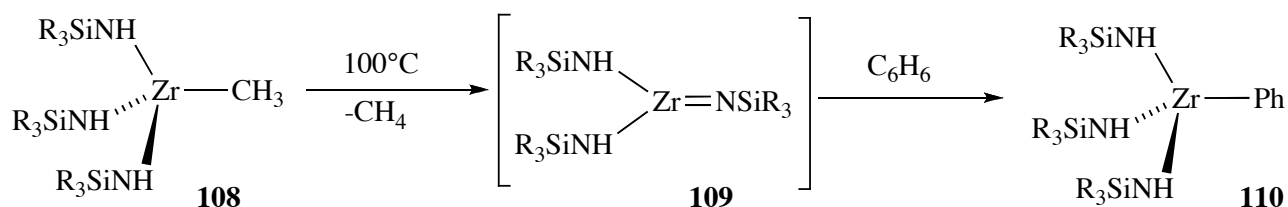


Scheme 2.14: Cp*MCH₃ undergoes methyl group exchange. M= Y, Sc.

Bercaw³⁰ reported similar exchange reactions with the related scandocene complexes [Sc(Me)(Cp*)] (**105**) together with the thermal decomposition of similar titanocene complexes [Ti(CH₃)₂(Cp*)].³¹

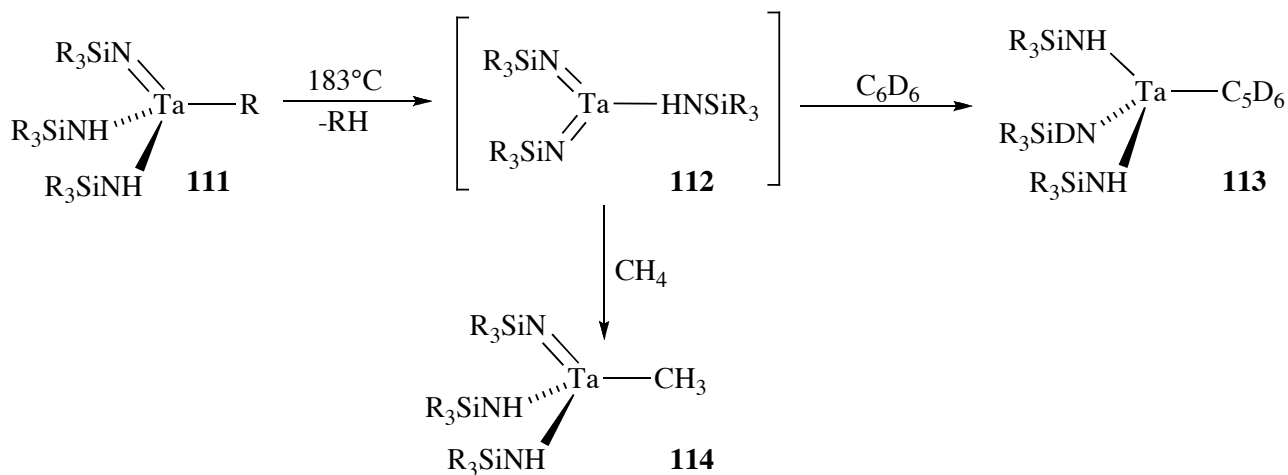
Another important class of transformations related to the activation of C-H bonds, is the reaction of alkane across metal-ligand multiple bonds (e.g. L_nM=X, where X= O, NR or CR₂).

Representative of this class of reactions are the 1,2-additions with $[\text{Zr}(\text{CH}_3)(^t\text{BuSiNH})_3]$ (**108**) studied by Wolczanski.³² Such complex eliminates methane to generate a reactive imido intermediate (**109**), which eventually reacts with benzene to yield complex $[\text{Zr}(\text{Ph})(^t\text{BuSiNH})_3]$ (**110**), as shown in Scheme 2.15. The imido complex can be trapped as THF adduct.



Scheme 2.15: 1,2 addition across a Zr=N bond.

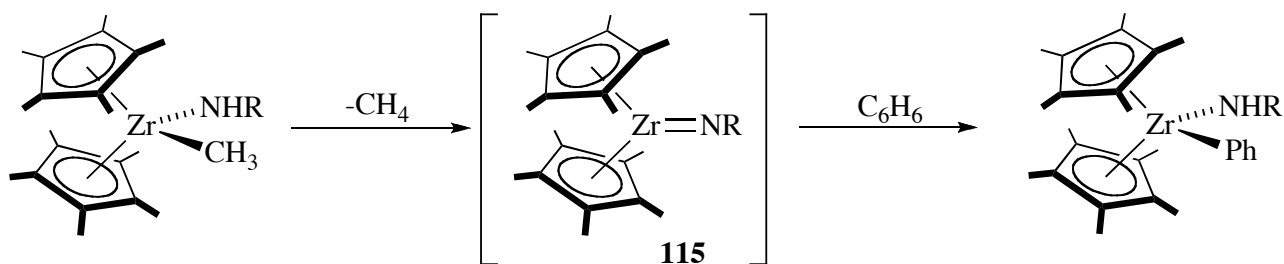
According to computational studies and experimental evidences σ -complexes do not appear to be involved in the reaction.³³ The transition state suggested by the authors is a four-centered species, undergoing concerted bond breaking/forming with little charge buildup. Wolczanski also studied the reactivity of tantalum imido system, such as **111**.³⁴ Scheme 2.16 shows the tantalum system **111** can form the bis-amido imido complex **112** by thermal elimination of an alkane.



Scheme 2.16: Tantalum system.

In this system the thermal activation occurs with more difficulty (above 180°C) but, once formed, **112** reacts immediately with methane and benzene to yield **113** or **114**. Another system investigated by the same group is the bis-siloxy amido titanium complex. The mechanism of the reaction is equivalent to the related imido complexes described above.

A notable work in the field of C-H activation promoted by early transition metal complexes has been done by the Bergman group.³⁵ In these laboratories the reactivity of complexes bearing zirconium-nitrogen double bonds (**115**) has been widely investigated (Scheme 2.17).



Scheme 2.17: The system studied by Bergman et al.

2.2 Aims

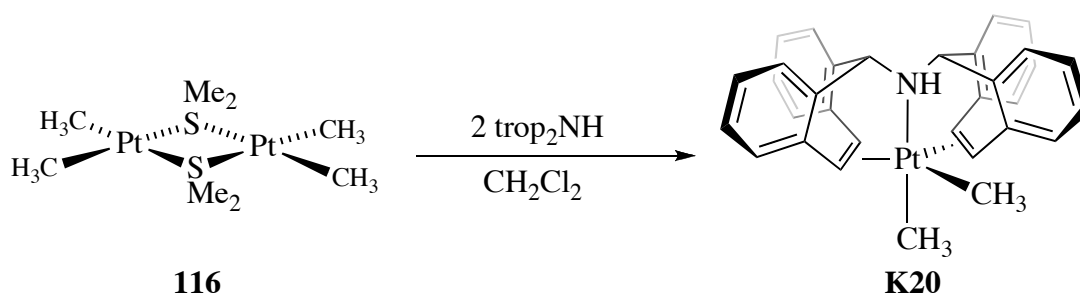
The *intra*-molecular C-H activation across a Rh-amide bond has been described for cyclohexyl- (see **K4**), 1-ethyl-phenyl- (see **(S,S)-K5**) and isopropyl- (see **(S,S)-K6**) groups in Chapter 1. Despite the fact that the activation occurs, for the moment, exclusively in an *intra*-molecular fashion, such examples represent a rare case of activation of alkanes along a M-amide bond. This type of process is normally observed only for complexes where M is an early transition metal such as Zr, Y, Sc, and Ta (Chapter 2.1.3), whereas when M is a late transition metal the complexes are known to undergo C-H activation through the oxidative addition mechanism, as discussed in Chapter 1.1.3 and 2.1.2.

The interest to explore the reactivity of M-amide bonds in late transition metals complexes with the ultimate aim to achieve *inter*-molecular C-H activation, prompted us to explore the coordination chemistry of platinum.

Platinum is actually known to be capable of activating alkanes, as already discussed in the introduction of this chapter. The first purpose of the project was, therefore, to develop a synthetic strategy for the preparation of Pt(II) trop_2NH complexes. Despite the fact that the coordination chemistry of trop_2NH was extensively explored for Rh(I) and Ir(I) through the work of T. Büttner,³⁶ the coordination properties of this ligand towards other type of metal was practically unexplored at the time. The possibility to exploit and prove the versatility of the bistropamine ligand, inspired us for the preparation and the study of Pt(II) and Pd(II) complexes, isoelectronic to Rh(I) and Ir(I). The question to be addressed was whether the coordination mode of the ligand would change on going from Rh(I) to Pt(II) and Pd(II). Moreover, we were especially curious whether tetracoordinate Pt(II) complexes would resemble in geometry the isoelectronic compounds of Rh(I) complexes, adopting saw-horse type structures. However, the ultimate aim, as already mentioned, was to understand if a Pt-amide bond would be reactive in the activation of small molecule in an *inter*-molecular fashion.

2.3 Synthesis of Pt(II) and Pd(II) Complexes

The first purpose of this project was to prepare new Pt(II) and Pd(II) complexes of trop₂NH. A fair number of Pt(II) compounds have been tried as precursors without success, among them: [PtCl₂(cod)], [PtCl₂(SMe₂)₂], [PtCl₂(PhCN)₂], [PtCl₂(PPh₃)], [PtCl₂(DMSO)₂], K₂PtCl₄ and PtCl₂. The complex, which showed the appropriate reactivity was [Pt(μ²-SMe₂)Me₂]₂ (**116**).³⁷ This platinum dimer bears labile bridging groups (SMe₂), which can be easily displaced by the trop ligand. Hence, the successful synthetic route for the preparation of the desired trop complex uses **116** together with a slight excess of the ligand in dichloromethane as solvent (Scheme 2.18). The reaction is clean and the product [Pt(Me)₂(trop₂NH)] (**K20**) can be isolated as yellow crystals.



Scheme 2.18: Synthesis of the platinum complex [Pt(Me)₂(trop₂NH)] (**K20**).

The characterization of the product was achieved by low temperature ¹H NMR spectroscopy (233 K). Two non-equivalent methyls were observed, which display two singlets at δ= 0.105 ppm and δ=1.175 ppm with platinum satellites of 67.3 Hz, as summarized in Table 2.1. The amine moiety must be coordinated to the metal because its chemical shift at δ= 2.53 ppm shows platinum satellites of 23.0 Hz. Moreover, the singlet for the two benzylic protons and the two doublets for the four olefinic protons display platinum satellites of 18.8 Hz, 38.4 Hz and 55.4 Hz, respectively (Table 2.1). From the presence of platinum satellites in the NH, the benzylic and the olefinic signals, it has assumed that the coordination of the ligand occurs in a tripodal fashion, similarly to that observed for Rh(I). Moreover, from the number of signals observed, it was deduced that the structure of the compound should be trigonal bipyramidal.

This feature was further confirmed by comparison of range and the magnitude of the chemical shifts and of the coupling constants reported in the literature for other trigonal bipyramidal platinum(II) complexes bearing olefins in the trigonal plane.³⁸

It is important to note that the room temperature ¹H NMR spectrum shows broad platinum satellites exclusively for the olefinic protons, probably caused by a slight movement of the olefinic

bonds around the metal. This could mean that the olefins are not tightly bond to the platinum center (vide infra).

The X-ray analysis confirmed the trigonal bipyramidal structure of the complex. Single crystals suitable for X-ray studies were obtained by slow evaporation of a saturated solution of **K20** in THF. In Figure 2.3 the ORTEP view of **K20** is shown.

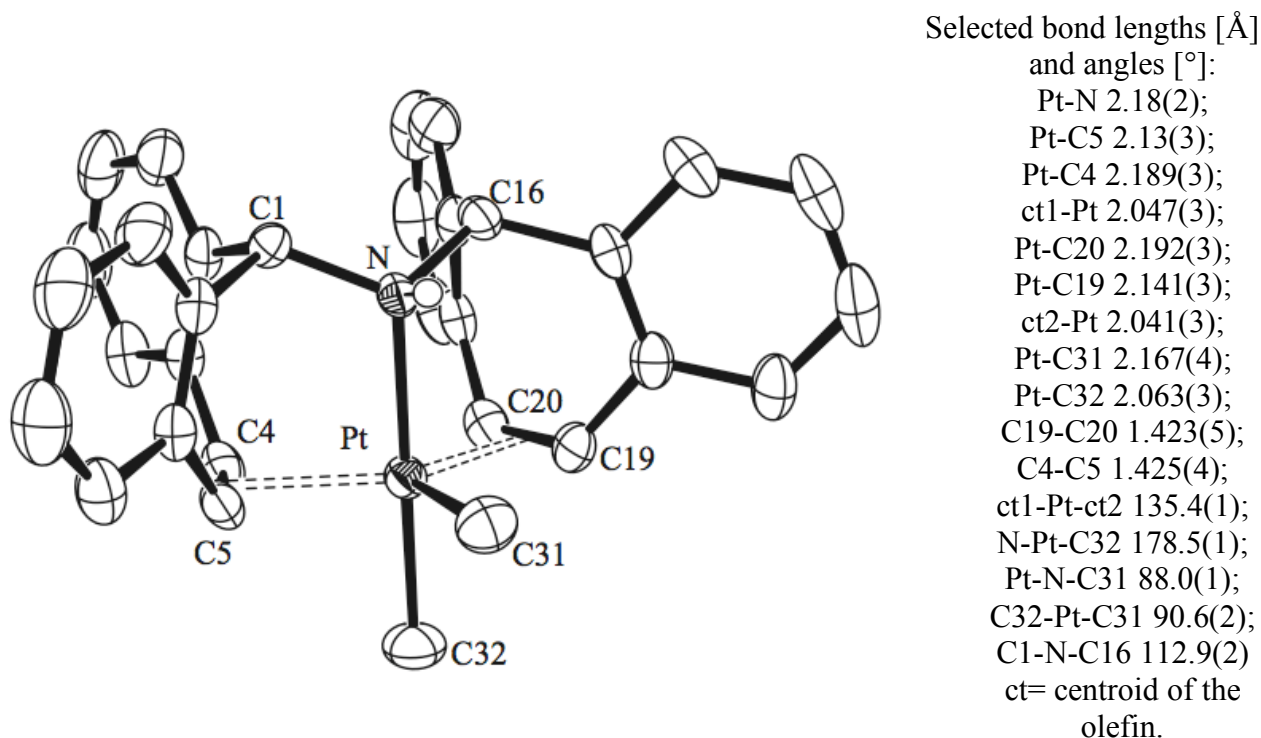


Figure 2.3: ORTEP view of **K20**. Thermal ellipsoids are drawn with 50% probability; all hydrogen atoms except at N1 are omitted for clarity.

A comparison of the structural parameters for **K20** and the known compound $[\text{Pt}(\text{Cl})_2(\text{dmbn})(\text{C}_2\text{H}_4)]$ (**117**) is given in Figure 2.4 (dmbn= 3,7-dimethylenebicyclo-[3.3.1]nonane).

The average of the Pt-C bond lengths of the olefins is shorter in **K20** (approx. 2.16 Å) than in **117** (approx. 2.29 Å), due, most likely, to the different ligand set in the two platinum(II) complexes: **K20** has stronger σ -donors in the two axial positions – the CH_3 group and the amine - and moreover the σ -donor methyl group in compound **K20** has replaced the π -acceptor ethylene molecule in **117**.



Pt-C5= 2.13(3) Å, Pt-C19= 2.141(3) Å
 Pt-C20= 2.192(3) Å, Pt-C4= 2.189(3) Å

Pt-C10/C11= 2.254(5) Å
 Pt-C3/C7= 2.475(7) Å
 Pt-C1'/C2'= 2.154(7) Å

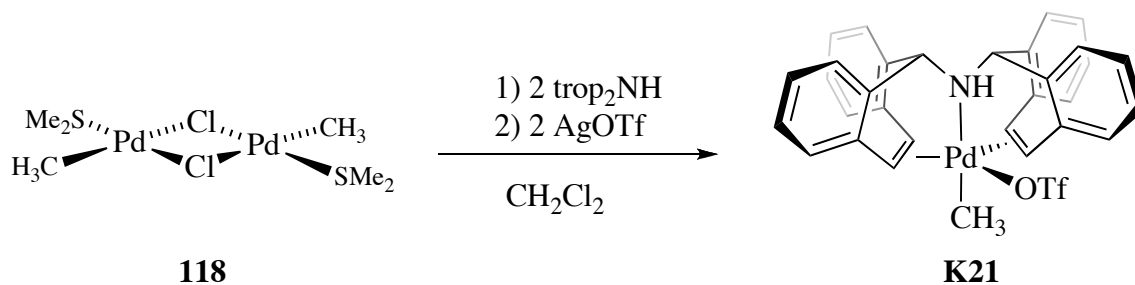
Figure 2.4: Schematic representation of complex **K20** and $[\text{Pt}(\text{Cl})_2(\text{dmbn})(\text{C}_2\text{H}_4)]$ (**117**).

The olefin-metal bond lengths have been compared to the previously discussed trop₂NH structures of rhodium(I) such as $[\text{Rh}(\text{OTf})(\text{trop}_2\text{NH})(\text{PPh}_3)]$ (**59**) and $[\text{RhCl}(\text{trop}_2\text{NH})(1,3\text{-bis-(1-phenyl-ethyl)imidazolin-2-ylidene})]$ (**(S-S)-K5**), discussed in Chapter 1.

The average Pt-C_{olefin} bond length varies from 2.19 Å (**(S-S)-K5**), to 2.18 Å (**44**) and 2.16 Å (**K20**) and the Pt-N bond changes from 2.14 Å (**(S-S)-K5**) to 2.15 Å (**44**) and 2.18 Å (**K20**).

At a first glance, one may conclude that the isoelectronic Rh(I) and Pt(II) complexes show rather similar properties both in the solid state and in solution with the only exception that the broadening of the olefinic proton signals indicate a dynamic behaviour which may be related to a lower strength of the olefin-platinum bond in solution.

Since the preparation of **K20**, using **116** as metal precursor, was straight forward, the synthesis of a Pd(II) complex was subsequently planned. The palladium precursor most similar to **116**, is indeed the Pd(II) dimer $[\text{Pd}(\mu^2\text{-Cl})(\text{Me})(\text{SMe}_2)]_2$ (**118**) depicted in Scheme 2.19. Despite the low yield reported for the preparation of **118** (44%),³⁹ compound **118** was employed for the synthesis of $[\text{Pt}(\text{Me})_2(\text{trop}_2\text{NH})]$ (**K21**), in a similar fashion to that reported for **K20** (Scheme 2.19).



Scheme 2.19: Synthesis $[\text{Pt}(\text{Me})_2(\text{trop}_2\text{NH})]$ (**K21**).

The ORTEP plot of the crystals of **K21** solved by X-ray analysis is shown in Figure 2.5.

The differences observed for the bond lengths in **K21** and **K20** are due to the replacement of the methyl group with the triflate counter anion and to the consequent lower ($d \rightarrow \pi^*$)-back donation from the metal center to the olefins. As expected, this replacement affects the chemical shifts of the olefins as well, which are shifted to lower frequencies in **K21**. For example the ^{13}C NMR spectrum of **K20** displays two signals at $\delta = 57.12$ ppm and $\delta = 62.71$ ppm for the $\text{C}=\text{C}_{\text{olefin}}$, whereas in **K22** the same signals are shifted to $\delta = 97.25$ ppm and $\delta = 98.9$ ppm. From the observation of the shift of the olefinic carbon signals towards high frequencies, it was deduced that the formation of cationic complexes would result in a lower Pt-C bond strength.

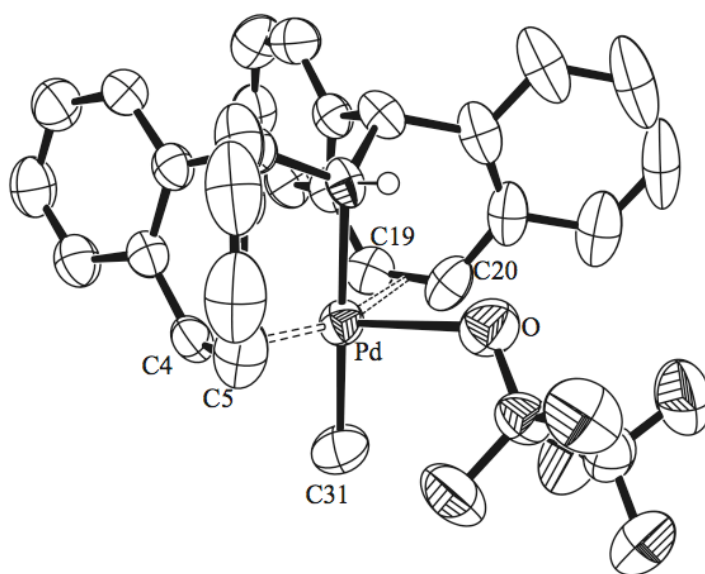


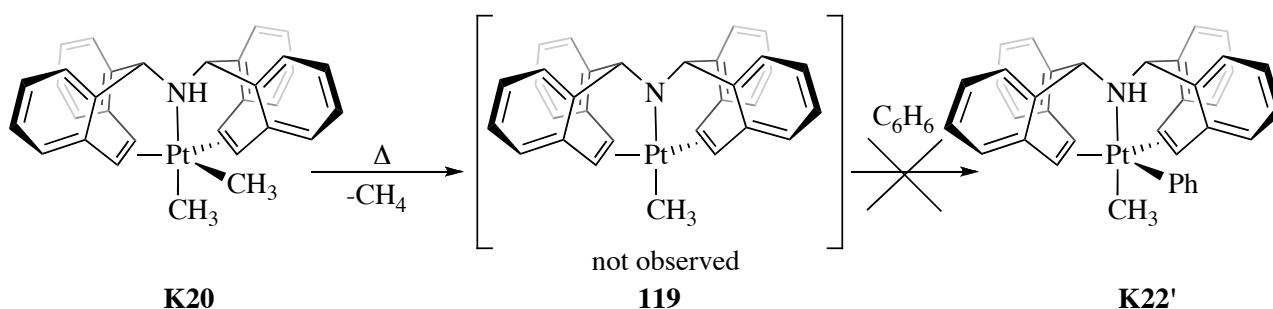
Figure 2.5: ORTEP view of $[\text{PdOTf}(\text{Me})(\text{trop}_2\text{NH})]$ (**K21**). Thermal ellipsoids are drawn with 50% probability; all hydrogen atoms except at N1 are omitted for clarity. Selected bond lengths [\AA] and angles [$^\circ$]: Pd-N 2.180(2); Pd-C4 2.231(3); Pd-C5 2.238(3); ct1-Pd 2.124(3); Pd-C19 2.255(3); Pd-C20 2.255(3); ct2-Pd 2.146(3); ct1-Pd-ct2 151.2(5); Pd-C31 2.043(1); C19-C20 1.386(4); C4-C5 1.388(4); N-Pt-C31 178.6(1). ct= centroid of the olefin.

2.3.1 Thermal Activation in Benzene

As already mentioned in the introduction, the main intent of the project was to explore the reactivity of Pt-amide bonds. Therefore, the generation *in situ* of the amide $[\text{Pt}(\text{Me})_2(\text{trop}_2\text{N})]$ (**119**) was subsequently planned. The idea was to form the platinum amide by elimination of methane formed through thermal activation of $[\text{Pt}(\text{Me})_2(\text{trop}_2\text{NH})]$ (**K20**), in an analogous fashion to that employed by Wolczanski and Bergman for the formation of reactive imido species (Chapter 2.1.3).

The examples reported by these groups clearly demonstrate that, once the imido intermediate is formed, it immediately reacts with benzene (see Scheme 2.15 and 2.16). The thermal activation

reaction was therefore performed in benzene with the intent to trap the amido complex by *inter*-molecular C-H activation of benzene (Scheme 2.20).



Scheme 2.20: Planned Thermal activation of [Pt(Me)₂(trop₂NH)] (**K20**) in benzene.

A new species formed after two days at relatively high temperature (80°C). Its formation was followed by NMR spectroscopy and was further confirmed by the great difference in solubility between the starting material (**K20**) and the thermal activation product (**K22'**). In fact, **K20** is almost insoluble in benzene, whereas **K22'** is soluble in this solvent. Moreover, the formation of [Pt(Me)(Ph)(trop₂NH)] (**K22'**) through activation of benzene from the amide **119** should be easily detectable by ¹H NMR spectroscopy: [Pt(Me)(Ph)(trop₂NH)] should resemble **K20** and therefore it should show the same patterns in the ¹H NMR spectrum.

Disappointingly, the inspection of the ¹H NMR spectrum revealed that the newly formed compound **K22** was not [Pt(Me)(Ph)(trop₂NH)] (**K22'**). Despite the fact that **K22** has one methyl group ($\delta = 1.58$ ppm, $^2J_{\text{PtH}} = 82.24$ Hz) and that methane actually developed from the reaction mixture, the new compound is asymmetric, in contrast with **K20** and in consequence with the hypothesized species [Pt(Me)(Ph)(trop₂NH)]. Moreover, **K22** displays only two olefinic signals ($\delta = 5.30$ ppm and $\delta = 5.78$ ppm) showing platinum satellites, each integrating to one proton. This observation suggests that only one trop unit is coordinated to the metal center. The signals of the non-coordinated olefins are found at $\delta = 6.52$ ppm and $\delta = 6.68$ ppm, values in the range of those found for the olefinic protons of the free ligand. Furthermore, the presence of a doublet in the aromatic range at $\delta = 8.27$ ppm displaying platinum satellites ($J_{\text{PtH}} = 73$ Hz) suggested the activation of one phenyl ring of the trop. Therefore, it was speculated that the new complex formed by the thermal activation of **K20** was the metallacycle **K22** derived by the *intra*-molecular C-H activation of a benzannulated group of the ligand (Figure 2.6).

X-ray analysis of suitable crystals of **K22**, grown by slow diffusion of *n*-hexane into a saturated solution of the compound in benzene, confirmed the hypothesized structure. In Figure 2.6 an ORTEP view of the single crystal is shown.

Complex **K22** has an almost planar geometry, in fact the angle N-Pt-C31 is $175.7(3)^\circ$ and the angle C31-Pt-ct1 is of $164.8(3)^\circ$. The crystal exhibits a new Pt-C30 bond of $2.042(8)$ Å (similar in length to the other Pt-C31 bond that is $2.037(8)$ Å).

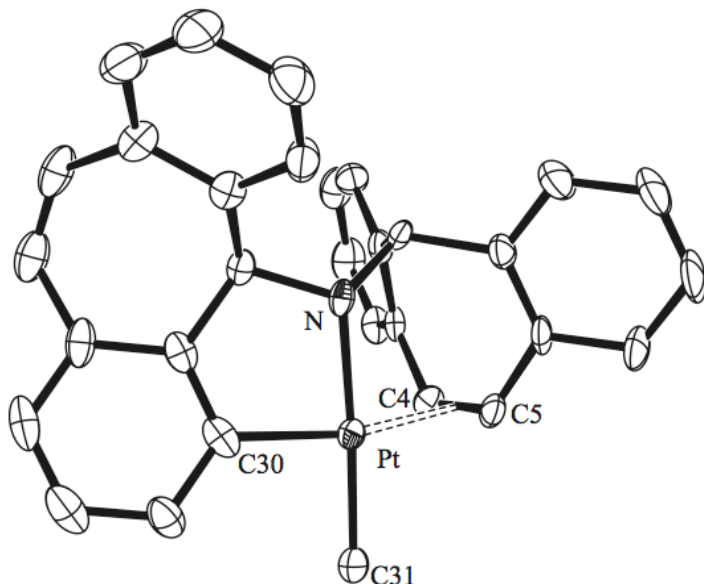
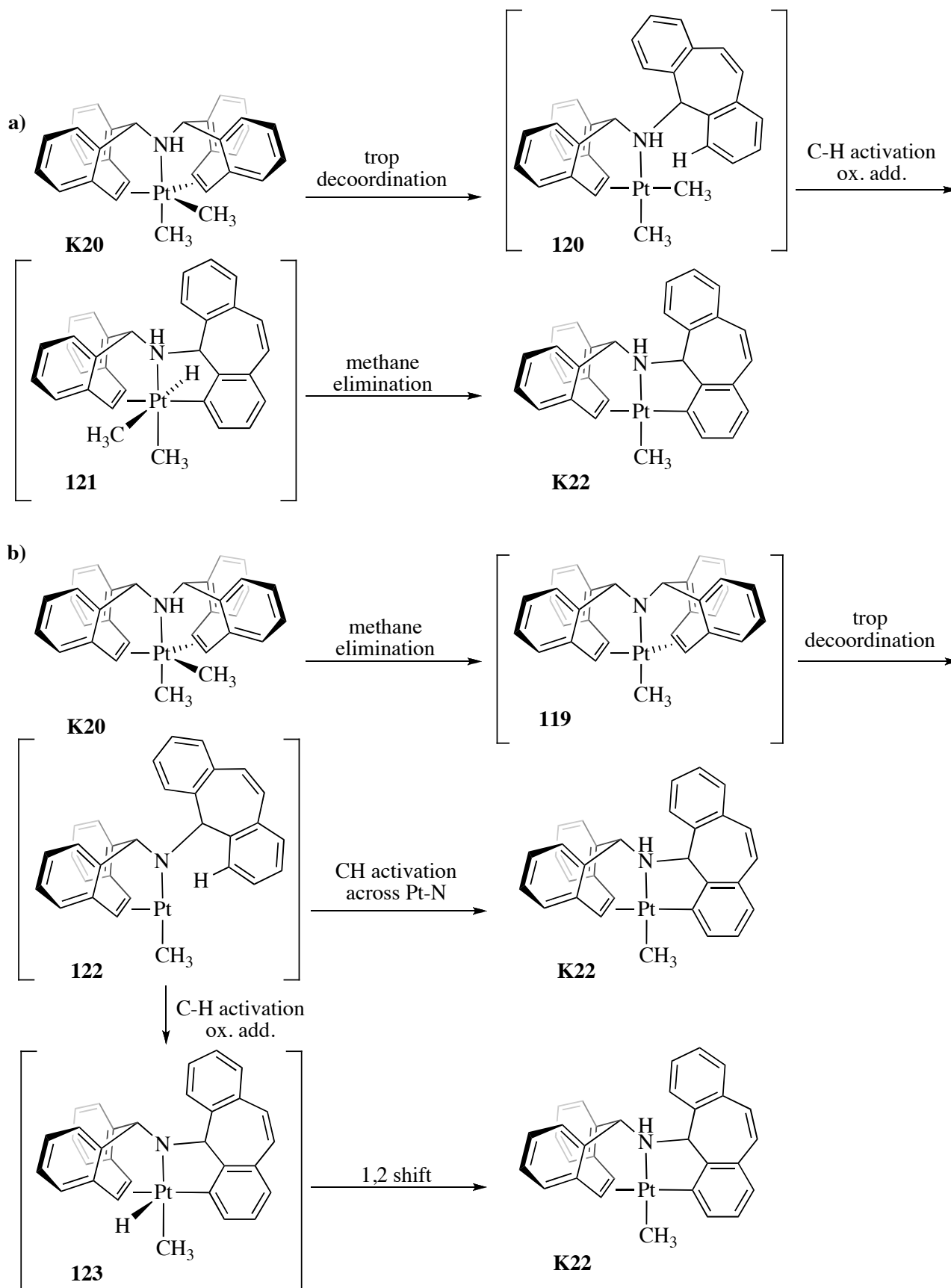


Figure 2.6: ORTEP view of **K22**. Thermal ellipsoids are drawn with 50% probability; all hydrogen atoms are omitted for clarity. Selected bond lengths [Å] and angles [°]: Pt-N 2.103(6); Pt-C4 2.169(7); Pt-C5 2.227(7); ct1-Pt 2.09(7); Pt-C30 2.042(8); Pt-C31 2.037(8); C30-Pt-N $80.2(3)$; C31-Pt-ct1 $164.8(3)$; C30-Pt-C31 $95.8(3)$; N-Pt-C31 $175.7(3)$. ct= centroid of the olefin.

We reasoned that the formation of **K22** from **K20** could follow two plausible mechanisms, which are sketched in Scheme 2.21a-b.

On the one hand, mechanism (a) takes into account the formation of the tetracoordinate species **120** formed after the decoordination of one olefinic unit of the trop ligand. The trop moiety is thus free to rotate and can approach the metal center to undergo an *intra*-molecular C-H activation by a classical oxidative addition (**121**). Subsequently, the elimination of methane yields the orthometallate product **K22**. On the other hand, mechanism (b) considers first the formation of an amido complex (**119**) by thermal elimination of methane from the methyl group and the NH of the trop ligand. The reactive amido intermediate undergoes *intra*-molecular C-H activation of the aromatic proton of the ligand, after decoordination of the ligand (**122**) leading to the isolated product **K22**. For sterical reasons, the latter mechanism is rather unlikely to be operative because the C-H bond of the benzannulated ring of the trop cannot be coplanar to the Pt-N, as it will be later demonstrated in Chapter 2.6. Another plausible route takes into account the formation of **123** by oxidative addition of the CH bond. The subsequent 1,2 proton shifts leads to **K22**.

The decoordination of one olefin unit, prior to its C-H activation – either by oxidative addition or 1,2 addition along the Pt-amide bond – has been proposed as a common step for both mechanisms. As already discussed, the broad platinum satellites in the ^1H NMR spectrum of **K20** were attributed to a weak coordination of the olefin to the platinum. In view of this, the reaction conditions employed – namely the high temperature – would probably promote the formation of such species.

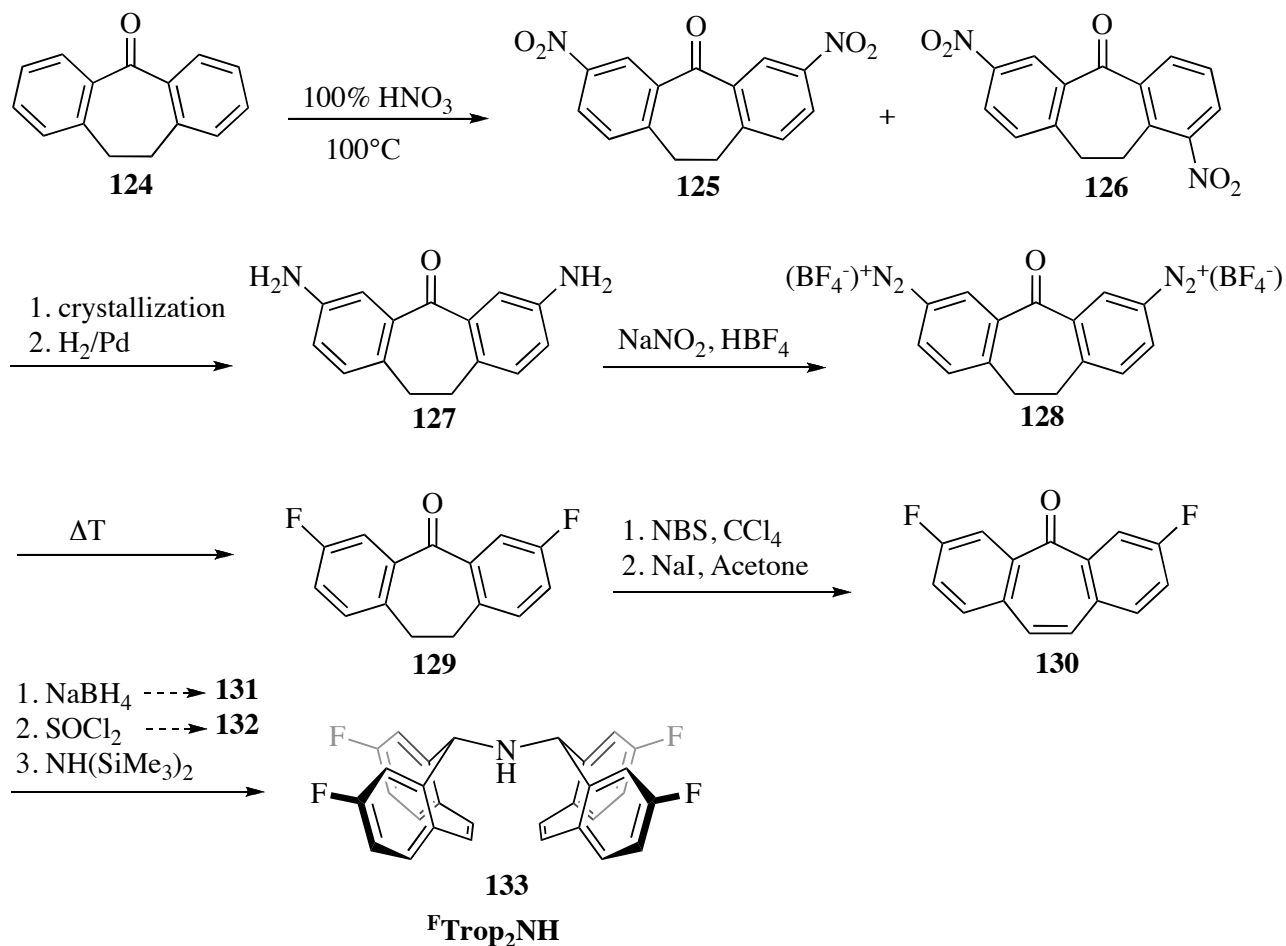
Scheme 2.21a-b: Proposed mechanisms for the formation of **K22**.

The strategy to avoid such process would be, either to modify the trop ligand in order to inhibit the *intra*-molecular C-H activation step, or to promote the formation of the amido complex at a lower temperature. Both strategies have been experimentally tested and will be described in Chapter 2.4 and Chapter 2.5 and 2.6, respectively.

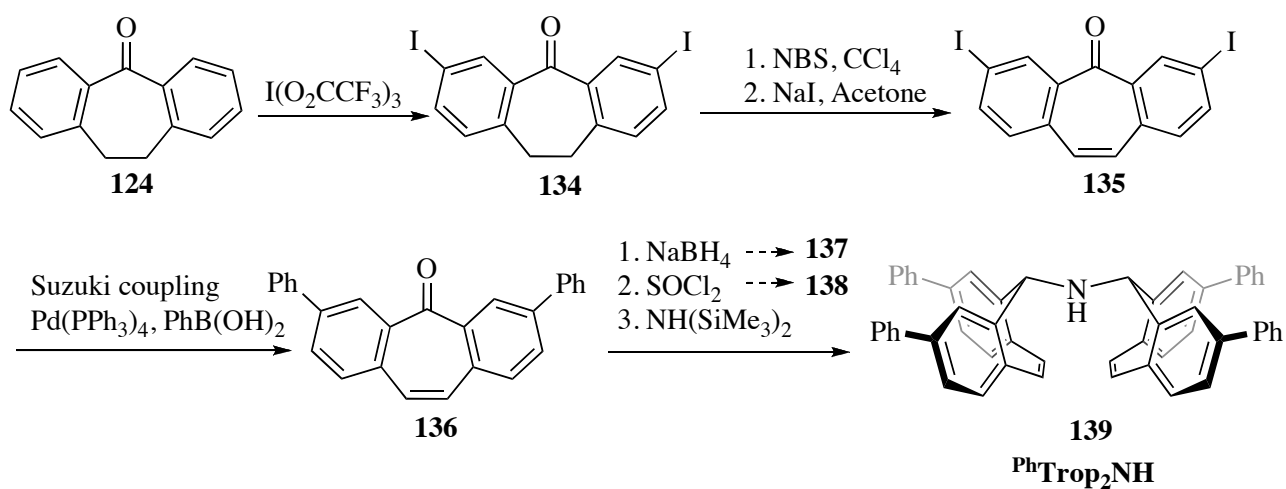
2.4 Synthesis of [Pt(Me)₂(^Ytrop₂NH)]

It was speculated that the *intra*-molecular C-H activation by oxidative addition might be avoided by the appropriate substitution of the aryl groups of the bis(5H-dibenzo[a,d]cyclohepten-5-yl)amine. Therefore, the bis(3,7-difluoro-5H-dibenzo[a,d]cyclohepten-5-yl)amine (^Ftrop₂NH) (**133**) and bis(3,7-diphenyl-5H-dibenzo[a,d]cyclohepten-5-yl)amine (^{Ph}trop₂NH) (**139**) were prepared as new ligands. It was reasoned that the two fluorine atoms in **133** would deactivate the aryl moiety towards electrophilic attack by the metal, whereas the phenyl-substituted ligand **139** would sterically prevent ligand activation in case of a nucleophilic attack from the platinum. The synthetic route for the fluorination of the trop ligand is sketched in Scheme 2.22 and has been already reported by Deblon.⁴⁰ The first steps were performed following the procedure published by Campbell et al., which employs fuming nitric acid for the nitration of the ketone **124**.⁴¹ The crude reaction yields a mixture of the isomers **125** and **126**, which were separated by fractional crystallization in acidic acid. The isolated isomer **125**, was subsequently reduced with dihydrogen at atmospheric pressure in presence of palladium on charcoal⁴² to obtain the diamine compound **127**. Successive reaction with sodium nitrite in tetrafluoroboric acid yields the diazonium salt **128**, which decomposes by thermal reaction to the fluorinated compound **129**.⁴² The introduction of the double bond was achieved by dibromination with N-bromosuccinimide in tetrachloromethane followed by reaction with sodium iodide in acetone to obtain 3,7-difluoro-5H-dibenzo[a,d]cyclohepten-5-one (**130**). Compound **130** can be reduced to the corresponding alcohol **131** by reaction with sodium hydride in methanol. Reaction with thionylchloride yields product **132**. The formation of the desired bis-(3,7-difluoro-5H-dibenzo[a,d]cyclohepten-5-yl)amine (**133**) was finally accomplished by reaction of the chloride **132** with hexamethyldisilylazane following the standard synthetic procedure.³⁶ The synthetic route used to obtain bis(3,7-diphenyl-5H-dibenzo[a,d]cyclohepten-5-yl)amine (^{Ph}trop₂NH) (**139**) is outlined in Scheme 2.23. The initial iodination of **124** with iodo-trifluoroacetate⁴³ allowed the isolation in good yield of the 3,7-diiodo-5H-dibenzo[a,d]cycloheptanone (**134**), which is a versatile substrate for further ligand modification. The double bond was introduced by the same procedure as discussed above (**135**). A standard Suzuki coupling with tetrakis-triphenylphosphine palladium (3 mol%) as catalysts and

phenylboronic acid yielded the 3,7-diphenyl-5H-dibenzo[a,d]cycloheptanone **136**. Reduction to the alcohol **137**, reaction with thionylchloride to **138** and subsequently with $[\text{NH}(\text{SiMe}_3)_2]$ leads to the formation of the desired phenyl-substituted ligand $^{\text{Ph}}\text{trop}_2\text{NH}$ (**139**).



Scheme 2.22: Synthetic strategy employed for the preparation **132**.



Scheme 2.23: Synthetic strategy employed for the preparation of **139**.

In order to test the coordination behavior of **133**, a preliminary reaction of ${}^F\text{trop}_2\text{NH}$ with the rhodium precursor $[\text{Rh}(\mu^2\text{-Cl})(\text{COD})]_2$ was attempted. The isolation of $[\text{Rh}(\mu^2\text{-Cl})({}^F\text{trop}_2\text{NH})_2]_2$ (**K23**) was achieved in an analogous fashion to that adopted for the complex $[\text{Rh}(\mu^2\text{-Cl})(\text{trop}_2\text{NH})_2]_2$.⁴⁵ An ORTEP view of the X-ray crystal structure obtained for **K32** is shown in Figure 2.7. It can be observed that the values of the bond lengths between the metal center and the bridging chlorine atoms, Rh-Cl1 [2.376(2) Å] and Rh-Cl2 [2.626(3) Å], are in the same range of those found for $[\text{Rh}(\mu\text{-Cl})(\text{trop}_2\text{NH})_2]_2$, which are 2.384(2) Å and 2.626(2) Å, respectively. Neither the Rh-N nor the Rh-C bond lengths are affected by the substitution of the ligand from trop_2NH to ${}^F\text{trop}_2\text{NH}$. From these observations it was reasoned that the fluorine in the 3,7-positions of the trop would not affect the coordination behaviour of the ligand. Therefore, no drastic changes in the structural properties were expected for the platinum complexes bearing **133** or **139**.

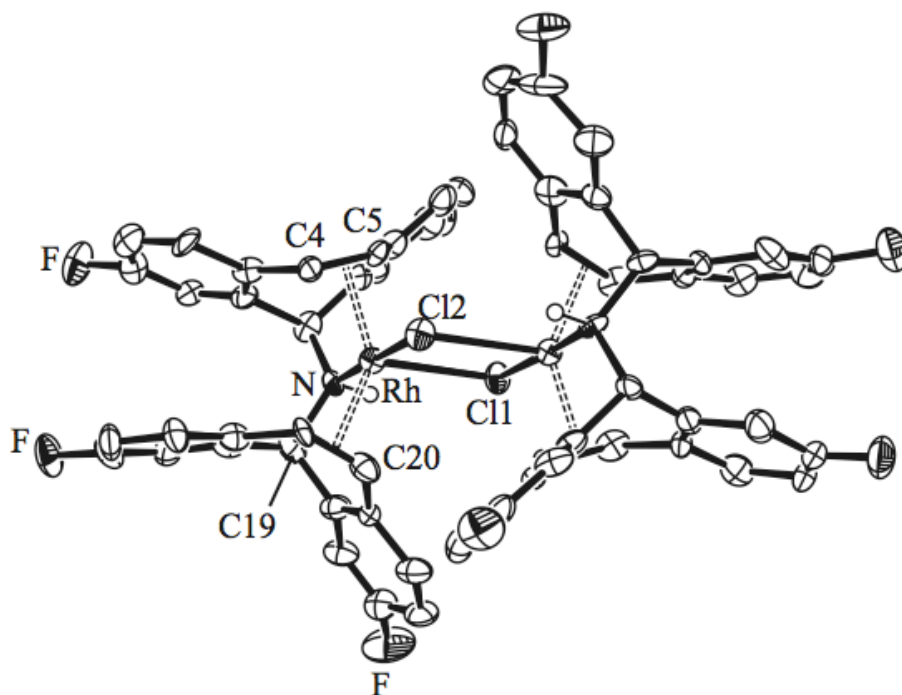
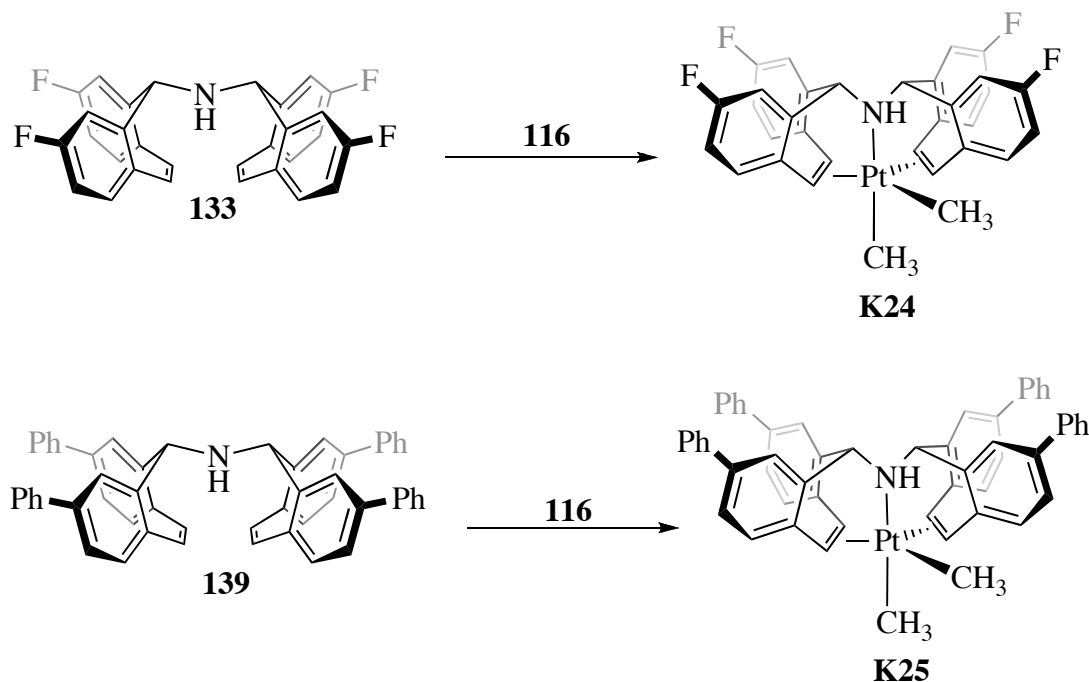


Figure 2.7: ORTEP view of $[\text{Rh}(\mu\text{-Cl})({}^F\text{trop}_2\text{NH})_2]_2$ (**K23**). Thermal ellipsoids are drawn with 50% probability; all hydrogen atoms except at N1 are omitted for clarity. Selected bond lengths [Å] and angles [°]: Rh-N 2.076(8); Rh-C4 2.161(8); Rh-C5 2.157(8); ct1-Rh 2.031(8); Rh-C20 2.154(8); Rh-C19 2.168(9); Rh-ct2 2.041(9); Rh-Cl1 2.376(2); Rh-Cl2 2.626(3); ct2-Rh-ct1 138.7(2); N-Rh-Cl1 93.9(2); N-Rh-Cl2 179.5(3). ct= centroid of the olefin.

The preparation of the platinum(II) methyl complexes $[\text{Pt}(\text{Me})_2({}^Y\text{trop}_2\text{NH})]$ (Y= F, **K24** and Y= Ph, **K25**) was performed analogously to $[\text{Pt}(\text{Me})_2(\text{trop}_2\text{NH})]$ (**K20**) (Scheme 2.23).

Scheme 2.23: Synthesis of **K24** and **K25**.

As expected, complexes **K24** and **K25** display similar spectroscopic features to **K20** as is confirmed by the ^1H NMR and ^{13}C NMR spectra (see Table 2.1).

Table 2.1: Characteristic ^1H NMR and ^{13}C NMR data for **K20**, **K24** and **K25**.

		$\text{CH}_3^{\text{axial}}$	$\text{CH}_3^{\text{equatorial}}$	$\text{CH}_{\text{benzyl}}$	$\text{CH}_{\text{olefin}}$
K20	$\delta^1\text{H}$ [J_{HH} (Hz)]	0.105 [67.3]	0.175 [67.3]	4.62 [18.8]	3.97 [38.4] 4.12 [55.4]
	$\delta^{13}\text{C}$ [J_{PtC} (Hz)]	-13.5 [725.0]	-6.97 [647.1]	71.8	57.12 [80.2] 62.71 [151.0]
K24	$\delta^1\text{H}$ [J_{HH} (Hz)]	0.074 [69.7]	0.165 [67.2]	4.71 [21.9]	3.97 [32.3] 4.07 [37.3]
	$\delta^{13}\text{C}$ [J_{PtC} (Hz)]	-14.78 [748.6]	-7.54 [651.5]	68.33	55.83 [76.9] 61.75 [155.6]
K25	$\delta^1\text{H}$ [J_{HH} (Hz)]	0.21 [68.35]	0.27 [66]	4.91 [20.5]	4.15 [n.d.] 4.25 [n.d.]
	$\delta^{13}\text{C}$ [J_{PtC} (Hz)]	-13.98 [n.d.]	-7.75 [n.d.]	71.9	57.2 [n.d.] 62.8 [n.d.]

Crystals of **K24** suitable for X-ray studies were obtained by slow evaporation of a saturated solution of in THF. Figure 2.7 shows an ORTEP view of the crystal structure. Despite the similar structural characteristics between **K24** and **K20**, the Pt-C31 bond length in **K24** is about 0.1 Å longer than in **K20**. For these reasons, we expected compound **K24** to be more reactive than **K20**.

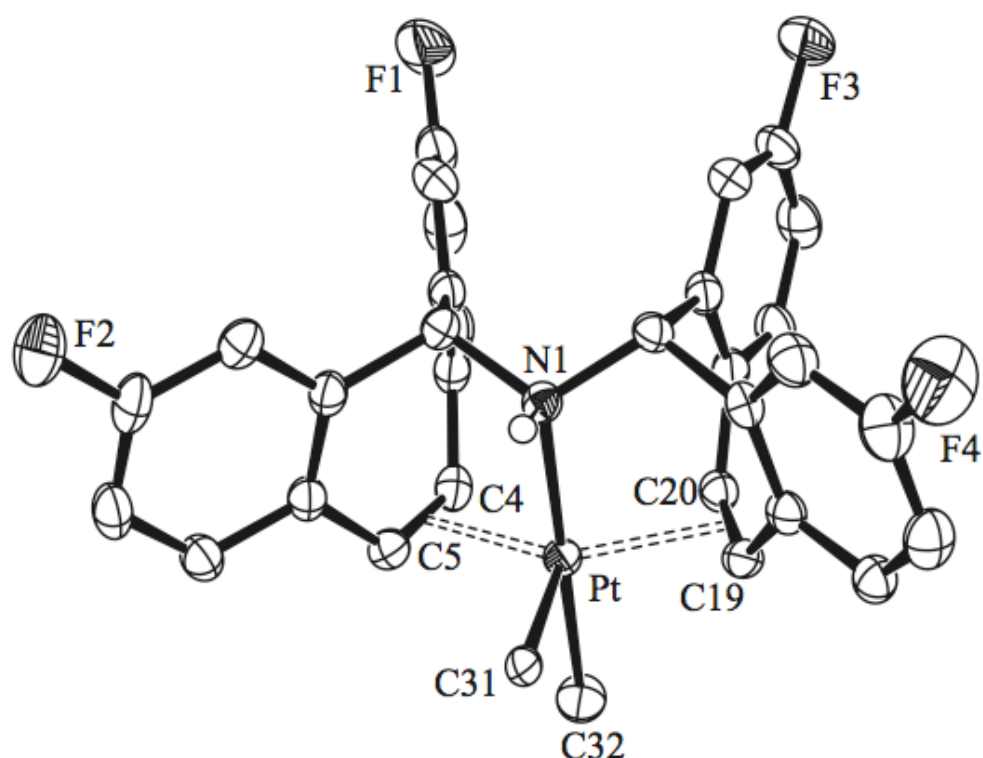
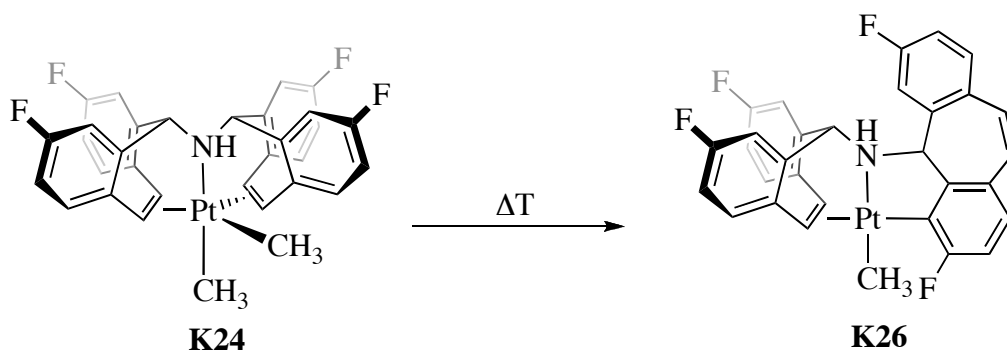


Figure 2.7: ORTEP view of $[\text{Pt}(\text{Ftrop}_2\text{NH})\text{Me}_2]$ (**K24**). Thermal ellipsoids are drawn with 50% probability; all hydrogen atoms except at N1 are omitted for clarity. Selected bond lengths [\AA] and angles [$^\circ$]: Pt-N 2.181(3); Pt-C4 2.180(4); Pt-C5 2.142(4); ct1-Pt 2.039(4); Pt-C20 2.190(3); Pt-C19 2.136(4); Pt-ct2 2.042(4); Pt-C31 2.261(4); Pt-C32 2.064(4); C31-Pt-N 86.6(1); ct2-Pt-ct1 136.1(3); C32-Pt-N 178.5(2). ct= centroid of the olefin.

The thermolysis reaction in benzene of complex **K24** yield to the *ortho*-metallation compound **K26** depicted in Scheme 2.24.



Scheme 2.24: Reactivity of **K24** at elevated temperatures.

The ^{19}F NMR spectroscopy immediately confirmed the loss of symmetry of the molecule because of the presence of four different signals at $\delta = -92.49$ ppm, $\delta = -112.28$ ppm, $\delta = -113.26$ ppm and $\delta = -113.37$ ppm. Furthermore, the peaks at lower frequencies display platinum

satellites of 179 Hz. Note that the ^{19}F NMR spectrum of complex **K24** shows only two signals at $\delta = -120$ and $\delta = -117$ ppm due to its higher symmetry.

On the contrary, complex $[\text{Pt}(\text{Me})_2(\text{Phtrop}_2\text{NH})]$ (**K25**) did not yield the *ortho*-metallate compound but decomposed to a mixture of unidentified species. In view of these results we hypothesized that, most likely, the C-H activation step proceeds by nucleophilic attack of the metal center onto the C-H bond. For the F-substituted ligand **128** the increased acidity of the proton leads to a faster orthometallation reaction. The increased steric hindrance at this position in complex **K25** prevents this attack and this compound undergoes non-selective decomposition reactions at high temperatures in solution.

2.5 Synthesis of $[\text{Pt}(\text{Me})(\text{X})(\text{trop}_2\text{NH})]$

Since the substitution of the trop ligand did not lead to the desired result, the synthesis of the amide under mild conditions – avoiding the high temperatures which may lead to the formation of cycloplatinate species – was planned. The results obtained for the isoelectronic rhodium compounds encouraged us to explore the possibility to form the amide by direct deprotonation of the amine function of the coordinated trop. The spectroscopic and structural data of $[\text{Pt}(\text{Me})_2(\text{trop}_2\text{NH})]$ and $[\text{Rh}(\text{PPh}_3)(\text{X})(\text{trop}_2\text{NH})]$ (where X is a generic anion) clearly demonstrate a similar coordination mode for the tripodal amine ligand and therefore an analogous behavior was expected in the presence of a base – namely the deprotonation from the amine to the amide. The idea was therefore to prepare complexes of general formula $[\text{Pt}(\text{Me})(\text{X})(\text{trop}_2\text{NH})]$ (where X is an appropriate counter anion), which would be eventually employed for the deprotonation reactions. In order to achieve this result, the cleavage of one of the two methyl groups under acidic conditions was investigated.

From the evaluation of the NMR spectroscopic data of complexes **K20** and **K24**, it was evident that the two methyl groups have different bond strengths to the platinum center.

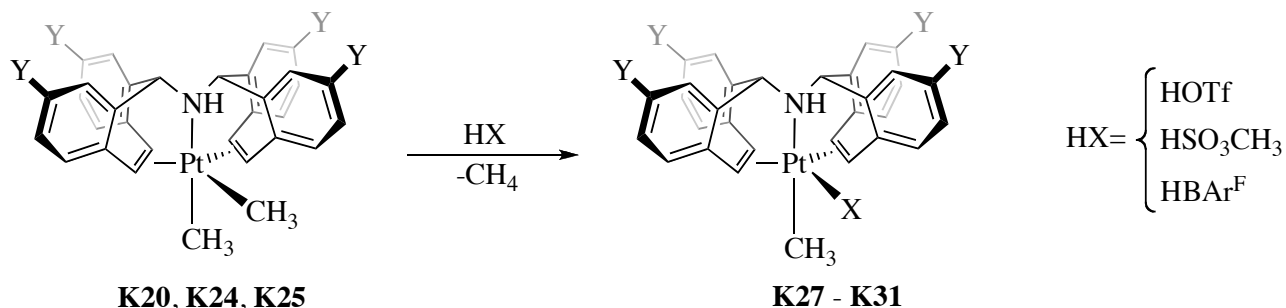
The methyl group in equatorial position was expected to be bound more weakly because of the longer Pt-C distances (see Table 2.2) and the smaller corresponding platinum satellites.

These expectations are fulfilled by the results obtained when **K20**, **K24** or **K25** are treated with acids.

Table 2.2: bond lengths of the methyl groups.

	CH ₃ equatorial	CH ₃ axial
$[\text{Pt}(\text{Me})_2(\text{trop}_2\text{NH})]$ K20	Pt-C31 2.167(4) Å	Pt-C32 2.063(3) Å
$[\text{Pt}(\text{Me})_2(\text{Ftrop}_2\text{NH})]$ K24	Pt-C31 2.261(4) Å	Pt-C32 2.064(4) Å

Reaction of **K20**, **K24** and **K25** with acids resulted in the production of methane and led to the formation of the desired platinum(II) complexes **K27**, **K28**, **K29**, **K30** and **K31** (Scheme 2.25), which bears one methyl group in the axial position.



K20: Y= H [Pt(Me)₂(Trop₂NH)]

K24: Y= F [Pt(Me)₂(^FTrop₂NH)]

K25: Y= Ph [Pt(Me)₂(^{Ph}Trop₂NH)]

K27: Y= H; X= OTf [Pt(OTf)(Me)(Trop₂NH)]

K28: Y= H; X= OMs [Pt(OMs)(Me)(Trop₂NH)]

K29: Y= H; X= BAr^F [Pt(Me)(Trop₂NH)]BAr^F

K30: Y= F; X= BAr^F [Pt(Me)(^FTrop₂NH)]BAr^F

K31: Y= Ph; X= BAr^F [Pt(Me)(^{Ph}Trop₂NH)]BAr^F

Scheme 2.25: Reactivity of complexes **K20**, **K24** and **K25** upon treatment with acids.

Depending on the acid used, it was possible to synthesize pentacoordinate and tetracoordinated platinum complexes of general formula [Pt(Me)(X)(trop₂NH)] and [Pt(Me)(trop₂NH)]⁺(X⁻) as it will be shown below (where X is a coordinating or non-coordinating counter anion).

[Pt(O₃SMe)(Me)(trop₂NH)] (**K28**) and [Pt(O₃SCF₃)(Me)(trop₂NH)] (**K27**) are two examples of pentacoordinated compounds. The crystal structure of **K28** shows that the MeSO₃⁻ belongs to the coordination sphere of the metal with a bond distance Pt-O1 of 2.31(3) Å (Figure 2.8). As expected, the methyl cleaved is the equatorial one: the CH₃ group in the axial position is still bound to the metal center with a distance Pt-C of 2.047(5) Å, slightly shorter than in **K20** and **K24**.

Comparing the Pt-C_{olefin} bond distances in **K28** and **K20**, it is evident that the bond lengths are in average longer for **K28** (2,175 Å) than in **K20** (2.163 Å), due to less electron density on the metal center and consequently less (d→π^{*})-back bond donation from the metal to the olefins. This is reflected in the ¹H NMR spectra of [Pt(O₃SMe)(Me)(trop₂NH)] (**K28**) and [Pt(O₃SCF₃)(Me)(trop₂NH)] (**K27**), where the olefinic resonances are shifted to higher frequencies (δ= 4.94 δ= 6.86 for **K28** and δ= 4.97 ppm and δ= 5.9 ppm for **K27**), whereas in [Pt(Me)₂(trop₂NH)] (**K20**) such signals are displayed at δ= 3.97 ppm and δ= 4.12 ppm. High

frequency shifts are observed for the olefinic carbon nuclei in the ^{13}C NMR spectra. Comparable differences were already observed for **K21** and were already discussed in Chapter 2.3.

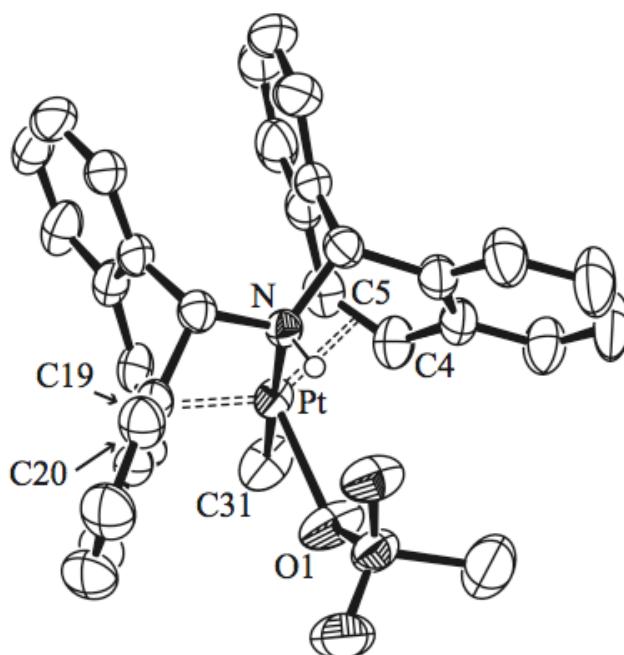


Figure 2.8: ORTEP view of **K28**. Thermal ellipsoids are drawn with 50% probability; all hydrogen atoms except at N1 are omitted for clarity. Selected bond lengths [\AA] and angles [$^\circ$]: Pt-N 2.169(3); Pt-C4 2.171(4); Pt-C5 2.148(4); ct1-Pt 2.039(4); Pt-C20 2.185(4); Pt-C19 2.197(4); Pt-ct2 2.075(4); Pt-C31 2.047(5); Pt-O1 2.312(3); NH-O2 1.973(5); C31-Pt-N 178.3(2); ct2-Pt-ct1 137.8(1); O1-Pt-N1 92.3(1). ct= centroid of the olefin.

On the other hand, complexes $[\text{Pt}(\text{Me})(\text{trop}_2\text{NH})]^+\text{BAr}^{\text{F}-}$ (**K29**), $[\text{Pt}(\text{Me})(^{\text{F}}\text{trop}_2\text{NH})]^+\text{BAr}^{\text{F}-}$ (**K30**) and $[\text{Pt}(\text{Me})(^{\text{Ph}}\text{trop}_2\text{NH})]^+\text{BAr}^{\text{F}-}$ (**K31**), are examples of tetracoordinated compounds. The structures of **K30** and **K31** were determined by X-ray diffraction studies and are shown in Figure 2.9 and Figure 2.10, respectively. The refinement of the data of **K30** was complicated by severe disordering and therefore the structure will not be discussed in detail. But the gross structural features as shown in the figure are unambiguously correctly presented.

Crystals of good quality were obtained for **K31**. The ORTEP plot in Figure 2.10 shows a distorted structure halfway between a planar and saw-horse type. Compared to structure **K20** (Figure II.3), structure **K31** has shorter Pt-N ($\Delta = 0.021 \text{ \AA}$) and Pt-CH₃ ($\Delta = 0.017 \text{ \AA}$) bond lengths; on the contrary the Pt-C_{olefins} are longer ($\Delta = 0.05 \text{ \AA}$). Moreover, the angle ct1-Pt-ct2 widens from 135.4° in the trigonal bipyramidal structure of **K20** to 159.9° in **K31**. Note that in the saw-horse type form of (**S,S**)-**K6** (Figure 1.8a-b) the angle ct1-Rh-ct2 is 147.03° .

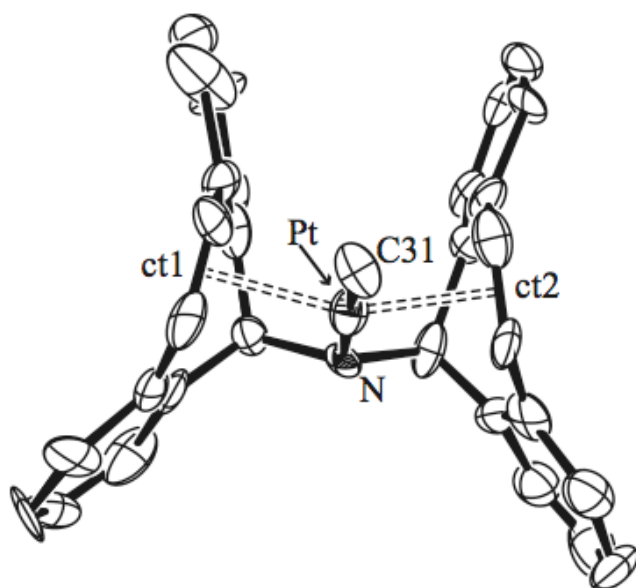


Figure 2.9:
ORTEP view of **K29**. Thermal ellipsoids are drawn with 50% probability; the counter anion (BAR^{F}) and all hydrogen atoms except at N1 are omitted for clarity. Selected bond lengths [\AA] and angles [$^{\circ}$]:
ct1-Pt 2.144;
Pt-ct2 2.084;
ct2-Pt-ct1 156.08.
ct= centroid of the olefin.

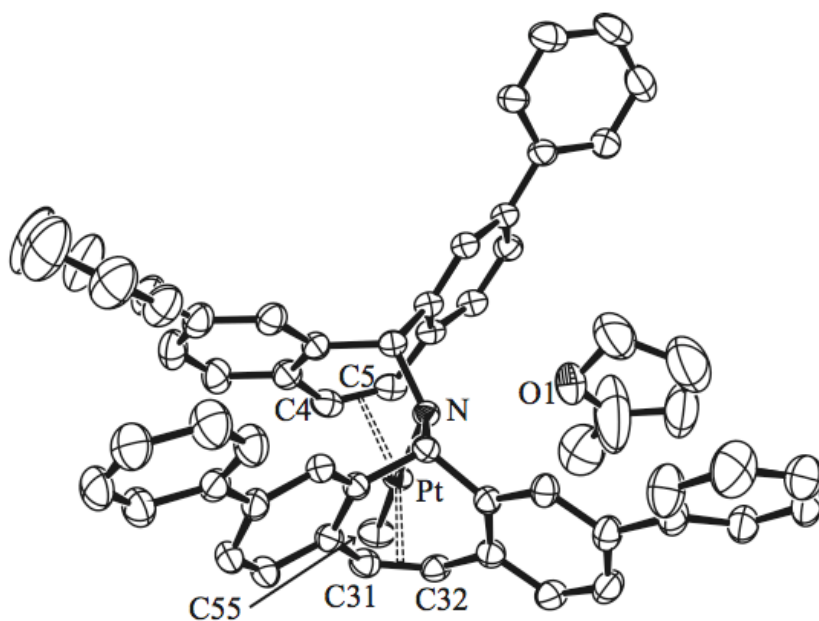
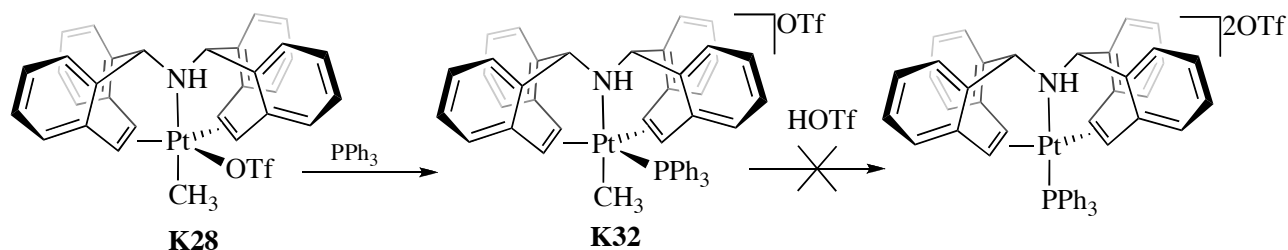


Figure 2.10:
ORTEP view of **K31**. Thermal ellipsoids are drawn with 50% probability; the counter anion (BAR^{F}) and all hydrogen atoms except at N1 are omitted for clarity. Selected bond lengths [\AA] and angles [$^{\circ}$]:
Pt-N 2.158(3);
Pt-C4 2.214(3);
Pt-C5 2.208(3);
ct1-Pt 2.104(3);
Pt-C31 2.212(3);
Pt-C32 2.221(3);
Pt-ct2 2.097(3);
Pt-C55 2.046(4);
 $\text{NH}\cdots\text{O1}$ 2.007(5);
 C55-Pt-N 177.1(1);
ct2-Pt-ct1 159.9(2).
ct= centroid of the olefin.

One molecule of solvent ($\text{C}_5\text{H}_{10}\text{O}$) is present in the crystal structure; the solvent interacts with the NH moiety of the trop ligand ($\text{NH}\cdots\text{O}$ bond length of 2.007 \AA). This can be taken as an indication that the NH function is rather acidic. The reaction at room temperature with an excess of acid did not allow the removal of the second methyl group. Reactions at high temperature were avoided in order to prevent the *ortho*-metallation. We hoped that the synthesis of a platinum

complex bearing an additional ligand in equatorial position as triphenylphosphine would allow the removal of the remaining group. Consequently, complex **K32** was synthesized (Scheme 2.24).



Scheme 2.24: Synthesis of $[\text{PtMe}(\text{trop}_2\text{NH})(\text{PPh}_3)]\text{OTf}$ **K32**.

The complex $[\text{PtMe}(\text{trop}_2\text{NH})(\text{PPh}_3)]\text{OTf}$ (**K32**) shows in the ^{31}P NMR spectrum a signal at $\delta = -15.01$ ppm with platinum satellites of 2596 Hz. The structure of **K32** has been confirmed by X-ray diffraction analyses on crystals obtained by slow evaporation of a saturated chloroform solution of the compound. Figure 2.12 shows an ORTEP plot of the structure determined with a single crystal X-ray diffraction study with selected bond lengths and angles. The triphenylphosphine is coordinated to the metal center and occupies the equatorial position within the plane of the trigonal bipyramid with a Pt-P distance of 2.425(2) Å. Reaction of compound **K32** with various acids did not give the desired results and the methyl group in the axial position could not be cleaved.

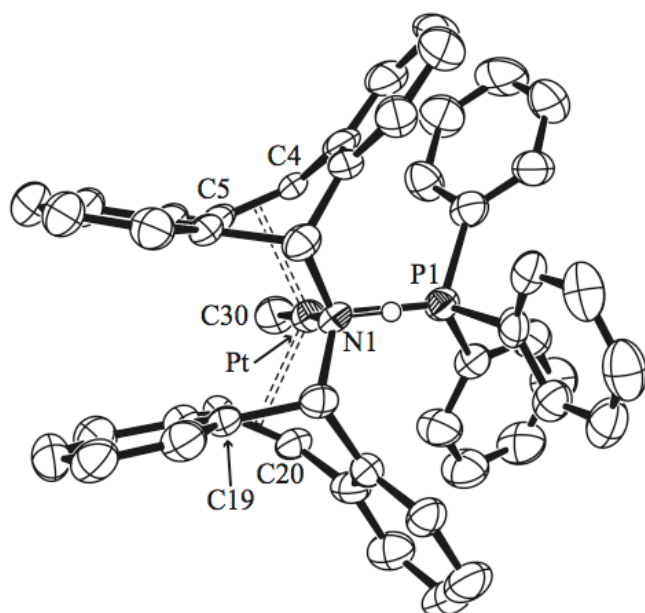


Figure 2.12: ORTEP view of **K32**.

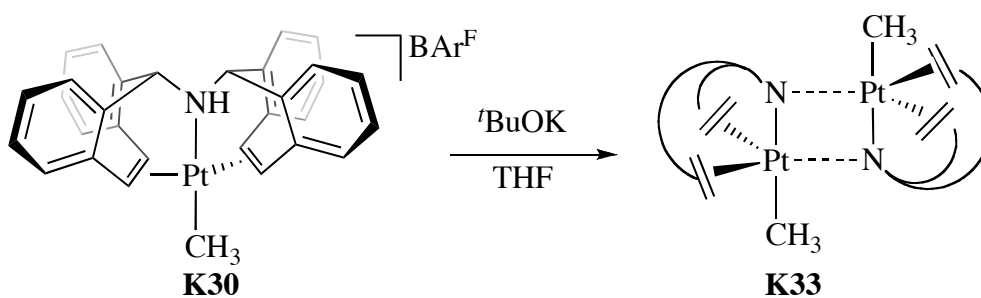
Thermal ellipsoids are drawn with 50% probability; the counter anion (OTf) and all hydrogen atoms except at N1 are omitted for clarity.

Selected bond lengths [Å] and angles [°]: Pt-N 2.195(5); Pt-C4 2.250(6); Pt-C5 2.215(6); ct1-Pt 2.121(6); Pt-C20 2.225(6); Pt-C19 2.179(6); Pt-ct2 2.088(6); Pt-C30 2.086(6); Pt-P1 2.425(2); C30-Pt-N 174.8(2); ct2-Pt-ct1 128.8(3); P1-Pt-N1 95.1(1).
ct= centroid of the olefin.

2.6 Deprotonation Reaction

Since the target complexes $[\text{Pt}(\text{Me})(\text{X})(\text{trop}_2\text{NH})]$ (where $\text{X} = \text{OTf}, \text{OMs}, \text{BAr}^{\text{F}}$) could be prepared in good yields, we moved our attention to the deprotonation step, following the same conditions used for the NHC rhodium complexes of Chapter 1.

As a preliminary test, the reaction was first tried in a J. Young NMR tube. One equivalent of potassium *tert*-butoxide was added to a freshly distilled $[\text{D}_8]$ -THF solution of the platinum amine complex $[\text{Pt}(\text{Me})(\text{trop}_2\text{NH})]\text{BAr}^{\text{F}}$ (**K30**), prepared under the exclusion of air or moisture. A change in the color of the reaction mixture from yellow to light green – the characteristic color of the amide – could be observed after the addition of the base (Scheme 2.25), but the green color vanished almost immediately. This behaviour is in marked contrast to the properties of the NHC Rh(I) complexes discussed in Chapter 1 where the green color of the amide complexes is persistent for extended periods of time at room temperature.



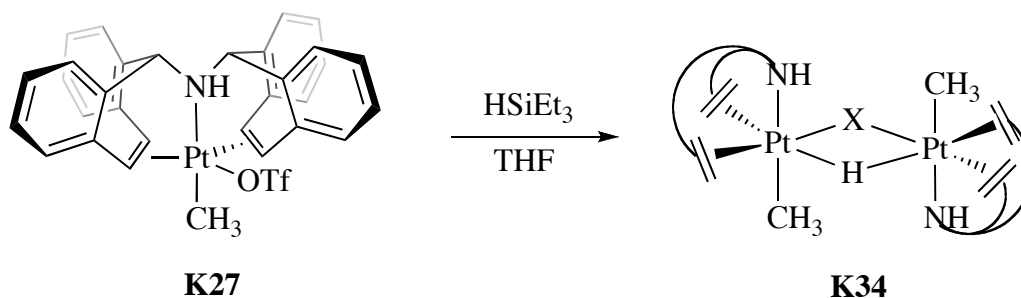
Scheme 2.25: Deprotonation of $[\text{PtMe}(\text{trop}_2\text{NH})]\text{BAr}^{\text{F}}$ (**K29**) to **K33**, with *t*BuOK.

The formed bright yellow species **K33** was not isolated but characterized in solution by NMR spectroscopy techniques. The ^1H NMR and ^{13}C NMR spectra clearly show the formation of a new compound still bearing the trop_2NH ligand. However, the formed complex does not display the NH signal anymore – in the platinum(II) complexes the NH is found in a range from 2 ppm to 5 ppm – and it has a high symmetry, as deduced by the number of signals observed both in the ^1H NMR spectrum. One singlet for the two benzylic protons was found at 4.65 ppm ($J_{\text{PtH}} = 29.5$ Hz) and two doublets were observed for the four olefinic protons at 4.49 ppm and 4.82 ppm ($J_{\text{PtH}} = 41.1$ Hz and $J_{\text{PtH}} = 64.4$ Hz). These observations – the high symmetry of the compound and the absence of the NH signal – exclude that **K33** did undergo an *intra*-molecular C-H activation of the benzannulated ring of the trop ligand. Compared to $[\text{PtMe}(\text{trop}_2\text{NH})]\text{BAr}^{\text{F}}$ (**K30**) the olefinic signals are shifted to lower frequency ($\Delta = 1.1$ ppm and 2.4 ppm, respectively) indicating a higher electron density on the metal center and the consequent increased ($\text{d} \rightarrow \pi^*$) – back donation from the platinum to the olefin.

Complex **K33** proved to be quite inert and did not react, for example, with HSiEt_3 . However, **K33** reacts with acid to give back **K30**. In summary, the absence of the NH function, the high symmetry of the complex, and the low frequency shift of the ^1H resonances for the olefinic nuclei lead us to propose that the dimeric species **K33**, depicted in Scheme 2.25, has formed.

Note, that this result strongly suggests that the *intra*-molecular C-H activation discussed previously in Chapter 2.3.1 does not proceed through a tetracoordinated amido complex with a saw-horse type structure but require the decoordination of one $\text{C}=\text{C}_{\text{trop}}$ unit (Scheme 2.21a).

In view of these results, we reasoned that a suitable substrate for the C-H activation could be offered prior the deprotonation reaction in order to trap the amido complex before the formation of the inert species **K33**. In a first attempt, triethylsilane (HSiEt_3) was tested as substrate. Disappointingly, HSiEt_3 reacts with the platinum(II) salt to quantitatively yield the hydride species **K34** (Scheme 2.26).



Scheme 2.26: Formation of $[\text{Pt}(\text{trop}_2\text{NH})(\mu^2-\text{H})(\mu^2-\text{X})\text{Me}]_2$ (**K34**).

No crystals suitable for X-ray diffraction studies were obtained and the complex was characterized by ^1H NMR, ^{13}C NMR and ^{195}Pt NMR spectroscopy. The ^1H NMR spectrum shows that the new compound is asymmetric, two signals were found for the benzylic protons at $\delta = 4.84$ ppm and 5.47 ppm; and four doublets for the olefins were detected ($\delta = 3.07$ ppm, 3.57 ppm, 4.97 ppm and 5.11 ppm). The formation of a dimeric species was doubtlessly clarified by means of ^1H NMR. The signals attributed to the hydride $\text{Pt}(\mu^2-\text{H})$ appeared at $\delta = -12.58$ ppm as a five-line multiplet, due to the overlapping of a doublet (one ^{195}Pt nuclei within the dimeric unit) and a triplet (two ^{195}Pt nuclei within the dimeric unit). Note that a singlet with two ^{195}Pt satellites is expected for a monomeric hydride compound. Moreover, the evaluation of the integrals allows us to state that there is only one hydride per molecular unit. Despite the fact that we could not determine the exact nature of the second bridging atom X, we could rationalize that the loss of symmetry of complex **K34**, with respect to the parental compound **K27**, was due to the presence of the unidentified X ligand.

However, the reaction clearly showed that silanes are not suitable for our purpose and should therefore be replaced by a more appropriate class of compounds. Since the reaction of **K30** in the presence of benzene resulted in the neat formation of **K33**, we speculated that fluoroarenes might be good substrates for further trials. These should not react with tetracoordinate platinum precursor complexes like **K27** and should show a higher reactivity with respect to benzene. Moreover, the possibility to follow the reaction by means of ^{19}F NMR spectroscopy represents an additional advantage. Pentafluorobenzene ($\text{C}_6\text{F}_5\text{H}$) seemed the ideal candidate for our next test. A preliminary reaction shows that $\text{C}_6\text{F}_5\text{H}$ does indeed not react with **K27** (differently from HSiEt_3). At this point we initiated a DFT calculations (performed by Dr. Jean-Valère Naubron) using a model system as is briefly outlined below.

2.6.1 DFT Calculations

DFT calculations were performed in order to see whether a C-H activation of C_6HF_5 across the Pt-N bond would be mechanistically possible or whether the calculated energy for the process would be prohibitive.

Computational Methods:

The simplified model **M2** was chosen in order to represent compound **C1** which is the transient amide complex intermediate in the deprotonation of **K27**.

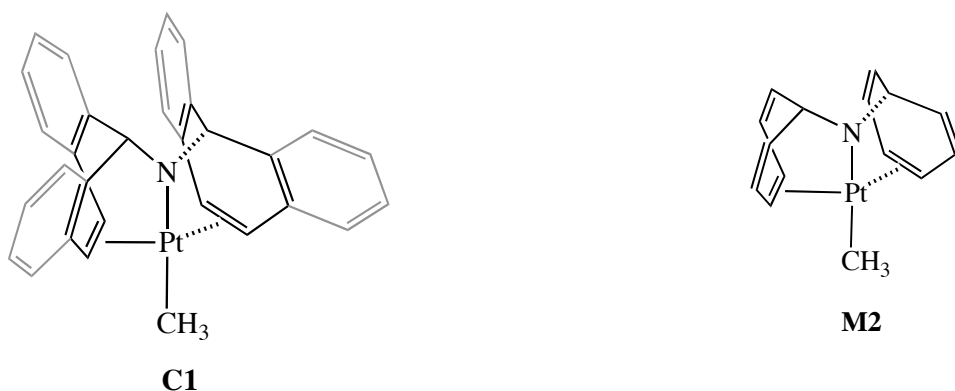


Figure 2.14: Simplified model **M2** to represent compound **C1**.

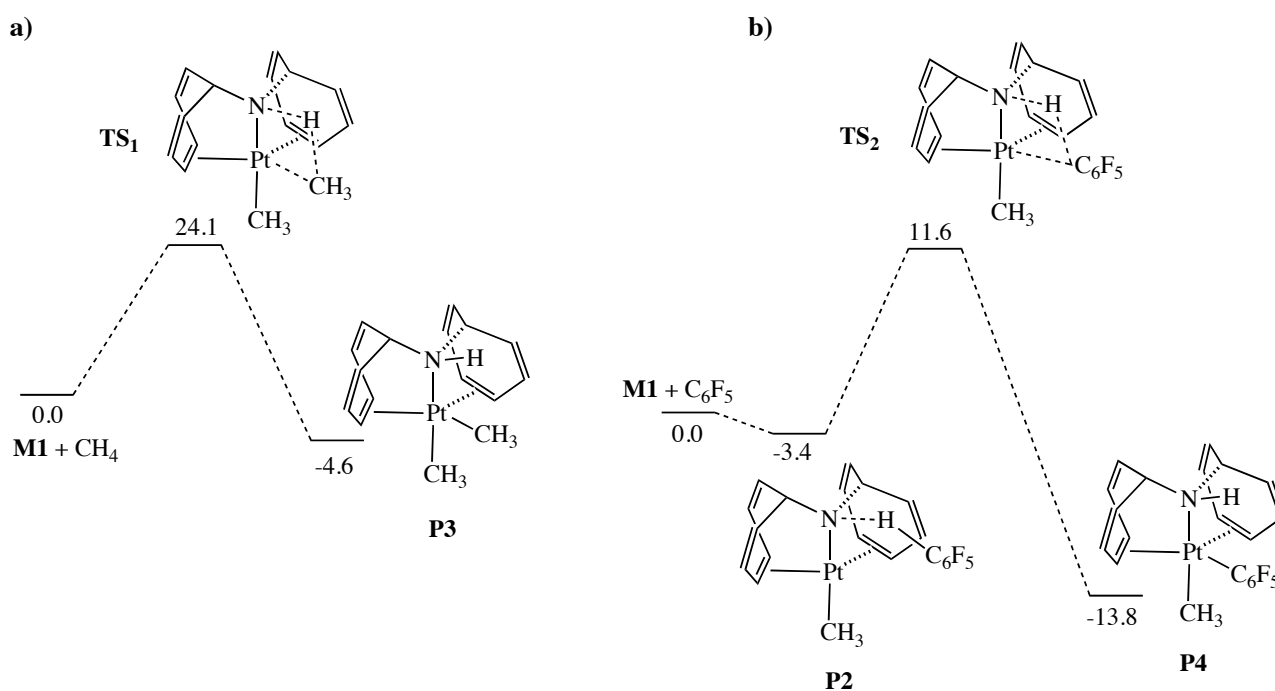
All calculations were carried out within the framework of DFT. For optimizations, we used the BP86 functional in combination the BSI basis set, which consists of the standard 6-31G(d) basis set for all atoms directly connected to the metal with the Lanl2mb basis function^{‡,§} for the Pt. The

[‡]A. D. Becke, *Phys. Rev. A* **1988**, 38, 3098. [§] J. P. Perdew, *Phys. Rev. B* **1986**, 33, 8822. * W. R. W. P.J. Hay, *J. Chem. Phys.* **1985**, 82, 299.

Lan12mb basis function incorporates the Hay and Wadt* small-core relativistic effective core potential and a minimal valence basis set for all atoms.

Results and Discussion:

The cleavage of a C-H bond across the N-Pt bond has been calculated for methane and pentafluorobenzene and the reaction profile for both processes are displayed in Scheme 2.27a-b.



Scheme 2.27a-b: Reaction profile for the C-H activation across the Pt-N bond calculated for methane (a) and pentafluorobenzene (b). Energies corrected for ZPE in kcal mol^{-1} .

For the mechanism of methane activation, it was found that most likely the alkane reacts with **M1** following a one step mechanism to form complex **P3**. The activation energy corresponding to this process is with $24.1 \text{ kcal mol}^{-1}$ rather high but thermally still feasible.

For the activation of $\text{C}_6\text{F}_5\text{H}$ a different reaction profile is calculated. First, the pre-complex **P2** is formed which corresponds to a loose complex between **M1** and $\text{C}_6\text{F}_5\text{H}$ (hydrogen bonded to the acidic NH function). This adduct is $3.4 \text{ kcal mol}^{-1}$ more stable than the educts. Subsequently, this species undergoes a concerted rearrangement to yield the final complex **P4**. The activation energy (15 kcal mol^{-1}) for this process is significantly lower when compared to the addition of methane, and in the order of the activation energy computed for the heterolytic cleavage of H_2 across the Rh-N bond in $[\text{Rh}(\text{trop}_2\text{N})(\text{PPh}_3)]$ (**K2**). Moreover, the formation of **P4** is more exothermic ($-13.8 \text{ kcal mol}^{-1}$) than the formation of **P3** ($-4.6 \text{ kcal mol}^{-1}$).

2.6.2 Activation of C₆F₅H

The reaction at room temperature of one equivalent of potassium *tert*-butoxide with [Pt(Me)(trop₂NH)]BAr^F (**K30**) in the presence of C₆F₅H – the sample was prepared in a J. Young NMR tube under anhydrous and inert conditions in freshly distilled [D₈]-THF – was subsequently carried out. The pentafluorobenzene immediately reacts after the addition of the base. The color of the reaction turned from yellow to green for few seconds, but, unlike the example reported previously no formation of **K33** was detected and above all, the ¹⁹F NMR spectrum unambiguously revealed the presence of new ¹⁹F signals.

Since the number of peaks observed in the ¹⁹F NMR spectrum was higher than initially expected, we performed a ¹⁹F – ¹⁹F COSY experiment, which allowed us to understand which signals belong to one spin system. By comparison with the literature data, the doublets of doublets at $\delta = -144.3$ ppm and at -155.1 ppm, with coupling constants of 8.8 Hz and 21.6 Hz respectively, were assigned to the ether 3-*tert*-butoxy-1,2,4,5-tetrafluorobenzene, formed by a nucleophilic displacement by *t*BuOK of the fluorine atom in *para*-position with respect to the hydrogen atom in C₆F₅H.⁴⁴

On the other hand, the five multiplets ($\delta = -115$ ppm, -117 ppm, -163.5 ppm, -165 ppm and -167.4 ppm) were identified as the second spin system present in solution. The presence of platinum satellites (³J_{PtF}) of 364 Hz and 469 Hz for the two signals at lower frequency clearly showed the formation of a new platinum compound. These NMR data are particularly similar to those published by Caulton et al. for a tridentate macrocycle [2.1.1]-(2,6)-pyridinophane (L) platinum system [Pt^{IV}(Me)₂(H)(L)]⁺, which reacts with two equivalents of C₆F₅H to yield an N-protonated bispentafluoroplatinum(II) complex by loss of two molecules of methane.⁴⁵ The ¹⁹F NMR spectrum at 22°C in CD₂Cl₂ of this species, display two broad multiplets at -164.2 ppm and -163.2 ppm attributed to the *meta*-CF; two triplets at -160.8 ppm and at -160.9 ppm (J_{FF} = 20 Hz) associated with the *para*-CF, and two broad singlets and multiplets at -122.1 ppm and -119.0 ppm assigned to the *ortho*-CF groups. These last two resonances display platinum satellites of 440 Hz and 400 Hz in the range of the ones we observed. Note that the structure of [Pt^{IV}(Me)₂(H)(L)]⁺ has been confirmed by X-ray diffraction studies. Because of the striking similarity between our spectroscopic data and those reported by Caulton, the new compound was identified as [Pt(trop₂NH)(C₆F₅)Me] (**K35**). In the beginning, we believed that the trop₂NH was still coordinated in a tripodal mode, resembling complex **K22'**. However, all resonances in the ¹H NMR spectrum at room temperature were extremely broad (see lower trace in Figure 2.27) indicating a dynamic process, which also includes the olefinic protons. This last feature it is clearly difficult to bring into accordance with a trigonal

bipyramidal structure. Moreover, the presence of five signals in the ^1F NMR spectrum indicates an asymmetric complex whereby C_s symmetry is expected for a complex comparable to **P4** in Scheme 2.26a-b.

By cooling the sample down to 220 K, a well resolved ^1H NMR spectrum is obtained (see upper trace in Figure 2.27).

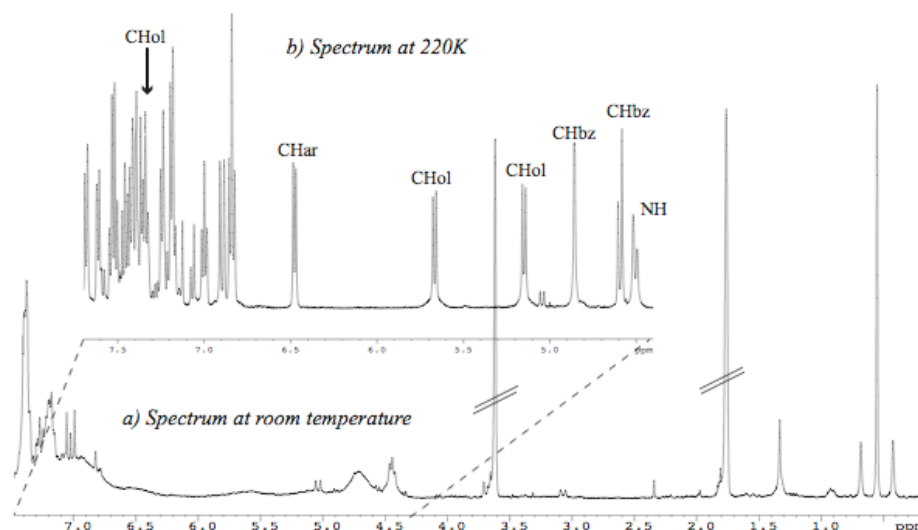
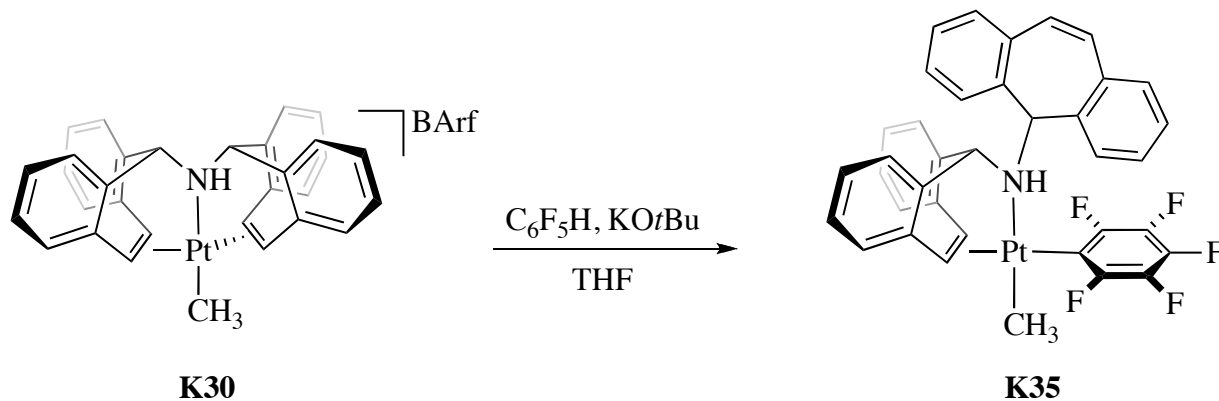


Figure 2.27: NMR spectrum **K35** at room temperature (a) and at 220K (b).

A detailed analysis of the spectrum clarifies that the new compound **K35** is asymmetric, as is depicted in Scheme 2.29 and one of the trop units has been displaced from the metal center.



Scheme 2.29: Activation reaction of pentafluorobenzene to yield **K35**.

The spectrum shows four doublets, and the ones at 5.15 ppm and 5.67 ppm (with coupling constant of 9.2 Hz) are attributed to the olefinic protons. The signal at 4.50 ppm is assigned to the amine NH of the trop and the one at 4.59 ppm is attributed to the benzylic proton of the decoordinates trop. A $^3J(HH)$ coupling constant of 11 Hz between these two protons indicates a dihedral angle of about 180° (estimated from the Karplus curve). Such a coupling was never

observed in the previously discussed complexes where the trop₂NH ligand coordinated in a κ^3 -fashion, which leads to a parallel alignment of the benzylic CH and the NH groups. The two missing signals for the olefinic protons are observed in the aromatic region (with no platinum satellites) clearly indicating that one of the two trop moieties is not coordinated to the metal center. In view of these observations, the highly dynamic behavior of the complex displayed at room temperature is simply explained by the decoordination/coordination of the olefin from/to the metal center. In the process, the asymmetric complex (with the nitrogen atom a stereogenic center) corresponds to the ground state structure and a trigonal bipyramidal structure is an intermediate (or transition state) for this process. That is in contrast to the computations, which showed **P4** to be a stable species, a trigonal bipyramidal form for **K35** is not stable may be attributed to the fairly high steric repulsion between the benzo groups in the trop₂NH ligand and the pentafluorophenyl group.

As it was already mentioned in Chapter 2.3, the olefins of the trop₂NH are not as tightly bound to the platinum center as in the rhodium (I) complexes. This property is manifested in the significant shift of the ¹H and ¹³C carbon resonances of nuclei of the olefinic units to higher frequencies in the platinum complexes when compared to analogous rhodium complexes. The formation of **K35** – bearing a κ^2 -trop₂NH ligand gives further evidence and shows that the olefinic groups of the trop₂N-type ligands are more weakly bound and easier to displace in the platinum compounds

2.7 Conclusions and Outlook

A satisfactory and straightforward method for the preparation of platinum (II) and palladium (II) complexes bearing the trop₂NH ligand was developed. The preparation exploits the well-known [Pt(μ^2 -SMe₂)Me₂]₂ (**116**) and [Pd(μ^2 -Cl)(Me)(SMe₂)]₂ (**118**), which bear labile SMe₂ groups readily displaced by the amine ligand. The striking similarities of the Pt(II) and Pd(II) compounds with respect to the Rh(I) complexes of trop₂NH described in Chapter 1 were verified by X-ray diffraction and NMR spectroscopic studies. We find that the geometry observed in isoelectronic pentacoordinate compounds is trigonal bipyramidal and very similar. This is different for tetracoordinated compounds: Pt(II) preferentially adopts a distorted square planar conformation (ct1-Pt-ct2 159.9° in **K31**), whereas Rh(I) assumes a saw-horse type geometry (ct1-Rh-ct2 147.03° in **(S,S)-K6**). A marked difference between the Rh(I) and Pt(II) complexes concerns the binding properties of the olefinic units: The binding strength of the olefin to the Pt(II) seems to be significantly weaker and this fact must be taken into consideration when the reactivity and the role of Pt(trop₂N) complexes for catalytic applications is discussed.

The preparation of a complex with a Pt-amide bond proved to be more challenging than expected. The first attempts to produce the amide by simple elimination of methane through thermal activation of **K20**, **K24** or **K25** – inspired by the examples reported by Wolczanski and Bergman – resulted exclusively in the formation of stable cycloplatinate compounds such as **K22** and **K26**. In the retro perspective and given that the platinum olefin interaction in the synthesized complexes is rather labile especially at higher temperatures, these findings are less surprising. In these cyclometallation reactions, we assume that the C-H activation process likely proceeds through a classical mechanism consisting in the oxidative addition to the metal center. The addition of the C-H bond across a Pt-amide bond seems less probable because a collinear arrangement of the Pt-N and C-H bond is required which is difficult to realize in the intra-molecular process.

We finally succeeded in the synthesis of a transient the Pt-amide complex, which was generated by a method which was already successfully applied for the synthesis of the analogous Rh(I) complexes. That is complexes of type $[\text{Pt}(\text{Me})(\text{X})(\text{trop}_2\text{NH})]$ ($\text{X} =$ generic anion) are deprotonated by one equivalent of $\text{KO}t\text{Bu}$ as base to give transient Pt-amide complexes, which were identified by their characteristic green color. These amides rapidly dimerize to give unreactive diplatinadiaza-cyclobutanes. With pentafluorobenzene as trapping agent we obtained evidence that the intermolecular addition of at least an activated C-H bond across a Pt-N is possible. This assumption is further bolstered by DFT calculations which show that this process has a reasonable activation barrier of about 15 kcal mol^{-1} . Future research work will concentrate on an extension of possible substrates for this C-H activation reaction (that is further C-H acidic compounds will be tested) and especially efforts will be undertaken to obtain a stable Pt-amide.

A way to overcome the problems in isolating such a species, may be to substitute the methyl in axial position with a more hindered substituted phenyl group, as outlined in Figure 2.28, which may prevent the dimerization of the amide.

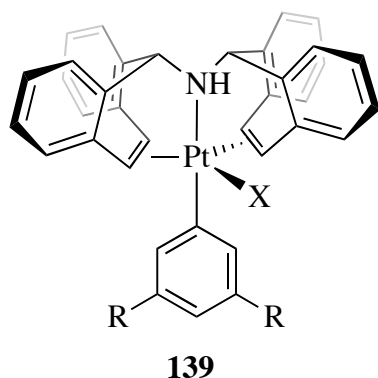


Figure 2.28: Conceivable platinum complex, bearing hindered substituted phenyl groups in axial position.

- ¹ a) J.A. Labinger, J.E. Bercaw, *Nature*, **2002**, 417, 507; b) B.A. Arndtsen, R.G. Bergman, T.A. Mobley, T.H. Peterson, *Acc. Chem. Res.*, **1995**, 28, 154; c) A.E. Shilov, G.B. Shul'pin, *Chem. Rev.*, **1997**, 97, 2879; d) R.H. Crabtree, *J. Chem. Soc., Dalton Trans.*, **2001**, 2437; e) U. Fekl, K.I. Goldberg, *Adv. Inorg. Chem.*, **2003**, 54, 259; f) S. Stahl, J.A. Labinger, J.E. Bercaw, *Angew. Chem. Int. Ed.*, **1998**, 37, 2181; g) W.D. Jones, *Top. Organomet. Chem.*, **1999**, 3, 9; h) R.H. Crabtree, *J. Organomet. Chem.*, **2004**, 689, 4083; k) M. Lersch, M. Tilset, *Chem. Rev.* **2005**, 105, 2471.
- ² J. Belli, C.M. Jensen, *Organometallics*, **1996**, 15, 1532.
- ³ A.E. Sherry, B.B. Waykand, *J. Am. Chem. Soc.*, **1990**, 112, 1259. B.B. Waykand A.E. Sherry, *J. Am. Chem. Soc.*, **1991**, 113, 5305.
- ⁴ R.H. Crabtree, J.M. Mihelcic, J.M. Quirk, *J. Am. Chem. Soc.*, **1979**, 101, 7738.
- ⁵ A.H. Janowicz, R.G. Bergman, *J. Am. Chem. Soc.*, **1982**, 104, 352.
- ⁶ J.K. Hoyano, W.A.G. Graham, *J. Am. Chem. Soc.*, **1982**, 104, 3723.
- ⁷ M.C. Keyes, V.G. Young, W.B. Tolman, *Organometallics*, **1996**, 15, 4133.
- ⁸ S. Geftakis, G.E. Ball, *J. Am. Chem. Soc.*, **1998**, 120, 9953.
- ⁹ D.R. Evans, T. Drovetskaya, R. Bau, C.A. Reed, P.D. Boyd, *J. Am. Chem. Soc.*, **1997**, 119, 3633.
- ¹⁰ R.H. Crabtree, E.M. Holt, M. Lavin, S.M. Morehose, *Inorg. Chem.*, **1985**, 24, 1986.
- ¹¹ S. Reinartz, P.S. White, M. Brookhart, J.L. Templeton, *J. Am. Chem. Soc.*, **2001**, 123, 12724.
- ¹² R.L. Brainard, W.R. Nutt, T.R. Lee, G.M. Whitesides, *Organometallics*, **1988**, 7, 2379.
- ¹³ M.W. Holtcamp, J.A. Labinger, J.E. Bercaw, *J. Am. Chem. Soc.*, **1997**, 119, 848.
- ¹⁴ J. Johansson, M. Tilset, J.A. Labinger, J.E. Bercaw, *J. Am. Chem. Soc.*, **2000**, 122, 10846.
- ¹⁵ a) G. Gerdes, P. Chen, *Organometallics*, **2006**, 25, 809; b) J.A. Labinger, J.E. Bercaw, M. Tilset, *Organometallics*, **2006**, 25, 805; c) G. Gerdes, P. Chen, *Organometallics*, **2003**, 22, 2217;
- ¹⁶ S.B. Harkins, J.C. Peters, *Organometallics*, **2002**, 21, 1753.
- ¹⁷ M.P. Brown, R.J. Puddephatt, C.E.E. Upton, *J. Chem. Soc., Dalton Trans.*, **1974**, 2457.
- ¹⁸ D.M. Crumpton, K.I. Goldberg, *J. Am. Chem. Soc.*, **2000**, 122, 962.
- ¹⁹ R.J. Puddephatt, *Coord. Chem. Rev.*, **2001**, 219, 221, 157.
- ²⁰ H.A. Jenkins, G.P.A. Yap, R.J. Puddephatt, *Organometallics*, **1997**, 16, 1946.
- ²¹ U. Fekl, A. Zahl, R. van Eldik, *Organometallics*, **1999**, 18, 4156.
- ²² U. Fekl, R. van Eldik, S. Lovell, K.I. Goldberg, *Organometallics*, **2000**, 19, 3535.
- ²³ S. Reinartz, P.S. White, M. Brookhart, J.L. Templeton, *Organometallics*, **2000**, 19, 3854.
- ²⁴ B.J. Wik, M. Lersch, M. Tilset, *J. Am. Chem. Soc.*, **2001**, 123, 12116.
- ²⁵ U. Fekl, W. Kaminsky, K.I. Goldberg, *J. Am. Chem. Soc.*, **2001**, 123, 6423.
- ²⁶ U. Fekl, W. Kaminsky, K.I. Goldberg, *J. Am. Chem. Soc.*, **2002**, 124, 6804.
- ²⁷ S. Reinartz, P.S. White, M. Brookhart, J.L. Templeton, *J. Am. Chem. Soc.*, **2001**, 123, 6425.
- ²⁸ S.-B. Zhao, G. Wu, S. Wang, *Organometallics*, **2008**, 27, 1030.
- ²⁹ P.L. Watson, *J. Am. Chem. Soc.*, **1983**, 105, 6491.
- ³⁰ M.E. Thompson, J.E. Bercaw, *Pure. Appl. Chem.*, **1984**, 56, 1.
- ³¹ C. McDade, J.C. Green, J.E. Bercaw, *Organometallics*, **1982**, 1, 1629.
- ³² C.C. Cummins, S.M. Baxter, P.T. Wolczanski, *J. Am. Chem. Soc.*, **1988**, 110, 8731.
- ³³ T.R. Cundari, T.R. Klinckman, P.T. Wolczanski, *J. Am. Chem. Soc.*, **2002**, 124, 7, 1481.
- ³⁴ C.P. Schaller, P.T. Wolczanski, *J. Am. Chem. Soc.*, **1993**, 32, 131.
- ³⁵ P.J. Walsh, F.J. Hollander, R.G. Bergman, *J. Am. Chem. Soc.*, **1988**, 110, 8729.
- ³⁶ T. Büttner, Diss. ETH No. 15503, Zürich, **2004**, "Synthesis and Reactivity of Penta Coordinated Rhodium Amine-Diolefin Complexes".
- ³⁷ G.S. Hill, M.J. Irwin, C.J. Levy, L.M. Rendina, R.J. Puddephatt, *Inorg. Syntheses*, **1998**, 32, 149.
- ³⁸ L. Mink, M.F. Rettig, R.M. Wing, *J. Am. Chem. Soc.*, **1991**, 113, 2065.
- ³⁹ P.K. Byers, A.J. Canty, H. jim, D. Kruis, B.A. Markies, J. Boersma, G. Van Koten, *Inorg. Syntheses*, **1998**, 32, 162.

- ⁴⁰ S. Deblon, Diss. ETH No. 13920, Zürich, **2000**, “Neue Tropyridenphosphane Koordinationverhalten und Anwendung in der homogenen Katalyse”.
- ⁴¹ T.W. Campbell, R. Ginsig, H. Schmid, *Helvetica Chimica Acta*, **1953**, 186, 1489.
- ⁴² J. Thompson, P. Anderson, S. Brichter, T. Lyle, E. Thies, *J. Med. Chem.*, **1990**, 33, 789.
- ⁴³ M. Schmeisser, K. Dahmen, P. Sartori, *Chem. Ber.*, **1976**, 100, 1633; b) J. Maletina, V. Orda, L. Yagupolski, *Zh. Org. Khim.*, **1974**, 10, 294,
- ⁴⁴ C.L. Cheong, B.J. Wakefield, *J.Chem.Soc. Perkin Trans.*, **1998**, 12, 3301.
- ⁴⁵ A.N. Vedernikov, M. Pink, K.G. Caulton, *Inorg. Chem.*, **2004**, 43, 3642.

3 Hydridophosphorane as Ligands for H₂ Activation

3.1 Introduction

Whereas in the first two chapters of this thesis the discussion was mainly addressed to the C-H activation of alkane across a M-amide bond – where the nitrogen of the amide is in α -position as in Figure 3.1a – in this chapter the attention will be shifted to a similar system where the active nitrogen is in β -position as shown in Figure 3.1b.

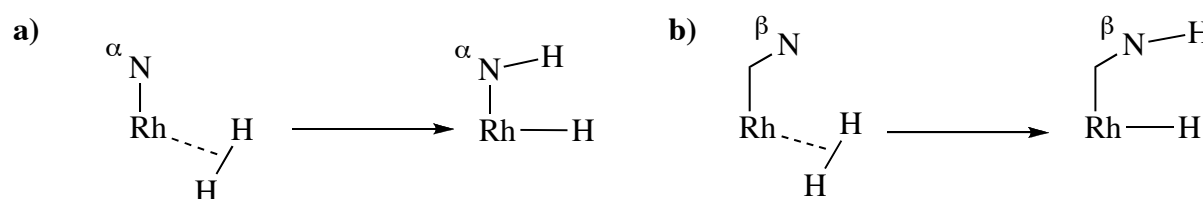


Figure 3.1a-b: amide in α -position (a) and amide in β -position (b).

The project was indented to be a parallel and preliminary study of a new type of cooperating ligand related to the Rh-amide system of trop_2NH , which is remarkably active in the heterolytic activation of dihydrogen. The new system was tested exclusively for the activation of dihydrogen, even if future projects could investigate on the activation of other small molecule as well.

The work is inspired by the hydrogenase enzymes and related artificial system; therefore, in the introduction the most important examples reported in the literature will be discussed.

3.1.1 Heterolytic Dihydrogen Activation in Complexes with Pendant Basic Group

As above mentioned, hydrogenase enzymes¹ can catalyze the conversion of protons to dihydrogen and its reverse (eq. 1) at impressive rates – dihydrogen is produced and oxidized at 6'000 - 9'000 and 28'000 molecules per second per hydrogenase molecule (30 °C), respectively.²



In order to reproduce such striking activity, it is of extreme importance to correctly understand the system and how the active site of the enzyme really is. Fortunately, studies in this direction outlined that two well-established classes of hydrogenases can actually exists: the Fe-only hydrogenase³ (Fe H₂-ases (**140**) in Figure 3.2a) and the NiFe hydrogenase ([NiFe] H₂-ases (**141**) in Figure 3.2b). The main difference between the two active sites is indeed the presence in the core of the hydrogenases itself of either a diiron unit or a nickel-iron cluster.

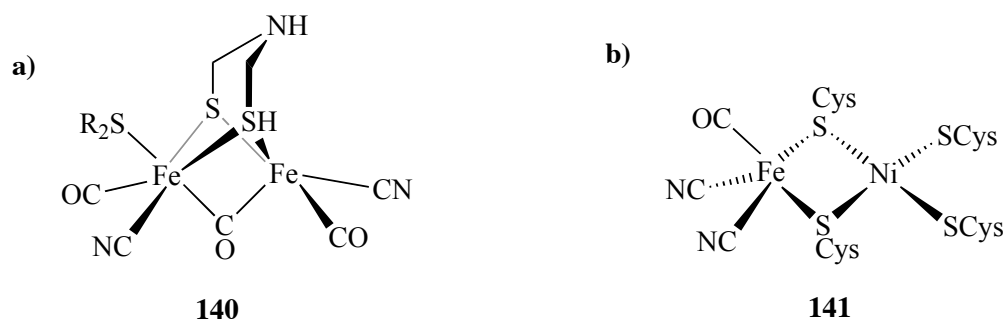
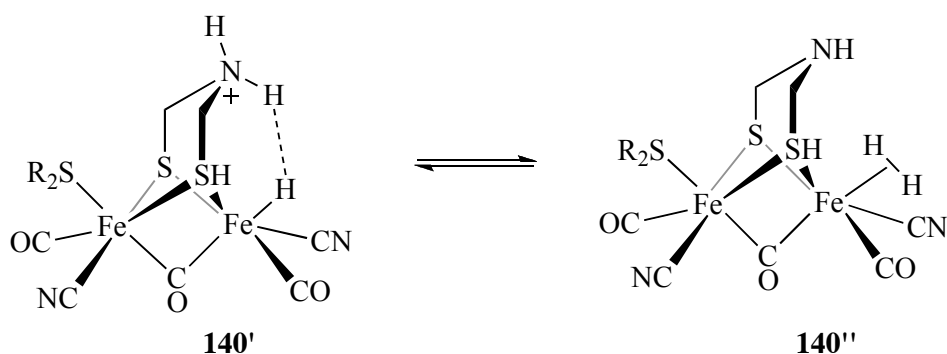


Figure 3.2a-b: Fe H₂-ases (**140**) and the [NiFe] H₂-ases (**141**).

The Fe H₂-ases⁴ (**140**) has been mainly found in bacteria and algae, but it can be present in eukaryotes as well, including humans.⁵ Its usual role is the reduction of protons to dihydrogen, but the oxidation is also possible. Recent structural studies of the Fe-only hydrogenase suggest that the site for hydrogen activation contains two Fe atoms bridged by a di(thiomethyl)amine ligand [HN(CH₂S⁻)₂].⁶ The ligand is thought to play an important role in the heterolytic cleavage of hydrogen in the transfer from the active site to the outer sphere of the enzyme via a proton-transfer pathway (**140'** and **140''** in Scheme 3.1).



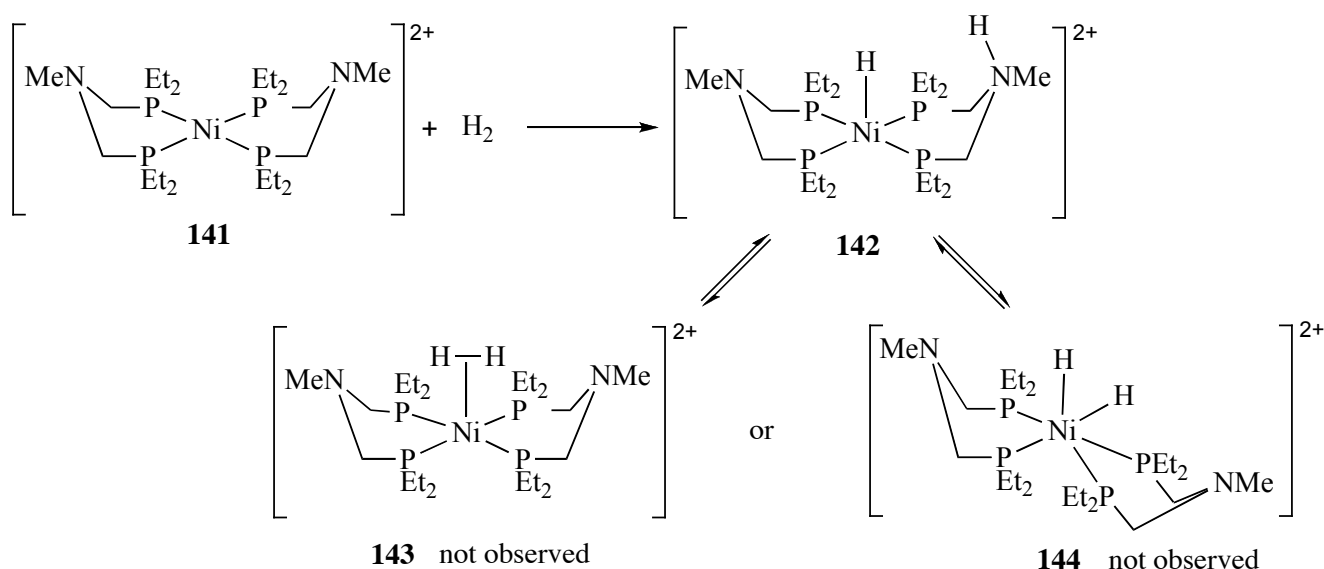
Scheme 3.1: the Fe H₂-ases.

On the other hand, in the cluster of [NiFe] H₂-ases⁷ (**141** in Figure 3.2b), the Fe atom has a similar coordination sphere to that observed in **140**. The Ni atom is bound to four sulfur atoms of cysteine residues, two of which are bridging the Fe center as well (μ^2 -coordination mode). The study on structural models for the [NiFe] H₂-ases suggested that the thiolate of the cysteine residue is enough basic to abstract a proton from a transiently formed H₂ ligand, similar to the mechanism depicted in Scheme 3.1.

Different models resembling hydrogenases enzymes have been study and some of these examples – where a basic appended ligand interacts with a coordinated dihydrogen molecule in a transition metal complex – will be discussed. These examples have a peculiar feature in common: the molecules possess both a proton acceptor – generally a basic ligand – and a free site for the

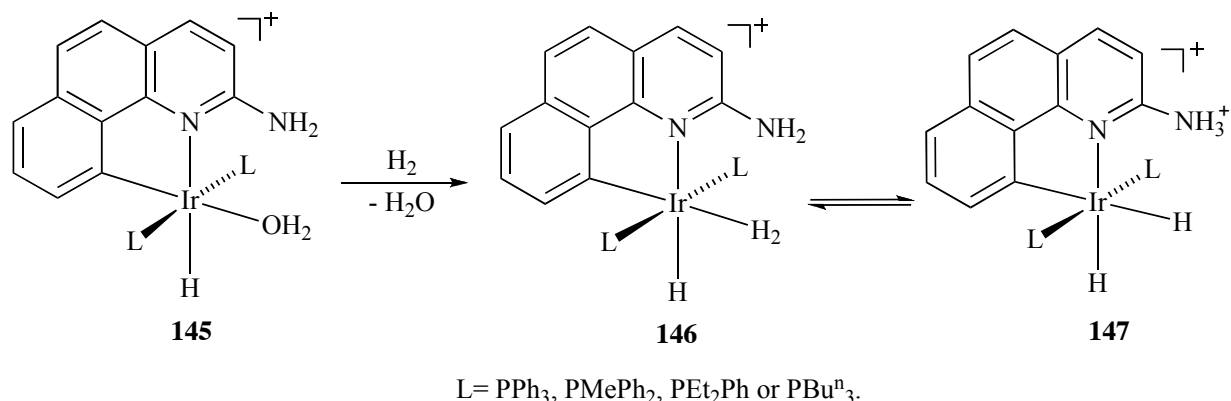
accommodation of the hydride. The most widespread pendant basic ligand is indeed the amino group.

An example is the one reported by DuBois et al., whose group synthesized the nickel complex $[\text{Ni}(\text{PNP})_2](\text{BF}_4)_2$ (**141**) which possesses both hydride – and proton acceptor sites where PNP = 1-(diethylphosphino)-*N*-((diethylphosphino)methyl)-*N*-methylmethanamine (Scheme 3.2).⁸ A rapid reaction was observed when hydrogen was bubbled through an acetonitrile or dichloromethane solutions of **141**. In fact, the formation of a new hydride species – $[\text{HNi}(\text{PNHP})-(\text{PNP})]^{2+}$ (**142**) – was detected by NMR spectroscopy. From the spectroscopic data it was deduced that the bridging N atom of the diphosphine ligand had been protonated. Furthermore, the ^1H NMR spectrum of **142** showed a highly dynamic behavior in solution, due to a rapid exchange processes. The high rate of exchange suggested an *intra*-molecular process and the author hypothesized that **142** is in equilibrium with an intermediate dihydrogen complex resembling either **143** or **144**.



Scheme 3.2: Reaction of $[\text{Ni}(\text{PNP})_2](\text{BF}_4)_2$ **83** with H_2 .

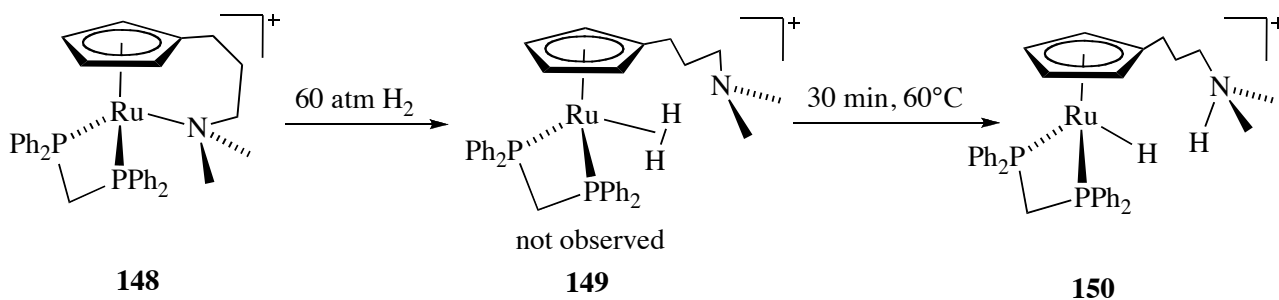
Crabtree and Eisenstein have shown that the presence of a basic appending NH_2 group in the 2-position of a 7,8-benzoquinolate ligand (shortened with bq- NH_2) is indispensable in order to achieve the activation of dihydrogen. In fact, when the aqua complex $[\text{IrH}(\text{bq}-\text{NH}_2)(\text{OH}_2)(\text{PPh}_3)]\text{BF}_4$ (**145**) reacts with H_2 , the product of the reaction is not the corresponding H_2 complex resembling **146**, but the dihydride **147** formed *via* heterolytic activation (Scheme 3.3).⁹



Scheme 3.3: Formation of compound **147**, upon reaction of H₂ with **145**.

Differently, in the known analogous bq-H system – which is not bearing any NH₂ group – the cationic complex [IrH(bq-H)(OH₂)(PPh₃)]BF₄ reacted with H₂ to give a cationic H₂ complex (similar to **146**). Exclusively upon addition of an external base, such as ^tBuLi, the deprotonation of the H₂ complex could take place to yield the neutral dihydride [Ir(H)₂(bq-H)(PPh₃)] (similar to **147**).

Approximately in the same years, Lau et al.¹⁰ synthesized the ruthenium complex [Ru(Cp)(dppm)((CH₂)₃NMe₂)] (**148**), where dppm means bis(diphenylphosphino)methane, depicted in Scheme 3.4. Compound **148** reacted with 60 atm H₂ within 30 minutes at 60°C, probably to form a μ²-H₂ complex intermediate **149**. This species could be subsequently deprotonated by the pendant amino group to form **150**.



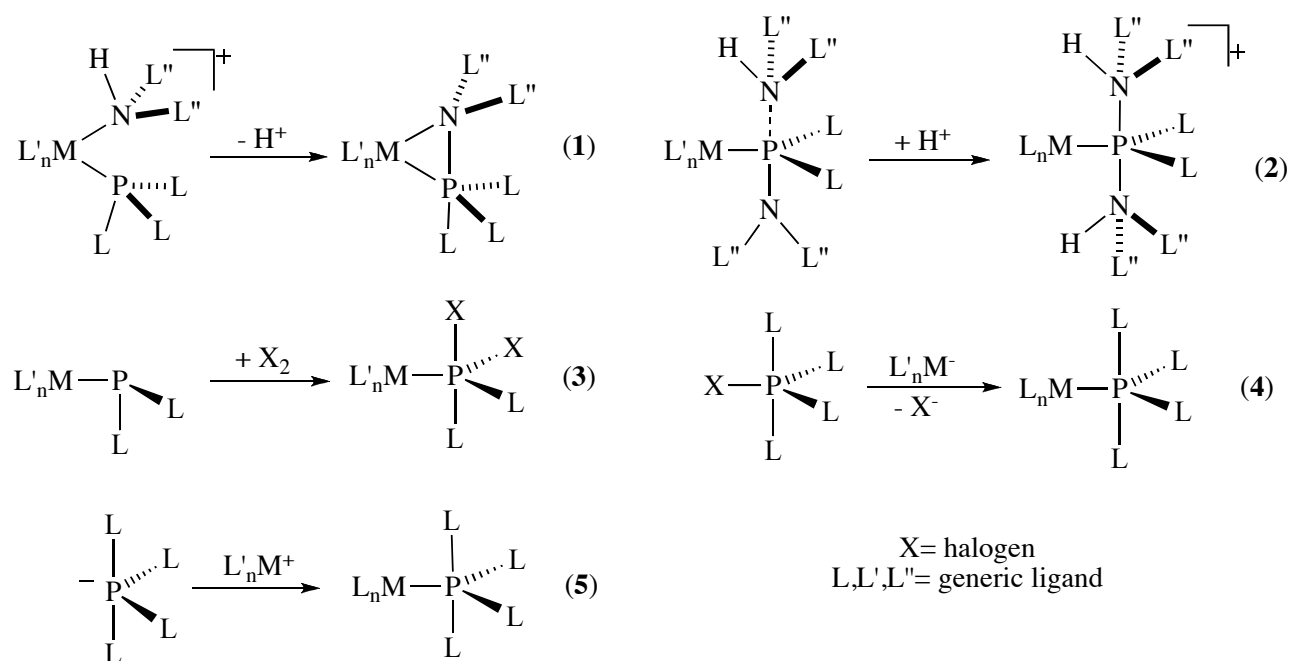
Scheme 3.4: Reactivity of [Ru(Cp)(dppm)((CH₂)₃NMe₂)] (**148**) with dihydrogen.

The interaction Ir–H^{δ-}⋯H^{δ+}–N between an iridium hydride and the protonated nitrogen of a sulfur-bonded thiopyridine ligand has been studied by Morris et al.¹¹ When a solution of complex **151** (Scheme 3.5) in CD₂Cl₂ is exposed to D₂ (1 atm) for 5 minutes, the intensities of the NH and IrH resonances in the ¹H NMR decrease by approximately 75%. It is important to note that this reaction does not occur in the presence of good hydrogen bond acceptors (e.g. THF), which prevent the H^{δ-}⋯H interaction, essential for rapid D/H exchange with D₂ gas.

Although the phosphorus atom in HPs does not possess a lone electron pair in the electronic ground state, reversible (ring)opening processes of the type $HP\cap X \rightleftharpoons P \dots XH$ ($X = N, O$; \cap = closed P-X interaction, \dots = open P-X interaction) make the P and X atoms available for coordination to metal centers and HPs may act as P-, N-, P,N-, P,O-, and N,N- ligands. The several preparative methods¹⁷ for the synthesis of metallaphosphoranides, which have been developed, are classified as follows and are depicted in Scheme 3.7 [equations (1) – (5)].

In equation (1) the deprotonation¹⁸ of the amine present in a phosphine-amine metal adduct will form the desired polycyclic species, similarly the protonation¹⁹ displayed in equation (2) will yield the desired metallaphosphoranide. Other options are the oxidative addition²⁰ of halogens to transition-metal phosphide complexes, as sketched in equation (3) or the nucleophilic substitution at the phosphorous atom of a phosphorane by a transition-metal anion,²¹ as outlined in equation (4).

Last, the electrophilic attack of an electron deficient transition-metal fragment at a phosphoranide²² is shown in equation (5).

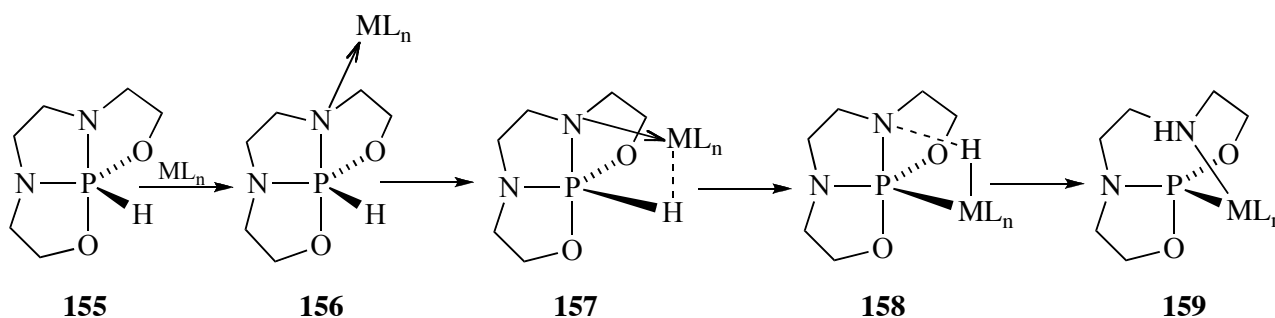


Scheme 3.7. Preparative methods for metallaphosphoranides.

Complexation of bicyclic and tricyclic HPs has been actively investigated during the last decade. Depending on the structure of the phosphorane fragment, complexation on a metal fragment leads either to a complex preserving the pentacoordinate phosphorous fragment or to a structure resulting from the opening of the hydridophosphorane and showing a tricoordinate phosphorous atom coordinated by the lone pair to the metal center.

The mechanism for the formation of hydridophosphorane – in their open form – complexes (resembling **159** in Scheme 3.6) is not yet clear. The hypothesized mechanisms for the formation of **159** sketched in Scheme 3.6 has been proposed by Gavrilov et al. and it does not take into account the participation of P(III)-tautomers.

The initial coordination of the hydridophosphorane fragment, such as **155**, may take place at the nitrogen in axial position (see **156**) and the hydride species **158** may then be formed by oxidative addition from the agostic intermedia **157**. The final reductive elimination leads to the metallaphosphorane **159**.



Scheme 3.6: Mechanism for the formation of a chelate metallacycles (**159**).

The cleavage of a P-X bond through a reductive elimination is frequently observed upon complexation of hydridophosphoranes. Cases where the pentacoordinated skeleton around the phosphorus center is retained are known only for tetracyclic HPs and tricyclic HPs (stabilization through a macrocyclic effect).^{14d}

3.2 Aims

The experiments discussed in this chapter aim to demonstrate that phosphoranido rhodium (I) complexes with bis(5H-dibenzo[ad]cyclohepten-5-yl)phosphate as co-ligand are capable to heterolytically cleave dihydrogen in a similar fashion as seen with hydrogenase enzymes and the model complexes mentioned above.

Preliminary DFT calculations performed conducted in our group give evidence that the process should be feasible and the incorporation of an hydridophosphoranide ligand into a Rh(trop₂NMe) or Rh(trop₂PPh) fragment should result in the formation of an active complex bearing the phosphorus ligand in the axial position. The molecule should have a vacant site (the missing equatorial corner in the saw horse type structure that is derived from a original bipyramidal structure) available for the approach of the H₂, whereas the active site of the molecule should be provided by the coordinated hydridophosphorane, which should bear a basic amine in β-position with respect to the metal, as it

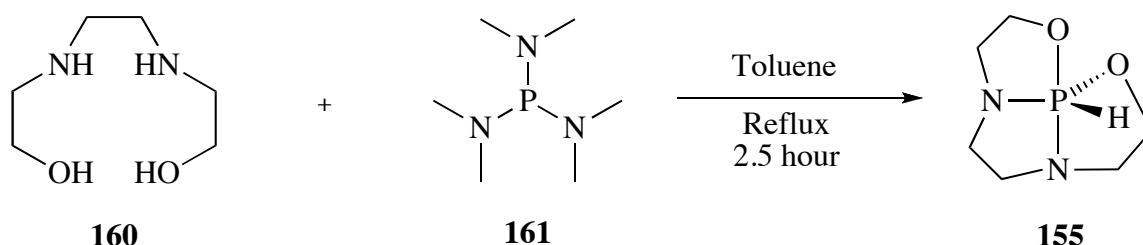
will eventually be discussed. The main aim was therefore to confirm that amide in β -position (Figure 3.1b) are as active in the heterolytical activation of dihydrogen as the already explored system with the amide function in α -position (Figure 3.1a).

Note that the function of the bistrong ligand would be exclusively that of forcing the complex into a saw-horse type geometry, which bears a free coordination site available for the incoming dihydrogen molecule. Differently from the examples of Chapter 1 and 2, the cooperative ligand is not the bistrong but rather the HP ligand: in the examples herein reported the bistrong ligand is barely a spectator ligand.

3.3 Attempted synthesis of metallaphosphorane

As already discussed in the introduction, the complexation of hydridophosphoranes commonly co-occurs with the fragmentation of the HP, leading to chelate complexes of type **159** (Scheme 3.6).⁹ Since our goal was to prove that the basic nitrogen of an amide in β -position could cooperate in the activation of dihydrogen, the preparation of a tricyclic hydridophosphorane was planned, rather than an acyclic one.

The stoichiometric reaction of 2,2'-(ethane-1,2-diylbis(azanediyl))diethanol (**160**) and hexamethylphosphinetriamine (**161**) in toluene gives the tricyclic hydridophosphorane **155** as a colorless oil after distillation in 49% yield (Scheme 3.7).⁹



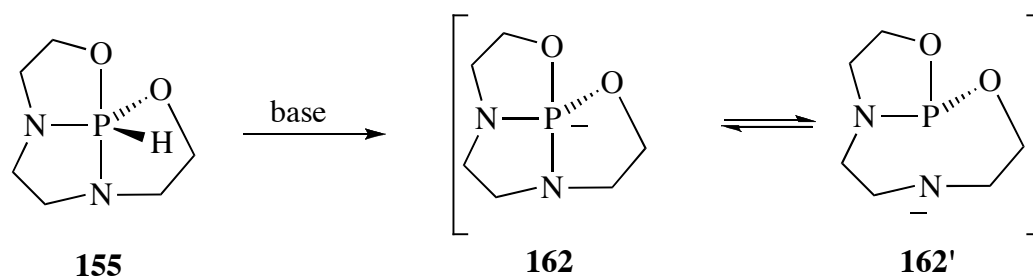
Scheme 3.7: Synthesis of the hydridophosphorane **155**.

Compound **155** shows in the $^{31}\text{P}\{^1\text{H}\}$ NMR a singlet at $\delta = -36.9$ ppm, while the ^1H NMR spectrum shows a doublet at $\delta = 6.9$ ppm with a $^1J_{\text{PH}} = 721$ Hz (PH signal). These data are according to those reported in the literature.

As second step, the synthesis of the rhodium complex was immediately after planned. We decided to attempt first the procedure sketched in equation (5) in Scheme 3.7, namely the direct electrophilic attack of an electron-deficient transition-metal fragment at a phosphoranide. Therefore, the study of the deprotonation reaction of hydridophosphorane **155** was attempted prior to the reaction of metallation.

The preparation of the phosphoranide was tried in different conditions: different solvents (such as DME and THF); different bases (such as $\text{Na}[\text{N}(\text{iPr})_2]$, $n\text{BuLi}$, $t\text{BuOK}$ or KH); different temperatures (-40°C , 22°C , 40°C) and also in the presence of additives (crown ether 18).

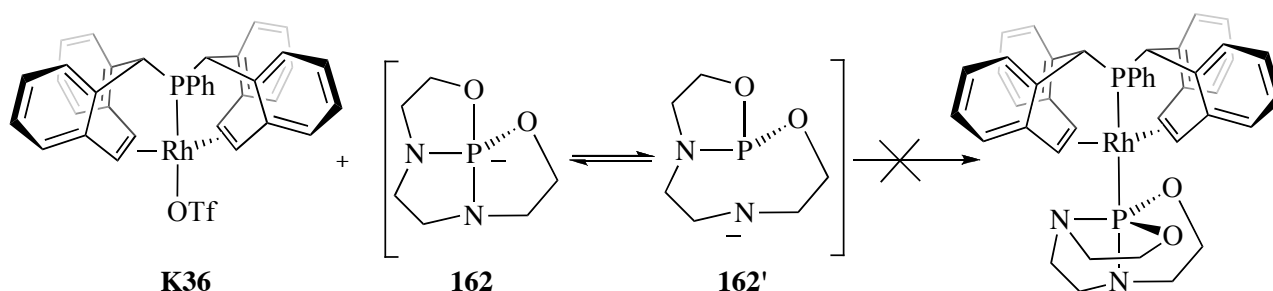
In the ^{31}P NMR spectrum of the reaction mixtures several resonances have been always detected, none of which was at low field – as expect for the phosphoranide. Therefore, such signals were attributed to the species **162'** formed by isomerization of the HP anion **162**, as outlined in Scheme 3.9.



Scheme 3.9: Direct deprotonation of the hydriphosphorane **155**.

Despite the fact that we could never observe so far the phosphoranide in solution by NMR techniques, we decided to react anyway the reaction mixture derived from the direct deprotonation of **155** with the proper Rh(I) precursor. The metal compound of our choice was $[\text{Rh}(\text{OTf})(\text{trop}_2\text{PPh})]$ (**K36**), which can be easily prepared from $[\text{Rh}(\mu\text{-Cl})(\text{trop}_2\text{PPh})_2]$ and silver triflate in diethylether.²³ The characteristic ^{31}P NMR signal for this species is the doublet at $\delta = 175.8$ ppm with a $^1J_{\text{PRh}}$ of 197.7 Hz.

Reaction of the crude phosphoranide (**162** and **162'**) and **K36**, shown in Scheme 3.8, yielded a mixture of different compounds. Among them **K39** has been observed (see chapter 3.4 for analytic details); the additional compound detected has resonances at 137.9 ppm (dd with $^1J_{\text{RhP}} = 40.3$ Hz and $^2J_{\text{PP}} = 220.4$ Hz) and at 23.5 ppm (dd with $^1J_{\text{RhP}} = 40.6$ Hz and $^2J_{\text{PP}} = 220.4$ Hz). Disappointingly, the clean formation of a single species has never been observed at any reaction conditions.

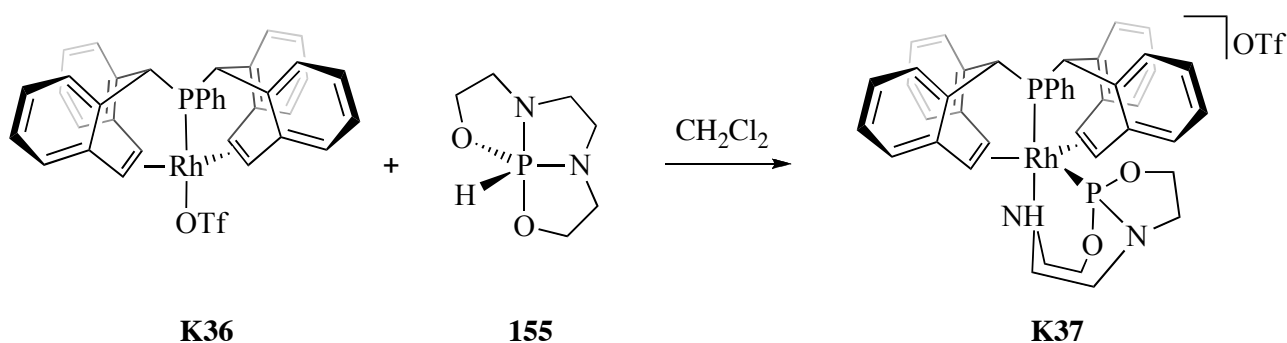


Scheme 3.8: Synthesis of $[\text{Rh}(\text{OTf})(\text{trop}_2\text{PPh})]$ **K36**.

However, it is important to note that the formation of a Rh(I) fragment, bearing the deprotonated HP (**162**) in his “close form”, was never detected in solution, in fact any signals was ever observed at negative frequencies in the ^{31}P NMR spectrum, even at low temperatures.

3.4 Synthesis of $[\text{Rh}(\text{trop}_2\text{PPh})(\text{HP})]$

Since the direct electrophilic attack of an electron deficient transition metal fragment at a phosphoranide did not produce the desired results, the preparation of the metallaphosphorane complex by direct reaction of the metal precursor **K36** with the available hydridophosphorane **155** was subsequently tested (Scheme 3.10).



Scheme 3.10: Synthesis of *cis*- $[\text{Rh}(\text{trop}_2\text{PPh})(\text{P}(\text{C}_6\text{H}_{13}\text{N}_2\text{O}_2))]$ (**K37**).

An immediate color change from red to yellow was observed upon addition of **155** to a solution of **K37** in DCM. The formation of a clean compound was confirmed by NMR analysis: **K37** is the only species present in solution after complete reaction.

The ^{31}P NMR spectrum, shown in Figure 3.4, shows two sets of *dd* at $\delta = 152.4$ ppm (with $^1J_{\text{RhP}} = 211.3$ Hz and $^2J_{\text{PP}} = 5.8$ Hz) and at $\delta = 137.5$ ppm (with $^1J_{\text{RhP}} = 163.4$ Hz and $J_{\text{PP}} = 5.8$ Hz).

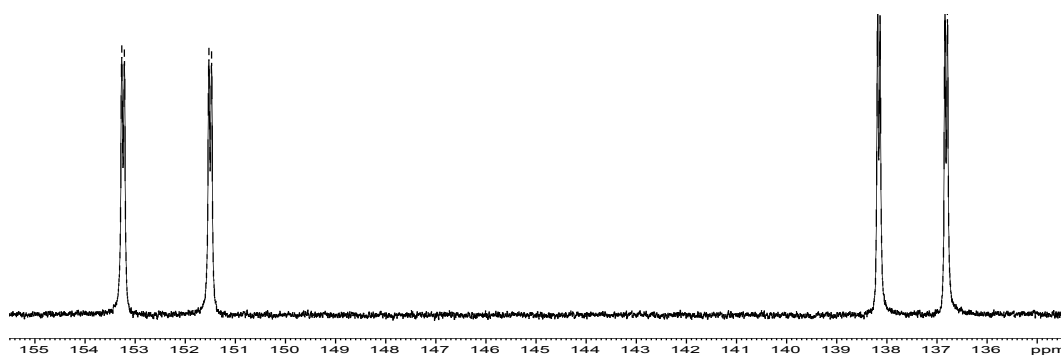


Figure 3.4: ^{31}P NMR spectrum of *cis*- $[\text{Rh}(\text{trop}_2\text{PPh})(\text{P}(\text{C}_6\text{H}_{13}\text{N}_2\text{O}_2))]$ (**K37**).

It is important to note that the resonances for pentacoordinate phosphorus (V) compounds appear typically in the negative region, whereas tricoordinate phosphorus (III) compounds have resonances

in the positive one. In this case, the phosphorus chemical shift attributed to the hydridophosphorane ($\delta = 152.4$ ppm) moiety is shifted to higher frequencies ($\Delta = 190$ ppm) with respect to **155**. This signal is indeed at relatively high frequencies; we therefore reasoned that the HP has coordinated in its open form, probably chelating the metal center through its nitrogen and phosphorous atoms. Moreover, the small values of $^2J_{PP}$ suggest a *cis* arrangement of the phosphorous atoms of the trophosphane and of the HP.²⁴ Therefore, we believed that the compound formed was *cis*-[Rh(trop₂PPh)(P(C₆H₁₃N₂O₂))] (**K37**).

We conclude that probably the formation of the *trans* product could be thermodynamically inhibited by the higher *trans* effect of the two phosphorus nuclei *trans* to each other.

The complex obtained was further characterized by ¹³C NMR and ¹H NMR spectroscopy. The ¹³C NMR spectrum shows that the olefinic and benzylic carbons and protons are no longer magnetically equivalent: four olefinic carbons are displayed ($\delta = 91.3$ ppm, 87.1 ppm, 64.8 ppm and 62.4 ppm) and furthermore two different benzylic carbons are present ($\delta = 54.0$ ppm and 48.5 ppm). The same patterns were observed in the ¹H NMR spectrum, depicted in Figure 3.5. The spectrum shows four different signals for the four olefinic protons ($\delta = 6.3$ ppm, 6.1 ppm, 5.3 ppm and 4.7 ppm) and two resonances for the two benzylic ones ($\delta = 5.0$ ppm and 3.9 ppm). These data clearly exclude the formation of a C_s-symmetrical complex and are in accord with the asymmetrical structure of **K37** (with the phosphorus center of the P(C₆H₁₃N₂O₂) ligand as center of asymmetry). The NH signal is found at 4.7 ppm.

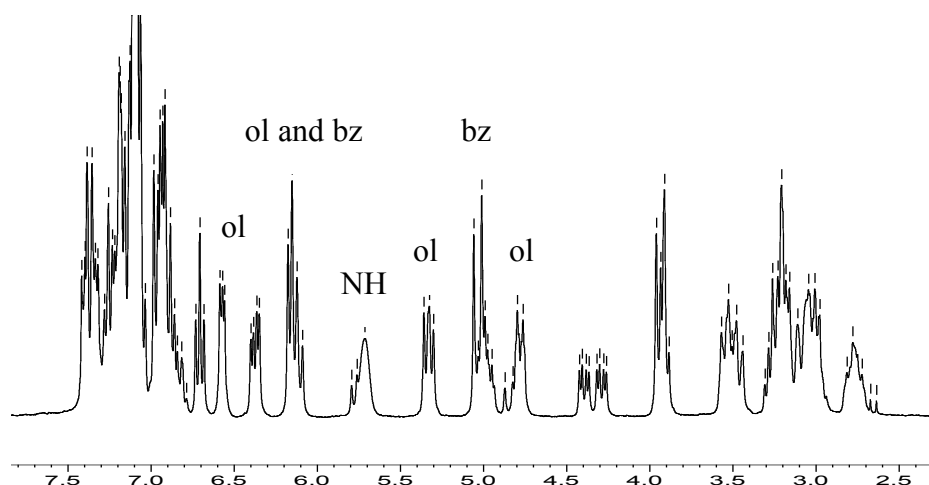


Figure 3.5: ¹H NMR spectrum for **K37**. ol= olefin and bz= benzyl.

The structure of *cis*-[Rh(trop₂PPh)(P(C₆H₁₃N₂O₂))] (**K37**) was further confirmed by X-ray diffraction.

Unfortunately the rather poor quality of the crystal (obtained by slow evaporation of a saturated dichloromethane solution of **K37**) did not allow a refinement of the data to a point where a detailed analysis of bond lengths and angles is meaningful. However, the gross structural features of the complex as shown in Figure 3.6 are clearly detected and are in accord with the NMR spectra.

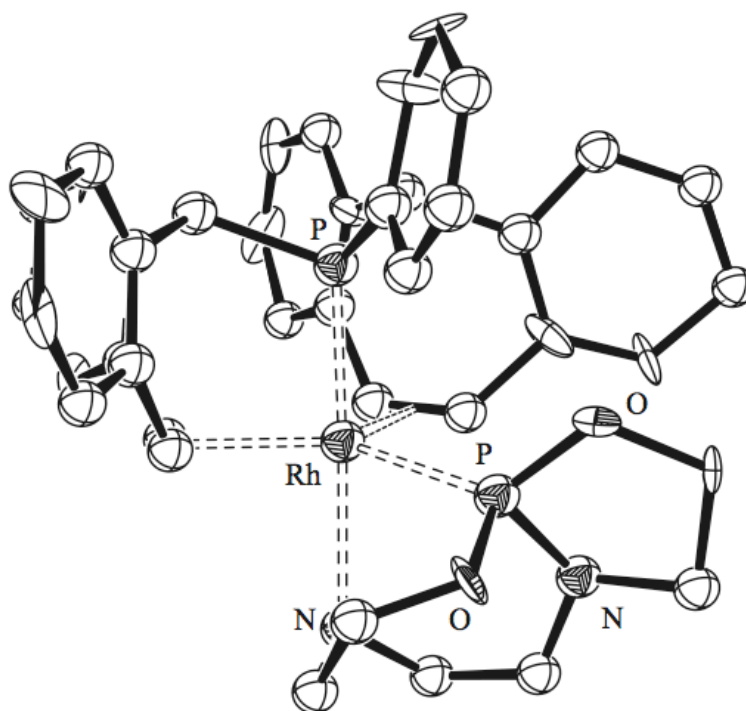
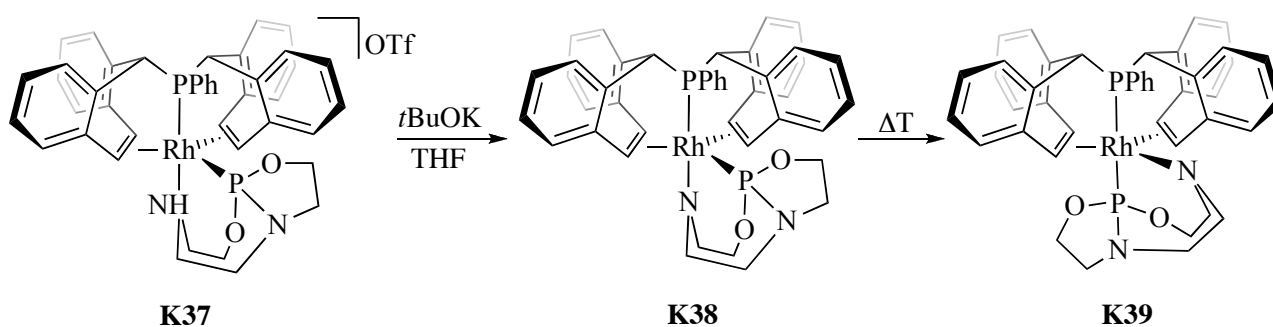


Figure 3.6: ORTEP view of *cis*-[Rh(trop₂PPh)(P(C₆H₁₃N₂O₂))] (**K37**).

The next step planned to obtain the desired metallaphosphoranide complex was the deprotonation of the coordinated amino function in *cis*-[Rh(trop₂PPh)(P(C₆H₁₃N₂O₂))] (**K37**), which eventually may proceed under ring closure and reconstitution of the λ^5, σ^5 -phosphoranido framework. Therefore, **K37** was reacted with one equivalent of potassium *tert*-butoxide in THF (Scheme 3.11).



Scheme 3.11: Deprotonation of **K37** and its isomerization to **K39**.

Indeed, the resulting amide was prepared quantitatively and its formation was confirmed by ^1H NMR, ^{31}P NMR and ^{13}C NMR spectroscopy. The ^{31}P NMR spectrum, depicted in Figure 3.7, showed two *dd* at $\delta = 137.0$ ppm (with $^1J_{\text{RhP}} = 137.9\text{ Hz}$ and $^2J_{\text{PP}} = 25.0\text{ Hz}$) and $\delta = 22.6$ ppm (with $^1J_{\text{RhP}} = 137.4\text{ Hz}$ and $^2J_{\text{PP}} = 25.0\text{ Hz}$).

The rather small coupling constant between the two phosphorus nuclei (25 Hz) indicates a *cis*-configuration of the two ^{31}P nuclei at the metal.

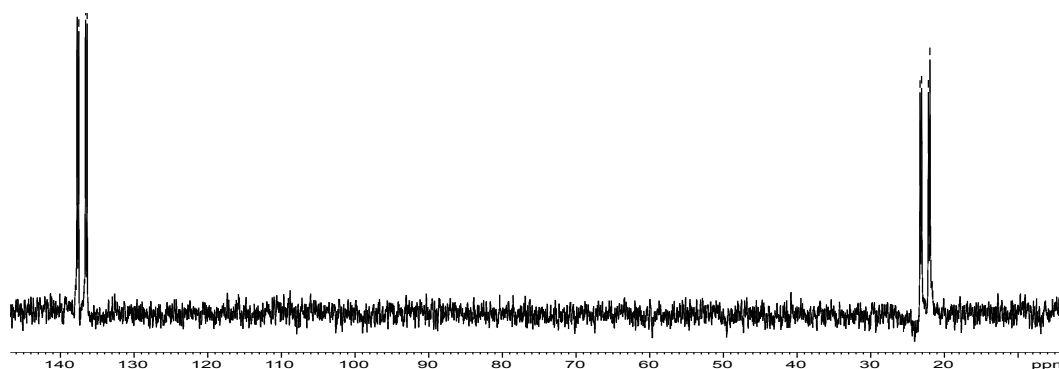


Figure 3.7: ^{31}P -NMR spectrum of *cis*-[Rh(trop₂PPh)(P(C₆H₁₂N₂O₂))] (**K38**).

While the resonance of the ^{31}P nucleus of trop₂PPh ligand ($\delta = 137.0$ ppm) is only mildly affected when compared to **K37** ($\delta = 152.4$ ppm), the resonance of the amidophosphite P(C₆H₁₃N₂O₂) ($\delta = 22.6$ ppm) is significantly affected upon deprotonation and shifted by about 110 ppm to lower frequencies compared to complex **K37** (for a comparative listing see Table 3.1a-b). However, the chemical shift of the latter still in the positive region of ^{31}P NMR spectrum (vs 85% H₃PO₄) excludes ring closure and formation of a symmetrical phosphoranido ligand. Furthermore, the ^1H NMR shows four resonances for the olefinic protons [$\delta = 4.9$ ppm (two signals overlapping) $\delta = 4.7$ ppm and $\delta = 4.5$ ppm] and two resonances for the benzylic protons ($\delta = 4.4$ ppm and 4.3 ppm) and hence indicates an asymmetric complex due to the open asymmetrical form of the P(C₆H₁₃N₂O₂) ligand in **K38**.

After 12 hours in solution at room temperature the formation of a second complex was detected by ^{31}P NMR spectroscopy. This new species was assigned to *trans*-[Rh(trop₂PPh)(P(C₆H₁₂N₂O₂))] (**K39**). Complete isomerization from *cis* to *trans* was achieved after heating a THF solution of *cis*-[Rh(trop₂PPh)(P(C₆H₁₂N₂O₂))] (**K38**) (Scheme 3.11).

trans-[Rh(trop₂PPh)(P(C₆H₁₃N₂O₂))] (**K39**) was analyzed by ^1H NMR, ^{13}C NMR and ^{31}P NMR spectroscopy. No crystals suitable for X-ray diffraction studies could be obtained. The ^{31}P NMR spectrum, displayed in Figure 3.8, showed two *dd* at $\delta = 24.1$ ppm (with $^1J_{\text{PRh}} = 128.5\text{ Hz}$ and $^2J_{\text{PP}} =$

743.1 Hz) and $\delta = 7.8$ ppm (with $^1J_{\text{PRh}} = 97.6$ Hz and $^2J_{\text{PP}} = 743.1$ Hz). The large coupling constant measured of 743 Hz is typical for a *trans* configuration of two phosphorus donors at a metal center.

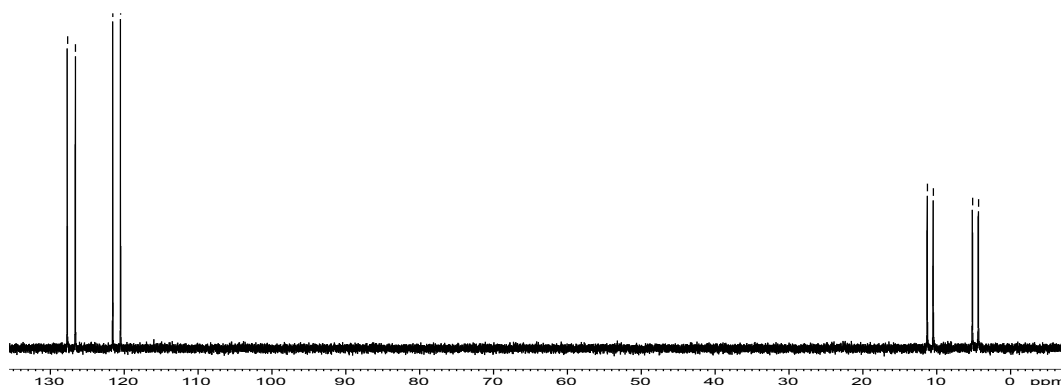


Figure 3.8: ^{31}P -NMR spectra of *trans*-[Rh(trop₂PPh)(P(C₆H₁₂N₂O₂))] (**K39**).

The ^1H NMR data show four resonances for the olefinic protons ($\delta = 5.7$ ppm, 5.4 ppm, 4.8 ppm and 4.7 ppm) and a multiplet centered at 4.7 ppm due to the two overlapping resonances of the benzylic protons.

The ^{13}C NMR confirmed the coordination of the trop ligand on the metal center displaying resonances at 68.2 ppm, 67.7 ppm, 66.4 ppm and 63.6 ppm for the olefinic carbons and at 50.3 ppm for both benzylic carbons. The slight shift to higher frequencies of the chemical shifts of olefinic carbons and protons in **K39** can be explained by the different *trans* effect of mutually exchanged N,P-donor centers in the equatorial plane of the trigonal bipyramidal structures of **K38** and **K39** trans to the olefinic units (P being the better donor leading to enhanced M→L back bonding and consequently to ^{13}C resonances at lower frequencies).

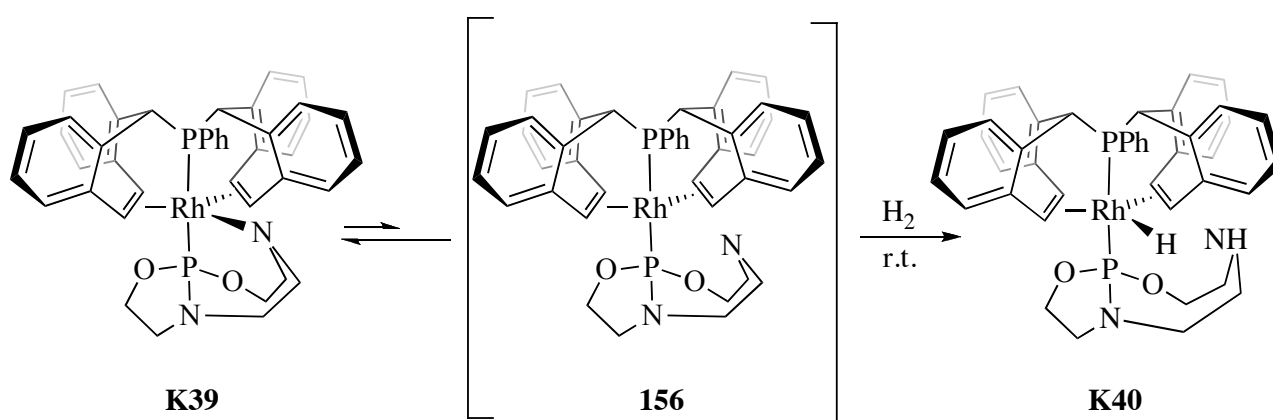
The proton and carbon chemical shifts attributed to the benzylic groups of the trop₂PPh ligand are not affected by the *cis* → *trans* isomerisation while the phosphorus chemical shift at $\delta = 124.1$ ppm is shifted slightly to lower frequencies in **K39** (vs. $\delta = 137$ ppm for **K38**).

The results lead us to conclude that the kinetic product of the deprotonation reaction is the *cis*-configured complex **K38**, which upon heating rearranges to the thermodynamically more stable product *trans* isomer **K39**. In combination with the observations of a single *cis*-isomer for the amino-phosphane complex **K37**, we conclude that the *trans*-effect and concomitantly the *cis*-directing effect which pushes a second strong donor ligand in *cis*-position to the first, increases in the order amine < aminophosphite < amide.

3.5 Reactivity of *trans*-[Rh(trop₂PPh)(HP)] with H₂

Despite the fact that **K39** did not bear the HP ligand in its pentacoordinated form, we reasoned that an equilibrium between species **K39** and **156** could be possible in solution, as depicted in Scheme 3.12. Compound **156** would have a free coordination site available for the side-on approach of the molecule of dihydrogen and would therefore be to some extent reactive. This hypothesis is actually supported by DFT calculations, as it will be discussed (Chapter 3.1.8).

In view of this possibility, the reaction of *trans*-[Rh(trop₂PPh)(P(C₆H₁₂N₂O₂))] (**K39**) in presence of dihydrogen gas was investigated (Scheme 3.12).



Scheme 3.12: Reactivity of *trans*-[Rh-(trop₂PPh)(P(C₆H₁₂N₂O₂))] (**K39**) with H₂.

Remarkably, the reaction occurred very cleanly at room temperature and yielded quantitatively the hydride species **K40**. As we will show below, it is reasonable to assume an equilibrium between species **K39** and **156** based on DFT calculations (see paragraph 3.6). In the equatorial position of its saw-horse type structure compound **156** has a free coordination site, which is available for a side-on binding of one molecule of dihydrogen. The pendant amido arm can then assist in the heterolytical cleavage of H₂ leading to the new rhodium-hydride complex **K40**.

The ¹H NMR spectrum shows a resonance (*ddd*) at δ = -7.1 ppm (¹J_{RhH} = 3.0 Hz, ²J_{PH} = 16.3 Hz and ²J_{PH} = 22.3 Hz), which is attributed to the hydride (Figure 3.9). This resonance lies in the range expected for terminal hydrides in rhodium complexes. Moreover, the relatively small coupling constants suggest a *cis* orientation of the hydride to the phosphorus nuclei. The molecule still contains the fully κ³-bound trop ligand (confirmed by ¹³C and ¹H NMR spectroscopy). Evaluation of the integrals suggested the formation of a monohydride complex, which excluded the formation of a dihydride species by oxidative addition of H₂. Therefore, the pendant amide assisted the metal in the heterolytical cleavage of H₂ leading to the new rhodium hydride complex **K40**, which is

bearing an amine function ($\delta_{\text{NH}} = 1.87$ ppm), as expected. Moreover, the ^{31}P NMR, shown in Figure 3.10, displayed two *dd* at $\delta = 155.9$ ppm (with $^1J_{\text{RhP}} = 137.4$ Hz and $^2J_{\text{PP}} = 608.8$ Hz) and $\delta = 142.9$ ppm (with $^1J_{\text{RhP}} = 163.2$ Hz and $^2J_{\text{PP}} = 608.8$ Hz). The relatively big coupling constants ($^2J_{\text{PP}}$) detected suggested a *trans* orientation of the two phosphorous atoms, which has been further confirmed by the rather small coupling constants ($^2J_{\text{PH}}$) – 16.3 Hz and 22.3 Hz, respectively – between the hydride and the two phosphorus atoms.

Note that the phosphorus chemical shift attributed to the ^{31}P nucleus of the $\text{P}(\text{C}_6\text{H}_{12}\text{N}_2\text{O}_2)$ ligand is significantly shifted to higher frequencies in a region comparable to the amino complex **K37**.

A Comparison of the NMR data of the compounds **K36**, **K37**, **K38**, **K39** and **K40** is given in Table 3.1a-b. The observed successive shift to lower frequencies of the ^{31}P nucleus of the trop ligand can be explained by the electronegativity of the group trans to phosphorus ($\text{OTf} > \text{NR}_3 > \text{PR}_3$) and the ionicity of the complexes (cationic complexes showing generally higher frequency shifted resonances than neutral ones).

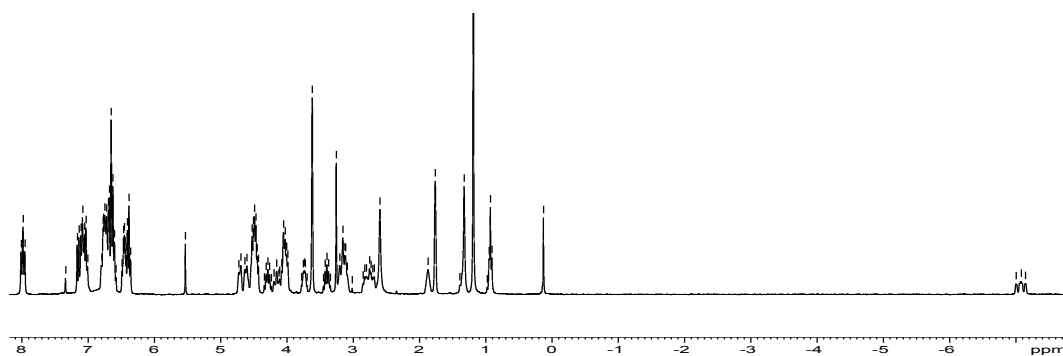


Figure 3.9: ^1H NMR spectra of **K40**. The hydride resonance is at -7 ppm.

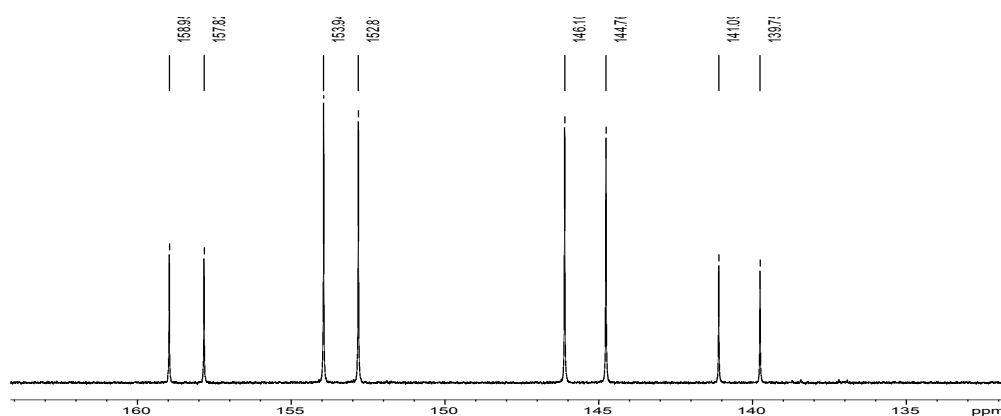


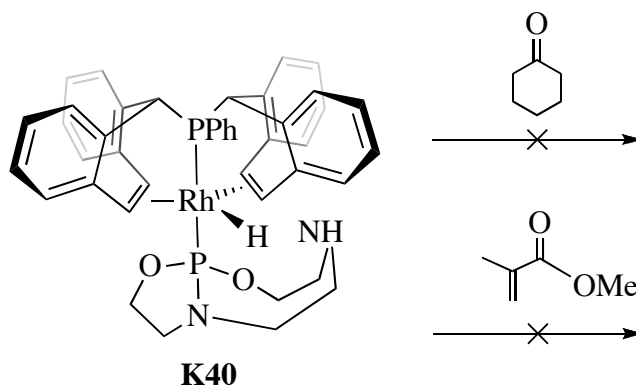
Figure 3.10: ^{31}P NMR spectra of *trans*- $[\text{RhH}(\text{trop}_2\text{PPh})(\text{P}(\text{C}_6\text{H}_{13}\text{N}_2\text{O}_2))]$ (**K40**).

Table 3.1a-b: ^1H (a) and ^{31}P NMR (b) data of complexes **K36**, **K37**, **K38**, **K39** and **K40**.

a)	^1H δ [ppm] _{olefin}				^1H δ [ppm] _{benzyl}	
trop ₂ PPh	6.7				4.5	
[Rh(trop ₂ PPh)(OTf)] (K36)	6.9	6.9	5.8	5.8	4.9	4.9
<i>cis</i> -[Rh(OTf)(trop ₂ PPh)(P(C ₆ H ₁₃ N ₂ O ₂))] (K37)	6.3	6.1	5.3	4.8	5.0	3.9
<i>cis</i> -[Rh(trop ₂ PPh)(P(C ₆ H ₁₂ N ₂ O ₂))] (K38)	4.9	4.7	4.5	4.5	4.4	4.3
<i>trans</i> -[Rh(trop ₂ PPh)(P(C ₆ H ₁₂ N ₂ O ₂))] (K39)	5.7	5.4	4.8	4.7	4.7	4.8
<i>trans</i> -[Rh(trop ₂ PPh)H(P(C ₆ H ₁₃ N ₂ O ₂))] (K40)	4.7		4.5	4.6	4.7	4.5

b)	^{31}P δ [ppm] _{tropPPh}	^{31}P δ [ppm] _{HP}	$^2J_{\text{PP}}$ [Hz]
trop ₂ PPh	-7.0		
HP (155)		-36.9	
[Rh(trop ₂ PPh)(OTf)] [†] (K36)	175.8		
<i>cis</i> -[Rh(OTf)(trop ₂ PPh)(P(C ₆ H ₁₃ N ₂ O ₂))] (K37)	152.4	137.5	5.8
<i>cis</i> -[Rh(trop ₂ PPh)(P(C ₆ H ₁₂ N ₂ O ₂))] (K38)	137.0	22.6	33.5
<i>trans</i> -[Rh(trop ₂ PPh)(P(C ₆ H ₁₂ N ₂ O ₂))] (K39)	124.1	7.8	743.1
<i>trans</i> -[Rh(trop ₂ PPh)H(P(C ₆ H ₁₃ N ₂ O ₂))] (K40)	155.9	142.9	608.8

In order to test whether the heterolytic splitting of H₂ across the Rh-N unit may be used for (catalytic) hydrogenations, a solution of *trans*-[RhH(trop₂PPh)(P(C₆H₁₃N₂O₂))] (**K40**) in THF was reacted with one equivalent of cyclohexanone (Scheme 3.13). However, the reduction of the ketone was not observed even after long reaction time or gentle heating of the solution. The change of the substrate to methyl methacrylate did likewise not produce the desired hydrogenated product.

**Scheme 3.13.** Attempted reduction of simple ketones.

3.6 DFT Calculations

Computational Methods:

In order to gain further insight in the mechanism of hydrogenation reaction DFT calculations were performed by Dr. Jean-Valère Naubron during his stay as post-doctoral fellow at the ETH. The simplified models **Ca** (X = N) and **Cb** (X = P) have been employed for the calculations (Figure 3.11).

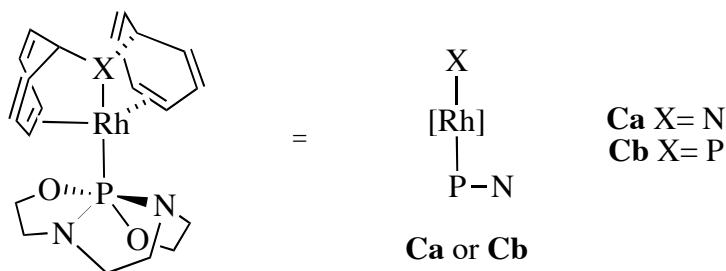


Figure 3.11. Simplified models used for DFT calculations.

The computations were performed within either the framework of full DFT or two layers ONIOM. All calculations were performed with the Gaussian 03 program packages[§].

Results and Discussion:

Two systems have been investigated: **Ca** having as co-ligand the trop₂NMe and **Cb** bearing the trop₂PMe. Preliminary conformational studies pointed out the most probable species existing in solution for **Ca** and **Cb** (Figure 3.12a-b).

The first system investigated has trop₂NMe as ligand. The relative stability of various isomers (Figure 3.12a) was inspected and accordingly conformer **C1a** corresponds to the structure in global energy minimum. **C1a** has the phosphoranido moiety in apical position *trans* to the nitrogen atom of the bistropamine ligand. The phosphoranide does not preserve its typical structure but is present in a *quasi* open-form: the nitrogen center closest to the metal center has a calculated distance of 2.445 Å from the rhodium atom (≈ 0.2 Å longer than normal Rh-N bonds in comparable complexes) and the distance P-N is 1.975 Å significantly longer than usual P-N bonds in λ^5, σ^5 -phosphoranes. The calculated bond lengths for the P-Rh and Rh-N bonds are 2.224 Å and

[§] R. D. Gaussian 03, M. J. Frisch, G. W. Trucks, H. B. Schlegel, G. E. Scuseria, M. A. Robb, J. R. Cheeseman, J. A. Montgomery, Jr., T. Vreven, K. N. Kudin, J. C. Burant, J. M. Millam, S. S. Iyengar, J. Tomasi, V. Barone, B. Mennucci, M. Cossi, G. Scalmani, N. Rega, G. A. Petersson, H. Nakatsuji, M. Hada, M. Ehara, K. Toyota, R. Fukuda, J. Hasegawa, M. Ishida, T. Nakajima, Y. Honda, O. Kitao, H. Nakai, M. Klene, X. Li, J. E. Knox, H. P. Hratchian, J. B. Cross, V. Bakken, C. Adamo, J. Jaramillo, R. Gomperts, R. E. Stratmann, O. Yazyev, A. J. Austin, R. Cammi, C. Pomelli, J. W. Ochterski, P. Y. Ayala, K. Morokuma, G. A. Voth, P. Salvador, J. J. Dannenberg, V. G. Zakrzewski, S. Dapprich, A. D. Daniels, M. C. Strain, O. Farkas, D. K. Malick, A. D. Rabuck, K. Raghavachari, J. B. Foresman, J. V. Ortiz, Q. Cui, A. G. Baboul, S. Clifford, J. Cioslowski, B. B. Stefanov, G. Liu, A. Liashenko, P. Piskorz, I. Komaromi, R. L. Martin, D. J. Fox, T. Keith, M. A. Al-Laham, C. Y. Peng, A. Nanayakkara, M. Challacombe, P. M. W. Gill, B. Johnson, W. Chen, M. W. Wong, C. Gonzalez, and J. A. Pople, Gaussian, Inc., Wallingford CT, 2004.

2.240 Å, respectively. The open form **C2a** (where the oxygen atom has interactions with the phosphorus and rhodium center) is less favorable by 9.5 kcal mol⁻¹. The least stable isomer is **C3a** has an intact phosphoranide as ligand but is 16.2 kcal mol⁻¹ less stable than **C1a**. Similar results have been obtained for compound **Cb**. Conformer **C3b** has a lower energy with respect to **C2b**.

In Figure 3.13a-b a sketch of the results obtained for the computed reaction profile for the heterolytical (a) and homolytical dihydrogen (b) splitting are shown. Starting point for the calculations was the most stable conformer **C1a**.

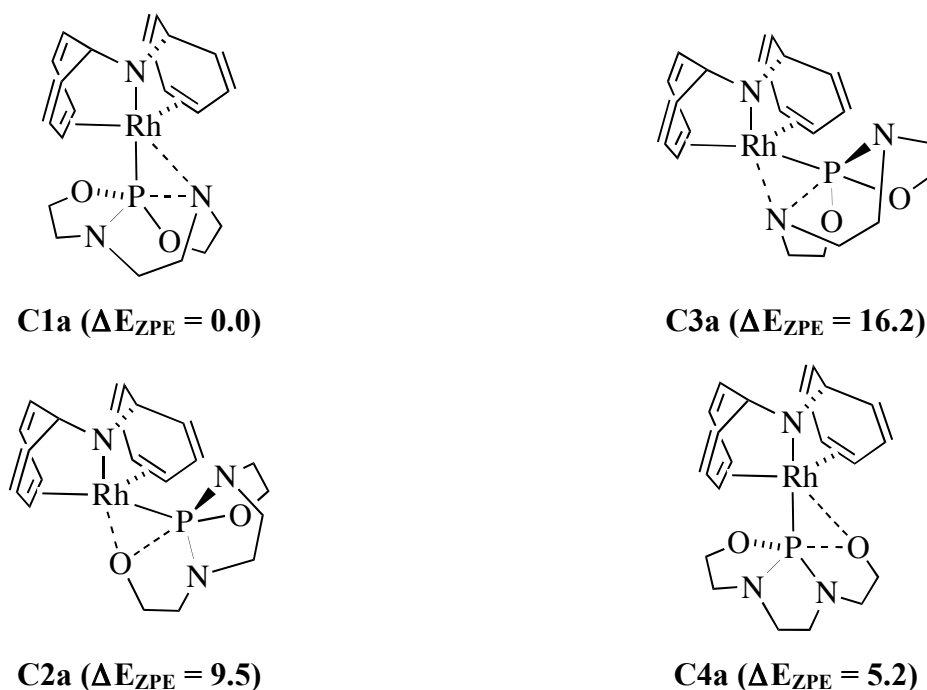


Figure 3.12a: Structures of the different conformers **C1a** – **C4a** computed by DFT methods (ONIOM B3PW91/BS1:HF/lanM2B). The relative energies (corrected for zero point energy, ZPE) are given in brackets (in kcal mol⁻¹).

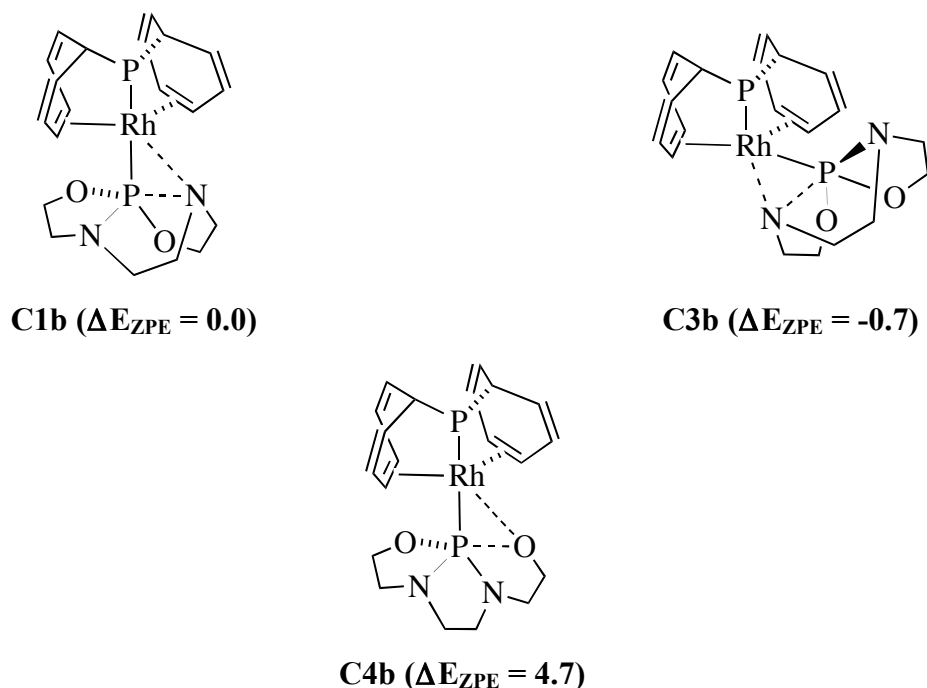


Figure 3.12b: Structures of the different conformers **C1b** – **C4b** computed by DFT methods (ONIOM B3PW91/BS1:HF/lanM2B). The relative energies (corrected for zero point energy, ZPE) are given in brackets (in kcal mol⁻¹).

In the heterolytic pathway (**a**) the first step – common for both mechanisms – is the approach of the dihydrogen molecule toward the open site of the complex to yield the intermediate **I3**, which is higher in energy by +10.8 kcal mol⁻¹. The energetic barrier calculated for this step is 10.2 kcalmol⁻¹ and the bond lengths calculated for **I3** show an elongation of the Rh-P bond (2.358 Å, longer 0.134 Å compared to **C1a**). A slight contraction of the Rh-N bond of 0.053 Å in respect to **C1a** can be observed. The Rh-N bond is slightly longer (2.259 Å, $\Delta_{3-\text{C1a}} = 0.019$ Å). Other important bond lengths calculated for **I3** are listed here: the Rh-H distance is 2.076 Å, the Rh-N distance is 1.895 Å and the H-H distance is 0.785 Å.

The activation of the dihydrogen molecule proceeds through the transition state **TS1** which somewhat lower in energy than **I3** at $\Delta E = 9.1$ kcalmol⁻¹. While this is physically not meaningful, it indicates that the potential energy surface is very flat in this region. The axial Rh-N and Rh-P bond lengths remain almost unchanged in this process (respectively 2.24 Å and 2.34 Å) but a significant elongation of the P-N bond (2.063 Å) concomitant with a stretching of the H-H bond (1.021 Å) is computed. As expected the Rh-H and N-H bonds are diminished in length (1.790 Å and 1.285 Å respectively). The NBO charge analysis shows the expected δ^+ , δ^- polarization of the dihydrogen molecule. The final product, the Rh(I) hydride complex **P4** is at 3.3 kcal mol⁻¹ that is the overall

reaction is endotherm and the reverse reaction, that is the facile loss of H₂ from a trop₂NR complex like **P4** has to be expected which is furthermore favored by a gain in entropy.

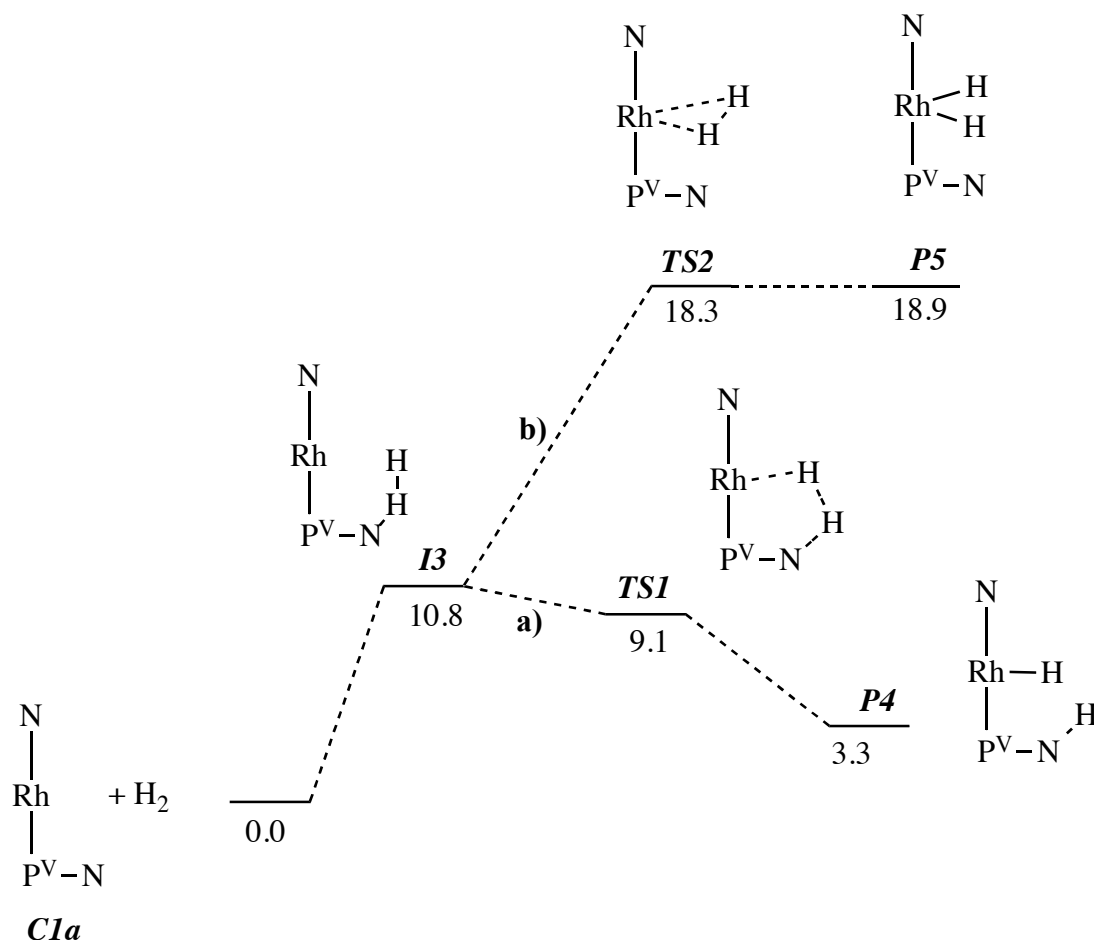


Figure 3.13a-b: Reaction profile for the heterolytic (a) and homolytic (b) H₂ activation by **C1a**.

The energies corrected for zero point energy are in kcalmol⁻¹. (Method: we used B3PW91/BS2 for energy calculations and ONIOM B3PW91/BS1:HF/lanM2B for geometry and frequency calculations. BS1: 6-311G(d) for H, C, N, O, P atoms and Lan12dz for Rh. BS2: 6-311+G(df,p) for H, C, N, O, P atoms and Lan12dz for Rh).

In the classical oxidative addition (b) that follows the formation of intermediate **I3** requires considerably more energy when compared to the heterolytic pathway (a) ($\Delta\Delta E = 9.2$ kcalmol⁻¹). Furthermore, the formation of the Rh(III) dihydride **P5** is energetically very unfavorable even when compared to **TS2**.

In conclusion the calculations clearly show that a heterolytic pathway A is the most favorable for the splitting of the H₂ molecule, however, the formed product – a remote amino Rh(I) hydride complex **P4** – is not expected to be stable with respect to the educts **C1a** and H₂.

We therefore turned our attention to the model complex **C1b** that is close to the experimentally investigated complex **K39** with a trop₂PPh ligand. The reaction profile calculated is shown in

Figure 3.14c-d. Qualitatively, the energy profile is very similar to the one discussed for the H₂ activation with a complex carrying trop₂NR type ligand. The formation of H₂ adduct **I6** is slightly more favourable and is the bifurcation point for the heterolytic pathway **TS3** → **P7** and oxidative addition **TS4** → **P8**. Again, clearly the heterolytic pathway is more favorable by about 7 kcal mol⁻¹. Furthermore, the remote amino Rh(I) hydride **P7** is thermodynamically stable while the Rh(III) dihydride **P8** is expected to decompose in an barrierless reaction to the starting materials.

The results from the computations are fully in accord with our experimental findings, which show that the trop₂PPh complex **K39** with an “open” phosphoranido ligand is capable of cleaving instantaneously molecular hydrogen.

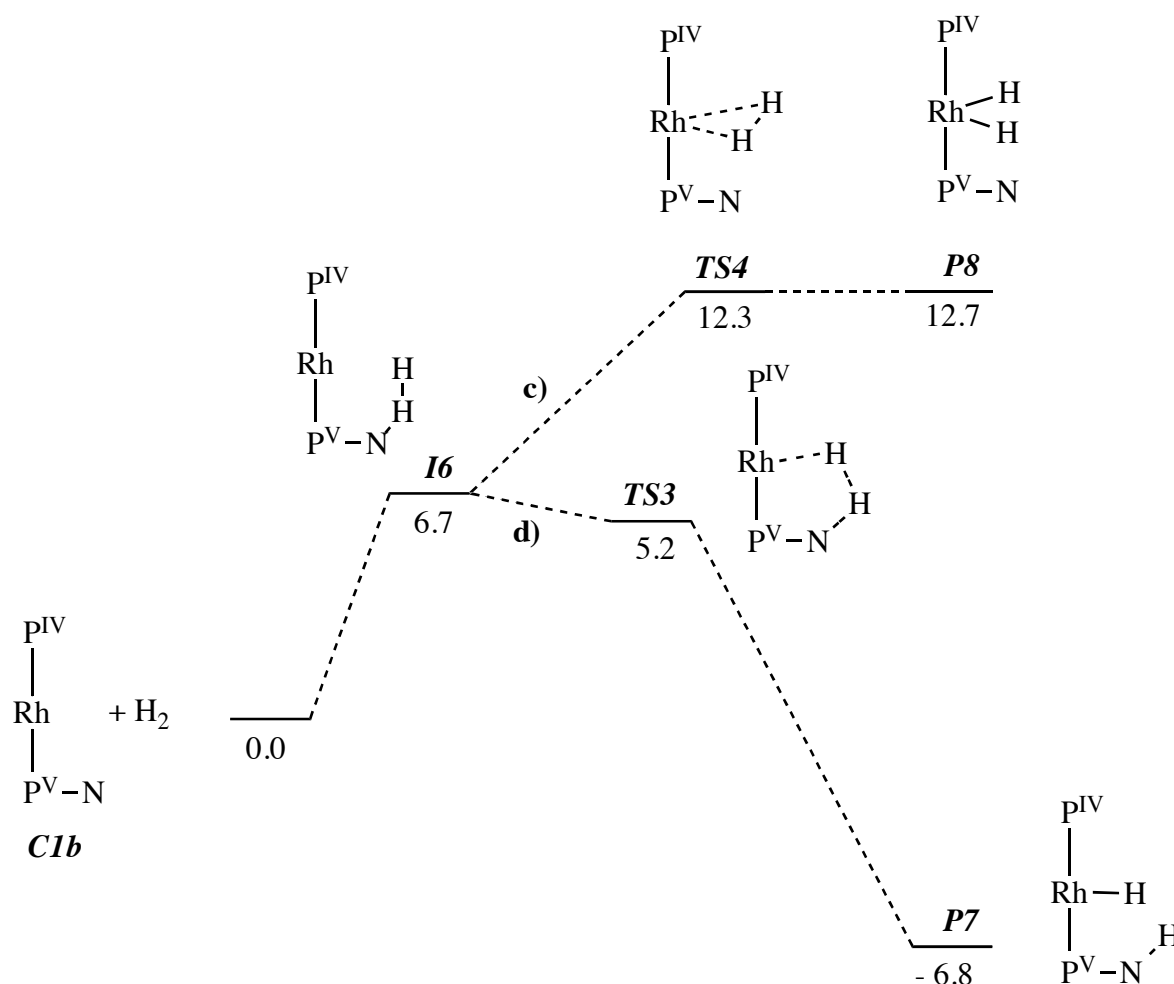


Figure 3.14c-d: Reaction profile for the heterolytical H₂ activation. The energies corrected for zero point energy are in kcalmol⁻¹. (Method: we used B3PW91/BS2 for energy calculations and ONIOM B3PW91/BS1:HF/lanM2B for geometry and frequency calculations. BS1: 6-311G(d) for H, C, N, O, P atoms and Lanl2dz for Rh. BS2: 6-311+G(df,p) for H, C, N, O, P atoms and Lanl2dz for Rh).

3.7 Conclusions and Outlook

Experimental work and DFT calculations discussed in this chapter show that phosphoranides as ligands are able to participate as cooperating ligands in the activation of small molecules like H₂.

Computations indicate that the most stable conformers are species **C1a** and **C1b** (Figure 3.15) that is in agreement with the structure we propose for the experimentally observed complex **K39** based on NMR data. This conformer bears the “opened” phosphoranido-type ligand in *trans* position to the heteroatom X of the trop ligand. The calculated distances for Rh-N and P-N are 2.445 Å and 1.975 Å. The rhodium-nitrogen interaction is weak.

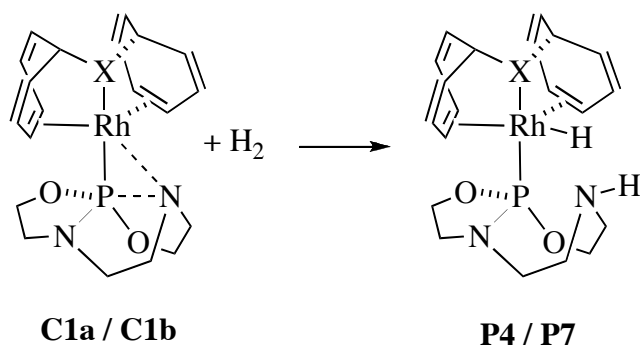


Figure 3.15: Conformers **C1a** and **C1b** are the most stable, according to DFT calculations. (X= PR or NR).

Species resembling **C1a** and **C1b** according to the calculation should be able to activate dihydrogen through a heterolytical reaction path which is also in agreement with the experimental findings made in the reaction between **K39** and H₂ which cleanly gives the remote amino Rh(I) hydride complex **K40**.

This reaction opens up new avenues for the application of complexes which are derived from λ⁵,σ⁵-phosphoranides. Specifically, future work will focus on the synthesis and application of complexes with non-noble metals like Co and Fe. Furthermore, the observation that the trop₂NR ligand leads to remote amino hydride complexes which should easily decompose to the corresponding phosphoranido complex and dihydrogen may lead to useful applications as dehydrogenation catalyst proceeding under deliberation of H₂ (a valuable chemical energy source). Both aspects are currently investigated.

In this preliminary study, we exploited the well-know hydridophosphoranides as cooperating ligand for the activation of dihydrogen.

¹ a) R. Cammack, *Nature*, **1999**, 21, 214. b) M.W.W. Adams, E.I. Stiefel, *Science*, **1998**, 282, 1842.
² M. Frey, *ChemBioChem*, **2002**, 3, 153-160.

- ³ a) Y. Nicolet, A.L. de Lacey, X. Vernède, V. M. Fernandez, E. C. Hatchikian, J.C. Fontecilla-Camps, *J. Am. Chem. Soc.*, **2001**, 123, 1596. b) Y. Nicolet, B. Lemon, J.C. Fontecilla-Camps, J.W. Peters, *Trends Biochem. Sci.*, **2000**, 25, 138.
- ⁴ a) Y. Nicolet, C. Piras, P. Legrand, C. E. Hatchikian, J.C. Fontecilla-Camps, *Struct. Fold. Des.*, **1999**, 7, 13. b) J.W. Peters, W.N. Lanzilotta, B.J. Lemon, L.C. Seefeldt, *Science*, **1998**, 282, 1853.
- ⁵ D.S. Horner, B. Heil, T. Happe, T.M. Embley, *Trends Biochem. Sci.*, **2002**, 27, 148-153. c) J.W. Peters, *Curr. Opin. Struct. Biol.*, **1999**, 9, 670.
- ⁶ G. Jaouen, *Bioorganometallics*, Wiley-VCH, **2006**, 404-417.
- ⁷ D. Sellmann, R. Prakash, F. W. Heinemann, *Eur. J. Inorg. Chem.*, **2004**, 1847.
- ⁸ D.L. DuBois, C.J. Curtis, *Inorg. Chem.*, **2003**, 42, 216-227.
- ⁹ D-H. Lee, B.P. Patel, E. Clot, O. Eisenstein, R.H. Crabtree, *Chem. Commun.*, **1999**, 297-298.
- ¹⁰ H.S. Chu, C.P. Lau, K.Y. Wong, *Organometallics*, **1998**, 17, 2768.
- ¹¹ A.J. Lough, S. Park, R. Ramachandran, R.H. Morris, *J. Am. Chem. Soc.*, **1994**, 116, 8356.
- ¹² M.D. Fryzuk, C.D. Montgomery, S.J Rettig, *J. Organometallics*, **1991**, 10, 467.
- ¹³ a) C. Marchi, G. Buono, *Tetrahedron Lett.*, **1999**, 40, 9251. b) C. Marchi, F. Fotiadu, G. Buono, *Organometallics*, **1999**, 18, 915. c) Y. Vannoorenberghe, G. Buono, *J. Am. Chem. Soc.*, **1990**, 112, 6142. d) G. Buono, J.R. Llinas, *J. Am. Chem. Soc.*, **1981**, 103, 4532. e) G. Buono, *Tetrahedron Lett.*, **1972**, 32, 3257.
- ¹⁴ a) K.N. Gavrilov, A.I. Polosukhin, O.G. Bondarev, S.E. Lyubimov, K.A. Lyssenko, P.V. Petrovskii, V.A. Davankov, *J. Mol. Catal. A: Chem.*, **2003**, 196, 39. b) O.G. Bondarev, I.S. Mikhel, V.N. Tsarev, P.V. Petrovskii, V.A. Danakov, K.N. Gavrilov, *Russ. Chem. Bull.*, **2003**, 52, 116. c) I.S. Mikhel, O.G. Bondarev, V.N. Tsarev, G.V. Grintselev-Knyazev, K.A. Lyssenko, V.A. Davankov, K.N. Gavrilov, *Organometallics*, **2003**, 22, 925. d) K.N. Gavrilov, A.V. Korostylev, A.I. Polosukhin, O.G. Bondarev, A.Y. Kovalevsky, V.A. Davankov, *J. Organomet. Chem.*, **2000**, 613, 148. e) K.N. Gavrilov, *Russ. J. Coord. Chem.*, **1998**, 24, 127. f) E.E. Nifant'ev, K.N. Gavrilov, G.I. Timofeeva, A.T. Teleshev, S.N. Krasnokutskii, E.Y. Zhorov, V.A. Pavlov, E.I. Klabunskii, *J. Organomet. Chem.*, **1990**, 397, 245.
- ¹⁵ a) R. Burgada, R. Setton, *Chem. Organophosphorus Compds.*, **1994**, 3, 185. b) T. Baily, R. Burgada, *Phosphorus Sulfur Relat. Elem.*, **1991**, 63, 33. d) B. Ben Jaafar, D. El Manouni, R. Burgada, *Phosphorus Sulfur Relat. Elem.*, **1990**, 47, 67. e) D. El Manouni, Y. Leroux, R. Burgada, *Tetrahedron*, **1986**, 42, 2435.
- ¹⁶ a) M. Fan, I.V. Shevchenko, R.H. Voorhies, S.F. Eckert, H. Zhang, M. Lattman, *Inorg. Chem.*, **2000**, 39, 4704. b) D.V. Khasnis, M. Lattman, U. Siriwardane, S.K. Chopra, *J. Am. Chem. Soc.*, **1989**, 111, 3103. c) Lattman M., M.M. Olmstead, P.P. Philip, D.W.H. Rankin, H.E. Robertson, *Inorg. Chem.*, **1988**, 27, 3012. d) S.K. Chopra, S.S.C. Chu, P. de Meester, D.E. Geyer, M. Lattman, S.A. Scott, *J. Organomet. Chem.*, **1985**, 294, 347. e) M. Lattman, S.K. Chopra, A.H. Cowley, Arif A.M., *Organometallics*, **1986**, 5, 677. f) M. Lattman, S.A. Morse, A.H. Cowley, J.G. Lasch, N.C. Norman, *Inorg. Chem.*, **1985**, 24, 1364. g) M. Lattman, B.N. Anand, S.C. Shirly, R.D. Rosenstein, *Organometallics*, **1984**, 3, 670. h) M. Lattman, B.N. Anand, S.C. Shirly, R.D. Rosenstein, Robert R., *Phosphorus Sulfur Relat. Elem.*, **1983**, 18, 303.
- ¹⁷ a) M. Lattman, S.K. Chopra, A.H. Cowley, A.M. Arif, *Organometallics* **1986**, 5, 677. b) E.G. Burns, S.S.C. Chu, P. Meester, M. Lattman, *Organometallics* **1986**, 5, 2383. c) M. Lattman, E.G. Burns, S.K. Chopra, A.H. Cowley, A.M. Arif, *Inorg. Chem.* **1987**, 26, 1926. For reviews see: a) C.D. Montgomery, *Phosphorus, Sulfur Silicon Relat. Elem.* **1993**, 84, 23. b) K.B. Dillon, *Chem. Rev.* **1994**, 94, 1441. c) H. Nakazawa, K. Kubo, K. Miyoshi, *J. Am. Chem. Soc.* **1993**, 115, 5863.
- ¹⁸ a) J. Wachter, B.F. Mentzen, B.F., J.G. Riess, *Angew. Chem., Int. Ed. Engl.* **1981**, 20, 28. b) P. Vierling, J.G. Riess, *J. Am. Chem. Soc.* **1981**, 103, 2466. c) F. Jeanneaux, A. Grand, J.G. Riess, *J. Am. Chem. Soc.* **1981**, 103, 4272. d) J.-M. Dupart, A. Grand, S. Pace, J.G. Riess, *J. Am. Chem. Soc.*

-
- 1982**, *104*, 2316. e) P. Vierling, J.G. Riess, *J. Am. Chem. Soc.* **1984**, *106*, 2432. f) J.-M. Dupart, A. Grand, J.G. Riess, *J. Am. Chem. Soc.* **1986**, *108*, 1167. g) P. Vierling, J.G. Riess, *Organometallics* **1986**, *5*, 2543. h) P. Vierling, G.J. Riess, A. Grand, A. *Inorg. Chem.* **1986**, *25*, 4144. i) D.V. Khasnis, J.M. Burton, H. Zhang, M. Lattman, *Organometallics* **1992**, *11*, 3745.
- ¹⁹ a) D.V. Khasnis, M. Lattman, U. Siriwardane, *Inorg. Chem.* **1989**, *28*, 681. b) D.V. Khasnis, M. Lattman, U. Siriwardane, U. *Inorg. Chem.* **1989**, *28*, 2594. c) D.V. Khasnis, M. Lattman, U.J. Siriwardane, *Chem. Soc., Chem. Commun.* **1989**, 1538. d) D.V. Khasnis, M. Lattman, U. Siriwardane, *Organometallics* **1991**, *10*, 1326. e) D.V. Khasnis, M. Lattman, U. Siriwardane, H. Zhang, *Organometallics* **1992**, *11*, 2074.
- ²⁰ a) E.A.V. Ebsworth, N.T. McManus, N.J. Pilkington, D.W.H. Rankin, *J. Chem. Soc., Chem. Commun.* **1983**, 484. b) E.A.V. Ebsworth, J. H. Holloway, N.J. Pilkington, D.W.H. Rankin, *Angew. Chem., Int. Ed. Engl.* **1984**, *23*, 630. c) W. Malisch, H.A. Kaul, E. Gross, U. Thewalt, U. *Angew. Chem., Int. Ed. Engl.* **1982**, *21*, 549.
- ²¹ a) M. Lattman, B.N. Anand, D.R. Garrett, M.A. Whitener, *Inorg. Chim. Acta* **1983**, *76*, L139. b) B.N. Anand, R. Bains, K. Usha, *J. Chem. Soc., Dalton Trans.* **1990**, 2315.
- ²² S.K. Chopra, J.C. Martin, *Heteroat. Chem.* **1991**, *2*, 71.
- ²³ F. Puschmann, Master Thesis, ETHZ – RWTH Aachen.
- ²⁴ P.S. Pregosin, R.W. Kunz, In *NMR Basic Principles and Progress*; P. Diehl, E. Fluck, R. Kostfeld, Eds.; Springer-Verlag: Berlin 1979.

4 Experimental Section

4.1 General Comments

General Techniques: All synthesis were performed in dried glassware under an atmosphere of argon using standard Schlenk techniques. The Argon was provided by PANGAS and further purified with Braun MB 100 HP gas purification system. Solvents were freshly distilled from sodium/benzophenone (THF), from sodium/tetraglyme/benzophenone (hexane, toluene) or calcium hydride (dichloromethane, acetonitrile) prior to use. Air sensitive compounds were stored and weighed in an argon filled glove box (Braun MB 150 B-G system) and reactions on small scale were performed directly in the glove box

Chemicals: Basic chemical were ordered at ABCR, Across, Aldrich, Fluka or Lancaster. The following organic compounds and metal precursor were prepared by literature methods: trop_2NH^1 , $[\text{Rh}(\mu\text{-Cl})(\text{COD})]_2$,² 1,3-dimethylimidazolium iodine³ (**55**), 1,3-dicyclohexylimidazolium chloride⁴ (**56**), 1,3-bis-((*S*)-1-phenyl-ethyl)imidazolium chloride⁵ (**57**), imidazolium triflate⁶ (**58**), phenylisocyanide⁷, 2-(trimethylsiloxy)phenyl isocyanide⁸ (**64**), $[\text{Pt}(\mu\text{-SMe}_2)(\text{Me})_2]_2$,⁹ $[\text{Pd}(\mu\text{-Cl})(\text{Me})(\text{SMe}_2)]_2$,¹⁰ 3,7-dinitro-5H-dibenzo[a,d]cycloheptan-5-on¹¹ (**125**), 3,7-diamino-5H-dibenzo[a,d]cycloheptan-5-on¹² (**127**), 3,7-difluoro-5H-dibenzo[a,d]cycloheptan-5-on (**129**), 3,7-difluoro-5H-dibenzo[a,d]cyclohepten-5-on (**130**), 3,7-difluoro-5H-dibenzo[a,d]cyclohepten-5-olo (**131**), 3,7-difluoro-5H-dibenzo[a,d]cyclohepten-5-chloro (**132**), $\text{I}(\text{O}_2\text{CCF}_3)_3$,¹³ 3,7-diiodo-5H-dibenzo[a,d]cycloheptanone (**134**), 3,7-diiodo-5H-dibenzo[a,d]cycloheptenone (**135**), $[\text{Rh}(\text{OTf})(\text{trop}_2\text{PPh})]^{14}$ (**K36**), hydridophosphorane¹⁵ (**155**), $[(3,5\text{-}(\text{CF}_3)_2\text{C}_6\text{H}_3)_4\text{B}]^+[\text{H}(\text{OEt}_2)_2]^-$ (“HBAr^F”).¹⁶

NMR spectra: were recorded on Bruker Avance 200, 250, 300, 400, 500 and 700 MHz spectrometers at room temperature (unless differently noted). Temperatures below room temperature were reached by evaporation of liquid nitrogen. The chemical shifts (δ) are expressed in ppm relative to TMS, CF_3Cl and H_3PO_3 for ^1H , ^{13}C , ^{19}F and ^{31}P respectively. For ^{103}Rh the frequency reference $\Xi = 3.16$ MHz was used (unless differently specified). Coupling constants J are given in Hertz [Hz] as absolute values. Where the first-order analysis is appropriate, the multiplicity of the signals is indicated as s, d, t, q and for m for singlets, doublets, triplets, quartets and multiplets, respectively. Otherwise the spin systems are specified explicitly. The abbreviation br is given for broadened signals. Quaternary carbons are indicated as C quart and aromatic units as CH ar. Simulation were performed with the MEXICO¹⁷ program package.

X-ray: crystallographic measurements were performed on Bruker SMART 1K and SMART APEX platforms with graphite-monochromated Mo- K_{α} radiation ($\lambda = 0.71073 \text{ \AA}$). The reflex intensities were measured by CCD area detectors. The collected frames were processed with the proprietary software SAINT¹⁸ and an absorption correction was applied (SADABS¹⁹). Solution and refinement of the structures was performed with SHELXS-97²⁰ and SHELXL-97²¹ respectively. In general, all non-hydrogen atoms were refined with anisotropic displacement parameters. Hydrogen atoms were placed in their idealized positions and allowed to ride on the respective carbon atoms.

IR spectra were recorded on a Perkin-Elmer-Spectrum 2000 FT-IR-Raman spectrometer with KBr beam splitter (range 600-4000 cm^{-1}). For solid compounds the ATR technique was applied. The absorption bands are described as follows: strong (s), very strong (vs), middle (m), weak (w) or broad (br).

Mass spectra High-resolution MALDI spectra were measured by the MS-service (Laboratorium für Organische Chemie, ETH Zürich) on an IonSpec HiResMALDI apparatus in a DCTB matrix.

Melting Points were determined with a Büchi melting point apparatus and are not corrected. Samples were prepared in a sealed glass capillaries.

Hydrogen Transfer Catalytic Experiments: The tested complex (0.1 mol %) was dissolved in a solution of KOtBu (0.01 eq) and acetophenone (1000 eq) in Ethanol (3 mL) in a Schlenk tube. The reaction progress was monitored by CG. Products were identified by comparison of GC retention times with those of authentic samples.

DFT Calculations: *Chapter II*: Full geometry optimizations were carried out followed by vibrational frequency calculations. All transition state structures reported are characterized by only one imaginary frequency. The transition state structures were slightly distorted along the normal mode of the imaginary frequency and geometry minimizations using the transition structure force constants as the initial Hessian were performed in order to obtain the two minimum structures attached to it. The energies of all structures were improved by performing single point calculations with an extended basis set, BP86/BS2. The basis set BS2 consisted of 6-311+G(df,p) for all atoms except Pt which is calculated with the Lanl2dz basis set. The Lanl2dz basis set include a double-zeta valence basis set (8s5p5d)/[3s3p2d] with the Hay and Wadt effective core potential (ECP)²² replacing core electrons up to 3p was used for the Pt atom. All energies were corrected for zero point energies. All calculations were carried out with the Gaussian 03 program.²³ All molecular drawings were produced with GaussView 3.09.²⁴ *Chapter III*: Calculation within two frameworks, full DFT and two layers ONIOM were carried out. For full DFT optimizations, the B3PW91 functional with a combination of the standard 6-31G(d) basis set has been used for all atoms

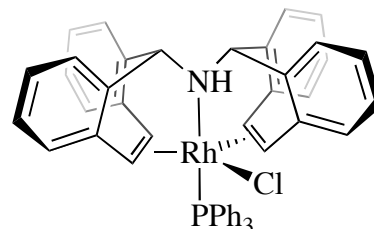
directly connected to the metal and the Lanl2dz basis functions for the Rh. The Lanl2dz basis set include a double-zeta valence basis set (8s5p5d)/[3s3p2d] with the Hay and Wadt effective core potential (ECP) replacing core electrons up to 3p was used for the Rh atom. In order to save computational time, we also tested a two-layered ONIOM method for geometry optimizations. In this method, the molecule is divided into high and low level layers, respectively a simplified model, called core, and the whole molecule, called real (Figure III.13). The ONIOM energy of the whole system is calculated using the equation: $E(\text{ONIOM}) = E(\text{high level, core}) + E(\text{low level, real}) + E(\text{low level, core})$; where $E(\text{high level, core})$ is the high level energy of the simplified model of the molecule, $E(\text{low level, real})$ is the energy of the whole system using low level method and $E(\text{low level, core})$ is the energy of the simplified model calculated with the low level method. The high level calculations were performed with the B3PW91²⁵ functional associated with the BSI' basis set. BSI' is a combination of the 6-311G(d) for all atoms except the metal for which we used the Lanl2dz basis functions. The low level calculations on the whole molecules have been done at HF/Lanl2mb level. The Lanl2mb basis function incorporates the Hay and Wadt small-core relativistic effective core potential and minimal valence basis set for all atoms. In all studies, full geometry optimizations were carried out followed by vibrational frequency calculations. All transition state structures reported in this paper are characterized by only one imaginary frequency. The transition state structures were slightly distorted along the normal mode of the imaginary frequency and geometry minimizations using the transition structure force constants as the initial Hessian were performed in order to obtain the two minimum structures attached to it. All reasonable possible conformations were inspected for each species and the results for the most stable conformations are given. In both frameworks, the energies of all structures were improved by performing single point calculations with an extended basis set, B3PW91/BS2. The basis set BS2 consisted of 6-311+G(df,p) for all atoms except Rh which is calculated with the Lanl2dz basis set. All energies were corrected for zero point energies. All calculations were carried out with the Gaussian 03 program. All molecular drawings were produced with GaussView 3.09.²⁶

4.2 Preparation and Characterization

[RhCl(trop₂NH)(triphenylphosphine)] (K1)

MF = C₄₈H₃₈ClNPRh

MW = 798.14 g/mol



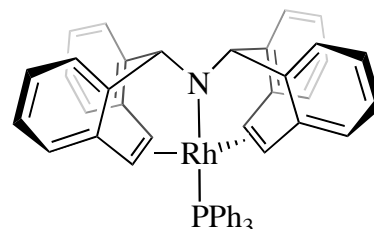
To a suspension of [Rh(μ -Cl)(trop₂NH)]₂ (500 mg, 0.467 mmol) in 40 mL of DCM a slight excess of PPh₃ (260 mg, 0.99 mmol) is added under aerobic condition. A bright yellow solution is immediately formed. The product was isolated as microcrystalline powder by addition of *n*-hexane in 90% yield.

The ¹H NMR and ³¹P NMR data are in agreement with those reported in the literature.

[Rh(trop₂N)(triphenylphosphine)] (K2)

MF = C₄₈H₃₇NPRh

MW = 761.69 g/mol



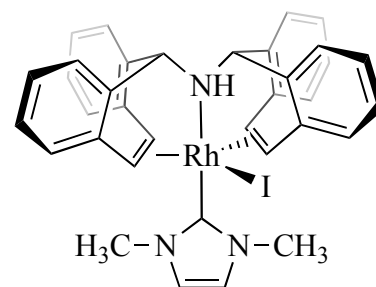
200 mg of [RhCl(trop₂NH)(PPh₃)] (K1) (80 mg, 0.262 mmol) were suspended in 50 ml dry THF and KO^tBu (30 mg, 0.267 mmol) was added. The solution turned immediately deep green and the mixture was almost homogeneous after 30 minutes. The KCl formed can be filtered off subsequently.

The ¹H NMR and ³¹P NMR data are in agreement with those reported in the literature.

[RhI(trop₂NH)(1,3-dimethylimidazolin-2-ylidene)] (K3)MF = C₃₅H₃₂IN₃Rh

MW = 724.45 g/mol

mp = 190°C decomposes



A solution of [Rh(trop₂N)(PPh₃)] was freshly prepared from [RhCl(trop₂NH)(PPh₃)] (80 mg, 0.10 mmol) and KO^tBu (17 mg, 0.15 mmol) in THF (1.5 mL). To this deep green solution 1,3-dimethylimidazolium iodide (34 mg, 0.15 mmol) was added. Within 15 minutes at RT the colour turned to brown and ³¹P-NMR showed complete conversion of [Rh(trop₂NH)(PPh₃)] (δ = 40.8 [d, ¹J_{RhP} = 124 Hz]) to free PPh₃ (δ = -5.8). Flash chromatography (silica, CH₂Cl₂/MeOH 96/4 → 92/8) gave [RhI(trop₂NH)(1,3-dimethylimidazolin-2-ylidene)], which was recrystallized from CH₂Cl₂/*n*-hexane. Yield 29 mg (40 %) as orange microcrystals. Single crystals suitable for X-ray structure analysis were grown by slowly diffusion of *n*-hexane into a saturated solution of [RhI(trop₂NH)(1,3-dimethylimidazolin-2-ylidene)] in CH₂Cl₂.

Rf (silica, CH₂Cl₂/MeOH 96/4): 0.39. m.p. 190°C dec.

¹H NMR (300.1 MHz, CDCl₃): δ = 4.28 (s, 3H, CH₃), 4.33 (s, 3H, CH₃), 4.65 (s, 1H, NH), 4.76 (s, 2H, CH benzyl), 4.92 (d, ³J_{HH} = 9.4 Hz, 2H, CH olefin), 5.11 (dd, ³J_{HH} = 9.4 Hz, ²J_{RhH} = 2.7 Hz, 2H, CH olefin), 6.83-6.93 (m, 6H, CH ar), 6.96 (d, ³J_{HH} = 2.0 Hz, 1H, CH imidazol), 7.01 (d, ³J_{HH} = 2.0 Hz, H, CH imidazol), 7.03-7.22 (m, 8H, CH ar), 7.32 (dd, ³J_{HH} = 7.3 Hz, ⁴J_{HH} = 0.9 Hz, 2H, CH ar).

¹³C{¹H} NMR (75.5 MHz, CDCl₃): δ = 40.4 (CH₃), 45.8 (CH₃), 69.9 (d, ¹J_{RhC} = 7.0 Hz, CH olefin), 70.4 (d, ¹J_{RhC} = 13.1 Hz, CH olefin), 72.5 (CH benzyl), 122.7 (CH imidazol), 124.1 (CH imidazol), 125.1 (CH ar), 125.8 (CH ar), 125.9 (CH ar), 127.2 (CH ar), 127.9 (CH ar), 128.1 (CH ar), 128.4 (CH ar), 130.0 (CH ar), 134.0 (C_{quart}), 134.4 (d, J_{RhC} = 1.2 Hz, C quart), 136.7 (d, J_{RhC} = 2.2 Hz, C_{quart}), 141.1 (C_{quart}), 168.1 (d, ¹J_{RhC} = 50.0 Hz, N₂C=Rh).

¹⁰³Rh NMR (15.8 MHz, CDCl₃): δ = 1547 (s).

ATR IR (neat, cm^{-1}): 3126 m, 3039 w, 1599 m, 1489 s, 1472 m, 1396 m, 1261 m, 1218 s, 1076 m, 983 m, 871m, 824 m, 749 s, 682s.

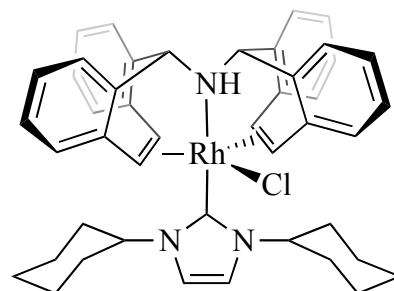
HRMS (MALDI, DCTB matrix): calcd for $[\text{C}_{35}\text{H}_{31}\text{N}_3\text{Rh}]^+$ m/z 596.1567; found 596.1558.

$[\text{RhCl}(\text{trop}_2\text{NH})(1,3\text{-dicyclohexylimidazolin-2-ylidene})]$ (K4)

MF = $\text{C}_{45}\text{H}_{48}\text{ClN}_3\text{Rh}$

MW = 769.24 g/mol

mp = 218°C decomposes



$[\text{RhCl}(\text{trop}_2\text{NH})(1,3\text{-dicyclohexylimidazolin-2-ylidene})]$ was prepared from $[\text{RhCl}(\text{trop}_2\text{NH})(\text{PPh}_3)]$ (80 mg, 0.10 mmol), $\text{KO}t\text{Bu}$ (17 mg, 0.15 mmol) and 1,3-dicyclohexylimidazolium chloride (32 mg, 0.12 mmol) as described above for $[\text{RhI}(\text{trop}_2\text{NH})(1,3\text{-dimethylimidazolin-2-ylidene})]$. Yield 49 mg (64%) as yellow microcrystals.

Rf (silica, $\text{CH}_2\text{Cl}_2/\text{MeOH}$ 96/4): 0.27. m.p. 218°C dec.

^1H NMR (300.1 MHz, CDCl_3): δ = 1.17 – 2.40 (m, 20 H, CH_2 , Cyc), 4.07 (s, 1H, NH), 4.42 (m, 1H, CH Cyc), 4.65 (m, 1H, CH Cyc), 4.86 (d, $^3J_{\text{HH}} = 8.7$ Hz, 2H, CH olefin), 5.92 (s, 2H, CH benzyl), 6.36 (dd, $^3J_{\text{HH}} = 8.7$ Hz, $^2J_{\text{RH}} = 2.5$ Hz, 2H, CH olefin), 6.91-7.43 (m, 18H, CH ar), 7.86 (d, $^3J_{\text{HH}} = 8.1$ Hz, 2H, CH imidazol).

$^{13}\text{C}\{^1\text{H}\}$ NMR (75.5 MHz, CDCl_3): δ = 25.1 (CH_2 Cyc), 25.4 (CH_2 Cyc), 26.0 (CH_2 Cyc), 35.2 (CH_2 Cyc), 35.8 (CH_2 Cyc), 58.4 (CH Cyc), 58.8 (CH Cyc), 71.0 (d, $^1J_{\text{RhC}} = 14.3$ Hz, CH olefin), 71.6 (CH benzyl), 71.9 (d, $^1J_{\text{RhC}} = 6.4$ Hz, CH olefin), 119.2 (CH imidazol), 119.6 (CH imidazol), 125.6 (CH ar), 125.7 (CH ar), 126.1 (CH ar), 127.5 (CH ar), 127.9 (CH ar), 128.1 (CH ar), 128.3 (CH ar), 129.9 (CH ar), 134.9 (C_{quart}), 135.0 (d, $J_{\text{RhC}} = 1.2$ Hz, C_{quart}), 137.0 (d, $J_{\text{RhC}} = 2.1$ Hz, C_{quart}), 139.9 (C_{quart}), 165.0 (d, $^1J_{\text{RhC}} = 49.3$, $\text{N}_2\text{C}=\text{Rh}$).

^{103}Rh NMR (15.8 MHz, CD_2Cl_2): δ = 1720 (s).

ATR IR (neat cm^{-1}): 3357 m br, 2927 s, 2854 m, 1624 m, 1490 m, 1447 m, 1421 w, 1350 w, 1235 m, 1194 m, 996 m, 748 vs, 695 s.

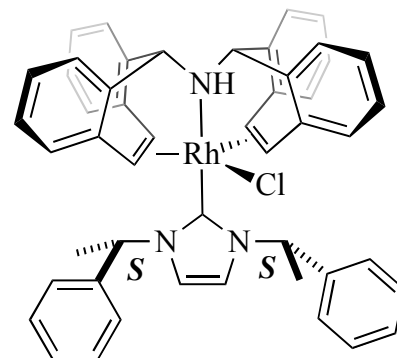
HRMS (MALDI, DCTB matrix): calcd. for $[\text{C}_{45}\text{H}_{47}\text{N}_3\text{Rh}]^+$ m/z 732.2819; found 732.2807.

**[RhCl(trop₂NH)(1,3-bis-((S)-1-phenyl-ethyl)imidazolin-2-ylidene)]
((S,S)-K5)**

MF = C₄₉H₄₄ClN₃Rh

MW = 813.25 g/mol

mp = 180°C decomposes



[RhCl(trop₂NH)(1,3-bis-(1-phenyl-ethyl)imidazolin-2-ylidene)] was prepared from [RhCl(trop₂NH)(PPh₃)] (80 mg, 0.10 mmol) and KO^tBu (17 mg, 0.15 mmol) and 1,3-bis-(1-phenyl-ethyl)imidazolium chloride (32 mg, 0.12 mmol) as described above for [RhI(trop₂NH)(1,3-dimethylimidazolin-2-ylidene)]. Yield 57 mg (70%) as yellow needle-shape crystals.

R_f (silica, CH₂Cl₂/MeOH 94/6): 0.21. m.p. 180°C dec.

¹H NMR (300.1 MHz, CDCl₃): δ = 1.93 (d, ³J_{HH} = 6.8 Hz, 3H, CH₃), 2.25 (d, ³J_{HH} = 6.8 Hz, 3H, CH₃), 4.73 (s, 1H, CH benzyl), 4.75 (s, 1H, CH benzyl), 4.88 (d, ³J_{HH} = 9.1 Hz, 1H, CH olefin), 4.98 (d, ³J_{HH} = 9.4 Hz, 1H, CH olefin), 5.02 (s, 1H, NH), 5.44 (dd, ³J_{HH} = 9.1 Hz, ²J_{RhH} = 2.1 Hz, 1H, CH olefin), 5.51 (dd, ³J_{HH} = 9.3 Hz, ²J_{RhH} = 2.1 Hz, 1H, CH olefin), 6.05 (d, ³J_{HH} = 7.3 Hz, 1H, CH ar), 6.57 (q, ³J_{HH} = 6.8 Hz, 1H, NCH(Ph)(CH₃)), 6.61 (dd, ³J_{HH} = 7.4 Hz, ⁴J_{HH} = 1.2 Hz, 1H, CH ar), 6.75 – 7.61 (m, 26H, CH ar and CH imidazol), 8.3 (q, ³J_{HH} = 6.9 Hz, 1H, NCH(Ph)(CH₃)).

¹³C{¹H} NMR (75.5 MHz, CDCl₃): δ = 22.9 (CH₃), 24.8 (CH₃), 57.8 (NCH(Ph)(CH₃)), 58.4 (NCH(Ph)(CH₃)), 67.5 (br, CH olefin), 69.5 (br, CH olefin), 72.2 (CH benzyl), 72.3 (CH benzyl), 120.5 (CH ar), 121.1 (CH ar), 125.1 (CH ar), 125.3 (CH ar), 125.7 (CH ar), 125.8 (CH ar), 127.2 (CH ar), 127.3 (CH ar), 127.1 (CH ar), 127.5 (CH ar), 127.9 (CH ar), 128.0 (CH ar), 128.3 (CH ar), 128.5 (CH ar), 128.6 (CH ar), 129.2 (CH ar), 129.4 (CH ar), 130.1 (CH ar), 134.2 (C quart), 134.7 (d, J_{RhC} = C quart), 134.9 (d, J_{RhC} = 0.9 Hz, C quart), 136.8 (d, J_{RhC} = 2.1 Hz, C quart), 137.3 (d, J_{RhC} = 1.8 Hz, C quart), 139.5 (C quart), 139.5 (C quart), 141.9 (C quart), 142.4 (C quart), 168.6 (d, 1J_{RhC} = 49.6 Hz, N₂C=Rh). Two of the olefinic resonances were not detected due to broadened lines.

^{103}Rh NMR (15.8 MHz, CD_2Cl_3): $\delta = 1744$ (s).

ATR IR (neat cm^{-1}): 3112 w, 2985 m, 1601 m, 1490 m, 1456 m, 1396 m, 1210 m, 1179 m, 1070m, 981 m, 825 m, 748 s, 691s.

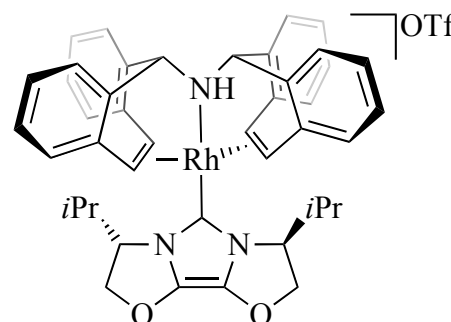
HRMS (MALDI, DCTB matrix): calcd. for $[\text{C}_{49}\text{H}_{43}\text{N}_3\text{Rh}]^+$ m/z 776.2506; found 776.2493.

[Rh(trop₂NH)((*S,S*)-ValinolCarben)]OTf ((*S,S*)-K6)

MF = $\text{C}_{47}\text{H}_{52}\text{F}_3\text{N}_3\text{O}_5\text{RhS}$

MW = 960.97 g/mol

mp = 250°C decomposes



$[\text{Rh}(\text{trop}_2\text{NH})(\text{ValinolCarben})]\text{OTf}$ was prepared from $[\text{Rh}(\text{Cl})(\text{trop}_2\text{NH})(\text{PPh}_3)]$ (80 mg, 0.10 mmol), $\text{KO}t\text{Bu}$ (17 mg, 0.15 mmol) and imidazolium triflate (50 mg, 0.13 mmol) as described above for $[\text{Rh}(\text{I})(\text{trop}_2\text{NH})(1,3\text{-dimethylimidazolin-2-ylidene})]$. Yield 58 mg (65%) as red microcrystals.

Rf (silica, $\text{CH}_2\text{Cl}_2/\text{MeOH}$ 94/6): 0.25. m.p. 250°C dec.

^1H NMR (500.2 MHz, CD_3CN): $\delta = 0.77$ (d, $^3J_{\text{HH}} = 6.8$ Hz, 3H, CH_3 *iPr*), 0.79 (d, $^3J_{\text{HH}} = 6.6$ Hz, 3H, CH_3 *iPr*), 1.13 (d, $^3J_{\text{HH}} = 6.6$ Hz, 3H, CH_3 *iPr*), 1.34 (d, $^3J_{\text{HH}} = 6.6$ Hz, 3H, CH_3 *iPr*) 2.19 (dh, $^3J_{\text{HH}} = 3.1$ Hz, $^3J_{\text{HH}} = 6.6$ Hz, 1H, CH *iPr*), 2.88 (h, $^3J_{\text{HH}} = 6.6$ Hz, 1H, CH *iPr*), 4.10 (s, 1H, NH), 4.71 (ddd, $^3J_{\text{HH}} = 7.7$ Hz, $^3J_{\text{HH}} = 3.3$ Hz, $^3J_{\text{HH}} = 3.1$ Hz, 1H, CH oxaz), 4.81 (dd, $^2J_{\text{HH}} = 9.2$ Hz, $^3J_{\text{HH}} = 3.7$ Hz, 1H, CH_2 oxaz), 4.99 – 5.06 (m, 4H, CH_2 and CH oxaz), 5.12 (s, 1H, CH benzyl), 5.16 (s, 1H, CH benzyl), 5.19 (d, $^3J_{\text{HH}} = 9.2$ Hz, 1H, CH olefin), 5.24 (d, $^3J_{\text{HH}} = 9.2$ Hz, 1H, CH olefin), 6.19 (dd, $^3J_{\text{HH}} = 9.2$ Hz, $^2J_{\text{RH}} = 2.9$ Hz, 1H, CH olefin), 6.50 (dd, $^3J_{\text{HH}} = 9.2$ Hz, $^2J_{\text{RH}} = 2.9$ Hz, 1H, CH olefin), 6.91 – 7.12 (m, 7H, CH ar), 7.17 (d, $^3J_{\text{HH}} = 7.3$ Hz, 1H, CH ar), 7.22 – 7.40 (m, 7H, CH ar), 7.52 (dd, $^3J_{\text{HH}} = 7.3$ Hz, $^4J_{\text{HH}} = 1.1$ Hz, 1H, CH ar).

$^{13}\text{C}\{^1\text{H}\}$ NMR (75.5 MHz, CD_3CN): $\delta = 14.1$ (CH_3 *iPr*), 16.4 (CH_3 *iPr*), 17.5 (CH_3 *iPr*), 18.5 (CH_3 *iPr*), 33.3 (CH *iPr*), 62.9 (CH oxaz), 63.3 (CH oxaz), 71.1 (CH_2 oxaz), 72.9 (d, $^1J_{\text{RhC}} = 8.2$ Hz, CH olefin), 75.0 (d, $^1J_{\text{RhC}} = 7.2$ Hz, CH olefin), 76.3 (CH benzyl), 77.1 (d, $^1J_{\text{RhC}} = 12.5$ Hz,

CH olefin), 77.3 (d, $^1J_{\text{RhC}} = 13.9$ Hz, CH olefin), 77.6 (CH benzyl), 126.6 (CH ar), 127.0 (CH ar), 127.1 (CH ar), 127.1 (CH ar), 127.5 (CH ar), 128.4 (CH ar), 128.4 (CH ar), 128.8 (CH ar), 128.9 (CH ar), 128.9 (CH ar), 129.0 (CH ar), 129.0 (CH ar), 129.1 (CH ar), 130.2 (CH ar), 130.6 (CH ar), 134.9 (CH ar), 135.2 (CH ar), 135.4 (CH ar), 135.6 (CH ar), 136.3 (C quart), 136.6 (C quart), 138.5 (C quart), 142.8 (C quart oxaz), 143.2 (C quart oxaz), $\text{N}_2\text{C}=\text{Rh}$ not detected.

^{19}F NMR (188.3 MHz, CD_3CN): $\delta = -79.3$ (s, SO_3CF_3^-).

^{103}Rh NMR (15.8 MHz, CD_3CN): $\delta = 1643$ (s).

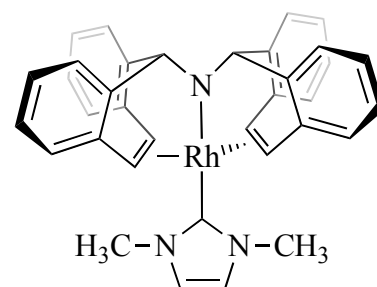
ATR IR (neat cm^{-1}): 3250 w, 2957 m, 1756 s, 1481 m, 1427 m, 1376 w, 1271 s, 1254 s, 1225 m, 1133 m, 1028 s, 930 m, 743 s, 637 s.

HRMS (MALDI, DCTB matrix): calcd. for $[\text{C}_{43}\text{H}_{43}\text{N}_3\text{O}_2\text{Rh}]^+$ m/z 736.2405; found 736.2392.

[Rh(trop₂N)(1,3-dimethylimidazolin-2-ylidene)] (K7)

MF = $\text{C}_{35}\text{H}_{31}\text{N}_3\text{Rh}$

MW = 596.55 g/mol



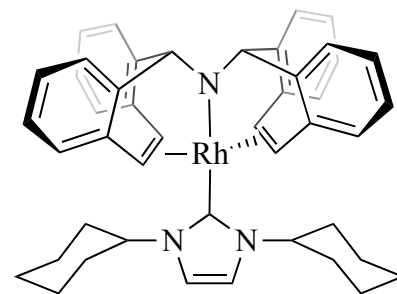
To a solution of [RhI(trop₂NH)(1,3-dimethylimidazolin-2-ylidene)] (**K3**) (30 mg, 0.041 mmol) in $[\text{D}_8]$ THF (0.45 mL) KOtBu (4.9 mg, 0.043 mmol, 1.05 eq) was added at RT. A dark green solution was formed immediately and the product was characterized by ^1H and ^{13}C NMR. Quantitative yield by NMR.

^1H NMR (300.1 MHz, $[\text{D}_8]$ THF): $\delta = 3.85$ (s, 6H, CH_3), 4.73 (s, 2H, CH benzyl), 5.42 (br s, 4H, CH olefin), 6.79 (m, 8H, CH ar), 7.02 (m, 8H, CH ar), 7.15 (s, 2H, CH imidazol).

$^{13}\text{C}\{^1\text{H}\}$ NMR (75.5 MHz, $[\text{D}_8]$ THF): $\delta = 33.46$ (s, CH_3), 1.56 (s, CH benzylic), 78.17 (d, $^1J_{\text{RhC}} = 12$ Hz, CH olefin), 121.65 (s, CH imidazol), 124.09 (CH ar), 124.76 (CH ar), 125.52 (CH ar), 127.03 (CH ar), 137.81 (C quart), 145.69 (C quart), 183.9 (d, $^1J_{\text{RhC}} = 42.7$ Hz, $\text{N}_2\text{C}=\text{Rh}$).

[Rh(trop₂N)(1,3-dicyclohexylimidazolin-2-ylidene)] (K8)MF = C₄₅H₄₇N₃Rh

MW = 732.78 g/mol



To a solution of [RhCl(trop₂NH)(1,3-dicyclohexylimidazolin-2-ylidene)] (**K4**) (30 mg, 0.039 mmol) in [D₈] THF (0.45 mL) KOtBu (4.6 mg, 0.041 mmol, 1.05 eq) was added at RT. A dark green solution was formed immediately and the product was characterized by ¹H and ¹³C NMR. Quantitative yield by NMR.

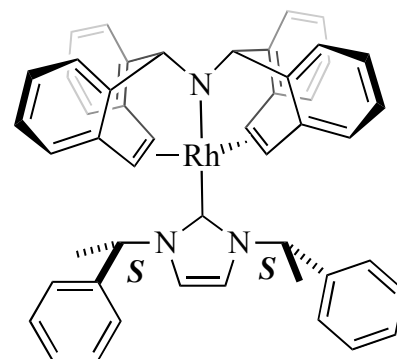
¹H NMR (300.1 MHz, [D₈] THF): δ = 1.26 – 2.14 (m, 20H, CH₂ Cyc), 4.44 (m, 2H, CH Cyc), 4.68 (s, 2H, CH benzylic), 5.34 (br s, 2H, CH olefin), 6.67 (m, 8H, CH ar), 7.02 (m, 8H, CH ar), 7.26 (s, 2H, CH imidazol).

¹³C{¹H} NMR (75.5 MHz, CDCl₃): δ = ¹³C{¹H} NMR (75.5 MHz, [D₈] THF): δ = 25.44 (CH₂ Cyc), 30.75 (CH₂ Cyc), 34.62 (CH₂ Cyc), 59.59 (CH Cyc), 77.21 (br s, CH olefin), 81.35 (br s, CH benzylic), 117.41 (s, CH imidazol), 124.31 (CH ar), 124.99 (CH ar), 125.42 (CH ar), 127.17 (CH ar), 137.58 (C quart), 145.52 (C quart), N₂C=Rh not detected.

[Rh(trop₂N)(1,3-bis-(1-phenyl-ethyl)imidazolin-2-ylidene)] ((*S,S*)-K9)

MF = C₄₉H₄₃N₃Rh

MW = 776.79 g/mol



To a solution of [RhCl(trop₂NH)(1,3-bis-(1-phenyl-ethyl)imidazolin-2-ylidene)] ((*S,S*)-K5) (30 mg, 0.037 mmol) in [D₈] THF (0.45 mL) KOtBu (4.3 mg, 0.039 mmol, 1.05 eq) was added at RT. A dark green solution was form immediately and the product was characterized by ¹H and ¹³C NMR. Quantitative yield by NMR.

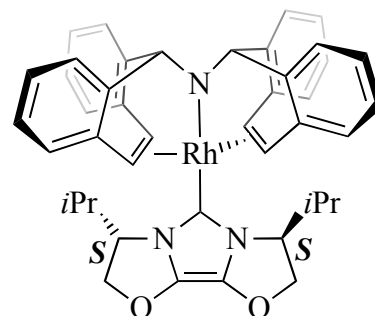
¹H NMR (300.1 MHz, [D₈] THF): δ = 1.99 (d, ³J_{HH} = 6.4 Hz, 6H, CH₃), 4.71 (s, 2H, CH benzyl), 5.83 (br d, ³J_{HH} = 7.8 Hz, 2H, CH olefin), 5.52 (br d, ³J_{HH}=7.8 Hz, 2H, CH olefin), 6.12 (br q, ³J_{HH}= 6.4 Hz, 1H, NCH(Ph)(CH₃)), 6.54 - 7.42 (m, 28H, CH ar and CH imidazol).

¹³C{¹H} NMR (75.5 MHz, [D₈] THF): δ = 22.0 (CH₃), 58.9 (NCH(Ph)(CH₃)), 77.8 (d, ¹J_{RhC} = 13.1 Hz, CH olefin), 77.9 (d, ¹J_{RhC} = 13.1 Hz, CH olefin), 81.5 (CH benzyl), 118.9 (CH imidazol), 124.4 (CH ar), 124.5 (CH ar), 124.8 (CH ar), 125.0 (CH ar), 125.6 (CH ar), 125.8 (CH ar), 126.4 (CH ar), 126.8 (CH ar), 127.1 (CH ar), 127.4 (CH ar), 127.6 (CH ar), 128.5 (CH ar), 137.2 (d, J_{RhC} = 0.9 Hz, C quart), 137.5 (d, J_{RhC} = 1.5 Hz, C quart), 142.1 (C quart), 145.4 (C quart), 145.5 (C quart), 183.9 (d, ¹J_{RhC} = 43.3 Hz, N₂C=Rh).

[Rh(trop₂N)((*S,S*)-ValinolCarbene)] ((*S,S*)-K10)

MF = C₄₃H₄₃N₃O₂Rh

MW = 736.73 g/mol



To a solution of [Rh(trop₂NH)(ValinolCarben)]OTf ((*S,S*)-K6) (30 mg, 0.031 mmol) in [D₈] THF (0.45 mL) KOtBu (3.7 mg, 0.033 mmol, 1.05 eq) was added at RT. A dark green solution was form immediately and the product was characterized by ¹H and ¹³C NMR. Quantitative yield by NMR.

¹H NMR (700.1 MHz, [D₈] THF, 220K): δ = 0.55 (d, ³J_{HH} = 6.6 Hz, 3H, CH₃ iPr), 0.60 (d, ³J_{HH} = 6.6 Hz, 3H, CH₃ iPr), 2.14 (m, 1H, CH iPr), 1.01 (d, ³J_{HH} = 6.3 Hz, 3H, CH₃ iPr), 1.30 (d, ³J_{HH} = 6.3 Hz, 3H, CH₃ iPr), 2.93 (m, 1H, CH iPr), 4.65 (s, 2H, CH bezylic), 4.74 – 5.06 (CH oxazolin, CH₂ oxazolin), 5.07 (d, ³J_{HH} = 9 Hz, 1H, CH olefin), 5.13 (d, ³J_{HH} = 8.4 Hz, 1H, CH olefin), 5.84 (d, ³J_{HH} = 9 Hz, 1H, CH olefin), 6.31 (d, ³J_{HH} = 8.4 Hz, 1H, CH olefin), 6.59 (q, 1H, J_{HH} = 7.5, CH ar), 6.66 (t, 1H, J_{HH} = 7.4, CH ar), 6.72 (t, 1H, J_{HH} = 7.3, CH ar), 6.81 (d, 1H, J_{HH} = 7.3, CH ar), 6.85 (d, 1H, J_{HH} = 7.3, CH ar), 6.89 (d, 1H, J_{HH} = 7.2, CH ar), 6.92 (d, 1H, J_{HH} = 7.3, CH ar), 6.97 (m, 2H, CH ar), 6.99 (t, 1H, J_{HH} = 7.2, CH ar), 7.04 (t, 1H, J_{HH} = 7.5, CH ar), 7.14 (m, 4H, CH ar), 7.44 (d, 1H, J_{HH} = 7.5, CH ar).

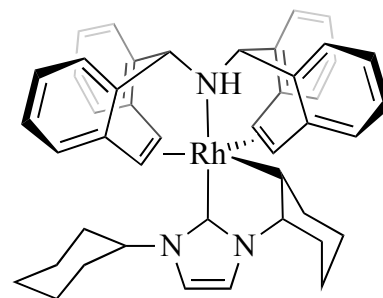
¹³C{¹H} NMR (176.1 MHz, [D₈] THF, 220K): δ = 13.2 (s, CH₃ iPr), 14.9 (s, CH₃ iPr), 17.4 (s, CH₃ iPr), 18.0 (s, CH₃ iPr), 30.7 (s, CH iPr), 31.9 (s, CH iPr), 60.4 (s, CH oxazolin), 61.3 (s, CH oxazolin), 72.9 (d, ¹J_{RhC} = 6.2 Hz, CH olefin), 74.4 (d, ¹J_{RhC} = 6.8 Hz, CH olefin), 75.5 (s, CH₂ oxazolin), 76.6 (s, CH₂ oxazolin), 78.6 (d, ¹J_{RhC} = 15.9 Hz, CH olefin), 79.1 (d, ¹J_{RhC} = 16.6 Hz, CH olefin), 80.8 (s, CH benzyl), 80.9 (s, CH benzyl), 124.6 (CH ar), 124.9 (CH ar), 125.0 (CH ar), 125.05 (CH ar), 125.1 (CH ar), 125.27 (CH ar), 125.31 (CH ar), 125.5 (CH ar), 125.9 (CH ar), 126.5 (CH ar), 126.63 (CH ar), 126.66 (CH ar), 127.5 (CH ar), 127.9 (CH ar), 128.1 (CH ar), 128.2 (CH ar), 136.9 (C quart), 137.1 (C quart), 137.9 (C quart), 138.6 (C quart), 143.2 (C quart), 143.7 (C quart), 146.1 (C quart), 146.5 (C quart), 160.6 (d, ¹J_{RhC} = 44 Hz, N₂C=Rh).

[Rh(trop₂NH)(1,3-dicyclohexylimidazolin-2-ylidene)] CHactivated (K11)

MF = C₄₅H₄₇N₃Rh

MW = 732.78 g/mol

mp = 220 °C decomposes



To a solution of [RhCl(trop₂NH)(1,3-dicyclohexylimidazolin-2-ylidene)] **K4** (100 mg, 0.13 mmol) in THF (2 mL) KOtBu (15 mg, 0.14 mmol, 1.05 eq) was added at RT. The deep green solution was stirred for one hour and subsequently heated at 70°C for 3 days. The solution's color changed from green to dark yellow. After filtration of the KCl formed, the solvent was narrowed and *n*-hexane was added. The product was obtained as a yellow powder (yield 78%). Suitable crystals for X-ray diffraction were obtained from slow diffusion of *n*-hexane in a THF solution of the product.

¹H NMR (700.1 MHz, [D₈] THF, 298K): δ = 0.10 (br d, 10 H, CH₂, activated Cyc), 0.25 (dq, 1H, J_{HH} = 2.9 Hz, ³J_{HH} = 11.7 Hz), 1.27 – 2.09 (m, 3H, CH₂ Cyc and NH), 2.24 (br t, 1H, ³J_{HH} = 11.7 Hz, CH activated Cyc), 2.45 (br d, 1H, ³J_{HH} = 11.7 Hz, CH₂ activated Cyc), 3.20 (d, 1H, ¹J_{HH} = 9.1 Hz, CH olefin), 3.56 (d, 1H, ¹J_{HH} = 9.6 Hz, CH olefin), 3.79 (d, 1H, ¹J_{HH} = 9.6 Hz, CH olefin), 3.94 (dt, 1H, J = 2.7 J = 11.7 Hz, CH activated Cyc), 4.29 (d, 1H, ¹J_{HH} = 9.1 Hz, CH olefin), 4.31 (s, 1H, CH benzylic), 4.39 (s, 1H, CH benzylic), 4.65 (m, 1H, CH Cyc), 6.54 (d, 1H, J_{HH} = 7.5, CH ar), 6.59 (m, 1H, CH ar), 6.67 (m, 2H, CH ar), 6.72 (m, 3H, CH ar), 6.83 (t, 1H, J_{HH} = 7.5, CH ar), 6.98 (br d, 2H, J_{HH} = 6.9, CH ar), 7.04 (m, 3H, CH ar), 7.12 (br d, 1H, J_{HH} = 1.9, CH ar), 7.14 (br d, 1H, J_{HH} = 7.2, CH ar), 7.22 (d, 1H, J_{HH} = 7.7, CH ar).

¹³C{¹H} NMR (176.1 MHz, [D₈] THF, 298K): δ = 25.3 (s, CH Cyc), 25.7 (s, CH Cyc), 26.0 (s, CH Cyc), 26.2 (s, CH Cyc), 29.3 (s, CH Cyc), 30.2 (s, CH Cyc), 33.4 (s, CH Cyc), 34.4 (s, CH Cyc), 35.1 (d, ¹J_{RhC} = 20 Hz, CH activated Cyc), 35.3 (s, CH Cyc), 51.7 (d, ¹J_{RhC} = 8.7 Hz, CH olefin), 54.7 (d, ¹J_{RhC} = 8.4 Hz, CH olefin), 56.4 (d, ¹J_{RhC} = 10 Hz, CH olefin), 57.9 (s, CH activated Cyc), 61.9 (d, ¹J_{RhC} = 8 Hz, CH olefin), 68.2 (s, CH Cyc), 72.3 (s, CH benzyl), 72.4 (s, CH benzyl), 116.1 (s, CH imidazolin), 116.5 (s, CH imidazolin), 119.6 (CH ar), 120.4 (CH ar), 122.6 (CH ar), 122.7 (CH ar), 126.0 (CH ar), 126.4 (CH ar), 126.6 (CH ar), 126.7 (CH ar), 126.9 (CH ar), 127.1 (CH ar), 127.3 (CH ar), 127.4 (CH ar), 127.8 (CH ar), 128.1 (CH ar), 129.3 (CH ar),

4 Experimental Section

129.7 (CH ar), 131.2 (C quart), 131.4 (C quart), 131.8 (C quart), 136.7 (C quart), 136.8 (C quart), 138.8 (C quart), 142.6 (C quart), 144.0 (C quart).

^{103}Rh NMR (22.1 MHz, $[\text{D}_8]$ THF, 298K): $\delta = 539$ (s). Relative to $\text{Rh}(\text{acac})_3$ $\Xi = 3.16$ MHz.

ATR IR (neat cm^{-1}): 3259.74 w, 2922.28 m, 2851.53 m, 2360.69 m, 2342.88 w, 1644.02 m, 1622.77 m, 1597.19 m, 1486.31 m, 1463.22 m, 1427.00 m, 1395.63 s, 1360.76 m, 1257.46 s, 1156.85 w, 1012.47 m, 993.07 w, 968.12 w, 932.20 w, 895.52 w, 876.23 w, 836.18 w, 800.15 m, 744.10 s, 689.99 s, 668.15 w, 645.77 w.

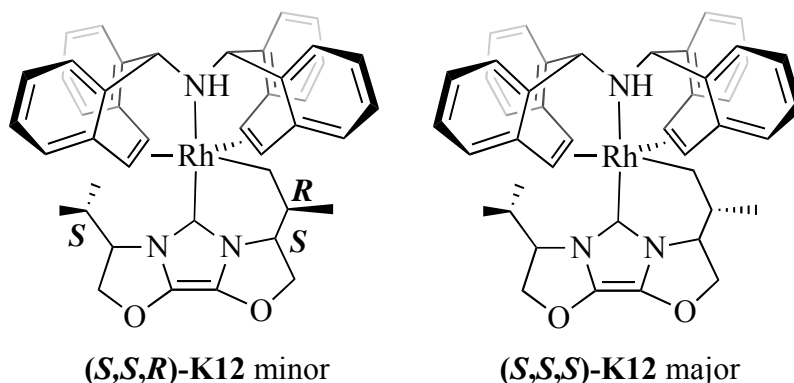
HRMS (MALDI, DCTB matrix): calcd. for $[\text{C}_{45}\text{H}_{47}\text{N}_3\text{Rh}]^+$ m/z 732.2819; found 733.2852 (100 %), 733.2852 (50.05 %), 734.2885 (12.26 %), 735.2918 (1.96 %), 736.2950 (0.23 %).

[Rh(trop₂NH)(ValinolCarben)] CHactivated (K12)

MF = C₄₃H₄₃N₃O₂Rh

MW = 736.73 g/mol

mp > 220 °C decomposes



To a solution of [Rh(trop₂NH)(ValinolCarben)]OTf ((S,S)-K6) (100 mg, 0.10 mmol) in THF (2 mL) KOtBu (12.3 mg, 0.11 mmol, 1.05 eq) was added at RT. The deep green solution was stirred for one hour and subsequently heated at 70°C for 3 days. The dark yellow solution was filtered and subsequently reduced in volume; *n*-hexane was added. The product was obtained as a yellow powder (yield 68%).

(S,S,R)-K12minor

¹H NMR (700.1 MHz, [D₈] THF, 298K): δ = 0.23 (br d, J_{HH} = 7.9 Hz, 1H, CH₂-Rh activated iPr), 0.51 (d, J_{HH} = 6.6 Hz, 3H, CH₃ activated iPr), 0.95 (d, ³J_{HH} = 6.8 Hz, 3H, CH₃ iPr), 1.08 (m, 1H, CH₂-Rh activated iPr), 1.25 (d, ³J_{HH} = 6.2 Hz, 3H, CH₃ iPr), 2.14 (m, 1H, CHCH₃ activated iPr), 3.1 (d sept, 1H, J_{HH} = 3.3 Hz, J_{HH} = 7.1 Hz, CH iPr), 3.89 (d, J_{HH} = 9.2 Hz, 1H, CH olefin), 3.75 (d, J_{HH} = 9.2 Hz, 1H, CH olefin), 4.26 (d, J_{HH} = 9.5 Hz, 1H, CH olefin), 4.27 (s, 1H, CH benzylic), 4.31 (s, 1H, CH benzylic), 4.37 (d, J_{HH} = 9.5 Hz, 1H, CH olefin), 4.54 (m, J_{HH} = 6.6 Hz, J_{HH} = 2.7 Hz, 1H, CH activated oxazolin), 4.67 (m, 2H, CH oxazolin and activated oxazolin), 4.73 (m, 2H, CH₂ oxazolin), 5.04 (1H, CH₂ activated oxazolin), 6.5 – 7.4 CH ar.

¹³C{¹H} NMR (176.1 MHz, [D₈] THF, 298K): δ = 12.6 (CH₃ activated iPr), 13.19 (s, CH₃ iPr), 17.86 (s, CH₃ iPr), 22.9 (d, ¹J_{RhC} = 28.7 Hz, CH₂-Rh activated iPr), 29.5 (s, CH iPr), 34.8 (CHCH₃ activated iPr), 51.56 (d, ¹J_{RhC} = 8.5 Hz, CH olefin), 55.14 (d, ¹J_{RhC} = 8.6 Hz, CH olefin), 51.73 (d, ¹J_{RhC} = 8.3 Hz, CH olefin), 59.73 (d, ¹J_{RhC} = 8.3 Hz, CH olefin), 61.25 (CH oxazolin), 62.4 (CH activated oxazolin), 72.03 (CH benzylic), 72.09 (CH benzylic), 74.87 (CH₂ oxazolin), 78.7 (CH₂ activated oxazolin), 120.3 (CH ar), 120.66 (CH ar), 122.36 (CH ar), 122.85 (CH ar), 24.18 (CH ar), 126.0 (CH ar), 126.17 (CH ar), 126.75 (CH ar), 126.85 (CH ar), 127.15 (CH ar), 127.35

(CH ar), 127.66 (CH ar), 128.17 (CH ar), 128.56 (CH ar), 128.87 (CH ar), 129.79 (CH ar), 132.13 (C quart), 132.58 (C quart), 136.09 (C quart), 136.55 (C quart), 138.81 (C quart), 139.36 (C quart), 143.81 (C quart), 143.83 (C quart), 153.5 (d, $^1J_{\text{RhC}} = 50$ Hz, $\text{N}_2\text{C}=\text{Rh}$).

^{103}Rh NMR (22.1 MHz, $[\text{D}_8]$ THF, 298K): $\delta = 520$ (s). Relative to $\text{Rh}(\text{acac})_3$ $\Xi = 3.16$ MHz.

(S,S,S)-K12major

^1H NMR (700.1 MHz, $[\text{D}_8]$ THF, 298K): $\delta = 0.52$ (m, 1H, CH_2 -Rh activated iPr), 0.87 (d, $J_{\text{HH}} = 6.3$ Hz, 3H, CH_3 activated iPr), 0.98 (d, $^3J_{\text{HH}} = 6.78$ Hz, 3H, CH_3 iPr), 0.62 (m, $J_{\text{HH}} = 2.6$ Hz, $J_{\text{HH}} = 8.7$ Hz, 1H, CH_2 -Rh activated iPr), 1.23 (d, $^3J_{\text{HH}} = 7.3$ Hz, 3H, CH_3 iPr), 1.50 (m, 1H, CHCH_3 activated iPr), 3.17 (d sept, $J_{\text{HH}} = 3.1$ Hz, $J_{\text{HH}} = 6.9$ Hz, 1H, CH iPr), 3.84 (d, $J_{\text{HH}} = 9.4$ Hz, 1H, CH olefin), 3.78 (d, $J_{\text{HH}} = 9.4$ Hz, 1H, CH olefin), 4.09 (d, $J_{\text{HH}} = \text{n.o.}$ Hz, 1H, CH olefin), 4.29 (s, 2H, CH benzylic), 4.31 (d, $J_{\text{HH}} = \text{n.o.}$ Hz, 1H, CH olefin), 4.09 (1H, CH activated oxazolin), 4.69 (m, 1H, CH oxazolin), 4.43 (1H, CH_2 activated oxazolin), 4.8 (m, 2H, CH_2 oxazolin), 5.05 (1H, CH_2 activated oxazolin), 6.5 – 7.4 CH ar.

$^{13}\text{C}\{^1\text{H}\}$ NMR (176.1 MHz, $[\text{D}_8]$ THF, 298K): $\delta = 20.8$ (CH_3 activated iPr), 13.34 (s, CH_3 iPr), 18.13 (s, CH_3 iPr), 24.9 (d, $^1J_{\text{RhC}} = 28.4$ Hz, CH_2 -Rh activated iPr), 28.92 (s, CH iPr), 40.9 (CHCH_3 activated iPr), 51.39 (d, $^1J_{\text{RhC}} = 7.9$ Hz, CH olefin), 51.56 (d, $^1J_{\text{RhC}} = 8.6$ Hz, CH olefin), 54.91 (d, $^1J_{\text{RhC}} = 8.6$ Hz, CH olefin), 59.43 (d, $^1J_{\text{RhC}} = 9.2$ Hz, CH olefin), 63.8 (CH activated oxazolin), 71.5 (CH oxazolin), 72.02 (CH benzylic), 72.09 (CH benzylic), 74.99 (CH_2 oxazolin), 82.1 (CH_2 activated oxazolin), 120.02 (CH ar), 120.32 (CH ar), 122.49 (CH ar), 122.83 (CH ar), 125.87 (CH ar), 126.63 (CH ar), 126.74 (CH ar), 126.89 (CH ar), 127.13 (CH ar), 127.31 (CH ar), 127.64 (CH ar), 127.74 (CH ar), 128.14 (CH ar), 128.66 (CH ar), 129.04 (CH ar), 129.74 (CH ar), 131.94 (C quart), 132.36 (C quart), 136.09 (C quart), 136.25 (C quart), 139.0 (C quart), 139.34 (C quart), 143.79 (C quart), 144.06 (C quart), 152.41 (d, $^1J_{\text{RhC}} = 50.6$ Hz, $\text{N}_2\text{C}=\text{Rh}$).

^{103}Rh NMR (22.1 MHz, $[\text{D}_8]$ THF, 298K): $\delta = 543$ (s). Relative to $\text{Rh}(\text{acac})_3$ $\Xi = 3.16$ MHz.

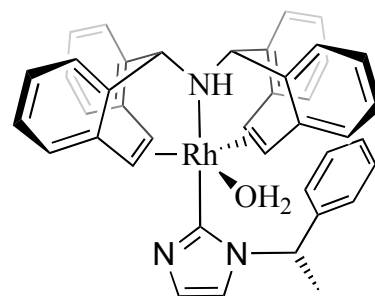
ATR IR (neat cm^{-1}): 2924.12 w, 2349.04 w, 1758.89 w, 1658.77 w, 1597.65 m, 1487.15 m, 1464.76 m, 1420.81 m, 1391.09 w, 1372.21 w, 1252.82 w, 1221.79 w, 1193.20 w, 1158.25 w, 1120.60 w, 1045.55 w, 977.84 w, 918.79 w, 879.04 w, 848.89 w, 820.57 w, 801.14 w, 745.79 s, 696.65 w, 637.16 w.

[Rh(trop₂NH)(1-(1-phenyl-ethyl)imidazolin-2-ylidene)] ((S)-K13)

MF = C₄₁H₃₆N₃ORh

MW = 689.65 g/mol

mp = 200 °C decomposes



To a solution of [Rh(Cl)(trop₂NH)(1,3-bis-(1-phenyl-ethyl)imidazolin-2-ylidene)] ((S,S)-K5) (80 mg, 0.098 mmol) in THF (1.5 mL) KOtBu (11.6 mg, 0.10 mmol, 1.05 eq) was added. The color of the solution became immediately green upon addition of the base. The reaction mixture was stirred at RT for 2 days. The salt formed was filtrated off and the product was dried under high vacuum (yield of 80%).

¹H NMR (700 MHz, [D₈] THF): δ = 0.63 (br s, NH), 1.59 (d, ³J_{HH} = 6.7 Hz, 3H CH₃), 3.17 (br s, 2H, H₂O), 4.04 (d, ³J_{HH} = 9.2 Hz, 1H, CH olefin), 4.07 (s, 1H, CH benzyl), 4.52 (d, ³J_{HH} = 9.3 Hz, 1H, CH olefin), 4.69 (s, 1H, CH benzyl), 5.15 (q, ³J_{HH} = 6.7 Hz, 1H, NCH(Ph)(CH₃)), 5.84 (t, ³J_{HH} = 1.37 Hz, 2H, NCH(Ph)(CH₃) (meta)), 5.93 (dd, ³J_{HH} = 9.31, ²J_{RhH} = 3.2, 1H, CH olefin), 6.56 (t, ³J_{HH} = 7.17, 2H, NCH(Ph)(CH₃) (para)), 6.59 (m, 1H, CH ar), 6.68-6.78 (m, 3 H, CH ar), 6.89 (d, ³J_{HH} = 9.2, 1H, CH olefin), 7.01 (d, ³J_{HH} = 1.4, 1H, CH imidazol), 7.02-7.04 (m, 1H, CH ar), 7.07 (d, ³J_{HH} = 1.4, 1H, CH imidazol), 7.08-7.11 (m, 3H, CH ar), 7.16 (d, ³J_{HH} = 1.37, 2H, NCH(Ph)(CH₃) (orto)), 7.19-7.26 (m, 3H, CH ar), 7.31-7.37 (m, 3H, CH ar), 7.40-7.45 (m, 2H, CH ar).

¹³C{¹H} NMR (75.5 MHz, [D₈] THF): δ = 24.3 (NCH(Ph)(CH₃)), 56.6 (NCH(Ph)(CH₃)), 67.2 (CH olefin), 70.4 (CH olefin), 70.5 (CH benzylic), 71.2 (CH benzylic), 73.6 (d, ¹J_{CRh} = 15.9 Hz, CH olefin), 79.8 (d, ¹J_{CRh} = 14.1 Hz, CH olefin), 116.8 (s, CH imidazol), 121.4 (s, NCH(Ph)(CH₃) (meta)), 124.4 (CH ar), 124.5 (CH ar), 125.0 (CH ar), 125.1 (CH ar), 125.9 (CH ar para), 126.9 (CH ar), 127.1 (CH ar), 127.4 (CH ar), 127.5 (CH ar), 127.6 (CH ar), 127.7 (CH ar), 127.8 (CH ar), 128.2 (CH ar), 128.2 (CH ar), 128.5 (CH ar), 128.5 (CH imidazol), 128.7 (CH ar meta), 129.2 (CH ar), 129.7 (CH ar), 134.7 (C quart), 134.9 (C quart), 136.05 (C quart), 137.6 (C quart), 136.9 (C quart), 137.1 (C quart), 137.4 (d, J = 2.5 Hz, C quart), 137.6 (d, J = 2.3 Hz, C quart), 140.6 (C quart), 141.7 (C quart), 157.6 (d, J_{RhC} = 38.8 Hz, C quart, Rh=C).

^{103}Rh NMR (15.8 MHz, CDCl_3): $\delta = -7083$ (s). Relative to $\text{Rh}(\text{acac})_3$ $\Xi = 3.16$ MHz.

ATR IR (neat cm^{-1}): 3022.67 w, 2922.51 w, 2851.07 w, 2117.96 w, 1655.16 w, 1598.49 m, 1488.34 m, 1467.41 w, 1407.44 w, 1379.10 w, 1260.27 m, 1221.97 w, 1192.22 w, 1091.71 m, 1020.45 m, 975.92 w, 937.20 w, 869.14 w, 799.78 m, 746.15 s, 696.27 s.

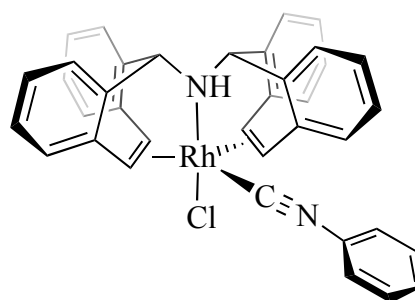
HRMS (MALDI, DCTB matrix): calcd. for $[\text{C}_{41}\text{H}_{35}\text{N}_3\text{Rh}]^+$ m/z 672.1886; found 672.1881 (100%), 673.1913 (45.56 %), 674.1946 (10.14 %), 675.1978 (1.47 %), 676.2011 (0.16 %).

[RhCl(trop₂NH)(CNC₆H₅)] (K14)

MF = $\text{C}_{37}\text{H}_{28}\text{ClN}_2\text{Rh}$

MW = 638.99 g/mol

mp > 220°C



$[\text{Rh}_2(\mu\text{-Cl})_2(\text{trop}_2\text{NH})_2]$ (100 mg, 0.093 mmol) are suspended in of CH_2Cl_2 (15 mL). Upon addition of phenylisocyanide (20 mg) the orange suspension turns into a yellow-brown solution. All volatile components are evaporated and the crude product is washed with Et_2O (3x 10 mL). The product is recrystallized from THF/hexane. Yield 82 mg (66%). Yellow crystals for X-ray structural analysis were grown from a concentrated solution of THF/hexane 1:3.

^1H NMR (300.1 MHz, CDCl_3): $\delta = 3.22$ (s, 1H, NH), 4.41 (s, 2H, CH benzylic), 5.35 (d, $^3J_{\text{HH}} = 9.3$ Hz, 2H, CH olefin), 5.58 (d, $^3J_{\text{HH}} = 9.3$ Hz, 2H, CH olefin), 6.74 (m, 2H, CH ar), 6.88 (m, 4H, CH ar), 6.98 (m, 2H, CH ar), 7.06 (m, 4H, CH ar), 7.13 (m, 3H, CH ar), 7.26 (m, 4H, CH ar), 7.70 (d, $^3J_{\text{HH}} = 7.7$ Hz, 2H, CH ar).

$^{13}\text{C}\{^1\text{H}\}$ NMR (75.5 MHz, CDCl_3): $\delta = 67.02$ (d, $^1J_{\text{RhC}} = 7.5$ Hz, CH olefin), 78.46 (d, $^1J_{\text{RhC}} = 9.06$ Hz, CH olefin), 72.82 (s, CH benzyl), 124.31 (CH ar), 124.61 (s, 2C, CH ar), 125.01 (CH ar), 126.71 (CH ar), 126.75 (CH ar), 127.65 (CH ar), 128.16 (CH ar), 128.77 (CH ar), 128.99 (CH ar), 129.17 (br s, CH ar), 129.49 (CH ar), 131.54 (C quart), 135.13 (C quart), 135.72 (C quart), 141.90 (C quart).

^{103}Rh NMR (12.7 MHz, CDCl_3): $\delta = 1005$ (s).

ATR IR (neat in cm^{-1}): 3235 w, 3009 w, 2131 s, 1600 w, 1481 w, 747 w, 726 w.

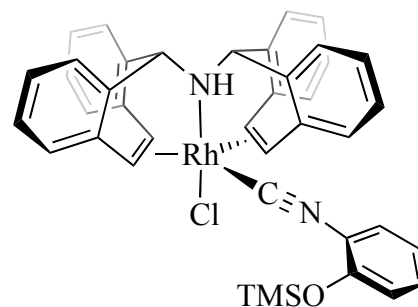
HRMS (MALDI, DCTB matrix): calcd. for $[\text{C}_{37}\text{H}_{28}\text{N}_2\text{Rh}]^+$ m/z 603.13; found 603.1291. Fragment intensity in %: 603.13 ($[\text{M}^+]$, 100), 604.13 ($[\text{M}^+] + 1$, 40.83), 605.13 ($[\text{M}^+] + 2$, 8.12), 606.14 ($[\text{M}^+] + 3$, 1.05).

$[\text{RhCl}(\text{trop}_2\text{NH})(\text{CNC}_6\text{H}_4\text{OSi}(\text{CH}_3)_3)]$ (K15)

MF = $\text{C}_{40}\text{H}_{36}\text{ClN}_2\text{ORhSi}$

MW = 727.17 g/mol

mp > 220°C



$[\text{Rh}_2(\mu\text{-Cl})_2(\text{trop}_2\text{NH})_2]$ (200 mg, 0.187 mmol) are suspended in of CH_2Cl_2 (50 mL). Upon addition of an excess of 2-(trimethylsilyloxy)phenyl isocyanide **63** (89 mg, 2.5 eq) the orange suspension turns into a clear yellow solution. The solvent's volume is narrowed to 5 ml and layered with *n*-hexane. The product was isolated as a bright yellow powder in 80% yield (217 mg).

^1H NMR (300.1 MHz, CDCl_3): δ = 0.28 (s, 9H, $-\text{OSi}(\text{CH}_3)_3$), 3.24 (s, 1H, NH), 4.40 (s, 2H, CH benzylic), 5.35 (d, $^3J_{\text{HH}} = 12$ Hz, 2H, CH olefin), 5.58 (d, $^3J_{\text{HH}} = 9$ Hz, 2H, CH olefin), 6.71-6.92 (m, 8 H, CH ar), 7.04 – 7.29 (m, 10 H, CH ar), 7.68 (d, $J = 9$ Hz, 2H, CH ar).

$^{13}\text{C}\{^1\text{H}\}$ NMR (75.5 MHz, CDCl_3): δ = 0.43 (s, $-\text{OSi}(\text{CH}_3)_3$), 66.92 (d, $^1J_{\text{RhC}} = 8.12$ Hz, CH olefin), 68.26 (d, $^1J_{\text{RhC}} = 9.21$ Hz, CH olefin), 72.78 (s, CH benzylic), 120.44 (CH ar), 121.41 (CH ar), 124.24 (CH ar), 124.97 (CH ar), 126.69 (CH ar), 127.77 (CH ar), 128.15 (CH ar), 128.71 (CH ar), 128.81 (CH ar), 128.98 (CH ar), 129.14 (CH ar), 130.22 (CH ar), 131.54 (C quart), 135.14 (C quart), 135.31 (C quart), 141.86 (C quart), 151.07 (C quart), 161.75 (d, $^1J_{\text{CRh}} = 37.75$ Hz, $\text{C}\equiv\text{N}(\text{C}_6\text{H}_4\text{OTMS})$).

^{103}Rh NMR (12.7 MHz, CDCl_3): δ = 1916 (s).

^{29}Si NMR (300 MHz, CDCl_3): δ = 24 (s).

ATR IR (neat in cm^{-1}): 3206 w, 3069 - 2907 w, 2233 w, 2132 w, 1599 s, 1488 s, 1471 s, 905 s, 728 s.

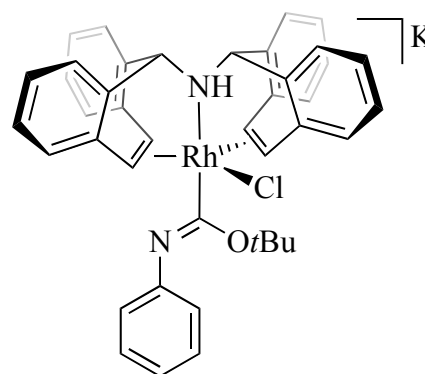
HRMS (MALDI, DCTB matrix): calcd. for $[\text{C}_{40}\text{H}_{36}\text{N}_2\text{ORhSi}]^+$ m/z 691.17; found 691.1663. Fragment intensity in %: 691.17 ($[\text{M}^+]$, 11.99), 692.1700 ($[\text{M}^+] + 1$, 6.00), 693.1737 ($[\text{M}^+] + 2$, 1.63), 619.1260 ($[\text{M}^+] - \text{TMS}$, 100).

[Rh(trop₂NH)(CN(Ph)OtBu)]K

MF = $\text{C}_{41}\text{H}_{37}\text{ClN}_2\text{ORh}$

MW = 712.10 g/mol

mp = 220 °C decomposes



To a suspension of $[\text{RhCl}(\text{trop}_2\text{NH})(\text{CNC}_6\text{H}_5)]$ (**K14**) in THF was added K^+OtBu^- (4.6 mg, 0.41 mmol, 1.05 eq) at room temperature. A dark green solution was formed immediately and after few minutes the color of the solution turned red-brown. The solvent was removed by reduced pressure and the product was dried overnight in high vacuum (quantitative yield).

^1H NMR (250.1 MHz, $[\text{D}_8]$ THF): δ = 1.69 (*s*, 9H, $-\text{OC}(\text{CH}_3)_3$), 2.78 (*s*, 1H, NH), 4.71 (*d*, $^3J_{\text{HH}} = 9$ Hz, 2H, CH olefin), 4.85 (*s*, 2H, CH benzylic), 5.94 (*dd*, $^3J_{\text{HH}} = 9$ Hz, $J = 2.8$ Hz, 2H, CH olefin), 6.66 – 6.82 (*m*, 9 H, CH ar), 6.95 – 7.06 (*m*, 10 H, CH ar), 7.15 (*d*, $J = 9$ Hz, 2H, CH ar).

$^{13}\text{C}\{^1\text{H}\}$ NMR (62.9 MHz, CDCl_3): δ = 30.78 (*s*, $-\text{OC}(\text{CH}_3)_3$), 70.04 (*d*, $^1J_{\text{RhC}} = 7.31$ Hz, CH olefin), 71.43 (*s*, CH benzylic), 73.80 (*d*, $^1J_{\text{RhC}} = 16$ Hz, CH olefin), 78.58 (*d*, $J = 1.68$ Hz, $\text{OC}(\text{CH}_3)_3$), 113.55 (*s*, 2C, CH ar), 122.62 (CH para to CN), 124.22 (*s*, 2C, CH ar), 124.62 (*s*, 2CH ar), 127.04 (*s*, 2CH ar), 127.24 (*s*, 4 CH ar, $-\text{CNC}_6\text{H}_5$), 127.73 (*s*, 2CH ar), 128.16 (*s*, 2CH ar), 129.51 (*s*, 2CH ar), 131.28 (*s*, 2CH ar), 134.25 (*d*, $J = 1.37$ Hz, C quart), 135.66 (*s*, C quart), 137.57 (*d*, $J = 2.59$ Hz, C quart), 140.25 (C quart), 154.31 (C quart, $\text{CN}(\text{OtBu})(\text{C}_6\text{H}_5)$), 189.53 (*d*, $^1J_{\text{CRh}} = 36.5$ Hz, $-\text{CN}(\text{OtBu})(\text{C}_6\text{H}_5)$).

^{103}Rh NMR (12.7 MHz, CDCl_3): δ = 1454 (*s*).

ATR IR (neat cm⁻¹): 2963.55 w, 2116.02 w, 1596.69 m, 1485.30 s, 1469.52 s, 1408.50 w, 1359.61 w, 1313.90 w, 1258.95 s, 1220.30 w, 1189.53 w, 1128.66 s, 1061.23 s, 1044.52 s, 1010.96 s, 974.56 m, 939.39 w, 896.30 w, 867.08 w, 802.53 s, 762.33 m, 744.80 vs, 701.09 s, 665.93 w, 636.25 w, 620.15 w, 607.21 w.

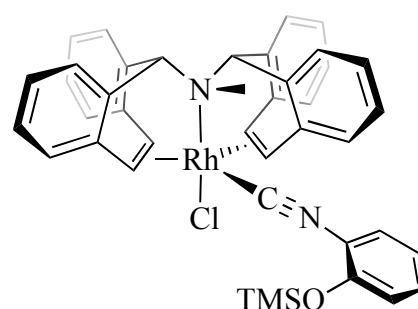
HRMS (ESI): calcd. for [C₄₁H₃₇ClN₂ORh]⁺ m/z 711.16; found 711.2. Fragment intensity in %: 705.1815 ([M⁺], 100), 706.1844 ([M⁺] + 1, 51.41), 707.1859 ([M⁺] + 2, 15.95), 708.1870 ([M⁺] + 3, 3.34).

[RhCl(trop₂NMe)(CNC₆H₄OSi(CH₃)₃)] (K16)

MF = C₄₁H₃₈ClN₂ORhSi

MW = 740.15 g/mol

mp > 220°C



[Rh₂(μ-Cl)₂(trop₂NMe)₂] (200 mg, 0.187 mmol) are suspended in of CH₂Cl₂ (50 mL). Upon addition of an excess of 2-(trimethylsilyloxy)phenyl isocyanide **xx** (89 mg, 2.5 eq) the orange suspension turns into a clear yellow solution. The solvent's volume is narrowed to 5 ml and layered with *n*-hexane. The product was isolated as a bright yellow powder in 80% yield (217 mg).

¹H NMR (300.1 MHz, CDCl₃): δ = 0.21 (*s*, 9H, -OSi(CH₃)₃), 1.86 (*s*, 3H, trop₂NCH₃), 3.78 (*s*, 2H, *CH* benzylic), 5.31 (*d*, ³J_{HH} = 9.3 Hz, 2H, *CH* olefin), 5.62 (*d*, ³J_{HH} = 9.3 Hz, 2H, *CH* olefin), 6.6-7.8 (16H, *CH* ar).

¹³C{¹H} NMR (75.5 MHz, CDCl₃): δ = 0.37 (*s*, -OSi(CH₃)₃), 56.98 (*s*, trop₂NCH₃) 66.28 (*d*, ¹J_{RhC} = 8.8 Hz, *CH* olefin), 64.49 (*d*, ¹J_{RhC} = 8.98 Hz, *CH* olefin), 82.37 (*s*, *CH* benzylic), 117.3 (*CH* ar), 124.61 (*s*, 2C, *CH* ar), 125.01 (*CH* ar), 126.71 (*CH* ar), 126.75 (*CH* ar), 127.65 (*CH* ar), 128.16 (*CH* ar), 128.77 (*CH* ar), 128.99 (*CH* ar).

ATR IR (neat cm⁻¹): 3008.54 w, 2960.22 w, 2130.36 m, 1952.31 w, 1595.99 m, 1578.52 w, 1551.25 w, 1514.11 w, 1488.71 s, 1470.42 m, 1451.55 m, 1400.05 m, 1291.10 m, 1276.63 m, 1254.18 s, 1219.84 w, 1189.19 w, 1157.98 w, 1124.95 w, 1105.30 m, 1065.86 m, 1044.43 w,

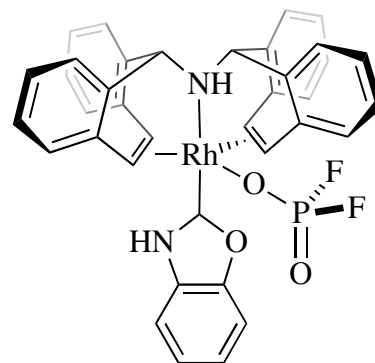
1027.06 m, 940.90 w, 904.64 s, 840.52 s, 768.60 m, 747.65 s, 731.23 s, 686.29 w, 654.37 w, 635.04 w, 627.49 w.

HRMS (MALDI): calcd. for $[C_{41}H_{38}N_2ORhSi]^+$ m/z 705.1808; found 711.1815; $[M^+] = 675.2$.

$[Rh(PF_2O_2)(trop_2NH)(C_7H_5NO)]$ (K18)

MF = $C_{37}H_{29}F_2N_2O_3PRh$

MW = 721.51 g/mol



This reaction has been performed in a young NMR tube. To a solution of **K15** (20 mg, 0.027 mmol) in CD_2Cl_2 (0.5 ml) only degassed by three freeze pump cycles is added Et_3PF_6 (6.8 mg). The solution is stirred at room temperature. After 24 hours we could detect the formation of the product and of POF_4^- and $PF_2O_2^-$. The reaction is not reproducible.

1H NMR (300.1 MHz, $CDCl_3$): $\delta = 3.61$ (s, 1H, NH trop), 4.92 (s, 2H, CH benzylic), 4.99 (d, $^3J_{HH} = 9$ Hz, 2H, CH olefin), 6.13 (d, $^3J_{HH} = 8.1$ Hz, 2H, CH olefin), 6.91 (m, 5H, CH ar), 7.18 (m, 7H, CH ar), 7.43 (m, 5H, CH ar), 7.71 (m, 3H, CH ar), 14.93 (s, 1H, NH carbene).

$^{13}C\{^1H\}$ NMR (75.5 MHz, $CDCl_3$): $\delta = 71.45$ (br s, CH olefin), 72.35 (br s, CH olefin), 72.63 (s, CH benzylic), 111.19 (CH ar), 113.08 (CH ar), 125.04 (CH ar), 125.81 (CH ar), 126.47 (CH ar), 126.61 (CH ar), 127.58 (CH ar), 127.93 (CH ar), 128.74 (CH ar), 128.92 (CH ar), 129.82 (CH ar), 129.94 (CH ar), 131.35 (C quart), 134.71 (C quart), 135.26 (C quart), 136.52 (C quart), 138.87 (C quart), 152.53 (C quart), 203.0 (Rh=C). The J_{RhC} for the olefin carbon were not detected due to broadened lines.

$^{31}P\{^1H\}$ NMR (101.25 MHz, d_6 -acetone): $\delta = -13.62$ (t, $^1J_{PF} = 967$ Hz, $PF_2O_2^-$).

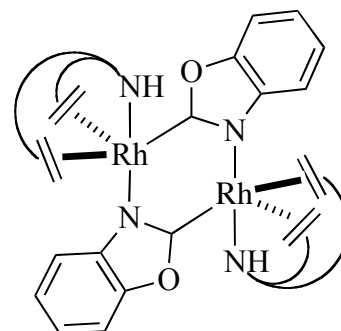
$^{31}F\{^1H\}$ NMR (101.25 MHz, d_6 -acetone): $\delta = -81.23$ (d, $^1J_{PF} = 967$ Hz, $PF_2O_2^-$).

HRMS (MALDI, DCTB matrix): calcd. for $[C_{37}H_{28}N_2ORh]^+$ m/z 619.1257; found 619.0

[Rh(trop₂NH)(μ-C₇H₄NO)] (K19)

MF = C₇₄H₅₆N₄O₂Rh₂

MW= 1239.07 g/mol



To a solution of **K15** (100 mg, 0.14 mmol) in CH₂Cl₂ (0.5 ml) is added Et₃PF₆ (55 mg, 0.23 mmol). The red solution is stirred at room temperature for 4 hours and then dried under vacuum. The red solid is dissolved in MeOH and KF is added. The solution is refluxed. After 15 minutes the colour changes to orange and a yellow precipitate forms and it is filtered. The product is obtained in 50% yield. The reaction is not reproducible.

¹H NMR (400.1 MHz, CD₂Cl₂): δ = 3.15 (s, 1H, NH trop), 4.88 (s, 2H, CH benzylic), 5.05 (d, ³J_{HH} = 9.29 Hz, 2H, CH olefin), 5.82 (dd, ³J_{HH} = 9.29 Hz, ³J_{HRh} = 2.74 Hz, 2H, CH olefin), 6.89-6.98 (m, 7H, CH ar), 7.14 (d, 2H, J_{HH} = 4 Hz, CH ar), 7.18 (d, 2H, J_{HH} = 8 Hz, CH ar), 7.27 (d, 4H, J_{HH} = 8 Hz, CH ar), 7.44 – 7.46 (m, 3H, CH ar), 7.55 (d, 2H, J_{HH} = 8 Hz, CH ar).

¹³C{¹H} NMR (75.5 MHz, CD₂Cl₂): δ = 68.62 (d, ¹J_{RhC} = 7.79 Hz, CH olefin), 68.96 (d, ¹J_{RhC} = 12.8 Hz, CH olefin), 71.97 (s, CH benzyl), 111.06 (CH ar), 113.69 (CH ar), 125.24 (CH ar), 125.91 (CH ar), 126.97 (CH ar), 127.11 (CH ar), 127.90 (CH ar), 128.22 (CH ar), 129.10 (CH ar), 129.17 (CH ar), 129.70 (CH ar), 130.07 (CH ar), 131.85 (C quart), 134.32 (C quart), 135.44 (C quart), 136.18 (C quart), 138.53 (C quart), 152.53 (C quart), 199.9 (Rh=C).

¹⁰³Rh NMR (12.7 MHz, CD₂Cl₂): δ = 1323 (s).

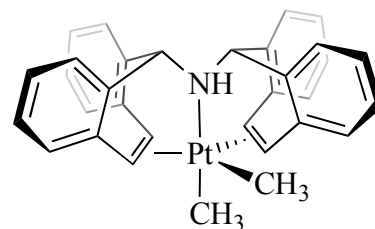
¹⁵N NMR (49.5 MHz, CD₂Cl₂): δ = 90.56 (s, NH trop)

HRMS (MALDI, DCTB matrix): calcd. for [C₃₇H₂₈N₂ORh]⁺ m/z 619.1257; found 619.0

[Pt(Me)₂(trop₂NH)] (K20)MF = C₃₂H₂₉NPt

MW = 621.65 g/mol

mp > 220°C



To a solution of [Pt(μ^2 -SMe₂)Me₂]₂ (**116**) (MW= 574.6 gmol⁻¹, 100 mg, 0.17 mmol) in CH₂Cl₂ trop₂NH (MW= 397.5 gmol⁻¹, 139 mg, 2 eq) is added. The solution color changed from colorless to yellow. The volume of the reaction solution is reduced under pressure and hexane is added. Yellow crystals grew over night (152 mg, yield 72%).

¹H NMR (400.1 MHz, CDCl₃, 2733K): δ = 0.105 (s, 3H, ²J_{PtH} = 67.3 Hz, CH₃ axial), 0.175 (s, 3H, ²J_{PtH} = 67.3 Hz, CH₃ equatorial), 2.53 (s, 1H, ²J_{PtH} = 23.15 Hz, NH), 3.97 (d, 2H, ³J_{HH} = 9.2 Hz, ²J_{PtH} = 38.4 Hz, CH olefin), 4.12 (d, 2H, ³J_{HH} = 9.2 Hz, ²J_{PtH} = 55.4 Hz, CH olefin), 4.62 (s, 2H, ²J_{PtH} = 18.8 Hz, CH benzylic), 6.76 (d, 2H, ³J_{HH}=7.2 Hz, CH ar), 6.82 (m, 2H, CH ar), 6.88 (d, 4H, ³J_{HH} = 4 Hz, CH ar), 7.04 (m, 4H, CH ar), 7.24 (t, 2H, ³J_{HH} = 7.6 Hz, CH ar), 7.4 (d, 2H; ³J_{HH}= 7.6 Hz, CH ar).

¹³C{¹H} NMR (100.6 MHz, CDCl₃, 233K): δ = -13.5 (s, ¹J_{PtC} = 725 Hz, CH₃ axial), -6.97 (s, ¹J_{PtC}= 647 Hz, CH₃ equatorial), 57.12 (s, ¹J_{PtC} = 80.18 Hz, CH olefin), 62.71 (s, ¹J_{PtC} = 150.99 Hz, CH olefin), 71.80 (s, CH benzylic), 123.8 (s, CH ar), 126.1 (s, CH ar), 127.4 (s, CH ar), 128.9 (s, CH ar), 129.1 (s, CH ar), 129.5 (s, CH ar), 130.1 (s, CH ar), 132.4(s, C quart), 134.9(s, C quart), 136.4(s C quart), 138.8(s, C quart).

¹⁵N NMR (40.55 MHz, CDCl₃, 233K): δ = - 101.55.

¹⁹⁵Pt NMR (64.3 MHz, CDCl₃, 273K): δ = - 4250.

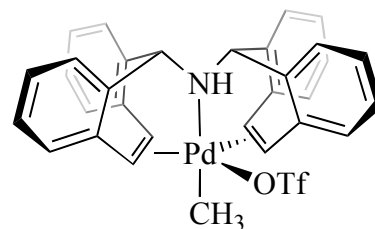
ATR IR (neat cm⁻¹): 2775 w, 2360 m, 2115 w, 1994 w, 1495 m, 1305 w, 1266 w, 1234 w, 1151 w, 1057 w, 933 m, 873 w, 656 w.

HRMS (MALDI, DCTB matrix): calcd. for [C₃₁H₂₆NOPt]⁺ 607.1713 m/z; found 607.1720.

[Pd(Me)(OTf)(trop₂NH)] (K21)MF = C₃₂H₂₆F₃NO₃PdS

MW = 668.03 g/mol

mp > 220°C



To a solution of [Pd(μ -Cl)(Me)(SMe₂)₂] (MW= 438.1 gmol⁻¹, 280 mg, 0.64 mmol) in CHCl₃, trop₂NH is added (MW= 397.5 gmol⁻¹, 508 mg, 2 eq). The solution turned immediately brow-green. After 30 minutes the solution is pale yellow and a solid precipitate ([Pd(Me)(Cl)(trop₂NH)]). The white solid (MW= 553.1 300 mg, 0.54 mmol) have been dissolved in CH₂Cl₂ and AgOTf was added (139 mg). The solution was stirred at room temperature for 2 hours and subsequently AgOtf was filtered off. The light pink solution was dried under vacuum. **K21** was obtained as off-white solid (280 mg, 34% yield).

¹H NMR (300.1 MHz, CD₃CN, 298K): δ = 1.19 (s, 3H, CH₃ axial), 3.57 (s, 1H, NH), 5.39 (s, 2H, CH benzylic), 5.97 (s, 2H, ³J_{HH} = 9.9 Hz, CH olefin), 6.74 (d, 2H, ³J_{HH} = 9.9 Hz, CH olefin), 6.99 ppm (dt, J_{HH} = 1.47 Hz, J_{HH} = 7.6 Hz, 2H, CH ar), 7.11 (dt, J_{HH} = 1.47 Hz, J_{HH} = 7.6 Hz, 2H, CH ar), 7.22 (m, 4H, CH ar), 7.38 (m, 4H, CH ar), 7.51 (m, 4H, CH ar).

¹³C{¹H} NMR (75.5 MHz, CD₃CN, 298K): δ = 11.58 (s, 1C; CH₃ axial), 70.12 (s, 2C, CH benzylic), 97.25 (s, 1C, CH olefin), 98.9 (s, 1C, CH olefin), 128.36 (s, CH ar), 128.49 (s, CH ar), 128.82 (s, CH ar), 129.04 (s, CH ar), 129.20 (s, CH ar), 129.22 (s, CH ar), 129.34 (s, CH ar), 130.7 (s, CH ar), 132.24 (C quart), 134.16 (C quart), 135.51 (C quart), 136.48 (C quart).

¹⁹F NMR (188.3 MHz, CD₃CN, 298K): δ = - 80 (s, -SO₃CF₃)

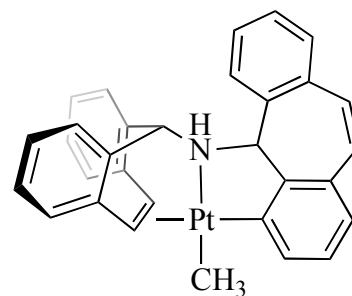
ATR IR (neat cm⁻¹): 3231.30 w, 3177.99 w, 3049.25 w, 2899.45 w, 2349.33 w, 1952.68 w, 1710.81 w, 1603.57 w, 1514.09 w, 1489.53 w, 1458.96 w, 1433.01 w, 1411.65 w, 1340.36 w, 1319.95 w, 1277.93 s, 1251.60 s, 1238.76 s, 1223.39 m, 1184.08 w, 1158.15 m, 1137.40 s, 1109.05 w, 1029.42 s, 1001.64 m, 979.25 m, 960.41 m, 947.96 w, 868.65 w, 824.24 m, 778.40 m, 764.34 m, 749.39 s, 727.25 m, 708.79 w, 662.32 w, 643.69 w, 632.34 s.

HRMS (MALDI, DCTB matrix): calcd. for [C₃₁H₂₆NOPd]⁺ m/z 518.1100; found 517.1084.

[Pt(Me)(tropNHortho-trop)] (K22)MF = C₃₁H₂₄NPt

MW = 605.16 g/mol

mp = 220 °C decomposes



[Pt(Me)₂(trop₂NH)] (**K20**) (MW= 621.65, 100 mg, 0.16 mmol) is suspended in 10 ml of dry benzene. The reaction is heated for 2 days under inert condition until all the starting is in solution. The volume of the reaction is lowered under reduced pressure and hexane is added. The product was isolated as yellow powder (63 mg, 65% yield).

¹H NMR (700.1 MHz, C₆D₆): δ = 1.58 (s, 3H, ²J_{PtH} = 82.24 Hz, CH₃), 4.65 (d, 1H, ³J_{HH} = 10.8 Hz, CH benzylic), 4.85 (d, 1H, 4.97 ³J_{HH} = 10.8 Hz, ²J_{PtH} = 50.6 Hz, NH), 5.28 (s, 1H, ³J_{PtH} = 18.8 Hz, CH benzylic), 5.3 (d, 1H, ³J_{HH} = 10.07 Hz, ²J_{PtH} = 35.2 Hz, CH olefin), 5.78 (d, 1H, ³J_{HH} = 10.07 Hz, ²J_{PtH} = 37.5 Hz, CH olefin), 6.93 (d, J_{HH} = 7.7 Hz, 1H, CH ar), 6.52 (d, J_{HH} = 11.6 Hz, 1H, CH olefin), 6.59 (m, 1H, CH ar), 6.68 (d, J_{HH} = 11.6 Hz, 1H, CH olefin), 6.9 (m, 6H, CH ar), 7.15 (m, 10H, CH ar), 7.3 (br d, J_{HH} = 7.7 Hz, 2H, CH ar), 8.27 (d, J_{HH} = 7.47 Hz, J_{PtH} = 72.99 Hz, 1H, CH meta ar).

¹³C {¹H} NMR (176.04 MHz, C₆D₆): δ = -8.15 (s, ¹J_{PtC} = 819.7 Hz, CH₃), 64.81 (s, ³J_{PtC} = 56.2 Hz, CH benzylic), 6.54 (s, ³J_{PtC} = 10 Hz, CH benzylic), 80.03 (s, ¹J_{PtC} = 57.1 Hz, CH olefin), 86.6 (s, ¹J_{PtC} = 87.4 Hz, CH olefin), 121.68 – 158.1 (CH ar).

ATR IR (neat cm⁻¹): 2963.87 m, 2903.01 w, 2865.63 w, 2799.87 w, 1951.17 w, 1599.51 w, 1571.49 w, 1546.36 w, 1484.79 m, 1442.96 w, 1425.04 w, 1309.05 w, 1260.29 s, 1186.37 w, 1157.53 w, 1057.07 s, 1017.25 s, 945.68 w, 874.68 w, 795.46 vs, 775.86 s, 750.87 s, 739.74 s, 699.08 m, 655.54 w, 632.97 w.

¹⁹⁵Pt NMR (64.6 MHz, C₆D₆, 298K): δ = - 3581.

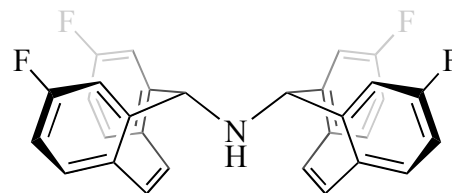
HRMS (MALDI, DCTB matrix): calcd. for [C₃₁H₂₆NPt]⁺ m/z 607.6228; found 607.1710; 591.1 [M⁺] – CH₃.

Bis(3,7-Difluor-5H-dibenzo[a,d]cyclohepten-5-yl)amine (^FtropNH₂) (**133**)

MF = C₃₀H₁₉F₄N

MW = 469.5 g/mol

mp = 200 °C



^Ftrop₂Cl (**132**) (MW= 262.7 gmol⁻¹, 1.7 g, 0.006 mol) are dissolved in toluene (30 ml) and an excess of 1,1,1,3,3,3-hexamethyl-disilazane is added (0.9 ml, d= 0.675 gml⁻¹, MW= 161.4 gmol⁻¹, 0.004 mmol). The mixture is refluxed for 5 hours and subsequently all the volatiles are removed under reduced pressure and the solid is recrystallized from hexane (1.1g, yield 73%). The product can be also purified by flash chromatography (2% AcOEt in hexane).

¹H NMR (500.1 MHz, CDCl₃): δ = 2.79 (br s, NH), 3.20 (d, J_{HH} = 5.7 Hz, NH), 3.76 (s, CH benzylic), 4.30 (m, NH), 4.34 (d, J_{HH} = 3.9 Hz, CH benzylic), 4.71 (br s, CH benzylic), 5.03 (d, J_{HH} = 3Hz, CH benzylic), 6.78 (s, CH ar), 6.95 – 7.06 (m, CH ar), 7.09 (dt, J_{HH}= 2.5, J_{HF}= 8.5 Hz, CH ar), 7.27 – 7.35 (m, CH ar), 7.46 (dd, J_{HH}= 6 Hz, J_{HF}=8.5 Hz, CH ar), 7.58 (dd, J_{HH}= 2.5 Hz, J_{HF}= 10 Hz, CH ar).

¹³C{¹H} NMR (125.8 MHz, CDCl₃): δ = 57.24 (s, CH benzylic), 58.16 (s, CH benzylic), 67.01 (s, CH benzylic), 65.33 (s, CH benzylic), 109.55 (d, J_{CF} = 23.7 Hz, CH ar), 109.82 (d, J_{CF} = 23.5 Hz, CH ar), 113.10 (d, J_{CF} = 22.3 Hz, CH ar), 113.21 (d, J_{CF} = 22.3 Hz, CH ar), 113.49 (d, J_{CF}= 21.6 Hz, CH ar), 114.37 (d, J_{CF} = 21.4 Hz, CH ar), 115.62 (d, J_{CF} = 21.5 Hz, CH ar), 116.09 (d, J_{CF}= 21.8 Hz, CH ar), 129.39 (d, J_{CF} = 36.4 Hz, CH ar), 129.67 (d, J_{CF} = 8.4 Hz, CH ar), 129.93 (d, J_{CF} = 6.0 Hz, CH ar), 130.53 (d, J_{CF} = 2.9 Hz, CH olefin), 130.57 (d, J_{CF} = 2.9 Hz, CH olefin), 130.79 (d, J_{CF}= 2.9 Hz, CH olefin), 131.60 (d, J_{CF} = 8.6 Hz, CH ar), 132.37 (d, J_{CF} = 8.2 Hz, CH ar), 141.39 (d, J_{CF} = 6.7 Hz, C quart), 141.78 (d, J_{CF} = 7.2 Hz, C quart), 141.7 (d, J_{CF} = 6.2 Hz, C quart), 141.93 (d, J_{CF} = 6.7 Hz, C quart), 163.14 (d, J_{CF} = 247.6 Hz, C-F), 163.41 (d, J_{CF} = 248.1 Hz, C-F), 164.4 (d, J_{CF} = 246.2 Hz, C-F), 164.49 (d, J_{CF} = 246.6 Hz, C-F).

¹⁹F NMR (188.3 MHz, CD₂Cl₂): δ = - 112.9, -113.6, -113.9, -114.4.

ATR IR (neat cm⁻¹): 3020.96 (w), 2359.63 (w), 2130.21 (m), 1599.37 (m), 1575.00 (w), 1489.32 (s), 1453.89 (w), 1412.88 (w), 1355.02 (vw), 1291.31 (w), 1276.18 (s), 1255.41 (s), 1223.21 (m), 1188.71 (m), 1161.56 (m), 1143.91 (m), 1126.92 (w), 1105.52 (w), 1089.38 (w), 1063.77 (vw),

1027.67 (vw), 991.93 (m), 980.31 (m), 953.78 (w), 904.12 (m), 894.53 (m), 869.08 (m), 833.14 (vs), 812.95 (m), 775.86 (s), 767.51 (s), 747.41 (s), 731.78 (s), 692.10 (s), 653.74 (w), 635.34 (w), 627.65 (w), 615.79 (w).

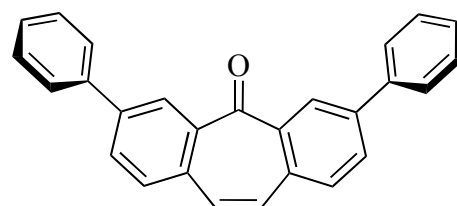
HRMS (MALDI, DCTB matrix): calcd. for $[C_{30}H_{20}F_4N]^+$ m/z 470.1532; found 470.1526 (100 %), 471.1560 (32.86 %), 472.1593 (5.22 %), 473.1626 (0.53 %).

3,7-Diphenyl-5H-dibenzo[a,d]cyclohepten-5-on (^{Ph}tropO) (136)

MF = $C_{27}H_{18}O$

MW = 358.43 g/mol

mp = 130 °C decomposes



A solution of 3,7-diiodo-5H-dibenzo[a,d]cycloheptanone (**135**) ($MW = 458.04 \text{ gmol}^{-1}$, 1.33 g, 0.003 mol), phenyloronic acid ($MW = 121.93 \text{ gmol}^{-1}$, 0.8 g 0.006 mol) and 3 ml of Na_2CO_3 (2M) in a mixture of DME and toluene is refluxed for 12 hours, until the solution colour is brown. The reaction is quenched with water and extracted three times with 30 ml of AcOEt. The solvent is dried over anhydrous $MgSO_4$, filtered and dried under reduced pressure (1.2 g). The raw product can be purified by flash chromatography (2% AcOEt in hexane). Quantitative yield.

1H NMR (300.1 MHz, $CDCl_3$): $\delta = 7.15$ (s, 1H, CH olefin), 7.42 (m, 1H, CH ar para), 7.49 (d, 2H, $^3J_{HH} = 7.2$ Hz, CH ar orto), 7.67 (d, 1H, $^3J_{HH} = 8.2$ Hz, CH ar), 7.75 (br d, $^3J_{HH} = 7.2$ Hz, 2H, CH ar meta), 7.93 (dd, 1H, $5J_{HH} = 2$ Hz, $^3J_{HH} = 8.2$ Hz, 2H, CH ar), 8.54 (d, 1H, $^5J_{HH} = 2$ Hz, CH ar).

$^{13}C\{^1H\}$ NMR (75.5 MHz, $CDCl_3$): $\delta = 127.15$ (s, 2C, CH ar meta), 127.97 (s, 1C, CH ar para), 128.67 (s, 1C, CH ar), 128.97 (s, 2C, CH ar ortho), 130.47 (s, 1C, CH ar), 131.27 (s, 1C, CH olefin), 131.65 (s, 1C, CH ar), 134.06 (C quart), 138.79 (C quart), 139.62 (C quart), 141.54 (C quart), 192.84 (C quart, C=O).

ATR IR (neat cm^{-1}): 2962.93 (w), 1897.48 (w), 1817.63 (w), 1673.11 (m), 1640.62 (w), 1619.76 (s), 1588.95 (s), 1480.79 (s), 1438.63 (s), 1390.06 (w), 1323.73 (s), 1259.97 (s), 1239.86 (w), 1212.26 (w), 1189.07 (s), 1172.31 (m), 1118.78 (s), 1095.68 (m), 1073.99 (m), 1027.18 (m), 999.78 (m), 967.33 (w), 927.10 (w), 910.63 (w), 879.38 (w), 860.97 (s), 803.59 (s), 767.35 (s), 751.94 (vs), 721.09 (vs), 695.36 (vs), 639.13 (w), 618.44 (w), 607.59 (w).

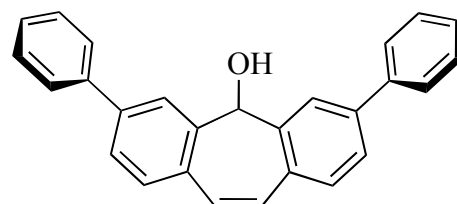
HRMS (MALDI, DCTB matrix): calcd. for $[C_{27}H_{18}O]^+$ m/z 358.1358; found 358.1386 (100 %), 359.1386 (29.42 %), 360.1419 (4.34 %), 361.1450 (0.43 %).

3,7-Diphenyl-5H-dibenzo[a,d]cyclohepten-5-ol (^{Ph}tropOH) (**137**)

MF = $C_{27}H_{20}O$

MW = 360.45 g/mol

mp = 170 °C decomposes



A suspension of 3,7-Diphenyl-5H-dibenzo[a,d]cyclohepten-5-on (**136**) (430 mg, 1.2 mmol) in 35 mL of MeOH is stirred overnight at room temperature after the addition $NaBH_4$ (23 mg, 0.6 mmol) and KOH (34 mg). Subsequently all volatiles are removed under reduced pressure. The row product is dissolved in CH_2Cl_2 and washed with water. The organic phase is dried over $MgSO_4$ and filtered. The volatiles are removed. The product is purified by flash chromatography (3% AcOEt in hexane). Product obtained: 280 mg (yield 65%).

1H NMR (300.1 MHz, $CDCl_3$): δ = 2.63 (d, J_{HH} = 4.9 Hz, OH), 5.57 (br s, CH benzylic), 7.15 (s, CH ar), 7.37 – 7.41 (m, 2H, CH ar), 7.46 – 7.50 (m, 7H, CH ar), 7.57 (dd, J_{HH} = 1.7 Hz, J_{HH} = 7.9 Hz, 2H, CH ar), 7.68 (br d, J_{HH} = 7.8 Hz, 5H, CH ar), 7.96 (br s, 2H, CH ar).

$^{13}C\{^1H\}$ NMR (75.5 MHz, $CDCl_3$): δ = 125.9 (s, CH ar), 127.6 (s, CH ar ortho), 127.8 (s, CH ar), 129.2 (s, CH ar meta), 129.6 (s, CH ar), 131.0 (s, CH ar), 132.2 (s, CH ar), 140.9 (C quart), 141.1 (C quart), 142.0 (C quart).

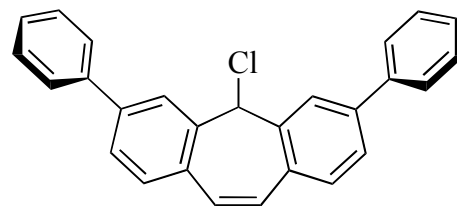
ATR IR (neat cm^{-1}): 3567.70 m, 3022.88 w, 1948.39 w, 1598.04 m, 1551.94 w, 1479.52 s, 1446.43 w, 1425.34 w, 1396.73 w, 1375.92 w, 1307.24 w, 1288.27 w, 1263.18 w, 1220.84 w, 1182.94 w, 1169.70 w, 1158.71 w, 1123.05 w, 1073.93 w, 1055.97 m, 1040.89 m, 1021.75 w, 1000.89 w, 976.18 w, 966.81 w, 922.97 w, 912.33 w, 874.81 w, 859.91 w, 841.05 s, 808.28 w, 780.25 w, 766.19 m, 753.17 s, 726.22 m, 697.27 s, 675.04 w, 632.03 w, 622.49 w, 607.35 m.

HRMS (MALDI, DCTB matrix): calcd. for $[C_{27}H_{21}O]^+$ m/z 361.4550; found 361.1587 (110 %), 362.1587 (29.43), 363.1653 (4.35), 364.1685 (0.43); 343.1 $[M^+] - H_2O$.

5-Chlor-3,7-Diphenyl-5H-dibenzo[a,d]cyclohepten (^{Ph}tropCl) (138)MF = C₂₇H₁₉Cl

MW = 378.89 g/mol

mp = 170 °C decomposes



A solution of 3,7-Diphenyl-5H-dibenzo[a,d]cyclohepten-5-ol (**137**) (1.5 g, 4.2 mmol) in CH₂Cl₂ is cooled to -10°C. Freshly distilled SOCl₂ (1 ml) is added drop wise and the solution is stirred at room temperature overnight. The raw product (1.6 g, quantitative yield) was used for the next step without further purification.

¹H NMR (300.1 MHz, CDCl₃): δ = 3.9 (s), 7.11 (s, *CH* ar), 7.15 (s, *CH* ar), 7.36 – 7.53 (m, *CH* ar), 7.60 – 7.77 (m, *CH* ar), 7.75 (br d, *CH* ar, J_{HH} = 8 Hz), 7.92 (dd, *CH* ar, J_{HH} = 2 Hz, J_{HH} = 8 Hz), 8.54 (d, *CH* ar, J_{HH} = 0.8 Hz).

ATR IR (neat cm⁻¹): 3566.50 w, 3025.62 w, 2964.50 w, 1910.29 w, 1806.77 w, 1671.97 w, 1599.18 m, 1550.72 w, 1482.73 m, 1447.14 w, 1431.49 w, 1393.99 w, 1309.20 w, 1288.91 w, 1260.93 m, 1207.83 w, 1182.56 w, 1160.82 w, 1076.91 m, 1056.28 m, 1041.20 m, 1024.84 m, 965.52 w, 914.93 w, 901.51 w, 879.96 m, 843.60 s, 792.65 s, 768.28 m, 754.27 s, 737.91 m, 691.75 s, 674.91 s, 658.94 m, 634.08 w, 621.88 w, 607.43 w.

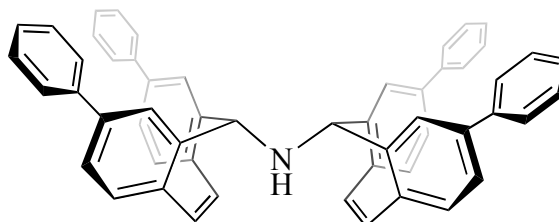
HRMS (MALDI, DCTB matrix): calcd. for [C₂₇H₁₉]⁺ m/z 343.1487; found 343.1481 (100 %), 344.1515 (29.38 %), 345.1549 (4.16 %), 346.1583 (0.38 %).

Bis(3,7-Diphenyl-5H-dibenzo[a,d]cyclohepten-5-yl)amine (^{Ph}tropNH₂) (**139**)

MF = C₅₄H₃₉N

MW = 701.89 g/mol

mp = 170 °C decomposes



^{Ph}trop₂Cl (**138**) (293 mg, 0.77 mmol) are dissolved in toluene and an excess of 1,1,1,3,3,3-hexamethyl-disilazane is added (90 μl, d= 0.675 gml⁻¹, MW= 161.4 gmol⁻¹, 0.82 mmol). The mixture is refluxed for 5 hours and subsequently all the volatiles are removed under reduced pressure. The row product (272 mg, quantitative yield) was used for the next step without further purification.

¹H NMR (300.1 MHz, CDCl₃): δ = 3.2 (br s, 1H, NH), 4.02 (br s, CH benzylic), 4.97 (br s, CH benzylic), 5.26 (br s, CH benzylic), 6.93 (s, CH ar), 7.09 (d, J_{HH} = 6.6 Hz, CH ar), 7.3 – 7.7 (CH ar), 8.01 (CH ar).

¹³C{¹H} NMR (75.5 MHz, CDCl₃): δ = 57.5 (s, CH benzylic), 66.3 (s, CH benzylic), 68.5 (s, CH benzylic), 121.4 (s, CH ar), 124.4 (s, CH ar), 125.3 (s, CH ar), 125.9 (s, CH ar), 127.08 (s, CH ar), 127.1 (s, CH ar), 127.2 (s, CH ar), 127.3 (s, CH ar), 127.5 (s, CH ar), 128.2 (s, CH ar), 128.3 (s, CH ar), 128.71 (s, CH ar), 127.73 (s, CH ar), 128.8 (s, CH ar), 130.0 (s, CH ar), 130.1 (s, CH ar), 130.4 (s, CH ar), 130.6 (s, CH ar), 130.9 (s, CH ar), 132.6 (s, C quart), 132.63 (s, C quart), 133.2 (s, C quart), 139.9 (s, C quart), 140.1 (s, C quart), 140.4 (s, C quart), 140.5 (s, C quart), 140.8 (s, C quart), 141.3 (s, C quart), 141.4 (s, C quart), 141.6 (s, C quart).

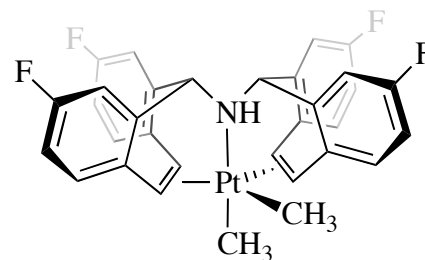
ATR IR (neat cm⁻¹): 3012.55 w, 2964.18 w, 2360.15 w, 2130.73 w, 1732.13 w, 1599.50 m, 1549.19 w, 1481.47 m, 1451.89 w, 1422.63 w, 1396.98 w, 1350.55 w, 1293.02 w, 1277.73 w, 1254.25 m, 1185.44 m, 1158.66 w, 1114.40 m, 1074.53 m, 1044.93 w, 1025.07 w, 968.93 w, 932.97 w, 900.44 m, 879.81 m, 855.73 m, 840.94 s, 793.89 m, 759.80 s, 694.84 s, 654.21 w, 627.54 w.

HRMS (MALDI, DCTB matrix): calcd. for [C₅₄H₄₀N]⁺ m/z 702.3161; found 702.3155 (100 %), 703.3189 (59.12 %), 704.3222 (17.16 %), 705.3256 (3.26 %), 706.3289 (0.46 %).

[Pt(Me)₂(^Ftrop₂NH)] (K24)MF = C₃₂H₂₅F₄NPt

MW = 694.16 g/mol

mp > 160 °C decomposes



K24 was prepared from ^Ftrop₂NH (**133**) (MW= 469.5 g mol⁻¹, 100 mg, 0.21 mmol) and [Pt(μ²-SMe₂)Me₂]₂ **xx** (MW= 574.6 g mol⁻¹, 61 mg, 0.12 mmol) in CH₂Cl₂ following the same procedure for [Pt(Me)₂(trop₂NH)] (**K20**). The product was isolated as yellow-greenish powder (95 mg, 65% yield).

¹H NMR (300.1 MHz, CD₂Cl₂): δ = 0.074 (s, 3H, ²J_{PtH} = 69.69 Hz, CH₃), 0.074 (s, 3H, ²J_{PtH} = 66.15 Hz, CH₃), 3.47 (s, 2H, ²J_{PtH} = 20.3 Hz, NH), 3.97 (d, 2H, ³J_{HH} = 9.29 Hz, ¹J_{PtH} = 32.3 Hz, CH olefin), 4.07 (d, 1H, ³J_{HH} = 9.29 Hz, ¹J_{PtH} = 37.3 Hz, CH olefin), 4.71 (s, 2H, ³J_{PtH} = 21.9 Hz, CH benzylic), 6.68 (dt, 2H, ³J_{HH} = 8.6 Hz, J_{HF} = 2.7 Hz, CH ar), 6.76 (dd, 2H, ³J_{HH} = 9.5 Hz, J_{HF} = 2.7 Hz, CH ar), 6.87 – 7.05 (m, 6H, CH ar), 7.42 (dd, 2H, ³J_{HH} = 8.6 Hz, J_{HF} = 5.9 Hz, CH ar).

¹³C {¹H} NMR (75.5 MHz, CD₃CN): δ = -17.78 (s, CH₃), -7.54 (s, CH₃), 55.62 (s, ¹J_{PtC} = 75.8 Hz, CH olefin), 61.27 (s, ¹J_{PtC} = 158.07 Hz, CH olefin), 68.33 (s, CH benzylic), 114.56 (d, J_{FC} = 21.02 Hz, CH ar), 114.83 (d, J_{FC} = 22.5 Hz, CH ar), 115.5 (d, J_{FC} = 21.2 Hz, CH ar), 116.1 (d, J_{FC} = 22.5 Hz, CH ar), 130.3 (d, J_{FC} = 7.9 Hz, CH ar), 131.1 (d, J_{FC} = 7.9 Hz, CH ar), 131.5 (d, J_{FC} = 2.9 Hz, C quart), 133.5 (d, J_{FC} = 7.3 Hz, C quart), 134.3 (d, J_{FC} = 3.1 Hz, C quart), 137.5 (d, J_{FC} = 7.3 Hz, C quart), 160.3 (d, J_{FC} = 240.9 Hz, C-F), 160.4 (d, J_{FC} = 242.6 Hz, C-F).

¹⁹⁵Pt NMR (64.6 MHz, CD₂Cl₂): δ = - 4220

¹⁹F NMR (188.3 MHz, CD₂Cl₂): δ = - 120 (s, 2F), -117 (s, 2F).

ATR IR (neat cm⁻¹): 3651.82 w, 2892.03 w, 1897.88 w, 1610.31 m, 1588.33 m, 1494.96 s, 1452.59 m, 1311.55 m, 1267.00 m, 1233.58 s, 1152.33 s, 1116.29 w, 1104.20 w, 1086.58 w, 1056.91 w, 979.75 m, 933.43 s, 874.18 m, 848.60 w, 823.44 m, 809.83 s, 796.18 s, 744.09 m, 723.68 w, 658.50 w, 635.48 w.

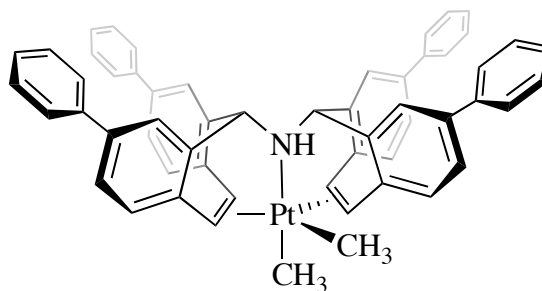
HRMS (MALDI, DCTB matrix): calcd. for $[\text{C}_{31}\text{H}_{22}\text{F}_4\text{Npt}]^+$ m/z 679.1336; found 679.1345 (100 %), 678.1322 (0.72 %), 680.1351 (86.44 %), 681.1378 (24.79 %), 682.1375 (19.84 %), 683.1410 (5.55 %), 684.1459 (0.96 %).

$[\text{Pt}(\text{P}^{\text{h}}\text{trop}_2\text{NH})\text{Me}_2]$ (**K25**)

MF = $\text{C}_{56}\text{H}_{45}\text{Npt}$

MW = 927.04 g/mol

mp = 220 °C decomposes



K25 was prepared from $\text{P}^{\text{h}}\text{trop}_2\text{NH}$ (**139**) (MW= 701.9 g mol^{-1} , 160 mg, 0.23 mmol) and $[\text{Pt}(\mu^2\text{-SMe}_2)\text{Me}_2]_2$ **xx** (MW= 574.6 g mol^{-1} , 65 mg, 0.11 mmol) in CH_2Cl_2 following the same procedure for $[\text{Pt}(\text{Me})_2(\text{trop}_2\text{NH})]$ (**K20**). The product was isolated as yellow powder (115 mg, 54% yield).

^1H NMR (300.1 MHz, CD_2Cl_2): δ = 0.21 (s, 3H, $^2J_{\text{PtH}} = 68.35$ Hz, CH_3), 0.27 (s, 3H, $^2J_{\text{PtH}} = 66.0$ Hz, CH_3), 2.92 (s, 1H, $^2J_{\text{PtH}} = 24$ Hz, NH), 4.15 (br d, 2H, $^3J_{\text{HH}} = 9.8$ Hz, CH olefin), 4.25 (br d, 2H, $^3J_{\text{HH}} = 9.8$ Hz, CH olefin), 4.91 (s, 2H, $^3J_{\text{PtH}} = 20.5$ Hz, CH benzylic), 7.05 (d, 2H, $J_{\text{HH}} = 7.9$ Hz, CH ar), 7.15 (m, 13H, CH ar), 7.35 (m, 2H, CH ar), 7.44 (m, 6H, CH ar), 7.57 (m, 9H, CH ar).

$^{13}\text{C}\{^1\text{H}\}$ NMR (75.5 MHz, CD_2Cl_2): δ = -13.98 (s, CH_3), -7.57 (s, CH_3), 57.2 (s, CH olefin), 62.8 (s, CH olefin), 71.9 (s, CH benzylic), 125.8 (s, CH ar), 126.31 (s, CH ar phenyl), 126.4 (s, CH ar), 126.7 (s, CH ar phenyl), 126.8 (s, CH ar), 127.2 (s, CH ar), 127.23 (s, CH ar), 127.8 (s, CH ar), 128.2 (s, CH ar phenyl), 128.7 (s, CH ar), 129.4 (s, CH ar), 132.4 (s, C quart), 134.4 (s, C quart), 136.5 (s, C quart), 136.9 (s, C quart), 137.6 (s, C quart), 138.6 (s, C quart), 139.9 (s, C quart).

^{195}Pt NMR (64.6 MHz, CD_2Cl_2): δ = - 4210

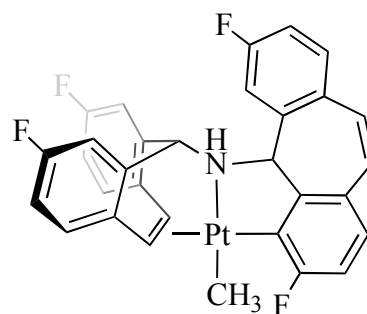
ATR IR (neat cm^{-1}): 3237.69 w, 2877.27 w, 1937.92 w, 1655.92 w, 1599.00 m, 1561.41 w, 1509.11 w, 1480.90 s, 1458.44 w, 1429.94 w, 1276.34 w, 1253.97 w, 1219.54 w, 1178.70 m, 1139.99 w, 1121.22 w, 1059.33 m, 1024.43 m, 999.12 w, 981.92 w, 892.33 m, 874.26 m, 848.37 m, 826.39 m, 785.98 w, 765.82 m, 755.25 s, 746.06 s, 718.88 w, 691.56 s, 671.45 m, 655.39 m, 630.04 w, 616.70 w.

HRMS (MALDI, DCTB matrix): calcd. for $[\text{C}_{55}\text{H}_{42}\text{NPt}]^+$ m/z 911.2965; found 911.2964 (100 %), 912.2979 (94.85 %), 913.3005 (41.31 %), 914.3010 (23.68 %), 914.3010 (23.68 %), 915.3032 (9.90 %), 916.3061 (2.63 %), 917.3093 (0.49 %), 908.2922 (1.46 %), 909.2956 (0.88 %), 910.2939 (61.70 %).

[Pt(^FtropNHortho-^Ftrop)Me] (K26)

MF = $\text{C}_{31}\text{H}_{21}\text{F}_4\text{NPt}$

MW = 678.58 g/mol



K26 is prepared from $[\text{Pt}(\text{Me})_2(\text{Ftrop}_2\text{NH})]$ (**K24**) following the same procedure reported for $[\text{Pt}(\text{Me})(\text{tropNHortho-trop})]$ (**K22**).

^1H NMR (500.2 MHz, CD_2Cl_2): δ = 1.06 (d, 3H, $^2J_{\text{PtH}} = 80.5$ Hz, $^4J_{\text{HF}} = 5.3$ Hz, CH_3), 4.49 (d, 1H, $^3J_{\text{HH}} = 10.8$ Hz, CH benzylic not coordinated), 4.72 (d, 1H, $^3J_{\text{HH}} = 10.8$ Hz, $^2J_{\text{HPt}} = 39.6$ Hz, NH), 5.26 (d, 1H, $^3J_{\text{HH}} = 8.99$ Hz, $^2J_{\text{PtH}} = 32.3$, CH olefin), 5.33 (d, 1H, $^2J_{\text{HPt}} = 19.8$ Hz, CH benzylic), 5.55 (d, 1H, $^3J_{\text{HH}} = 8.99$ Hz, $^2J_{\text{PtH}} = 40.9$, CH olefin), 6.76 (d, 1H, $^3J_{\text{HH}} = 11.9$ Hz, CH olefin not coordinated), 6.78 (m, 2H, CH ar), 6.93 (d, 1H, $^3J_{\text{HH}} = 11.9$ Hz, CH olefin not coordinated), 7.00 (m, 2H, CH ar), 7.11 (dt, 1H, $J_{\text{HF}} = 2.8$ Hz, $J_{\text{HF}} = 8.3$, CH ar), 7.17 (m, 2H; CH ar), 7.26 (dt, 1H, $J_{\text{HF}} = 2.7$ Hz, $J_{\text{HF}} = 8.4$ Hz, CH ar), 7.43 (dd, 1H, $J_{\text{HF}} = 6.2$ Hz, $J_{\text{HF}} = 8.6$ Hz, CH ar), 7.57 (dd, 1H, $J_{\text{HF}} = 7.6$ Hz, $J_{\text{HF}} = 8.6$ Hz, CH ar), 7.73 (dd, 1H, $J_{\text{HF}} = 8.6$ Hz, $J_{\text{HF}} = 5.7$ Hz, CH ar).

$^{13}\text{C}\{^1\text{H}\}$ NMR (125.8 MHz, CD_2Cl_2 , 298K): δ = -15.95 (s, CH_3), 64.47 (s, CH benzylic not coordinated), 65.72 (s, CH benzylic), 79.78 (s, CH olefin), 84.97 (s, CH olefin), 109.29 (d, $J_{\text{CF}} = 24.6$ Hz, CH olefin not coordinated), 113.63 (d, $J_{\text{CF}} = 37.7$ Hz, CH ar), 114.88 (d, $J_{\text{CF}} = 21.4$ Hz, CH ar), 115.35 (d, $J_{\text{CF}} = 22.7$ Hz, CH ar), 116.962 (d, $J_{\text{CF}} = 21.2$ Hz, CH ar), 116.97 (d, $J_{\text{CF}} = 21.1$ Hz, CH ar), 117.64 (d, $J_{\text{CF}} = 22.6$ Hz, CH ar), 128.00 (s, CH olefin not coordinated), 129.67 (d, $J_{\text{CF}} = 8.6$ Hz, CH ar), 130.96 (d, $J_{\text{CF}} = 8.4$ Hz, CH ar), 131.28 (d, $J_{\text{CF}} = 8.3$ Hz, CH ar), 132.17 (d, $J_{\text{CF}} = 8.3$ Hz, CH ar), 132.29 (s, CH olefin not coordinated), 136.06 – 137.34 (C quart), 159.18 – 164.86 (C-F).

^{195}Pt NMR (64.6 MHz, CD_2Cl_2 , 298K): $\delta = -3563$.

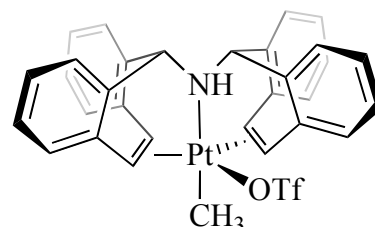
^{19}F NMR (188.3 MHz, CD_2Cl_2): $\delta = -92.49$ (s, 1F, $^3J_{\text{PtF}} = 179$ Hz, F metaPt), -112.28 (s, 1F), -113.26 (s, 1F), -113.37 (s, 1F).

[Pt(OTf)(Me)(trop₂NH)] (K27)

MF = $\text{C}_{32}\text{H}_{26}\text{F}_3\text{NO}_3\text{PtS}$

MW = 756.69 g/mol

mp = 210 °C decomposes



To a solution of $[\text{Pt}(\text{Me})_2(\text{trop}_2\text{NH})]$ (**K20**) (100 mg, 0.16 mmol) in 30 ml CH_2Cl_2 is slowly added HOTf (MW= 150.07 g mol^{-1} , $d = 1.696$ g ml^{-1} , 15 μl , 1 eq). The solution colour turns from yellow to red and evolution of gas (methane) is observed. The solution is stirred at room temperature for 1 hour. The volatiles are removed under reduced pressure and the solid is washed with Et_2O (5 x 1 ml) until pH neutral. The product is obtained as yellow solid (91 mg, 75% yield).

^1H NMR (400.1 MHz, CD_3CN , 298 K): $\delta = 0.67$ (s, 3H, $^2J_{\text{PtH}} = 58.8$ Hz, CH_3 axial), 4.55 (s, 1H, $^2J_{\text{PtH}} = 28.55$ Hz, NH), 4.97 (d, 2H, $^3J_{\text{HH}} = 9.2$ Hz, $^2J_{\text{PtH}} = 36.4$ Hz, CH olefin), 5.5 (s, 2H, $^2J_{\text{PtH}} = 24.8$ Hz, CH benzylic), 5.9 (d, 2H, $^3J_{\text{HH}} = 9.2$ Hz, $^2J_{\text{PtH}} = 64$ Hz, CH olefin), 6.76 (d, 2H, $^3J_{\text{HH}} = 7.2$ Hz, CH ar), 6.82 (m, 2H, CH ar), 6.88 (d, 4H, $^3J_{\text{HH}} = 4$ Hz, CH ar), 7.04 (m, 4H, CH ar), 7.24 (t, 2H, $^3J_{\text{HH}} = 7.6$ Hz, CH ar), 7.4 (d, 2H, $^3J_{\text{HH}} = 7.6$ Hz, CH ar).

$^{13}\text{C}\{^1\text{H}\}$ NMR (100.6 MHz, CD_3CN , 298K): $\delta = -8.6$ (s, $^1J_{\text{PtC}} = 547$ Hz, CH_3 axial), 69.53 (s, CH benzylic), 75.7 (s, $^1J_{\text{PtC}} = 214.5$ Hz, CH olefin), 76.23 (s, $^1J_{\text{PtC}} = 105.7$ Hz, CH olefin), 128.45 (s, CH ar), 128.5 (s, CH ar), 128.93 (s, CH ar), 128.98 (s, CH ar), 129.1 (s, CH ar), 129.3 (s, CH ar), 129.8 (s, CH ar), 130.8 (s, $J_{\text{PtH}} = 11.4$ Hz, CH ar), 132.2 (s, $J_{\text{PtH}} = 56.9$ Hz, C quart), 134.7 (s, $J_{\text{PtH}} = 19.2$ Hz, C quart), 135.3 (s, $J_{\text{PtH}} = 31.8$ Hz, C quart), 136.8 (s, $J_{\text{PtH}} = 14.2$ Hz, C quart).

^{195}Pt NMR (64.6 MHz, CD_3CN , 298K): $\delta = -4752$

^{19}F NMR (188.3 MHz, CD_3CN , 298K): $\delta = -77.89$ (s, $-\text{SO}_3\text{CF}_3$)

^{15}N NMR (40.55 MHz, CD_3CN , 298K): $\delta = 98.44$

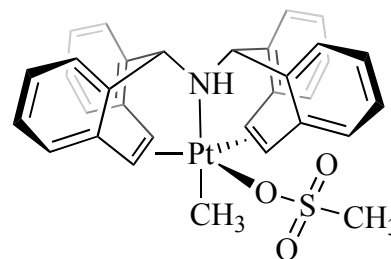
ATR IR (neat cm⁻¹): 2972.08 w, 2899.99 w, 2161.98 w, 1602.70 w, 1492.26 m, 1421.05 w, 1348.69 w, 1325.80 w, 1277.86 w, 1237.22 s, 1224.55 m, 1172.49 m, 1140.30 s, 1112.71 w, 1025.52 m, 1014.79 s, 992.12 m, 951.21 w, 904.88 w, 829.19 m, 782.60 w, 752.98 s, 744.05 s, 730.07 m, 703.99 w, 670.29 w, 645.87 w, 619.55 w, 606.86 m.

[Pt(OMs)(Me)(trop₂NH)] (**K28**)

MF = C₃₂H₂₈NO₃PtS

MW = 702.72 g/mol

mp = 220 °C decomposes



K28 was prepared from [Pt(Me)₂(trop₂NH)] (**K20**) (100 mg, 0.16 mmol) in 30 ml CH₂Cl₂ and HOMs (MW= 96.10 g mol⁻¹, d= 1.481 g ml⁻¹, 11 μl, 0.17 mmol), following the same procedure reported for [Pt(OTf)(Me)(trop₂NH)] (**K27**). The product was recrystallized from CH₂Cl₂ and hexane, yellow crystals grew overnight (94 mg, 83% yield).

¹H NMR (300.1 MHz, CDCl₃, 298 K): δ = 0.85 (s, 3H, ²J_{PtH} = 54 Hz, CH₃ axial), 2.00 (s, 3H, SO₃CH₃), 4.94 (d, 2H, ³J_{HH} = 9.0 Hz, ²J_{PtH} = 33 Hz, CH olefin), 5.27 (s, 2H, ²J_{PtH} = 25.8 Hz, CH benzylic), 6.86 (d, 2H, ³J_{HH} = 9.0 Hz, ²J_{PtH} = 89.1 Hz, CH olefin), 6.89 (dt, 2H, ³J_{HH} = 8.2 Hz, ³J_{HH} = 1.4 Hz, CH ar), 7.00 (m, 4H, CH ar), 7.11 (d, 2H, ³J_{HH} = 7.2 Hz, CH ar), 7.23 (m, 2H, CH ar), 7.36 (m, 4H, CH ar), 7.47 (d, 2H, ³J_{HH} = 7.2 Hz, CH ar).

¹³C{¹H} NMR (75.5 MHz, CDCl₃, 298K): δ = -3.43 (s, ¹J_{PtC} = 568 Hz, CH₃ axial), 71.16 (s, CH benzylic), 75.94 (s, ¹J_{PtC} = 234 Hz, CH olefin), 78.99 (s, ¹J_{PtC} = 105.1 Hz, CH olefin), 127.5 (s, CH ar), 127.7 (s, CH ar), 127.9 (s, CH ar), 128.5 (s, CH ar), 128.7 (s, CH ar), 128.9 (s, J_{PtH} = 11 Hz, CH ar), 130.3 (s, J_{PtH} = 13.8 Hz, CH ar), 130.4 (s, CH ar), 132.9 (s, 1C, J_{PtH} = 63.2 Hz, C quart), 134.3 (s, 1C, J_{PtH} = 16.6 Hz, C quart), 135.5 (s, 1C, J_{PtH} = 34.8 Hz, C quart), 136.2 (s, 1C, J_{PtH} = 14.2 Hz, C quart).

¹⁹⁵Pt NMR (64.3 MHz, CDCl₃): δ = - 4371.

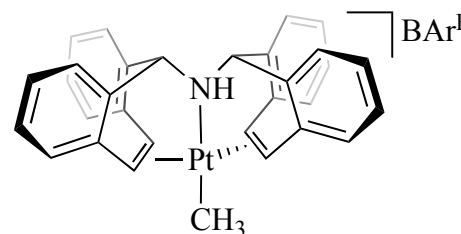
ATR IR (neat cm⁻¹): 3662.94 w, 3047.37 w, 2968.43 w, 2901.38 w, 1602.24 w, 1492.89 m, 1459.51 w, 1420.96 w, 1350.31 w, 1326.79 w, 1305.97 w, 1278.86 w, 1261.22 m, 1236.08 s, 1223.96 s, 1170.39 m, 1140.20 s, 1113.79 w, 1044.01 w, 1025.90 s, 1014.91 s, 993.57 m, 957.59 w,

948.11 w, 906.22 w, 880.19 w, 829.83 m, 800.96 w, 783.11 w, 764.94 m, 752.20 s, 742.36 s, 731.50 s, 702.96 m, 645.91 w, 619.85 w, 607.18 m.

[Pt(Me)(trop₂NH)]BAr^F (**K29**)

MF = C₆₃H₃₈BF₂₄NPt

MW = 1470.83 g/mol



K29 was prepared under inert condition from [Pt(Me)₂(trop₂NH)] (**K20**) (100 mg, 0.16 mmol) in 20 ml dry THF and HOEt₃BAr^F (MW= 938.15 gmol⁻¹, 151 mg, 1 eq), following the same procedure reported for [Pt(OTf)(Me)(trop₂NH)] (**K27**). The product was recrystallized from THF and hexane; yellow crystals grew overnight (186 mg, 79% yield).

¹H NMR (700.1 MHz, [D₈] THF): δ = 0.95 (s, 3H, ²J_{PtH} = 55.5 Hz, CH₃), 4.79 (s, 1H, ²J_{Pt} = 28.1 Hz, NH), 5.24 (d, 2H, ³J_{HH} = 9.1 Hz, ²J_{PtH} = 34.7 Hz, CH olefin), 5.81 (s, 2H, ³J_{PtH} = 20.5 Hz, CH benzylic), 6.91 (d, 2H, ³J_{HH} = 9.1 Hz, ²J_{PtH} = 94.2 Hz, CH olefin), 6.99 (dt, 2H, J_{HH} = 0.8 Hz, J_{HH} = 7.7 Hz, CH ar), 7.15 (t, 2H, J_{HH} = 7.1 Hz, CH ar), 7.17 (d, 2H, J_{HH} = 7.2 Hz, CH ar), 7.33 (d, 2H, J_{HH} = 7.6 Hz, CH ar), 7.36 (dt, 2H, J_{HH} = 7.4 Hz, J_{HH} = 1.1 Hz, CH ar), 7.40 (dt 2H, J_{HH} = 1.2 Hz, J_{HH} = 7.5 Hz, CH ar), 7.50 (br d, 2H, J_{HH} = 7.1 Hz, CH ar), 7.54 (d, 2H, J_{HH} = 7.6 Hz, CH ar), 7.63 (m, 4H, CH ar), 7.84 (m, 8H, CH ar).

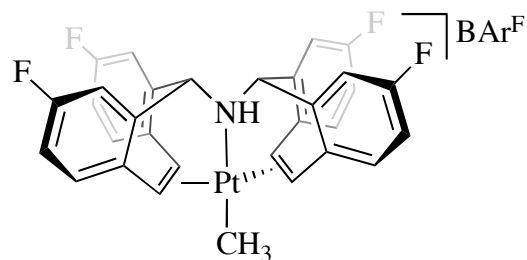
¹³C{¹H} NMR (176.1 MHz, [D₈] THF): δ = - 5.72 (s, 3H, ¹J_{PtC} = 583.7 Hz, CH₃), 70.84 (s, 2H, CH benzylic), 82.32 (s, ¹J_{PtC} = 105.4 Hz, CH olefin), 87.95 (s, ¹J_{PtC} = 191.7 Hz, CH olefin), 117.2 (s, CH ar para BAr^F), 124.60 (q, ¹J_{BC} = 272.1 Hz, C-F₃ BAr^F), 127.95 (s, J_{PtC} = 39.9 Hz, CH ar), 128.23 (s, CH ar), 128.79 (s, CH ar), 128.91 (s, CH ar), 128.98 (br s, CH ar), 129.16 (br s, CH ar), 129.36 (br s, C-CF₃ BAr^F), 129.61 (br s, CH ar), 130.78 (s, CH ar), 134.64 (s, CH ar ortho BAr^F), 133.01 (s, J_{PtC} = 70.2 Hz, C quart), 133.64 (s, C quart), 135.63 (s, J_{PtC} = 38.7 Hz, C quart), 136.53 (s, C quart), 161.85 (q, J_{CF} = 50.5 Hz, C-B BAr^F).

¹⁹F NMR (188.3 MHz, [D₈] THF): δ = - 62.75 (s, 24F, BAr^F).

[Pt(Me)(^Ftrop₂NH)]BAr^F (K30)

MF = C₆₃H₃₄BF₂₈NPt

MW = 1542.79 g/mol



K30 was prepared under inert condition from [Pt(Me)₂(^Ftrop₂NH)] (**K24**) (100 mg, 0.14 mmol) in 20 ml dry THF and HOEt₃BAr^F (MW= 938.15 gmol⁻¹, 135 mg, 1 eq), following the same procedure reported for [Pt(OTf)(Me)(trop₂NH)] (**K27**). The product was recrystallized from THF and hexane; yellow crystals grew after few days (216 mg, 66% yield).

¹H NMR (700.1 MHz, CD₂Cl₂): δ = 1.08 (s, 3H, ²J_{PtH} = 61.67 Hz, CH₃), 3.44 (s, 2H, ²J_{PtH} = 29.1 Hz, NH), 5.59 (d, 2H, ³J_{HH} = 8.5 Hz, ¹J_{PtH} = 39.1 Hz, CH olefin), 5.72 (s, 2H, ³J_{PtH} = 20.8 Hz, CH benzylic), 6.93 (dt, 2H, ³J_{HH} = 8.1 Hz, J_{HF} = 2.5 Hz, CH ar), 7.06 (dd, 2H, ³J_{HH} = 8.5 Hz, J_{HF} = 2.4 Hz, CH ar), 7.22 (d, 2H, ³J_{HH} = 8.5 Hz, ¹J_{PtH} = 91.2 Hz, CH olefin), 7.26 (dt, 2H, ³J_{HH} = 8.1 Hz, J_{HF} = 2.5 Hz, CH ar), 7.29 (dd, 2H, ³J_{HH} = 8.3 Hz, J_{HF} = 2.5 Hz, CH ar), 7.50 – 7.47 (m, 4H, CH ar), 7.6 (s, 4H, CH ar BAr^F), 7.78 (s, 8H, CH ar BAr^F).

¹³C{¹H} NMR (176.04 MHz, CD₂Cl₂): δ = -4.28 (s, CH₃), 70.93 (s, CH benzylic), 87.36 (br s, CH olefin), 98.97 (br s, CH olefin), 115.71 (d, J_{FC} = 23.41 Hz, CH ar), 116.96 (d, J_{FC} = 21.4 Hz, CH ar), 117.4 (m, CH ar), 117.48 (s, CH BAr^F), 118.55 (d, J_{FC} = 23.8 Hz, CH ar), 124.59 (q, ¹J_{BC} = 272.5 Hz, C-F₃ BAr^F), 128.9 (m, C-CF₃ BAr^F), 130.1 (br s, C quart), 131.55 (d, J_{FC} = 8.9 Hz, CH ar), 132.22 (d, J_{FC} = 8.5 Hz, CH ar), 134.80 (s, CH BAr^F), 135.7 (d, J_{FC} = 7.7 Hz, C quart), 136.6 (d, J_{FC} = 8.8 Hz, C quart), 161.75 (q, J_{CF} = 50.1 Hz, C-B BAr^F), 162.9 (d, J_{FC} = 256.7 Hz, C-F), 163.9 (d, J_{FC} = 254.3 Hz, C-F).

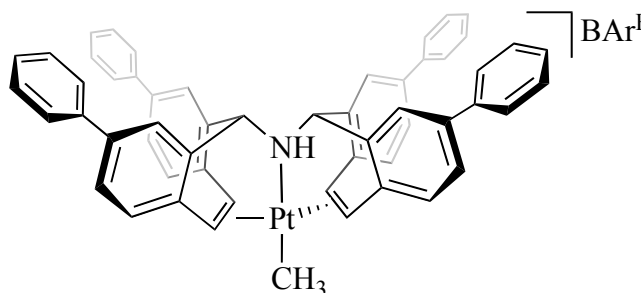
¹⁹⁵Pt NMR (64.6 MHz, CD₂Cl₂): δ = - 4601.

¹⁹F NMR (188.3 MHz, CD₂Cl₂): δ = - 62.75 (s, 24F, BAr^F), - 106.33 (br s, 2F, ^Ftrop), -108.25 (s, 2F, ^Ftrop).

[Pt(Me)(^{Ph}trop₂NH)]BAr^F (K31)

MF = C₈₇H₅₄BF₂₄NPt

MW = 1775.22 g/mol



K31 was prepared under inert condition from [Pt(Me)₂(^{Ph}trop₂NH)] (**K25**) (100 mg, 0.11 mmol) in 20 ml dry THF and HOEt₃BAr^F (MW= 938.15 gmol⁻¹, 101 mg, 1 eq), following the same procedure reported for [Pt(OTf)(Me)(trop₂NH)] (**K27**). The product was obtained as yellow powder after removal of the solvent (155 mg, 81% yield).

¹H NMR (700.1 MHz, CD₂Cl₂): δ = 1.19 (s, 3H, CH₃), 5.73 (d, 2H, ³J_{HH} = 8.4 Hz, ¹J_{PtH} = 41.3 Hz, CH olefin), 6.09 (s, 2H, ³J_{PtH} = 23.8 Hz, CH benzylic), 7.21 – 7.32 (m, 10H, CH ar), 7.41 – 7.67 (24 H, CH ar, CH olefin, CH ar BAr^F), 7.77 – 7.87 (12 H, CH ar, CH ar BAr^F).

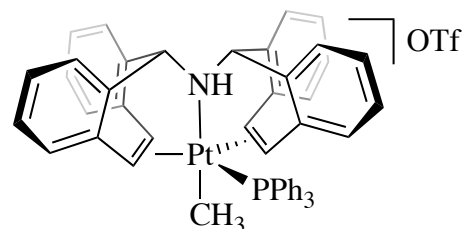
¹³C {¹H} NMR (176.04 MHz, CD₂Cl₂): δ = -4.81 (s, CH₃, ¹J_{PtC} = 599 Hz), 72.71 (s, CH benzylic), 88.28 (s, CH olefin, J_{PtC} = 97 Hz), 100.53 (s, CH olefin, J_{PtC} = 175.3 Hz), 117.51 (CH BAr^F), 126.45 (CH ar), 126.92 (CH ar), 127.00 (CH ar), 127.61 (CH ar), 128.22 (CH ar), 128.49 (CH ar), 128.63 (CH ar), 128.95 (CH ar), 128.17 (CH ar), 129.17 (CH ar), 129.55 (CH ar), 130.05 (CH ar), 131.60 (C quart), 132.54 (C quart), 134.87 (CH BAr^F), 135.43 (C quart), 135.61 (C quart), 138.21 (C quart), 138.57 (C quart), 143.92 (C quart), 143.97 (C quart), 162.02 (q, J_{CF} = 49.8 Hz, C-B BAr^F).

¹⁹F NMR (188.3 MHz, CD₂Cl₂): δ = - 62.75 (s, 24F, BAr^F).

[Pt(Me)(trop₂NH)(PPh₃)]OTf (K32)MF = C₅₃H₄₉F₃NO₃PtS

MW = 1063.07 g/mol

mp = 179 °C



To a solution of [Pt(Me)(trop₂NH)]OTf **K27** (100 mg, 0.13 mmol) in 50 ml CH₂Cl₂ is added PPh₃ (MW= 262.29 gmol⁻¹, 34.7 mg, 1 eq). The solution is stirred for 3 hours at room temperature and its colour slowly turns from yellow to colourless. The volume of the solvent is reduced to 2/3 and the product is crystallized by slow evaporation of CH₂Cl₂. Pale crystals are obtained after few days (123 mg, 89% yield).

¹H NMR (300.1 MHz, CDCl₃, 298 K): δ = 0.95 (d, 3H, ²J_{PtH} = 60.6 Hz, ³J_{PH} = 6.6 Hz, CH₃ axial), 2.49 (s, 1H, ²J_{PtH} = 21.5 Hz, NH), 4.98 (d, 2H, ²J_{PtH} = 12.6 Hz, CH benzylic), 5.44 (m, 4H, CH olefin), 6.76 – 6.86 (m, 8, CH ar), 6.93 – 7.08 (m, 10H, CH ar), 7.15 – 7.20 (m, 4H, CH ar), 7.37 (br m, 6H, CH ar), 7.52 – 7.59 (m, 3H, CH ar).

¹³C{¹H} NMR (75.5 MHz, CDCl₃, 298K): δ = -11.71 (d, ¹J_{PtC} = 562 Hz, ²J_{PC} = 11.3 Hz, CH₃ axial), 68.87 (s, CH benzylic), 71.19 (d, ¹J_{PtC} = 114.21 Hz, ²J_{PC} = 4.7 Hz, CH olefin), 78.39 (m, ²J_{PC} = 32.7 Hz, CH olefin), 127.8 (d, J_{PC} = 1.98 Hz, CH ar), 128.19 (s, CH ar), 128.37 (s, CH ar), 128.60 (s, CH ar), 129.10 (s, CH ar), 129.10 (s, CH ar), 129.16 (d, J_{PC} = 1.52 Hz, CH ar), 129.34 (s, CH ar), 129.48 (s, CH ar), 129.77 (d, J_{PC} = 1.83 Hz, CH ar), 131.17 (d, J_{PC} = 2.3 Hz, CH ar), 130.09 (C quart), 130.17 (C quart), 130.24 (C quart), 132.44 (br d, J_{PC} = 30 Hz, C quart), 133.69 (d, J_{PC} = 3.5 Hz, C quart), 134.08 (d, J_{PC} = 2.4 Hz, C quart), 137.02 (C quart).

¹⁹F NMR (188.3 MHz, CDCl₃, 298K): δ = - 78.8 (s, -SO₃CF₃)

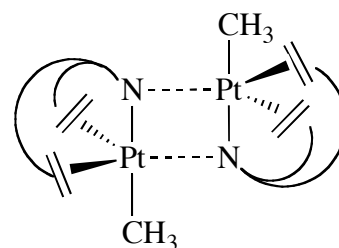
³¹P{¹H} NMR (121.5 MHz, CDCl₃): δ = -15.01 (s, ¹J_{PtP} = 2596 Hz, PPh₃)

¹⁹⁵Pt NMR (64.6 MHz, CDCl₃, 298K): δ = - 3937 (d, ¹J_{PtP} = 2596 Hz)

ATR IR (neat cm⁻¹): 3209.76 w, 2970.36 w, 1966.85 w, 1600.36 w, 1481.88 m, 1435.17 m, 1256.54 s, 1223.35 m, 1149.15 m, 1097.04 m, 1028.26 s, 998.54 w, 893.32 w, 826.74 w, 752.98 s, 695.05 s, 635.35 s.

[Pt(Me)(trop₂N)]₂ (K33)MF = C₆₂H₅₀N₂Pt₂

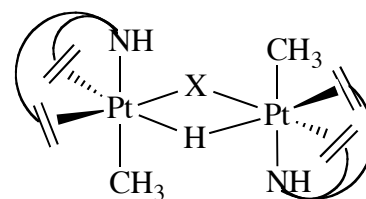
MW = 1213.23 g/mol



In a young NMR tube 20 mg (0.013 mmol) [Pt(Me)(trop₂NH)]BAr^F (**K29**) are dissolved in 0.4 ml of [D₈] THF. To this solution *t*BuOK (MW= 112.21, 1.5 mg) is added. The solution colour turned green immediately after the addition of the base. After few minutes the colour turns yellow. The yield is quantitative.

¹H NMR (500.1 MHz, [D₈] THF): δ = 0.44 (s, ²J_{PtH}= 54.5 Hz, 3H, CH₃), 4.49 (d, ³J_{HH}= 9.2 Hz, ³J_{PtH}= 41.1 Hz, 2H, CH olefin), 4.65 (s, ³J_{PtH}= 29.5 Hz, 2H, CH benzylic), 4.82 (d, ³J_{HH}= 9.2 Hz, ³J_{PtH}= 64.4 Hz, 2H, CH olefin), 6.59 (br s, 2H, CH ar), 6.71 (br s, 4H, CH ar), 6.81 (d, ³J_{HH}= 7.2 Hz, 2H, CH ar), 6.97 (t, ³J_{HH}= 7.5 Hz, 2H, CH ar), 7.09 (t, ³J_{HH}= 6.9 Hz, 2H, CH ar), 7.17 (d, ³J_{HH}= 7.5 Hz, 3H, CH ar), 7.29 (d, ³J_{HH}= 7.5 Hz, 1H, CH ar).

¹³C{¹H} NMR (125.8 MHz, [D₈] THF): δ = -4.37 (s, ¹J_{PtH}= 575.2 Hz, CH₃), 62.20 (s, CH olefin), 68.97 (s, CH olefin), 77.37 (s, CH benzylic), 124.54 (s, CH ar), 125.18 (s, CH ar), 125.52 (s, CH ar), 125.63 (s, CH ar), 126.11 (s, CH ar), 127.61 (s, CH ar), 128.18 (s, CH ar), 130.54 (s, CH ar), 134.33 (s, C quart), 138.23 (s, C quart), 144.38 (s, C quart), 144.86 (s, C quart).

[Pt(X)(trop₂NH)Me(H)]₂ (K34)MF = C₆₂H₅₃N₂Pt₂X

In a young NMR tube 20 mg (0.025 mmol) [Pt(OTf)(Me)(trop₂NH)] (**K27**) are dissolved in 0.5 ml of THF. To this solution Et₃SiH (MW= 116.27 gmol⁻¹, d= 0.728, 4.23 μl) is added. The solution colour turned from pale yellow to deep yellow. The yield is quantitative.

¹H NMR (400.1 MHz, CDCl₃, 240K): δ = 0.66 (s, 3H, CH₃), 3.07 (s, 1H, NH), 3.57 (d, ³J_{HH}= 9.6 Hz, 1H, CH olefin), 4.84 (s, 1H, CH benzylic), 4.97 (d, ³J_{HH}= 8.9 Hz, 1H, CH olefin), 5.11 (d, ³J_{HH}= 8.9 Hz, 1H, CH olefin), 5.47 (s, 1H, CH benzylic), 6.28 (d, 1H, J_{HH}= 7.5 Hz, CH ar), 6.78 (m, 2H, CH ar), 6.83 - 6.89 (m, 3H, CH ar), 6.94 - 7.00 (m, 3H, CH ar), 7.16 (d, 1H, J_{HH}= 7.3 Hz, CH ar), 7.24 (t, 1H, J_{HH}= 7.5 Hz, CH ar), 7.35 (t, 1H, J_{HH}= 7.3 Hz, CH ar), 7.41 (t, 1H, J_{HH}= 7.3 Hz, CH ar), 7.55 - 7.59 (m, 2H, CH ar), 7.76 (d, 1H, J_{HH}= 7.2 Hz, CH ar).

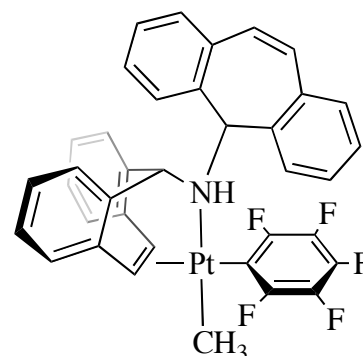
¹³C{¹H} NMR (100.6 MHz, CDCl₃): δ = -7.68 (s, CH₃), 68.73 (br s, CH olefin + CH benzylic), 69.34 (s, CH benzylic), 69.54 (s, CH olefin), 73.89 (s, CH olefin), 74.78 (s, CH olefin), 127.88 (br s, 2C, CH ar), 128.48 (br s, 2C, CH ar), 128.66 (s, CH ar), 128.79 (br s, 2C, CH ar), 129.17 (s, CH ar), 129.28 (s, CH ar), 129.62 (br s, 2C, CH ar), 130.62 (s, CH ar), 130.43 (s, CH ar), 131.08 (br s, 2C CH ar), 131.40 (s, C quart), 132.10 (s, C quart), 134.07 (s, C quart), 134.49 (s, C quart), 134.64 (s, C quart), 135.75 (s, C quart), 139.94 (s, C quart), 136.64 (s, C quart).

¹⁹⁵Pt NMR (64.3 MHz, CDCl₃): δ = - 3841 (s).

[Pt(trop₂NH)Me(C₆F₅)] (K35)

MF = C₃₇H₂₆F₅NPt

MW = 774.68 g/mol



To a solution of **K29** (100 mg, 0.07 mmol) and C₆HF₅ (MW= 168.06 gmol⁻¹, d= 1.51 gmL⁻¹, 37.8 μL, 5 eq) in 20 ml THF is added *t*BuOK (MW= 112.21 gmol⁻¹, 12 mg, 1.5 eq). The colour of the solution changes from yellow to green for few minutes. The volume of the solvent is reduced and hexane is added. After first filtration of the white salt formed the product can be crystallized for a solution of THF/hexane as yellow crystals (51 mg, 68% yield).

¹H NMR (500.1 MHz, [D₈] THF, 220K): δ = 0.51 (s, ²J_{PHH}= 71.1 Hz, 3H, CH₃), 4.50 (s, ³J_{HH}= 10.7 Hz, 1H, NH), 4.59 (s, ³J_{HH}= 10.7 Hz, 1H, CH benzylic not coordinated), 4.86 (s, 1H, CH benzylic), 5.15 (d, ³J_{HH}= 9.18, 1H, CH olefin), 5.67 (d, ³J_{HH}= 9.18, 1H, CH olefin), 6.47 (d, J_{HH}= 7.65 Hz, CH ar), 6.84 (t, J_{HH}= 8.03 Hz, 2H, CH ar), 6.89 (d, J_{HH}= 12.24 Hz, 1H, CH olefin not coordinated), 6.99 (t, J_{HH}= 7.65 Hz, 1H, CH ar), 7.18 (m, 1H, CH ar), 7.24 (d, J_{HH}= 0.02 Hz, 1H, CH ar), 7.34 (d, J_{HH}= 13.77 Hz, 1H, CH ar), 7.35 (d, J_{HH}= 13.77 Hz, 1H, CH ar), 7.39 – 7.47 (m, 4H, CH ar), 7.52 (q, J_{HH}= 7.65 Hz, 2H, CH ar), 7.61 (d, J_{HH}= 7.27 Hz, 1H, CH ar), 7.58 (d, J_{HH}= 7.65 Hz, 1H, CH ar), 7.81 (d, J_{HH}= 7.65 Hz, 1H, CH ar).

¹³C{¹H} NMR (125.8 MHz, [D₈] THF, 220K): δ = -13.2 (s, CH₃), 66.46 (s, CH benzylic), 69.78 (s, CH benzylic not coordinated), 77.73 (s, CH olefin), 88.38 (s, CH olefin), 127.13 (s, CH ar), 127.55 (s, CH ar), 127.92 (s, CH ar), 128.22 (s, CH ar), 128.29 (s, CH ar), 128.77 (s, CH ar), 128.83 (s, CH ar), 129.05 (s, CH ar), 129.15 (s, CH ar), 129.25 (s, CH ar), 129.32 (s, CH ar), 129.54 (s, olefin not coordinated), 129.52 (s, CH ar), 131.26 (s, CH ar), 131.61 (s, CH ar), 131.76 (s, CH olefin not coordinated), 131.94 (s, C quart), 133.23 (s, C quart), 133.59 (s, C quart), 135.65 (s, C quart), 135.97 (s, C quart), 135.99 (s, C quart), 136.65 (s, C quart), 137.46 (s, C quart), C-F quart not detected.

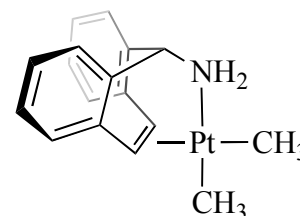
^{19}F NMR (376.4 MHz, $[\text{D}_8]$ THF): $\delta = -115$ (d, $^3J_{\text{FF}} = 32$ Hz, $^3J_{\text{FPt}} = 364$ Hz, *Fortho*), -117 (d, $^3J_{\text{FF}} = 32$ Hz, $^3J_{\text{FPt}} = 469$ Hz, *Fortho*), -163.5 (m, *Fmeta*), -165 (t, $^3J_{\text{FF}} = 20$ Hz, *Fpara*), -167.4 (m, *Fmeta*).

[Pt(tropNH₂)Me₂]

MF = C₁₇H₁₉NPt

MW = 432.42 g/mol

mp > 160 °C decomposes



To a solution of [Pt(μ^2 -SMe₂)Me₂]₂ (**116**) (MW= 574.6 gmol⁻¹, 100 mg, 0.17 mmol) in CH₂Cl₂ tropNH₂ (MW= 207.10 gmol⁻¹, 70.4 mg, 2 eq) is added. The solution color changed from colorless to yellow. The volume of the reaction solution is reduced under pressure and hexane is added. The product is isolated as pale yellow powder (119 mg, yield 81%).

^1H NMR (300.1 MHz, CDCl₃, 298 K): $\delta = 0.74$ (s, 3H, $^2J_{\text{PtH}} = 105$ Hz, CH₃), 0.78 (s, 3H, $^2J_{\text{PtH}} = 96$ Hz, CH₃), 2.78 (s, 2H, $^2J_{\text{PtH}} = 30$ Hz, NH), $.28$ (s, 2H, $^2J_{\text{PtH}} = 32.4$ Hz, CH olefin), 5.77 (s, 1H, $^2J_{\text{PtH}} = 27$ Hz, CH benzylic), 7.33 (br m, 6H, CH ar), 7.51 (br m, 2H, CH ar).

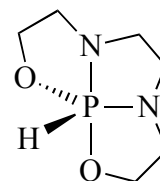
$^{13}\text{C}\{^1\text{H}\}$ NMR (75.5 MHz, CD₂Cl₂): $\delta = -13.1$ (s, $^1J_{\text{PtC}} = 750$ Hz, CH₃), -1.18 (s, $^1J_{\text{PtC}} = 818$ Hz, CH₃), 62.06 (s, $^3J_{\text{PtC}} = 15.4$ Hz, CH benzylic), 81.80 (s, $^1J_{\text{PtC}} = 67.8$ Hz, CH olefin), 127.28 (s, CH ar), 128.35 (s, CH ar), 128.80 (s, CH ar), 128.95 (s, CH ar), 135.63 (s, C quart), 135.75 (s, C quart).

^{195}Pt NMR (64.6 MHz, CD₂Cl₂): $\delta = -3560$.

HRMS (MALDI, DCTB matrix): calcd. for [C₁₆H₁₆NPt]⁺ m/z 417.093; found 417.0927 (100 %).

C₆H₁₃PN₂O₂ (155)MF = C₆H₁₃PN₂O₂

MW = 176.15 g/mol



2,2'-(ethane-1,2-diylbis(azanediy))diethanol (5.0 g, 33 mmol) was suspended in toluene (110 ml). Hexamethylphosphinetriamine (6.2 ml, 33 mmol) was added drop wise and the mixture was refluxed for one hour. The yellowish mixture was filtrated *via* cannula and the solvent was removed under reduce pressure. The row product was purified by distillation at 75 °C under reduced pressure. The pure product was obtained as colorless oil in 49% yield.

¹H NMR (300.1 MHz, CDCl₃, 298 K): δ = 3.13 - 2.95 (br m, CH₂), 3.96 (br m, CH₂), 6.87 (d, J_{PH} = 721 Hz, P-*H*).

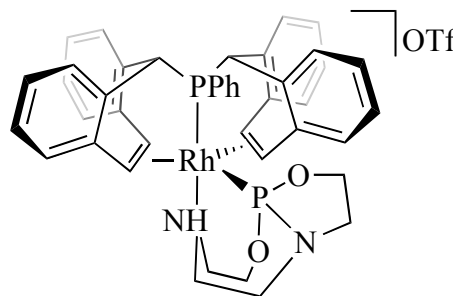
³¹P {¹H} NMR (121.5 MHz, CDCl₃): δ = - 36.92 (s)

³¹P-NMR (121.5 MHz, CDCl₃): δ = - 36.92 (d, J_{HP} = 721 Hz)

***cis*-[Rh(OTf)(trop₂PPh)(P(C₆H₁₃N₂O₂))] (K37)**MF = C₄₃H₄₀F₃N₂O₅P₂RhS

MW = 918.70 g/mol

MP > 220°C (Decomposition)



[RhOTf(trop₂PPh)] (500 mg, 673 μmol) is dissolved in CH₂Cl₂. C₆H₁₂N₂O₂PH (**155**) (118 mg, 673 μmol) is added to the red solution. The solution's color turns immediately yellow and after 30 minutes, a yellow precipitate forms. The yellow precipitate is filtrated, washed two times with hexane and dried over night under vacuum (yield 96%).

¹H NMR (300.1 MHz, CD₂Cl₂, 298 K): δ = 2.72 (br m, 2H, CH₂ HP), 3.15 (br m, 4H, CH₂ HP), 3.50 (br m, 2H, CH₂ HP), 3.91 (br m, 2H, CH₂ HP), 3.93 (d, ²J_{PH} = 14.4 Hz, CH benzylic), 4.31 (ddd, J_{HH} = 5 Hz, J_{HH} = 12.4 Hz, J = 32 Hz, 2H, CH₂ HP), 4.78 (d, ³J_{HH} = 10.2 Hz, CH olefin), 4.99 (d, 1H, ²J_{HP} = 14.4 Hz, CH benzylic), 5.31 (d, ³J_{HH} = 3.7 Hz, 1H, CH olefin), 5.76 (br s, 1H, NH), 6.14 (dd, ³J_{PH} = 7.2 Hz, ³J_{HH} = 16.2 Hz, 1H, CH olefin), 6.35 (dd, ³J_{PH} = 4.8 Hz, ³J_{HH} = 10.8 Hz, 1H, CH olefin), 6.57 (br m, 4H, CH ar), 6.71 (m, 7H CH ar), 6.71 (m, 3H, CH ar), 6.88 (br m, 2H, CH ar), 7.15 (br m, 3H, CH ar), 7.37 (br m, 2H, CH ar).

¹³C{¹H} NMR (75.5 MHz, CD₂Cl₂): δ = 44.9 (s, CH₂ HP); 48.5 (dd, J_{CP} = 13.3 Hz, J_{CP} = 6.6 Hz, CH benzylic), 49.4 (br m, CH₂ HP), 54.0 (br m, CH benzylic), 62.4 (m, CH olefin), 64.8 (dm, J_C = 30 Hz, CH olefin), 65.4 (d, J_{CP} = 6.3 Hz, CH₂ HP), 68.749 (d, J_{CP} = 13.5 Hz, CH₂ HP), 87.1 (dm, J_{CP} = 12 Hz, CH olefin), 91.3 (s br, CH olefin), 125.9 (br, CH ar), 126.5 (br, CH ar), 127.7-127.4 (br, CH ar), 127.9 - 127.8 (br, CH ar), 128.3 - 128.038 (br, CH ar), 128.7-128.6 (br, CH ar), 128.8 (br, CH ar), 129.1-129.1 (br, CH ar), 130.7 - 130.6 (br, CH ar), 130.8 (br, CH ar), 131.3 (br, CH ar), 131.4 (br, CH ar), 131.6 (br, CH ar), 132.2 (br, CH ar), 132.5 - 132.3 (br, CH ar), 132.7 (br, CH ar), 134.0 (m, C quart), 135.0 (s, C quart), 135.9 (m, C quart), 136.6 (m, C quart), 139.8 (m, C quart).

¹⁵N NMR (40.55 MHz, CD₂Cl₂, 298K): δ = -12.

³¹P{¹H} NMR (121.5 MHz, CD₂Cl₂): δ = 137.5 (dd, ¹J_{RhP} = 163.4 Hz, ²J_{PP} = 5.8 Hz, P trop), 152.4 (dd, ¹J_{RhP} = 211.3 Hz, ²J_{PP} = 5.8 Hz, P HP).

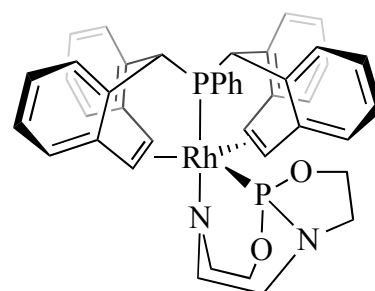
ATR IR (neat cm^{-1}): 3187 w, 3060 s, 2950 w, 2829 w, 1574-1434 m, 1333-1089 s, 1052-626 st, 877 s.

HRMS (MALDI, DCTB matrix): calcd. for $[\text{C}_{42}\text{H}_{40}\text{N}_2\text{O}_2\text{P}_2\text{Rh}]^+$ m/z 769.1620; found m/z (fragment, abundance in %): 769.16 ($[\text{M}^+]$, 100), 770.16 ($[\text{M}^++1]$, 46.54), 771.17 ($[\text{M}^++2]$, 10.98), 772.17 ($[\text{M}^++3]$, 1.75), 773.17 ($[\text{M}^++4]$, 0.21), 593 ($[\text{M}^+] - \text{HP}$).

***trans*-[Rh(OTf)(trop₂PPh)(P(C₆H₁₂N₂O₂))] (K38)**

MF = $\text{C}_{42}\text{H}_{39}\text{N}_2\text{O}_3\text{P}_2\text{Rh}$

MW = 768.62 g/mol



Cis-trop₂PPhRhP(C₆H₁₃N₂O₂) (300 mg, 327 μmol) was solved in THF. By adding potassium *tert*-butoxide (36.7 mg, 327 μmol), the yellow solution gets darker and greenish. The product was not isolated. The yield was quantitative by NMR.

^1H NMR (400.1 MHz, d_8 -THF, 298 K): δ = 2.39 (m, 1H, CH_2 HP), 2.57 (m, 1H, CH_2 HP), 2.86 (m, 1H, CH_2 HP), 2.96 (m, 1H, CH_2 HP), 3.09-3.16 (m, 2H, CH_2 HP), 3.36 (m, 1H, CH_2 HP), 3.47 (m, 2H, CH_2 HP), 3.83 (q, J = 7.6 Hz, 1H, CH_2 HP), 4.15 (quint, J = 8 Hz, 1H, CH_2 HP), 4.29-4.27 (m, 1H, CH_2 HP), 4.28 (d, $^2J_{\text{PH}}$ = 12.8 Hz, CH benzylic), 4.42 (d, $^2J_{\text{PH}}$ = 13.2 Hz, CH benzylic), 4.54 (q, J = 7.2 Hz, 2H, CH olefin), 4.73 (t, J = 8.4 Hz, 1H, CH olefin), 4.96 (t, J = 8.8 Hz, 1H, CH olefin), 6.41 (d, J = 8 Hz, 1H, CH ar), 6.71-6.53 (m, 8H, CH ar), 6.88-6.76 (m, 5H, CH ar), 6.95-6.93 (m, 2H, CH ar), 7.03-7-7.01 (m, 1H, CH ar), 7.39 (t, J = 8.4 Hz, 2H, CH ar), 7.65 (t, J = 9.2 Hz, 2H, CH ar).

$^{13}\text{C}\{^1\text{H}\}$ NMR (75.5 MHz, $[\text{D}_8]$ THF): δ = 45.1 (CH HP), 46.5 (d, J = 7.7 Hz, CH HP), 49.2 (br m, 2 CH HP), 49.3 (CH HP), 50.8-50.6 (br m, CH benzylic), 51.8 (d, J = 18.5 Hz, CH benzylic), 60.3 (d, J = 15.8 Hz, CH HP), 61.7 (m, 2 CH olefin), 65.7 (d, J = 9.6 Hz, CH HP), 66.9 (CH olefin), 67.4 (CH olefin), 123.2 (m, CH ar), 124.6 (d, J = 3.4 Hz, CH ar), 124.8 (CH ar), 124.9 (d, J = 3.1 Hz, CH ar), 126.1 (br m, CH ar), 126.2 (CH ar), 126.6 (d, J = 10.3 Hz, CH ar), 127.9-127.4 (br m, CH ar), 129.3-128.6 (br m, CH ar), 129.6-129.3 (br m, CH ar), 134.6-134.3 (br m, CH ar).

133.2 (d, $J = 12.6$ Hz, CH ar), 133.5 (d, $J = 7.0$ Hz, CH ar), 133.8 (m, C quart), 136.1 (t, C quart), 136.8 (m, C quart), 141.5 (m, C quart).

$^{31}\text{P}\{^1\text{H}\}$ NMR (121.5 MHz, $[\text{D}_8]$ THF): $\delta = 7.8$ (dd, $^1J_{\text{PRh}} = 97.6$ Hz, $^2J_{\text{PP}} = 743.1$ Hz, P HP), 124.1 (dd, $^1J_{\text{PRh}} = 128.5$ Hz, $^2J_{\text{PP}} = 743.1$ Hz, P trop).

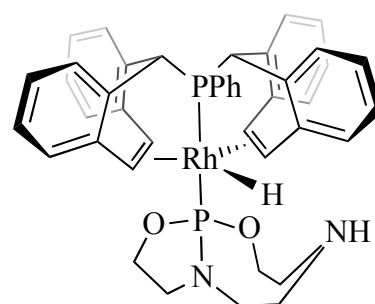
ATR IR (neat cm^{-1}): 2936 w, 2860 s, 1594 - 1408 s, 1247 - 915 s, 839 m, 766 - 640 s.

HRMS (MALDI, DCTB matrix): 769.16 ($\text{M}+\text{H}^+$, 100), 770.16 ($\text{M}+\text{H}^++1$, 46.54), 771.17 ($\text{M}+\text{H}^++2$, 10.98), 772.17 ($\text{M}+\text{H}^++3$, 1.75), 773.17 ($\text{M}+\text{H}^++4$, 0.21), 593 ($\text{M}^+ - \text{HP}$)

***trans*-[Rh(H)(trop₂PPh)(P(C₆H₁₃N₂O₂))] (K40)**

MF = C₄₂H₄₁N₂O₃P₂Rh

MW = 770.64 g/mol



To a THF solution of *trans*-[Rh(OTf)(trop₂PPh)(P(C₆H₁₂N₂O₂))] (20 mg, 26 μmol) was added H₂. The solution's color became lighter. The yield was quantitative by NMR.

^1H NMR (300.1 MHz, $[\text{D}_8]$ THF, 298 K): $\delta = -7.079$ (ddd, $^1J_{\text{RhH}} = 3.0$ Hz, $^2J_{\text{PH}} = 16.3$ Hz, $^1J_{\text{PH}} = 22.3$ Hz, 1H, Rh-H), 1.870 (s, 1H, NH), 2.77 (br m, 2H, CH₂ HP), 3.17 (br m, 3H, CH₂ HP), 3.39 (br m, 1H, CH₂ HP), 3.73 (br m, 1H, CH₂ HP), 4.03 (br m, 3H, CH₂ HP), 4.15 (br m, 1H, CH₂ HP), 4.28 (br m, 1H, CH₂ HP), 4.48 (br m, 4H, CH olefin and CH benzylic), 4.62 (d, $^2J_{\text{HP}} = 4.5$ Hz, CH olefin), 4.71 (d, $^2J_{\text{HP}} = 4.5$ Hz, CH olefin), 6.49 (br m, 4H, CH ar), 6.67 (br m, 10H, CH ar), 7.08 (br m, 5H, CH ar), 7.98 (t, $J = 8.7$ Hz, 2H, CH ar).

$^{13}\text{C}\{^1\text{H}\}$ NMR (75.5 MHz, $[\text{D}_8]$ THF): $\delta = 46.9$ (CH₂ HP), 48.1 (CH₂ HP), 48.5 (CH₂ HP), 48.9 (CH₂ HP), 51.3 - 50.9 (br m, CH₂ HP, CH olefin, CH benzylic) 52.0 (d, $J_{\text{RhC}} = 6.2$ Hz, CH olefin), 52.2 (d, $J_{\text{RhC}} = 6.7$ Hz, CH olefin), 56.6 (d, $J_{\text{PC}} = 4.19$ Hz, CH₂ HP), 58.1 (d, $J_{\text{PC}} = 3.99$ Hz, CH benzylic), 66.6 (CH₂ HP), 121.9 (d, $J = 0.6$ Hz, CH ar), 123.4 (d, $J = 3.2$ Hz, CH ar), 125.6 (d, $J = 1.77$ Hz, CH ar), 126.9 (d, $J = 4.83$ Hz, CH ar), 127.1 (d, $J = 3.1$ Hz, CH ar), 127.8 - 127.6 (br m, CH ar), 128.4 - 128.3 (br m, CH ar), 128.7 (d, $J = 1.5$ Hz, CH ar), 128.7 (d, $J = 1.4$ Hz, CH

ar), 128.9 (d, $J = 2.94$ Hz, CH ar), 129.1 (d, $J = 2.9$ Hz, CH ar), 129.3 (d, $J = 1.06$ Hz, CH ar), 132.1 - 132.3 (m, CH ar), 132.1 - 132.0 (m, C quart), 134.1 (br d, $J = .8$ Hz, CH ar) 135.8 (d, $J = 1.36$ Hz, C quart), 136.0 (d, $J = 1.1$ Hz, C quart), 136.7 (d, $J = 2.8$ Hz, C quart), 143.4 (d, $J = 4.6$ Hz, C quart).

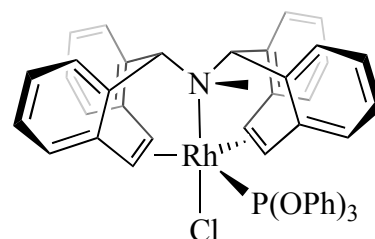
$^{31}\text{P}\{^1\text{H}\}$ NMR (121.5 MHz, $[\text{D}_8]$ THF): 155.9 (dd, $^1J_{\text{PRh}} = 137.4$ Hz, $^1J_{\text{PP}} = 608.8$ Hz, P trop), 142.9 (dd, $^1J_{\text{PRh}} = 163.2$ Hz, $^1J_{\text{PP}} = 608.8$ Hz, P_{HP}).

[RhCl(trop₂NMe)(P(OPh)₃)]

MF = C₄₀H₄₀ClNO₃PRh

MW = 860.18 g/mol

MP > 220 °C (Decomposition)



To a solution of $[\text{Rh}(\mu\text{-Cl})(\text{trop}_2\text{NMe})_2]$ (200 mg, 0.23 mmol) in CH_2Cl_2 is added AgOTf (MW = 256.93 g mol^{-1} , 60 mg). The solution is allowed to stirred for 2 hours at room temperature and the white solid (AgCl) is filtered off. The product was recrystallized from a solution of CH_2Cl_2 /hexane as dark orange crystals in 69% yield.

^1H NMR (300.1 MHz, CDCl_3 , 298 K): $\delta = 2.08$ (s, 3H, NCH_3), 3.81 (s, 2H, CH benzylic), 5.51 (dd, $^3J_{\text{HH}} = 9.8$ Hz, $^3J_{\text{HP}} = 27.0$ Hz, 4H, CH olefin), 7.24 - 6.74 (br m, 31 H, CH ar).

$^{13}\text{C}\{^1\text{H}\}$ NMR (75.5 MHz, CDCl_3): $\delta = 67.7$ (br m, CH olefin), 72.9 (br m, CH olefin), 82.9 (CH benzylic), 121.2 (d, $^3J_{\text{PC}} = 4.5$ Hz, CH ar, OPh), 124.05 (CH ar, OPh), 125.05 (CH ar), 125.3 (CH ar), 127.12 (CH ar), 128.07 (CH ar), 128.72 (CH ar), 128.9 (CH ar), 129.1 (CH ar), 129.4 (CH ar, OPh), 133.8 (C quart), 135.14 (br s, C quart), 135.4 (C quart), 139.1 (C quart), 152.4 (d, $^2J_{\text{PC}} = 11.3$ Hz, C quart OPh).

$^{31}\text{P}\{^1\text{H}\}$ NMR (121.5 MHz, CDCl_3): 117 - 111 (br m).

ATR IR (neat cm^{-1}): 3014 (C-H s), 1588-1413 (C=C, s), 1224-1004 (C-N s, C-O, P-O s), 893 (P(III)), 766-617 (=C-H).

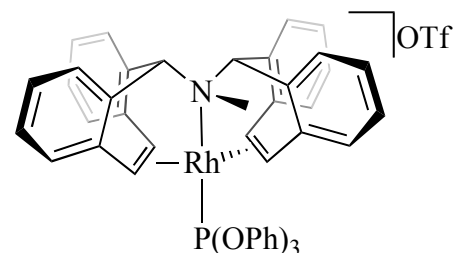
HRMS (MALDI, DCTB matrix): m/z (fragment, abundance in %): 824.18 ($[\text{M}^+]$, 100), 825.18 ($[\text{M}^++1]$, 56.12), 826.19 ($[\text{M}^++2]$, 15.59), 827.19 ($[\text{M}^++3]$, 2.69), 514.1 ($[\text{M}^+] - \text{P(OPh)}_3$).

[Rh(trop₂NMe)(P(OPh)₃)]OTf

MF = C₅₀H₄₀F₃NO₆PRhS

MW = 973.80 g/mol

MP > 220 °C (Decomposition)



[Rh(Cl)(trop₂NMe)(P(OPh)₃)₂] (200 mg, 370 μmol) forms a orange suspension in DCM. After adding P(OPh)₃ (210 μl, 820 μmol) drop wise, the solution gets darker. The solution is allowed to stir for 1.5 hour at room temperature. After this time not everything was in solution. Some more P(OPh)₃ (70 μl, 267 μmol) was added. Half of the solvent was removed under reduced pressure; the solution was then topped with hexane. Dark red crystals grew over night, which were filtrated and dried. The yield was 74%.

¹H NMR (300.1 MHz, [D₈] THF, 298 K): δ = 0.88 (d, J_{HP} = 4.8 Hz, 3H, NCH₃), 5.72 (d, J_{HP} = 8.9 Hz, 2H, CH benzylic), 5.78 (d, ³J_{HH} = 12.4 Hz, 2H, CH olefin), 6.92 (br m, 3H, CH ar), 7.02 (br m, 2H, CH ar), 7.09 (br m, 2H, CH ar), 7.35 - 7.18 (m, 27H, CH olefin and CH ar), 7.47 - 7.38 (br m, 5H, CH ar), 7.66 - 7.58 (br m, 2H, CH ar).

¹³C {¹H} NMR (75.5 MHz, [D₈] THF): δ = 44.2 (NCH₃), 77.9 (br m, CH benzylic and CH olefin), 89.18 (d, J_{RhC} = 12.22 Hz, CH olefin), 115.3 (CH ar), 118.4 (CH ar), 119.9 (CH ar), 120.2 (d, J = 4.83 Hz, CH ar), 120.3 (d, J = 4.83 Hz, CH ar), 122.7 (CH ar), 125.9 (d, J = 1.81 Hz, CH ar), 126.4 (CH ar), 126.6 (CH ar), 126.8 (CH ar), 127.8 (CH ar), 128.2 (CH ar), 129.2 (CH ar), 129.4 (d, J = 1.13 Hz, CH ar), 129.8 (CH ar), 130.3 (d, J = 1.28 Hz, CH ar), 130.5 (CH ar), 131.9 (C quart), 133.8 (C quart), 135.2 (d, J = 2.41 Hz, C quart), 135.3, 136.6 (d, J = 1.36 Hz, C quart), 149.6 (d, J = 2.04 Hz, C quart), 150.4 (s, C quart).

³¹P {¹H} NMR (121.5 MHz, [D₈] THF): 109.7 (d, ¹J_{PRh} = 201.0 Hz, P(OPh)₃).

ATR IR (neat cm⁻¹): 2921 (C-H s), 1732-1425 (C=C, s), 1259-1027 (C-N s, ar C-O, P-O s), 892 (P(III)), 777-635 (=C-H).

HRMS (MALDI, DCTB matrix): 824.18 (M^+ -OTf, 100), 825.18 (M^{+1} -OTf, 53.85), 826.19 (M^{+2} -OTf, 14.81), 827.19 (M^{+3} -OTf, 2.77), 828.19 (M^{+4} -OTf, 0.40), 514.1 (M^+ -OTf - P(OPh)₃).

4.3 Literature

- ¹ T. Büttner, *Dissertation* ETHZ nr. 15503, Zürich, **2004**.
- ² G. Giordano, R.H. Crabtree, *Inorg. Syntheses*, **1990**, 28, 88.
- ³ A.J. Arduengo III, US Patent, 5.077.414.
- ⁴ E.A. Mistyukov, *Mendeleev Commun.*, **2006**, 258.
- ⁵ W.A. Herrmann, L.J. Goossen, G.R.J. Artus, C. Kcher, *Organometallics*, **1997**, 16, 2472.
- ⁶ F. Glorius, G. Altenhoff, R. Goddard, C. Lehmann, *Chem. Commun.*, **2002**, 2704.
- ⁷ Weber W. P.; Gokel G. W., Ugi I. K., *Angew. Chem. Int. Ed.*, **1972**, 6, 530
- ⁸ P. Jutzi, U. Gilge, *J. Organomet. Chem.*, **1983**, 246, 159.
- ⁹ G.S. Hill, M.J. Irwin, C.J. Levy, L.M. Rendina, R.J. Puddephatt, *Inorg. Syntheses*, **1998**, 32, 149.
- ¹⁰ P.K. Byers, A.J. Canty, H. jim, D. Kruis, B.A. Markies, J. Boersma, G. Van Koten, *Inorg. Syntheses*, **1998**, 32, 162.
- ¹¹ T.W. Campbell, R. Ginsig, H. Schmid, *Helvetica Chimica Acta*, **1953**, 186, 1489.
- ¹² J. Thompson, P. Anderson, S. Brichter, T. Lyle, E. Thies, *J. Med. Chem.*, **1990**, 33, 789.
- ¹³ M. Schmeisser, K. Dahmen, P. Sartori, *Chem. Ber.*, **1976**, 100, 1633; b) J. Maletina, V. Orda, L. Yagupolski, *Zh. Org. Khim.*, **1974**, 10, 294,
- ¹⁴ F. Puschmann, Master Thesis, ETHZ.
- ¹⁵ K.N. Gavrilov, V.A. Davankov, *J. Org. Chem.*, **2000**, 613, 148-158.
- ¹⁶ M. Bookhart, B. Grant, A.F. Volpe Jr., *Organometallics*, **1992**, 11, 3920.
- ¹⁷ A.D. Bain, G.J. Duns, *Can. J. Chem.*, **1996**, 74, 819.
- ¹⁸ SAINT, *Reference manual*, Siemens Energy and Automation, Madison, WI, **1994-1996**.
- ¹⁹ G.M. Sheldrick, SADABS, *Empirical Absorption Correction Program*, University of Göttingen, Germany, **1997**.
- ²⁰ G.M. Sheldrick, SHELXS-97, *Program for Crystal Structure Solution*, University of Göttingen, Germany, **1997**.
- ²¹ G.M. Sheldrick, SHELXS-97, *Program for Crystal Structure Refinement*, University of Göttingen, Germany, **1997**.
- ²² W. R. W. P.J. Hay, *J. Chem. Phys.* **1985**, 82, 299.
- ²³ R. D. Gaussian 03, M. J. Frisch, G. W. Trucks, H. B. Schlegel, G. E. Scuseria, M. A. Robb, J. R. Cheeseman, J. A. Montgomery, Jr., T. Vreven, K. N. Kudin, J. C. Burant, J. M. Millam, S. S. Iyengar, J. Tomasi, V. Barone, B. Mennucci, M. Cossi, G. Scalmani, N. Rega, G. A. Petersson, H. Nakatsuji, M. Hada, M. Ehara, K. Toyota, R. Fukuda, J. Hasegawa, M. Ishida, T. Nakajima, Y. Honda, O. Kitao, H. Nakai, M. Klene, X. Li, J. E. Knox, H. P. Hratchian, J. B. Cross, V. Bakken, C. Adamo, J. Jaramillo, R. Gomperts, R. E. Stratmann, O. Yazyev, A. J. Austin, R. Cammi, C. Pomelli, J. W. Ochterski, P. Y. Ayala, K. Morokuma, G. A. Voth, P. Salvador, J. J. Dannenberg, V. G. Zakrzewski, S. Dapprich, A. D. Daniels, M. C. Strain, O. Farkas, D. K. Malick, A. D. Rabuck, K. Raghavachari, J. B. Foresman, J. V. Ortiz, Q. Cui, A. G. Baboul, S. Clifford, J. Cioslowski, B. B. Stefanov, G. Liu, A. Liashenko, P. Piskorz, I. Komaromi, R. L. Martin, D. J. Fox, T. Keith, M. A. Al-Laham, C. Y. Peng, A. Nanayakkara, M. Challacombe, P. M. W. Gill, B. Johnson, W. Chen, M. W. Wong, C. Gonzalez, and J. A. Pople, Gaussian, Inc., Wallingford CT, 2004.
- ²⁴ V. GaussView, Roy Dennington II, Todd Keith, John Millam, Ken Eppinnett

²⁵ a) A. D. Becke, *J. Chem. Phys.* **1993**, 98, 5648; b) J. A. C. J. P. Perdew, S. H. Vosko, K. A. Jackson, M. R. Pederson, D. J. Singh, C. Fiolhais, *Phys. Rev. B* **1992**, 46, 6671.

²⁶ V. GaussView, Roy Dennington II, Todd Keith, John Millam, Ken Eppinnett, W. Lee Hovell, and Ray Gilliland, Semichem. Inc., Shawnee Mission, KS, 2003.

5 Appendix

5.1 List of Abbreviations

Å	Åmstöm (10^{-10} m)
BAr ^F	Tetrakis[(3,5-trifluoromethyl)phenyl]borate
bpma	bis(pyridylmethyl)amine
Cy	cyclohexyl
CH ₂ Cl ₂	dichloromethane
cod	cyclooctadiene
C ₆ D ₆	deuterated benzene
COSY	correlation spectroscopy
Cp*	η^5 -pentamethylcyclopentadienyl
δ	chemical shift
dppe	bis(diphenylphosphino)ethane
dppm	bis(diphenylphosphino)methane
DMSO	dimethylsulfoxide
DMBN	3,7-dimethylenebicyclo-[3.3.1]nonane
ee	enantiomeric excess
GC	gas chromatography
HP	hydridophosphorane
Hz	hertz
HPLC	high pressure liquid chromatography
HMQC	heteronuclear Multiple Quantum Coherence
HMBC	heteronuclear Multiple Bond Correlation
ICy	1,3-dicyclohexylimidazolium chloride
IMe	1,3-dimethylimidazolium iodine
IMes	1,3-dimesityl-4,5-imidazol-2-ylidene
IR	infra red
J	coupling constant
Me	methyl
M	metal
NMR	nuclear magnetic resonance
NHC	N-heterocyclic carbene
NOESY	Nuclear overhauser effect spectroscopy
n-BuLi	n-Buthyl Litiums
NBS	N-bromo succinimide
OTf	triflate
ppm	parts per million
PGSE	pulsed field gradient spin-echo
SIMes	1,3-dimesityl-4,5-dihydroimidazol-2-ylidene,
<i>t</i> BuOK	potassium <i>tert</i> -butoxide
THF	tetrahydrofurane
TP [']	tris-(3,5-dimethylpyrazolyl)borate)
tmeda	N,N,N',N'-tetramethylethylenediamine
TFE	trifluoroethanol
TOF	turnover frequency
trop	5H-dibenzo[a,d]cyclohepten-5-yl

ZPE zero point energy

5.2 Crystallographic Data

[RhCl(trop₂NH)(1,3-bis-((S)1-phenyl-ethyl)imidazolin-2-ylidene)] ((S,S)-K5)

Identification code	[Rh(Cl)(trop ₂ NH)(1,3-bis-(1-phenyl-ethyl)imidazolin-2-ylidene)]
Empirical formula	C ₄₉ H ₄₄ ClN ₃ Rh
Formula weight	813.25 g/mol
Temperature	293(2) K
Wavelength	0.71073 Å
Crystal system	Monoclinic
Space group	P2
Unit cell dimensions	a = 13.7685(13) Å α = 90° b = 11.5451(11) Å β = 104.472(2)° c = 13.9549(13) Å γ = 90°
Volume	2147.9(4) Å ³
Z	5
Calculated density	1.440 mg/m ³
Absorption coefficient	0.686 mm ⁻¹
F(000)	956
Crystal size	0.35 x 0.27 x 0.25 mm
Data collection	Siemens SMART PLATFORM with CCD Detector Graphite monochromator
Detector distance	50 mm
Solution by	direct methods
Refinement method	full matrix least-squares on F ² SHELXTL
θ (deg)	1.51 to 24.71
Limiting indices hkl	-15 to +16, -13 to +13, -9 to +16
Reflections collected / unique	10831 / 7031 [R(int) = 0.0405]
Completeness to theta = 24.71	99.90%
Max. and min. transmission	0.8473 and 0.7953
Data / restraints / parameters	7031 / 1 / 525
Goodness-of-fit on F ²	1.024
Final R indices [I > 2σ(I)]	R1 = 0.0485, wR2 = 0.0841
R indices (all data)	R1 = 0.0804, wR2 = 0.0943
Absolute structure parameter	-0.01(3)
Largest diff. peak and hole	0.457 and -0.716 eÅ ⁻³

[Rh(trop₂NH)((S)-ValinolCarben)]OTf ((S,S)-K6)

Identification code	[Rh(trop ₂ NH)(ValinolCarben)]OTf
Empirical formula	C ₄₅ H ₃₉ Cl ₂ F ₃ N ₃ O ₅ RhS
Formula weight	964.68 g/mol
Temperature	150(2) K
Wavelength	0.71073 Å
Crystal system	Triclinic
Space group	P1
Unit cell dimensions	a = 11.7963(13) Å α = 83.705(2)° b = 12.2576(13) Å β = 88.446(2)° c = 14.7809(16) Å γ = 85.107(2)°
Volume	2116.3(4) Å ³
Z	2
Calculated density	1.514 mg/m ³
Absorption coefficient	0.642 mm ⁻¹
F(000)	984
Crystal size	0.51 x 0.36 x 0.21 mm
Data collection	Siemens SMART PLATFORM with CCD Detector Graphite monochromator
Detector distance	50 mm
Solution by	direct methods
Refinement method	full matrix least-squares on F ² SHELXTL
θ (deg)	1.39 to 28.28
Limiting indices hkl	-15 to +15, -16 to +16, -19 to +19
Reflections collected / unique	22064 / 19250 [R(int) = 0.0135]
Completeness to theta = 24.71	99.30%
Max. and min. transmission	0.8769 and 0.7354
Refinement method	full matrix least-squares on F ²
Data / restraints / parameters	19250 / 3 / 1085
Goodness-of-fit on F ²	1.023
Final R indices [I > 2σ(I)]	R1 = 0.0424, wR ₂ = 0.1089
R indices (all data)	R1 = 0.0450, wR ₂ = 0.1121
Absolute structure parameter	-0.050(16)
Largest diff. peak and hole	1.160 and -0.754 eÅ ⁻³

[Rh(trop₂NH)(1,3-dicyclohexylimidazolin-2-ylidene)] CHactivated (K11)

Identification code	[Rh(trop ₂ NH)(1,3-dicyclohexylimidazolin-2-ylidene)CHactiv]
Empirical formula	C ₄₉ H ₄₆ N ₃ Rh ₁ O ₁
Formula weight	795.81 g/mol
Temperature	200K
Wavelength	0.71073
Crystal system	Monoclinic
Space group	P2(1)/c
Unit cell dimensions	a = 17.0981 Å α = 90.0° b = 12.8812 Å β = 110.344° c = 19.7886 Å γ = 90.0°
Volume	4082.91 Å ³
Z	4
Crystal size	0.9 x 0.8 x 0.5 mm
Calculated density	1.335 mg/m ³
Absorption coefficient	0.59 mm ⁻¹
F(000)	1538.0
Data collection	Siemens SMART PLATFORM with CCD Detector Graphite monochromator
Solution by	direct methods
Refinement method	full matrix least-squares on F ² SHELXTL
θ (deg)	1.71 o 28.31
Limiting indices hkl	-22 =< h =< 21, -17 =< k =< 17, -26 =< l =< 20
Reflections collected / unique	31197/ 10170 R(sigma) = 0.0599
Refinement method	full matrix least-squares on F ² SHELXTL
Data / restraints / parameters	10170 / 5 / 468
Goodness-of-fit on F ²	0.943
Final R indices [I>2sigma(I)]	R1 = 0.0507
R indices (all data)	R2 = 0.0813 wR2 = 0.1453
Absolute structure parameter	0.11
Largest diff. peak and hole	1.19 and -0.52 eÅ ⁻³

[RhCl(trop₂NH)(CNC₆H₅)] (K14)

Identification code	[RhCl(trop ₂ NH)(CNC ₆ H ₅)]
Empirical formula	C ₄₁ H ₃₆ ClN ₂ ORh
Formula weight	711.09 g/mol
Temperature	200(2) K
Wavelength	0.71073 Å
Crystal system	Monoclinic
Space group	P21/n
Unit cell dimensions	a = 12.0753(8) Å α = 90° b = 19.9639(13) Å c = 14.5432(9) Å γ = 90°
Volume	3333.1(4) Å ³
Z	4
Calculated density	1.417 Mg/m ³
Absorption coefficient	0.628 mm ⁻¹
F(000)	1464
Crystal size	0.75 x 0.35 x 0.18 mm
Data collection	Siemens SMART PLATFORM with CCD Detector Graphite monochromator
Detector distance	50 mm
Solution by	direct methods
Refinement method	full matrix least-squares on F ² SHELXTL
range for θ (deg)	1.92 to 28.27°
Limiting indices hkl	-15 ≤ h ≤ 16, -26 ≤ k ≤ 26, -18 ≤ l ≤ 18
Reflections collected / unique	29331 / 7869 [R(int) = 0.0195]
Completeness to theta = 28.27	95.4 %
Max. and min. transmission	0.8953 and 0.6502
Refinement method	Full-matrix least-squares on F ²
Data / restraints / parameters	7869 / 1 / 430
Goodness-of-fit on F ²	1.049
Final R indices [I > 2σ(I)]	R1 = 0.0229, wR2 = 0.0583
R indices (all data)	R1 = 0.0295, wR2 = 0.0623
Largest diff. peak and hole	0.340 and -0.325 eÅ ⁻³

[RhCl(trop₂NMe)(CNC₆H₄OSi(CH₃)₃)] (K16)

Identification code	[RhCl(trop ₂ NMe)(CNC ₆ H ₄ OSi(CH ₃) ₃)]
Empirical formula	C ₄₁ H ₃₈ N ₂ O ₁ Si ₁ Cl ₁ Rh ₁
Formula weight	741.19 g/mol
Temperature	298K
Wavelength	0.71073 Å
Crystal system	Triclinic
Space group	P-1
Unit cell dimensions	a = 15.1106 Å α = 80.922° b = 15.6483 Å β = 87.395° c = 16.2350 Å γ = 67.250°
Volume	3495.34
Crystal size	1.80 x 0.9 x 0.9 mm
Z	4
Calculated density	1.408 mg/m ³
Absorption coefficient	0.63 mm ⁻¹
F(000)	1528.0
Data collection	Siemens SMART PLATFORM with CCD Detector Graphite monochromator
Solution by	direct methods
Refinement method	full matrix least-squares on F ² SHELXTL
θ (deg)	1.71 to 28.36
Limiting indices hkl	-20 ≤ h ≤ 20, -20 ≤ k ≤ 20, -21 ≤ l ≤ 21
Reflections collected / unique	36700 / 17301 R(int) = 0.0568
Refinement method	Full-matrix least-squares on F ²
Data / restraints / parameters	17301 / 0 / 855
Goodness-of-fit on F ²	0.941
Final R indices [I > 2σ(I)]	R1 = 0.0451
R indices (all data)	R2 = 0.0653 wR2 = 0.1081
Absolute structure parameter	0.09
Largest diff. peak and hole	0.83 and -0.62 eÅ ⁻³

[Rh(PF₂O₂)(trop₂NH)(C₇H₅NO)] (K18)

Identification code	[Rh(PF ₂ O ₂)(trop ₂ NH)(C ₇ H ₅ NO)]	
Empirical formula	C ₃₇ H ₂₈ N ₁ O ₃ F ₂ P ₁ Rh ₁	
Formula weight	706.5 g/mol	
Temperature	294(2) K	
Wavelength	0.71073 Å	
Crystal system	Monoclinic	
Space group	P21/c	
Unit cell dimensions	a = 9.1297(9) Å	α = 90.092°
	b = 23.436(4) Å	β = 102.041°
	c = 15.847(2) Å	γ = 89.992°
Volume	3316.1(9) Å ³	
Z	4	
Calculated density	4.513 Mg/m ³	
Absorption coefficient	1.995 mm ⁻¹	
F(000)	4500	
Data collection	Siemens SMART PLATFORM with CCD Detector Graphite monochromator	
Detector distance	50 mm	
Solution by	direct methods	
Refinement method	Full-matrix least-squares on F ² SHELXTL	
range of θ (deg)	2.54 to 34.30 deg.	
Limiting indices hkl	-14 ≤ h ≤ 14, -36 ≤ k ≤ 33, -24 ≤ l ≤ 23	
Reflections collected / unique	42413 / 12946 [R(int) = 0.0683]	
Completeness to theta = 34.30	93.5 %	
Refinement method	Full-matrix least-squares on F ²	
Data / restraints / parameters	12946 / 0 / 410	
Goodness-of-fit on F ²	0.908	
Final R indices [I > 2σ(I)]	R1 = 0.0600, wR2 = 0.1957	
R indices (all data)	R1 = 0.1644, wR2 = 0.2145	
Largest diff. peak and hole	2.106 and -0.381 e. Å ⁻³	

[Rh(trop₂NH)(μ-C₇H₄NO)]₂ (K19)

Identification code	[Rh(trop ₂ NH)(μ-C ₇ H ₄ NO)] ₂
Empirical formula	C ₄₀ H ₃₂ N ₂ O ₂ Rh
Formula weight	675.59 g/mol
Temperature	200(2) K
Wavelength	0.71073 Å
Crystal system	Monoclinic
Space group	P21/c
Unit cell dimensions	a = 11.1081(5) Å α = 90.101° b = 14.3965(6) Å β = 101.979° c = 19.9690(7) Å γ = 89.973°
Volume	3123.9(2) Å ³
Z	4
Calculated density	1.436 Mg/m ³
Absorption coefficient	0.586 mm ⁻¹
F(000)	1388
Data collection	Siemens SMART PLATFORM with CCD Detector Graphite monochromator
Detector distance	50 mm
Solution by	direct methods
Refinement method	full matrix least-squares on F ² SHELXTL
Range of θ (deg)	3.39 to 34.48 deg
Limiting indices hkl	-17 ≤ h ≤ 17, -20 ≤ k ≤ 22, -31 ≤ l ≤ 30
Reflections collected / unique	26495 / 11456 [R(int) = 0.0577]
Completeness to theta = 34.48	86.8 %
Refinement method	Full-matrix least-squares on F ²
Data / restraints / parameters	11456 / 0 / 409
Goodness-of-fit on F ²	1.056
Final R indices [I > 2σ(I)]	R1 = 0.0544, wR2 = 0.1313
R indices (all data)	R1 = 0.0800, wR2 = 0.1494
Largest diff. peak and hole	1.992 and -1.106 e. Å ⁻³

[Pt(Me)₂(trop₂NH)] (K20)

Identification code	[Pt(Me) ₂ (trop ₂ NH)]
Empirical formula	C ₃₂ H ₂₉ N ₁ Pt ₁
Formula weight	622.66 g/mol
Temperature	23°C
Wavelength	0.71073
Crystal system	Monoclinic
Space group	C2/c
Unit cell dimensions	a = 27.3675 Å α = 90.0° b = 9.7848 Å β = 124.397° c = 21.5814 Å γ = 90.0°
Volume	4768.65 Å ³
Z	8
Calculated density	1.735 mg/m ³
Absorption coefficient	5.91 mm ⁻¹
F(000)	2448.0
Crystal size	0.32 x 0.22 x 0.21 mm
Data collection	Siemens SMART PLATFORM with CCD Detector Graphite monochromator
Solution by	direct methods
Refinement method	full matrix least-squares on F ² SHELXTL
θ (deg)	1.71 to 28.27
Limiting indices hkl	-35 ≤ h ≤ 34, -7 ≤ k ≤ 12, -28 ≤ l ≤ 28
Reflections collected / unique	14905 / 5539 R(int) = 0.0206
Refinement method	Full-matrix least-squares on F ²
Data / restraints / parameters	5539 / 0 / 307
Goodness-of-fit on F ²	1.122
Final R indices [I > 2σ(I)]	R1 = 0.0228
R indices (all data)	R2 = 0.0305; wR2 = 0.0555
Largest diff. peak and hole	0.42 and -1.29 eÅ ³

[Pd(Me)(OTf)(trop₂NH)] (K21)

Identification code	[Pd(Me)(OTf)(trop ₂ NH)]
Empirical formula	C ₃₂ H ₂₆ N ₁ Pd ₁ S ₁ O ₃ F ₃
Formula weight	668.03 g/mol
Temperature	23°C
Wavelength	0.71073
Crystal system	Monoclinic
Space group	Cc
Unit cell dimensions	a = 13.8428 Å α = 90.0° b = 18.0166 Å β = 94.652° c = 11.1032 Å γ = 90.0°
Volume	2760.02 Å ³
Z	4
Calculated density	1.608 mg/m ³
Absorption coefficient	0.80 mm ⁻¹
F(000)	1352.0
Crystal size	0.35 x 0.22 x 0.17 mm
Data collection	Siemens SMART PLATFORM with CCD Detector Graphite monochromator
Solution by	direct methods
Refinement method	full matrix least-squares on F ² SHELXTL
θ (deg)	1.71 to 28.28
Limiting indices hkl	-18 ≤ h ≤ 17, -23 ≤ k ≤ 23, -14 ≤ l ≤ 14
Reflections collected / unique	12211 / 6141 R(int) = 0.0180
Refinement method	Full-matrix least-squares on F ²
Data / restraints / parameters	6141 / 2 / 370
Goodness-of-fit on F ²	1.016
Final R indices [I > 2σ(I)]	R1 = 0.0249
R indices (all data)	R2 = 0.0306, wR2 = 0.0588
Absolute structure parameter	0.04
Largest diff. peak and hole	0.18 to -0.20 eÅ ⁻³

[Pt(Me)(tropNHortho-trop)] (K22)

Identification code	[Pt(Me)(tropNH-ortho-trop)]
Empirical formula	C ₃₁ H ₂₄ NPt
Formula weight	605.61 g/mol
Temperature	200(2) K
Wavelength	0.71073 Å
Crystal system	Monoclinic
Space group	C2/c
Unit cell dimensions	a = 15.052(3) Å α = 90° b = 11.389(2) Å β = 94.70(3)° c = 29.933(6) Å γ = 90°
Volume	5113.7(18) Å ³
Crystal size	1.2 x 0.5 x 0.8 mm
Z	8
Calculated density	1.011 Mg/m ³
Absorption coefficient	1.413 mm ⁻¹
F(000)	1616
Data collection	Siemens SMART PLATFORM with CCD Detector Graphite monochromator
Detector distance	50 mm
Solution by	direct methods
Refinement method	full matrix least-squares on F ² SHELXTL
range of θ (deg)	1.37 to 28.30°
Limiting indices hkl	-19 ≤ h ≤ 14, -13 ≤ k ≤ 14, -29 ≤ l ≤ 39
Reflections collected / unique	15317 / 5725 [R(int) = 0.0760]
Completeness to theta = 28.30°	89.90%
Data / restraints / parameters	5725 / 0 / 327
Goodness-of-fit on F ²	1.084
Final R indices [I > 2σ(I)]	R1 = 0.0560, wR2 = 0.1391
R indices (all data)	R1 = 0.0712, wR2 = 0.1464
Largest diff. peak and hole	3.008 and -3.775 e. Å ⁻³

[Rh(μ -Cl)(^Ftrop₂NH)]₂ (K23)

Identification code	[Rh(μ -Cl)(^F trop ₂ NH)] ₂
Empirical formula	C ₆₂ H ₄₂ Cl ₆ F ₈ N ₂ Rh ₂
Formula weight	1385.52 g/mol
Temperature	273(2) K
Wavelength	0.71073 Å
Crystal system	Triclinic
Space group	P1
Unit cell dimensions	a = 11.1097(13) Å α = 64.956 b = 11.4231(13) Å β = 85.871 c = 13.3230(16) Å γ = 61.608
Volume	1329.7(3) Å ³
Crystal size	1.2 x 1.5 x 0.5 mm
Z	1
Calculated density	2.101 mg/m ³
Absorption coefficient	0.812 mm ⁻¹
F(000)	874
Data collection	Siemens SMART PLATFORM with CCD Detector Graphite monochromator
Detector distance	50 mm
Solution by	direct methods
Refinement method	full matrix least-squares on F ² SHELXTL
θ (deg)	1.71 to 28.28 deg
Limiting indices hkl	-14 \leq h \leq 14, -15 \leq k \leq 15, -17 \leq l \leq 17
Reflections collected / unique	11729 / 10490 [R(int) = 0.0389]
Completeness to θ = 28.28	91.2 %
Refinement method	Full-matrix least-squares on F ²
Data / restraints / parameters	10490 / 3 / 727
Goodness-of-fit on F ²	1.031
Final R indices [I > 2 σ (I)]	R1 = 0.0342, wR2 = 0.0901
R indices (all data)	R1 = 0.0382, wR2 = 0.0938
Absolute structure parameter	0.00
Largest diff. peak and hole	0.672 and -0.637 eÅ ⁻³

[Pt(Me)₂(^Ftrop₂NH)] (K24)

Identification code	[Pt(Me) ₂ (^F trop ₂ NH)]
Empirical formula	C ₃₂ H ₂₅ F ₄ NPt
Formula weight	694.62 g/mol
Temperature	273(2) K
Wavelength	0.71073 Å
Crystal system	Monoclinic
Space group	C2/c
Unit cell dimensions	a = 27.6810(13) Å α = 90° b = 9.8283(5) Å β = 124.8770(10)° c = 21.9749(11) Å γ = 90°
Volume	4904.6(4) Å ³
Z	8
Calculated density	1.049 Mg/m ³
Absorption coefficient	1.474 mm ⁻¹
F(000)	1606
Data collection	Siemens SMART with CCD Detector Graphite monochromator
Detector distance	50 mm
Solution by	direct methods
Refinement method	full matrix least-squares on F ²
Theta range for data collection	1.79 to 28.31°
Limiting indices hkl	-36 ≤ h ≤ 36, -13 ≤ k ≤ 13, -29 ≤ l ≤ 29
Reflections collected / unique	24805 / 6075 [R(int) = 0.0915]
Completeness to theta = 28.31°	99.8 %
Data / restraints / parameters	6075 / 0 / 356
Goodness-of-fit on F ²	0.987
Final R indices [I > 2σ(I)]	R1 = 0.0305, wR2 = 0.0727
R indices (all data)	R1 = 0.0359, wR2 = 0.0743
Largest diff. peak and hole	2.046 and -1.322 eÅ ⁻³

[Pt(OMs)(Me)(trop₂NH)] (K28)

Identification code	[Pt(OMs)(Me)(trop ₂ NH)]
Empirical formula	C ₃₃ H ₃₀ NO ₃ SCl ₃ Pt
Formula weight	822.09 g/mol
Temperature	23°C
Wavelength	0.71073
Crystal system	Tetragonal
Space group	P4(3)
Unit cell dimensions	a= 11.0604 Å α= 90.0° b = 11.0604 Å β = 90.0° c = 25.5290 Å γ = 90.0°
Volume	3123.02 Å ³
Z	4
Calculated density	1.748 mg/m ³
Absorption coefficient	4.85 mm ⁻¹
F(000)	1616.0
Crystal size	0.38 x 0.36 x 0.36
Data collection	Siemens SMART PLATFORM with CCD Detector Graphite monochromator
Solution by	direct methods
Refinement method	full matrix least-squares on F ² SHELXTL
θ (deg)	1.71 to 28.49
Limiting indices hkl	-14 ≤ h ≤ 14, -14 ≤ k ≤ 14, -33 ≤ l ≤ 32
Reflections collected / unique	36882 / 7364 R(int) = 0.0265
Refinement method	Full-matrix least-squares on F ²
Data / restraints / parameters	7364 / 4 / 407
Goodness-of-fit on F ²	1.049
Final R indices [I>2σ(I)]	R1= 0.0234
R indices (all data)	R2= 0.0281 wR2 = 0.0531
Absolute structure parameter	-0.0116
Largest diff. peak and hole	0.46 and -0.55 eÅ ⁻³

[Pt(Me)(^{Ph}trop₂NH)]BAR^F (K31)

Identification code	[Pt(Me)(^{Ph} trop ₂ NH)]BAR ^F
Empirical formula	C ₉₂ H ₆₄ B ₁ N ₁ F ₂₄ Pt ₁ O ₁
Formula weight	1861.34 g/mol
Temperature	200K
Wavelength	0.71073 Å
Crystal system	Triclinic
Space group	P-1
Unit cell dimensions	a = 13.6527 Å α = 72.034° b = 17.2363 Å β = 86.981° c = 19.4634 Å γ = 78.770°
Volume	4273.28 Å ³
Crystal size	1.8 x 1.55 x 0.6 mm
Z	2
Calculated density	1.447 mg/m ³
Absorption coefficient	1.74 mm ⁻¹
F(000)	1860.0
Data collection	Siemens SMART PLATFORM with CCD Detector Graphite monochromator
Detector distance	50 mm
Solution by	direct methods
Refinement method	full matrix least-squares on F ² SHELXTL
θ (deg)	1.71 to 28.39
Limiting indices hkl	-18 ≤ h ≤ 18, -23 ≤ k ≤ 22, -25 ≤ l ≤ 26
Reflections collected / unique	44925 / 21226 R(int) = 0.0728
Refinement method	full matrix least-squares on F ² SHELXTL
Data / restraints / parameters	21226 / 0 / 1086
Goodness-of-fit on F ²	1.107
Final R indices [I > 2σ(I)]	R1 = 0.0443
R indices (all data)	R2 = 0.0484 wR2 = 0.1321
Absolute structure parameter	0.14
Largest diff. peak and hole	2.59 and -0.93 e Å ⁻³

[Pt(Me)(trop₂NH)(PPh₃)]OTf (K32)

Identification code	[Pt(Me)(trop ₂ NH)(PPh ₃)]OTf
Empirical formula	C ₅₃ H ₄₀ N ₁ O ₃ F ₃ S ₁ Cl ₉ Pt ₁ P
Formula weight	1373.08 g/mol
Temperature	?
Wavelength	0.71073
Crystal system	Monoclinic
Space group	P2(1)/c
Unit cell dimensions	a = 11.8840 Å α = 90.00° b = 21.7836 Å β = 98.807° c = 21.5109 Å γ = 90.00°
Volume	5503.01 Å ³
Z	4
Calculated density	1.657 mg/m ³
Absorption coefficient	3.11 mm ⁻¹
F(000)	2712.0
Crystal size	1.5 x 1.0 x 1.0 mm
Data collection	Siemens SMART PLATFORM with CCD Detector Graphite monochromator
Detector distance	50 mm
Solution by	direct methods
Refinement method	full matrix least-squares on F ² SHELXTL
θ (deg)	1.71 to 28.29
Limiting indices hkl	-15 ≤ h ≤ 15, -29 ≤ k ≤ 28, -28 ≤ l ≤ 22
Reflections collected / unique	42051 / 13629 R(int) = 0.1146
Refinement method	full matrix least-squares on F ² SHELXTL
Data / restraints / parameters	13629 / 0 / 653
Goodness-of-fit on F ²	0.735
Final R indices [I > 2σ(I)]	R1 = 0.0533
R indices (all data)	R2 = 0.1239 wR2 = 0.0970
Absolute structure parameter	0.12
Largest diff. peak and hole	1.21 and -1.10 e Å ⁻³

***cis*-[Rh(OTf)(trop₂PPh)(P(C₆H₁₃N₂O₂))] (K37)**

Identification code	<i>cis</i> -[Rh(OTf)(trop ₂ PPh)(P(C ₆ H ₁₃ N ₂ O ₂))]
Empirical formula	C ₄₃ H ₄₀ N ₂ O ₅ P ₂ RhF ₃ S
Formula weight	918.70 g/mol
Temperature	273(2) K
Wavelength	0.71073 Å
Crystal system	Triclinic
Space group	P1
Unit cell dimensions	a = 11.1097(13) Å α = 64.956° b = 11.4231(13) Å β = 85.871° c = 13.3230(16) Å γ = 61.608°
Volume	1329.7(3) Å ³
Crystal size	0.5 x 1.4 x 1.5 mm
Z	4
Calculated density	2.101 mg/m ³
Absorption coefficient	0.812 mm ⁻¹
F(000)	874
Data collection	Siemens SMART PLATFORM with CCD Detector Graphite monochromator
Detector distance	50 mm
Solution by	direct methods
Refinement method	full matrix least-squares on F ² SHELXTL
θ (deg)	1.71 to 28.28 deg.
Limiting indices hkl	-14 ≤ h ≤ 14, -15 ≤ k ≤ 15, -17 ≤ l ≤ 17
Reflections collected / unique	11729 / 10490 [R(int) = 0.0389]
Completeness to theta = 24.71	91.2 %
Refinement method	Full-matrix least-squares on F ₂
Data / restraints / parameters	10490 / 3 / 727
Goodness-of-fit on F ²	1.031
Final R indices [I > 2σ(I)]	R1 = 0.0342, wR2 = 0.0901
R indices (all data)	R1 = 0.0382, wR2 = 0.0938
Absolute structure parameter	0.00
Largest diff. peak and hole	0.672 and -0.637 eÅ ⁻³

[RhCl(trop₂NMe)(P(OPh)₃)]

Identification code	[RhCl(trop ₂ NMe)(P(OPh) ₃)]
Empirical formula	C ₅₀ H ₄₂ N ₁ O ₃ P ₁ Cl ₁ Rh ₁
Formula weight	874.21 g/mol
Temperature	298K
Wavelength	0.71073 Å
Crystal system	Monoclinic
Space group	P2(1)/n
Unit cell dimensions	a = 16.0450 Å α = 90.0° b = 15.5360 Å β = 98.184° c = 17.4340 Å γ = 90.0°
Volume	4301.60 Å ³
Z	4
Calculated density	1.459 mg/m ³
Absorption coefficient	0.67 mm ⁻¹
F(000)	1936.0
Crystal size	1.8 x 0.5 x 0.4 mm
Data collection	Siemens SMART PLATFORM with CCD Detector Graphite monochromator
Detector distance	50 mm
Solution by	direct methods
Refinement method	full matrix least-squares on F ² SHELXTL
θ (deg)	1.71 to 28.35
Limiting indices hkl	-20 ≤ h ≤ 21, -20 ≤ k ≤ 20, -23 ≤ l ≤ 23
Reflections collected / unique	45105 / 10725 R(int) = 0.0533
Refinement method	Full-matrix least-squares on F ₂
Data / restraints / parameters	10725 / 0 / 533
Goodness-of-fit on F ²	0.949
Final R indices [I > 2σ(I)]	R1 = 0.0455
R indices (all data)	R2 = 0.0691 wR2 = 0.1149
Absolute structure parameter	0.07
Largest diff. peak and hole	0.86 and -0.59 e Å ⁻³

[Rh(trop₂NMe)(P(OPh)₃)]OTf

Identification code	[Rh(trop ₂ NMe)(P(OPh) ₃)]OTf
Empirical formula	C ₅₀ H ₄₀ N ₁ O ₆ F ₃ PSRh
Formula weight	973.79 g/mol
Temperature	298 K
Wavelength	0.71073 Å
Crystal system	Triclinic
Space group	P-1
Unit cell dimensions	a = 10.9449 Å α = 95.492 ° b = 11.6952 Å β = 101.855 ° c = 19.6662 Å γ = 116.015 °
Volume	2164.04 Å ³
Z	4
Calculated density	1.494 mg/m ³
Absorption coefficient	0.55 mm ⁻¹
F(000)	996.0
Crystal size	1.5 x 0.5 x 0.15 mm
Data collection	Siemens SMART PLATFORM with CCD Detector Graphite monochromator
Detector distance	50 mm
Solution by	direct methods
Refinement method	full matrix least-squares on F ² SHELXTL
θ (deg)	1.72 to 30.56
Limiting indices hkl	-15 ≤ h ≤ 15, -16 ≤ k ≤ 16, -28 ≤ l ≤ 28
Reflections collected / unique	46437 / 13217 R(int) = 0.0728
Refinement method	Full-matrix least-squares on F ₂
Data / restraints / parameters	13217 / 0 / 569
Goodness-of-fit on F ²	1.023
Final R indices [I > 2σ(I)]	R1 = 0.0558
R indices (all data)	R2 = 0.0718 wR2 = 0.1568
Absolute structure parameter	0.10
Largest diff. peak and hole	1.32 and -0.74 eÅ ⁻³

Curriculum Vitae

Name Federica Alessia Maria Ricatto
Nationality Italian
Date of Birth April 15th, 1980, Milano

Education

1986-1991 Primary School, Milano
1991-1994 Secondary School, Milano
1994-1999 “Liceo Scientifico Leonardo da Vinci”, Milano
1999 “Diploma di Maturità Scientifica” (mark 96/100)
1999-2005 Studies in Chemistry at “Universtità degli Studi di Milano”, Milano
2002-2003 Erasmus Project in Oslo, Norway
2005 Degree of “Dottore in Chimica” (mark 110/110)
Diploma thesis under the supervision of Prof. Dr. Cenini “*Chiral porphyrin complexes of cobalt(II) and ruthenium(II) in catalytic cyclopropanation and amination reactions*” (Universtità degli Studi di Milano)
2005-2008 Ph.D. position in chemistry at the ETHZ Zürich in the group of Prof. Dr. Grützmacher

During my Ph.D. I taught undergraduate courses in inorganic and analytical chemistry.

Publications and Presentations

- Caselli, A., Gallo, E.; Ragaini, F.; Ricatto, F.; Abbiati, G.; Cenini, S.; “*Chiral porphyrin of cobalt (II) and ruthenium (II) in catalytic cyclopropanation and amination reactions*”, *Inorganica Chimica Acta*, **2006**, 359(9), 2924-2932.
- “*Intra-molecular C-H Activation of N-Heterocyclic Carbene Ligands across a Rhodium(I) Amide Bond*”, XXIII COMC (Conference on Organometallic Chemistry, Rennes, France **2008**), Poster Presentation.
- “*Synthesis of amine olefin platinum complexes with unusual saw-horse structure*”, XVII EuCheMS (Conference on Organometallic Chemistry, Sofia, Bulgaria **2007**), Oral Presentation.

Acknowledgment

First of all I would like to thank Prof. Grützmacher for the unique opportunity to join his research group and for the freedom he gave me during these years to explore the “trop chemistry”.

My greatest thanks go to Prof. Togni not only for having accepted to be my co-referent but also for the pleasant ski-weekends and dinners with him and his research group.

I would like to thank Prof. Mezzetti for his helpful advises and Prof. Pregosin for his NMR and bridge lessons.

Thank to Dr. Schönberg for having “pushed” me to do some sport and out-door activities: “mens sana in corpore sano”!

I am grateful to Dr. Rügger for his advices and for his priceless help in solving complex NMR issues.

Thank to all the Grüzys: Betta, Catherine, Friederike, Georgina, Judith, Katrin, Karin, Monica, Swarna, Alex, Carlos, Coen, Daniel, Detlev, Flo A., Flo P., Jan-Valere, Joe, Martin, Matthias, Nick, Urs, Theo, Timo, Torsten, Pascal, Samuel, Sebastian, Simone and all the students who joined the group – in particular Ladina – for the pleasant atmosphere. I would especially like to thank my lab-mate Matthias for having constantly provided alternative rock music and for his helpful discussions in chemistry. Moreover, I deeply appreciated his “Italian touch” and his interest in my homeland! Thanks to Timo for having shared the joy – and the suffering! – of the “final steps” at the ETH and having organized our ski-trips, Theo for his helpful corrections and Jan-Valere for his calculations. Thank to Katrin for her gorgeous recipes, Fritzzy for her positive attitude and her British-humor, Florian (P.) for his energy and Simone, Carlos and Nick for being able to speak Italian! Thank to the whole Togni group for the nice evenings together. In particular, I would like to thank the Italian crew: Franceso & Isa, Luca, Pietro & Sheila, Nick and Serena for the nice coffee breaks at the bistro. Many thanks to my friend Aline for her friendship and the nice poker-evenings she organized. Thank to Checca & Checco for the countless nights spent together playing games and drinking wine. Thank to the neighbours of Imbisbühlstrasse 67 in particular Pierre and Ilona; thank to Francesca and her horses Delfin & Karina and to my cats: Pepe, Votan and Oreste.

I would also like to thank my whole family: my sister Manuela, my grandmother Maria my parents Lydia & Mario and my partner’s parents Simonetta & Sandro for the constant support.

Last but not least, I would like to thank my partner Marco for having made our “Swiss adventure” a particular pleasant journey!

GRAZIE A TUTTI DI CUORE!!!